Notes on Shell Structures

Pierre Hoogenboom

Contents

Sagitta 1
Radius/thickness 1
Objective 1
Summary 3
Corbel arch 3
Corbel dome 4
Treasury of Atreus 4
Cables and arches 5
Catenary or funicular 5
Pressure line 6
Middle third rule 7
Optimal arch 7
Barlow's formula 8
Drafting spline 9
B-spline 9
NURBS 9
Continuity 11
Zebra analysis 11
Finite element mesh 11
NURBS finite elements 11
Polygon meshes 11
Section forces and moments 12
Definition of membrane forces, moments and shear forces 13
Thickness 13
Shell force flow 13
Pantheon 14
Edge disturbance 14
Compatibility moment 15
Comparison of an arch and a dome 15
Plastic deformation in shell edges 16
Form finding 16
Fully stressed dome 16
Approximation of the fully stressed dome 17
Buckling of the fully stressed dome 17
Optimal dome 18
Global coordinate system 19
Local coordinate system 19
Line curvature 20
Surface curvature 20
Paraboloid 21
Principal curvatures 22
Savill building 22
Gaussian curvature 23
Mean curvature 24
Orthogonal parameterisation 25
Catenoid 26
Tractricoid 26
Interpretation 27
Sillogue water tower 27
Differential geometry 31
Curvilinear coordinate system 31
Shell displacement and load 32
Lamé parameters 32

Equation of Gauß 33
Intrinsic property 35
Curved roofs with tiles 35
Equations of Codazzi 36
Helicoid 36
In plane curvature 37
Shell membrane equations 38
Membrane forces in a spherical dome 38
Derivation of membrane equation 1 40
Derivation of membrane equation 3 40
Duomo di Firenze 42
Saint Paul's Cathedral 43
Derivation of membrane equation 7 44
Derivation of membrane equation 9 45
Soap bubbles and soap films 46
Beam calculation of a simply supported tube 47
Shell calculation of a simply supported tube 47
Shell calculation of the stresses 48
Statically determinate 49
Tube shear stress 49
Shell calculation of the tube deformation 49
Bernoulli's hypothesis 50
Shear stiffness 51
Gap 52
Monocoque 52

Structural models overview 53
Shell theory 54
Sanders-Koiter equations 54
Ping pong ball 56
Compatibility equation 57
Rigid translation 58
Shell differential equations 58
Differential equation type 59
Shallow shell differential equation 59
Plate boundary conditions 60
Reissner-Mindlin theory 62
Edge shear stresses 62
Reinforced concrete plate edges 63
Edges that are not in the *x* or *y* direction 63
Palazzetto dello sport 64
$nxy \neq nyx$ 66
Derivation of equation 18 67
Shell boundary conditions 68
Canopy example, shell boundary conditions 70
Diaphragm boundary condition 70
Overview of the shell variables 71
Generalised edge disturbance 72
Beam supported by springs 72
Influence length 74
Influence length of a cylinder edge 74
Influence lengths of all shells 75
Finite element mesh 75
Boiler drums 76
Saturn V 77

Finite difference method 79
Canopy example, finite difference solution 80
Shell finite elements 82
Element aspect ratio 83
Mesh refinement 84
Model accuracy 84
Result extrapolation 84
Bohemian dome 85
Selecting the element type 86
Integration points 86
Locking and hourglass modes 87
Finite element boundary conditions 88
Canopy finite element boundary conditions 88
Canopy finite element analysis 89
Singularities 92
The largest model that your PC can process 93
Moore's law 94
Arithmetic accuracy 94
Finite element benchmarks 94
Modelling thick shells 95
Averaging at nodes 96
Influence of coordinate system on the FEM results 97
Tensors 97
Principal directions 98
Principal values 98
Trajectories 98
Membrane forces around a square opening 98
Ellipsoid 99
Stresses 100
Von Mises stress 101
Principal stresses 101
Top and bottom face principal stresses 102
Hypar curvature 102
Zeckendorf plaza 102
Hypar membrane forces 103
Checking membrane reinforcement 104
Designing membrane reinforcement 104
Timber grid shell design 105
Particle-spring method 106
Spring back analysis 107
Timber grid shell analysis 107

Inextensional deformation 109
Viking ship Oseberg 109
Liquid storage tanks 111
Analysis of the liquid storage tank 111
Rijswijk shell roof 112
Spotting inextensional deformation 112
Vibration mode shapes 112
Strain energy 113
Theorema egregium 113
Shells behaving like a plate 114
Shell design 114
Plotting Gaussian curvature 115

Kresge Auditorium 115
Deitingen petrol station 116
Gauß-Bonnet theorem 116
Corollary 117
Force on a sphere 117
Force on a shell of positive Gaussian curvature 118
Force on a cylinder 118
Force on a shell of negative Gaussian curvature 119
Moments due to a force 120
Plate twisting 120
Gaussian curvature of boats 121
Prestressing tents 122
Umbilics 124
Umbilical patterns 124
Monkey saddle 125
Hypar edge moments 126
Berenplaat hypar roof 127
Paaskerk hypar roof 127
Surprising flexibility 128
Parameterisation of a paraboloid in the principal curvature directions 129

Sudden collapse 135
Tucker High School 135
Cylinder buckling shapes 136
Buckling of a beam supported by springs 137
Ring buckling of an axially compressed cylinder 138
Differential equation for shell buckling 139
Buckling load factor 140
Design check of buckling 141
Catelan's surface 142
Imperfection sensitivity 142
Experiment 143
Puzzle 143
Exceptions to imperfection sensitivity 144
Koiter's law 144
Knock down factor 145
Linear buckling analysis 145
Ship design 146
Nonlinear finite element analysis 146
Mystery solved 147
Measuring shape imperfections 147
Stiffeners 149
CNIT 149
Buckling, yielding or crushing? 152
Buckling curves for computational analysis 153

Hyperboloid 155
Gravity 155
Ferrybridge 155
Modal analysis 156
Rigid body modes 157
Equation of motion 157
Wave numbers 158
Festoon 159
Vibration experiments 159

Resonance 160
In-extensional deformation 160
Hemispheres 160
Resonance of a wine glass 161
Spheres 161
Cylinders 161
Membrane force 163
Shell vibration literature 163
Natural frequency of a square shell 163
Enneper's surface 164
Measuring vibrations 164
Spectrum 165
Fast Fourier transform 166
Sampling theorem 166
Transient analysis 166
Damping ratio 167
Damping ratio distribution 167
Acceptable vibrations 168
Shell acoustics 168
Design improvements 169
Bausschinger effect 169
Fatigue 169

Limit state function 171
Limit State 171
Approximation of the limit state function 171
Monte Carlo analysis 172
Turkstra's rule 173
Drawing a number 174
Software 174
Human error 175
Annual failure probability 175
Changing the period of a Gumbel distribution 176
Weakest link 176
Personal safety 176
Calculating with probabilities 177
Henk 177
Economic safety 177
Safety index β 179
Strength of chains 179
Statistical size effect 180
Professional size effect 181

Literature 183

Appendices

Optimal arch 191
Optimal dome 193
Curvature tensor 196
Membrane force tensor 197
Asymmetric tensors 198
Compatibility equation 199
Cylinder equation 200
Section forces and moments in thick shells 201

Stresses in thick shells ……. 203
Increase of the Gaussian curvature …….. 205
Umbilical patterns …… 206
Buckling equations …….. 211
3D reinforcement ……. 212
Tensors ……. 214

Symbols

a …….…… radius of curvature [m]
$a_1, a_2, a_3, a_4, a_5, a_6$ ……... gradients of a tensor field
b , c …….. dimensions [m]
C …….. knock down factor [-]
d ……. imperfection amplitude [m]
d …….. diameter of distributed point load [m]
E ……..…… Young's modulus [N/mm^2]
f_y ……. yield strength [N/mm^2]
f_n ……. natural frequency [Hz]
h ……... finite element size [m]
k_G ……..… Gaussian curvature [1/m^2]
k_m ……..… mean curvature [1/m]
k_x , k_y ……..…….. in plane curvature of parameter lines [1/m]
k_{xx} , k_{yy} , k_{xy} ……..…….. curvature tensor [1/m]
l ..…….. span [m]
m_{xx} , m_{yy} , m_{xy} …… moment tensor [kNm/m]
n_{xx} , n_{yy} , n_{xy} , n_{yx} …… membrane force tensor [kN/m]
n_{cr} …… critical membrane force [kN/m] often determined by a linear buckling analysis of a shell without imperfections
n_p …… plastic membrane force [kN/m] calculated by hand from crushing or yielding of a cross-section
n_{ult} …… membrane force [kN/m] just before a shell collapses often determined by a nonlinear finite element analysis
p_x , p_y , p_z ……..…….. distributed load [kN/m^2]
P ……... concentrated load [kN]
q_x , q_y , q_z ……..…… distributed edge load or support reaction [kN/m]
s ……... sagitta [m]
t …….. shell thickness [m]
t …….. time [s]
u , v ……... curvilinear coordinates [m or -]
u_x , u_y , u_z …… displacements [m]
V …….. concentrated shear force in a shell edge [kN]
v_x , v_y …….. out of plane shear forces [kN/m]
x , y , z ……. local Cartesian coordinates [m]
$\overline{x}$, $\overline{y}$, $\overline{z}$ ……. global Cartesian coordinates [m]

α_x , α_y ……. Lamé parameters [- or m]
β …….. reliability index [-]
Γ …….. increase in Gaussian curvature due to load [1/m^2]
δ_i …… invariants of the gradient of a tensor field
ε_{xx} , ε_{yy} , γ_{xy} …… strain tensor of the middle surface [-]

$\kappa_{xx}, \kappa_{yy}, \rho_{xy}$ …….. curvature deformation tensor [1/m]

λ …….. load factor [-]

λ_{cr} …….. buckling load factor of a perfect shell structure [-]

λ_{ult} …….. collapse load factor of an imperfect shell structure [-]

ν …….. Poisson's ratio [-]

ρ ……. mass density [kg/m^3]

$\sigma_{xx}, \sigma_{yy}, \sigma_{zz}, \sigma_{yz}, \sigma_{xz}, \sigma_{xy}$ .. stress tensor [N/mm^2]

$\varphi_x, \varphi_y, \varphi_z$ …… rotation of a pin perpendicular to the middle surface [1/m]

ϕ ……..… Airy stress function [kNm]

∇^2 …… Laplace operator (pronounce nabla squared)

Sagitta

The height of an arch is called the *rise* or the *sagitta* (pronounce with emphasis on "git") (Latin for arrow). When the sagitta s and the span l are known, we can calculate the radius a of a circular arch.

$$a = \frac{1}{2}s + \frac{1}{8}\frac{l^2}{s}$$

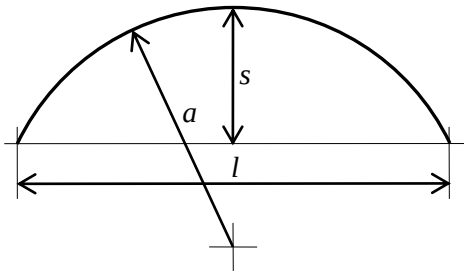

For example the dome of the palazzetto dello sport (fig. 1)(p. 64) has a span of 58.5 m, and sagitta of 20.9 m. The radius is

$$a = \frac{20.9}{2} + \frac{58.5^2}{8 \times 20.9} = 30.9\ \text{m}.$$





Figure 1. Palazzetto dello sport in Rome [www.galinsky.com]

Radius/thickness

The palazzetto dello sport has ribs which are 330 mm thick. The shell between the ribs is 120 mm thick. The ratio radius/thickness is

$$\frac{a}{t} = \frac{30.9}{0.12} = 260.$$

When we include the ribs the ratio is

$$\frac{a}{t} = \frac{30.9}{0.33} = 94.$$

Table 1 shows this ratio for several shell structures. Clearly, a large ratio shows that little material is used. For example, if your design has a ratio a / t = 500, it is really efficient.

Objective

The objective of these notes is to predict the behaviour of shell structures. After completing the course you can answer the following questions about your shell designs. Will it deflect too much? Will it yield? Will it crack or break? Will it vibrate annoyingly? Will it buckle? Will it be safe? What causes this and how can I improve it?

Exercise: Psychologists say that a person or animal needs an objective in order to determine how to look at something. For example, when you are tired, a chair is a thing-to-sit-on and when you need to replace a light bulb, a chair is a thing-to-stand-on. Rephrase the former sentence using the words “engineer”, “model”, “predict”.

Table 1. Dimensions of shell structures

structure	location, year, architect	geometry	dimensions	radius *a*	thickness *t*	ratio *a* / *t*
chicken egg	150 10^6 BC	surface of revolution	60 mm length	20 mm minimum	0.2–0.4 mm	100
Treasury of Atreus (p. 4)	Μυκηνες Greece 1100 BC	surface of revolution	14.5 m diameter	16 m	≈ 0.8 m	20
Pantheon (p. 14)	Rome 126 AD	hemisphere	43.4 m diameter	21.7 m	1.2 m at the top	18
Viking ship Oseberg (p. 109)	Tønsberg Norway 820 AD	ellipsoid part	21.58 m long 5.10 m wide			
Duomo di Firenze (p. 42)	Italy 1420 Brunelleschi	octagonal dome	44 m diameter	22 m		
St. Paul’s Cathedral (p. 43)	London 1675 Wren	cone and hemisphere	35 m diameter	15.25 m		
Jena planetarium [1]	Germany 1925 Bauersfeld	hemisphere	25 m diameter	12.5 m	60 mm	200
Algeciras market hall [1]	Spain 1934 Torroja	spherical cap on 8 supports	47.6 m diameter	44.1 m	90 mm	490
beer can (p. 143)	1935	cylinder	66 mm diameter	33 mm	0.08 mm	410
Hibbing water filter plant [1]	Minnesota 1939 Tedesko	ellipsoid of revolution	45.7 m diameter	47.24–5.33 m	900–150 mm	35–525
Brynmawr rubber factory [1]	Brynmawr UK, 1947 Arup	elpar on a rect. plan	19.6 x 25.3 m	25.0–32.9 m	90 mm	300–400
Kresge Auditorium (p. 115)	Cambridge 1955 Saarinen	segment of a sphere on 3 points	48.0 m between supports	33.0 m	90 mm	370
Kaneohe Foodland [1]	Hawaii 1957 Bradshaw	intersection of 2 tori on 4 supports	39.0 x 39.0 m between supports	39.0–78.0 m	76–178 mm	500–1000
Palazzetto dello sport (p. 63)	Rome 1957 Nervi	spherical cap with ribs	58.5 m diameter	30.9 m	0.12 m shell 0.33 m ribs	260 or 94
CNIT (p. 149)	Paris 1957 Esquilan	intersection of 3 cylinders on 3 supports	219 m between supports	89.9–420.0 m	1.91–2.74 m total 0.06 – 0.12 m outer layers	47–153
Zeckendorf Plaza (p. 102)	Denver, USA 1958 Tedesko	4 hypars	40 x 34 m height 8.5 m	40 m	76 mm	528
Ferrybridge cooling towers (p. 155)	Ferrybridge UK 1960	hyperboloid	height 115 m	44 m	130 mm repaired … mm	350
Paaskerk (p. 127)	Amstelveen 1963 Van Asbeck	hypar on 2 points	25 x 25 m height 10.3 m	31 m		
Tucker gym (p. 135)	Henrico USA 1965 Hanson	4 hypars	47 x 49 m height 4.6 m	127 m	90 mm	1400

Deitingen petrol station (p. 116)	Switserland 1968 Isler	segment of a sphere on 3 points	span 31.6 m height 11.5 m	52 m	90 mm	580
Saturn V (p. 76)	Houston USA 1965-1975	cylinders and stiffeners	height 111 m	5 m		
oil tanker (p. 146)	~1970	all curvatures with stiffeners	length 300 m width 30 m		20 mm	
Savill building (p. 22)	Windsor UK 2005 Howells	freeform	length 98 m width 24 m	143 m	300 mm	41
Sillogue water tower (p. 27)	Dublin 2007 Collins	surface of revolution	height 39 m top diameter 38 m	24.8 m	786 mm	32

Summary
Shell structures display four phenomena that are different from other structures. These phenomena are listed below. An engineer working with shell structures needs to understand these.

- Arches are thick because pressure lines (p. 6) need go through the middle third (p. 7). Shells are thin because hoop forces (p. 13) push and pull the pressure lines into the middle third.
- Large moments occur in supported edges. This is called edge disturbance (p. 14, 72). It happens because the deformed shell needs to connect to the undeformed support.
- Shells with special curvatures and particular supports behave like flat plates. This is called inextensional deformation (p. 109).
- Small shape imperfections often cause a large reduction of the buckling load. This is called imperfection sensitivity (p. 142).

Corbel arch
When piling blocks we can shift each block a little compared to the previous one. In this way we can make an arch without formwork (fig. 2). This arch is called a *corbel arch*. It can be analysed best starting from the top. The top block needs to be supported below its centre of gravity. Therefore, it can be shifted up to half its length *c*. The top two blocks need to be supported in their centre of gravity too. Therefore, they can be shifted up to one-fourth of *c*. The shifts produce a row of fractions $\frac{1}{2}, \frac{1}{4}, \frac{1}{6}, \frac{1}{8}...$ The shape of the arch is described by

$$x = nb, \quad y = \sum_{\eta=1}^{n} \frac{c}{2\eta}.$$

Where *b* and *c* are the block height and length. If *x* goes to infinity then *y* goes to infinity. So, there is no theoretical restriction to the span that can be created in this way. However, for large spans and small blocks the arch will become extremely high.

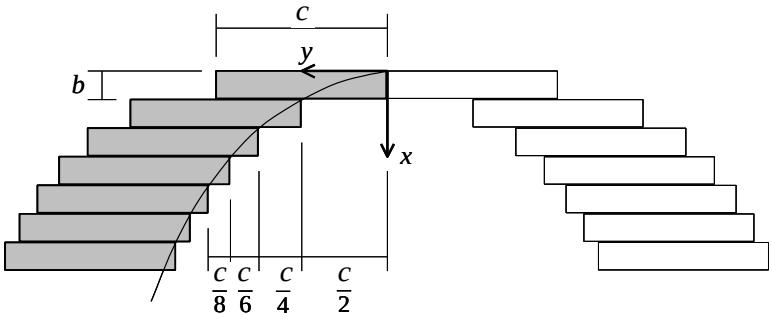

Figure 2. Pile of shifted blocks

Corbel dome

The concept of a corbel arch (p. 3) can be used for building domes too. The following program computes the coordinates *x* and *y*. In the derivation was used that the top block has a small angle.

```
x:=0: y:=0: M:=0: A:=0:
for n from 1 to 100 do
  M:=M+2/3*((y+a)^3-y^3):
  A:=A+(y+a)^2-y^2:
  x:=n*b:
  y:=M/A:
end do;
```

Treasury of Atreus

In ancient Greece was a civilisation called Mycenaean (pronounce my-se-nee-an with emphasis on my). It flourished for 500 years until 1100 BC.[1] The Mycenaeans buried their kings in corbel dome tombs (p. 4). Some still exist. One is called the treasury of Atreus (fig. 3, 4). It is located in the ancient city of Μυκηνες (pronounce me-kee-ness with emphasis on kee). It has a span of 14.5 m, a radius of curvature of 16 m and a thickness of approximately 0.8 m. Therefore, $a/t = 20$.

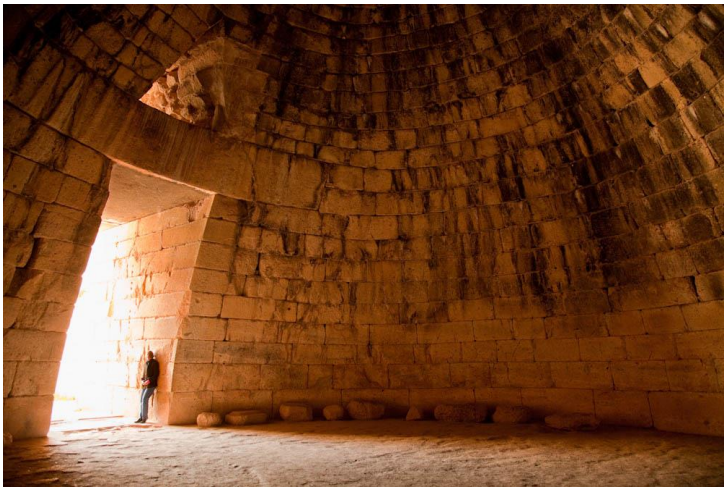

Figure 3. Interior of the treasury of Atreus [gjclarthistory.blogspot.com]

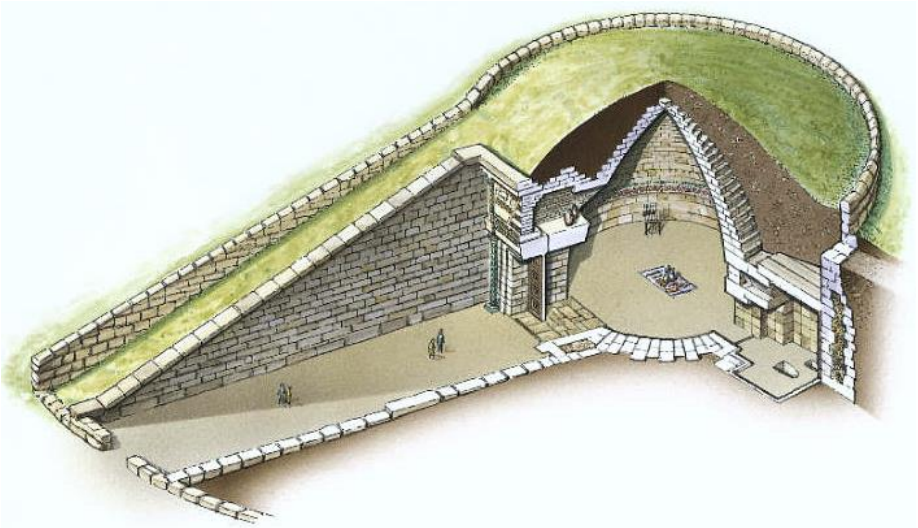

Figure 4. Structure of the treasury of Atreus [gjclarthistory.blogspot.com]

[1] The following dates provide a time frame: Around 2560 BC the oldest of the three large pyramids close to Cairo was build. In 753 BC the city of Rome was founded [Wikipedia].

Cables and arches
In 1664, Robert Hooke was curator of experiments of the Royal Society of London. He took his job very seriously and every week he showed an interesting experiment to the members of this society, which included Isaac Newton.[2] The members were enthusiastic about the experiments and published scientific papers on them. Often they forgot to mention that it was Hooke's idea they had started with. He became rather tired of this, therefore, he kept some discoveries to himself. He formulated them in Latin and published the mixed up letters [2]. One went like this.

abcccddeeeeefggiiiiiiiillmmmmnnnnnooprrsssttttttuuuuuuuux.

When Hooke died in 1703, the executor of his will gave the solution to this anagram.

Ut pendet continuum flexile, sic stabit contiguum rigidum inversum.

which can be translated as,

As hangs a flexible cable, so inverted, stand the touching pieces of an arch.

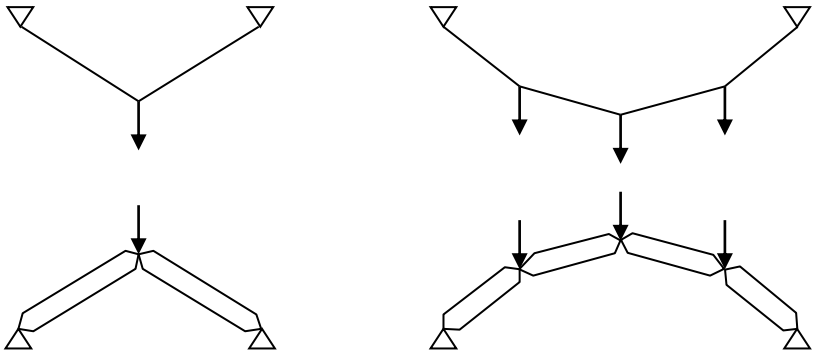

Figure 5. Hooke's discovery

Though not telling the world, it is likely that Hooke shared this discovery with his best friend Christopher Wren, who designed St Paul's Cathedral (p. 43) and supervised its construction (1669–1708).

Catenary or **funicular**
A chain hanging between two points will adopt a shape that is called *catenary* (emphasise ca) or *funicular* (emphasise ni) (fig. 6).

$$y = \frac{T}{q}\left(\cosh\frac{qx}{T} - \cosh\frac{ql}{2T}\right)$$

T is the horizontal support reaction and q is the self-weight of the chain per unit length. This shape is the solution to the differential equation

$$T\frac{d^2y}{dx^2} = q\sqrt{1+\left(\frac{dy}{dx}\right)^2},$$

and the boundary conditions

[2] Robert Hooke (1635–1703) also encouraged Isaac Newton (1643–1727) to use his mathematical expertise on the motions of the planets. Newton discovered his laws around 1684 [Wikipedia].

$$x = -\frac{1}{2}l \quad \rightarrow \quad y = 0$$
$$x = \frac{1}{2}l \quad \rightarrow \quad y = 0$$

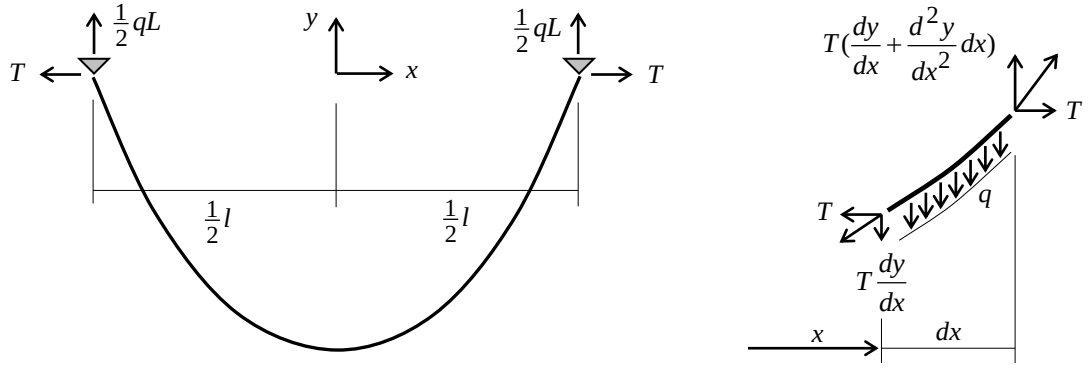

Figure 6. Catenary, T/q = 4 m, l = 14 m

The chain length is

$$L = \frac{2T}{q}\sinh\frac{ql}{2T}.$$

Challenging exercise: In 1690, Jakob Bernoulli wrote the following question in the journal *Acta Eruditorum*. What is the shape of a hanging chain? (Translated from Latin.) This problem had not been solved before. He got the right answer from three people; Gottfried Leibniz, Christiaan Huygens and his brother Johann Bernoulli [3]. (You can find these names in your history book too.) If you can derive the chain differential equation and solve it, you might be just as smart as they were.

Pressure line

In the analysis of an arch it is common to draw the pressure line for dead load. The procedure is demonstrated in an example (fig. 7) for a uniformly distributed vertical load. We first divide the distributed load into concentrated loads. Then we draw the loads head to tail in a *Magnitude plan*. We select a pole O somewhere to the left of the loads. We draw the rays Oa through Og (fig. 7, green lines). We proceed to draw the green curve in a *Line of action plan*. For this we start at the left support and draw a line parallel to ray Oa until we cross the line of action of force P_1. Next we draw a line parallel to ray Ob and so forth. The position of the pole O determines the shape of the pressure line. We make adjustments to the pole to design the shape. When you have done this a few times, you know what adjustments to make.

An arch constructed to follow a pressure line will carry loads P1 through P6 in pure axial compression. Often the pressure line is called funicular (p. 5). However, the shape is more like a parabola. In fact, if we would divide the uniformly distributed load in an infinite number of very small concentrated loads, the result would be a perfect parabola.

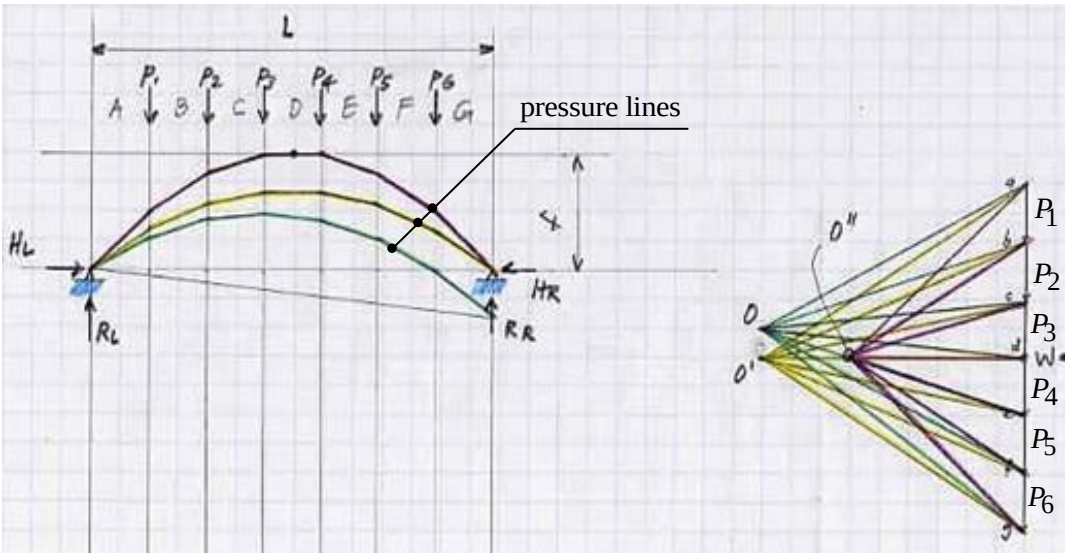

Figure 7. Line of action plan *Magnitude plan*

Exercise: In figure 7, line Oa is a vector that represents a force. Lines Oa, Ob and P1 can be rearranged into a parallelogram of forces. Draw this parallelogram of forces in the line of action plan. Do you see that the magnitude plan is a clever rearrangement of all parallelograms of forces in the line of action plan?

Exercise: In figure 7, suppose that $P_1 = P_2 = .. = P_6 = 10$ kN. What is the largest force in an arch that follows the O″ (purple) pressure line?

Middle third rule

There is no tensile stress in a rectangular cross-section, if the resulting force F is within the middle third of the thickness (fig. 8). F causes a normal force $N = F$ and a moment $M = F\,e$, where e is the eccentricity. There is no tension when e is smaller than $\frac{1}{6}t$. Since e is equal to M / N there is no tension when $-\frac{1}{6}t \le \frac{M}{N} \le \frac{1}{6}t$, which is called the *middle third rule*.

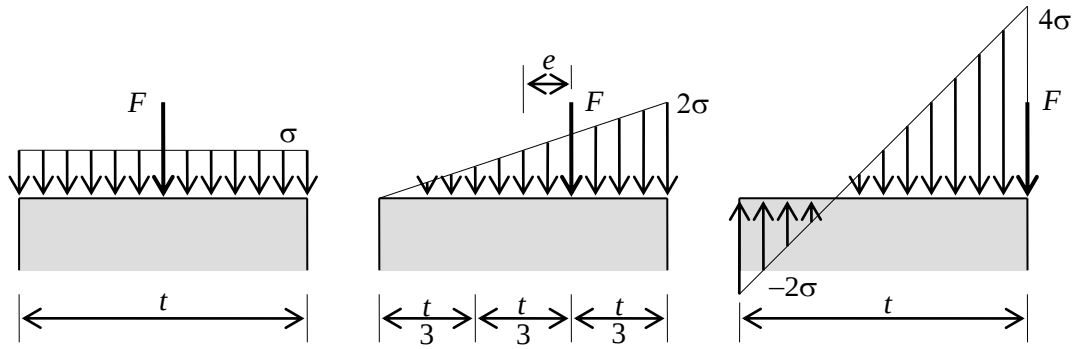

Figure 8. Stress distribution due to an eccentric normal force

Using the pressure line (p. 6) and the middle third rule we can design an arch which has no tensile stresses.

Optimal arch

Suppose we want to build an arch with as little material as possible. The arch has a span l and carries an evenly distributed line load q. The sagitta of this optimal arch is about 40% of its span. To be exact, the shape of this arch is a parabola with a ratio sagitta to span of $\sqrt{3}$ to 4 (fig. 9). The material volume of this arch is

$$V = \frac{q l^2}{\sqrt{3} f},$$

where f is the material compressive strength. The *abutment force* (horizontal component of the support reaction) is

$$R_h = \frac{1}{6}\sqrt{3} q l \approx 0.29 q l$$

These results are mathematically exact, however, self-weight of the arch and buckling have been neglected (derivation in appendix on p. 191.).

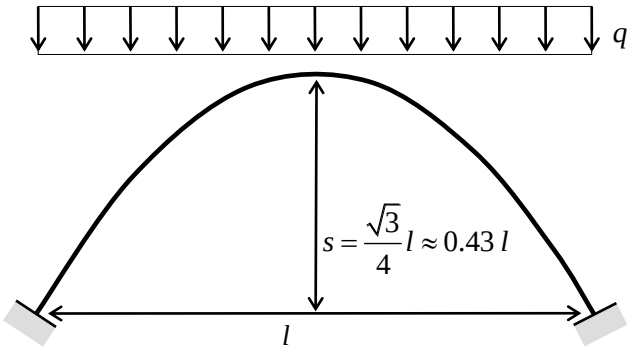

Figure 9. Optimal arch proportions

Barlow's formula

A cylindrical shell with a radius a [m] is loaded by a uniformly distributed force p [kN/m²] (fig. 10). The normal force n [kN/m] in the shell wall is

$n = p\,a$.

This equation is called Barlow's formula.[3] For the derivation we replace the load by compressed water. Subsequently, we cut the shell and water in halves (fig. 11). In the cut the water pressure is p and the shell forces are n. Vertical equilibrium gives $n + n = p\,2a$, which simplifies to $n = p\,a$. Q.E.D.

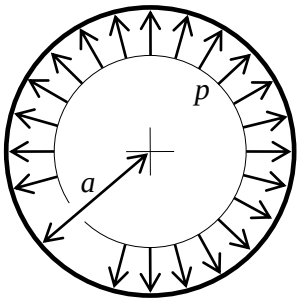

Figure 10. Cylindrical shell loaded by an evenly distributed force

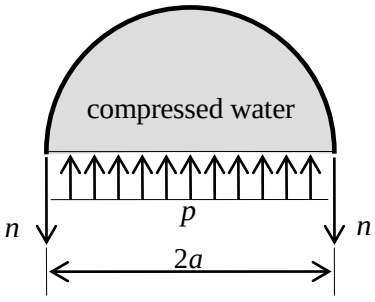

Figure 11. Derivation of Barlow's formula

Exercise: Show that the normal force n [kN/m] in a pressurised spherical shell is $n = \frac{1}{2} p\,a$.

[3] Peter Barlow (1776–1862) was an English scientist interested in steam engine kettles [Wikipedia].

Drafting spline
A spline is a flexible strip of metal, wood or plastic. Designers use it for drawing curved lines (fig. 12). For example when designing and building boats a spline is an indispensible tool. The spline is fixed in position by weights. Traditionally, the weights have a whale shape and are made of lead. Often they are called ducks.

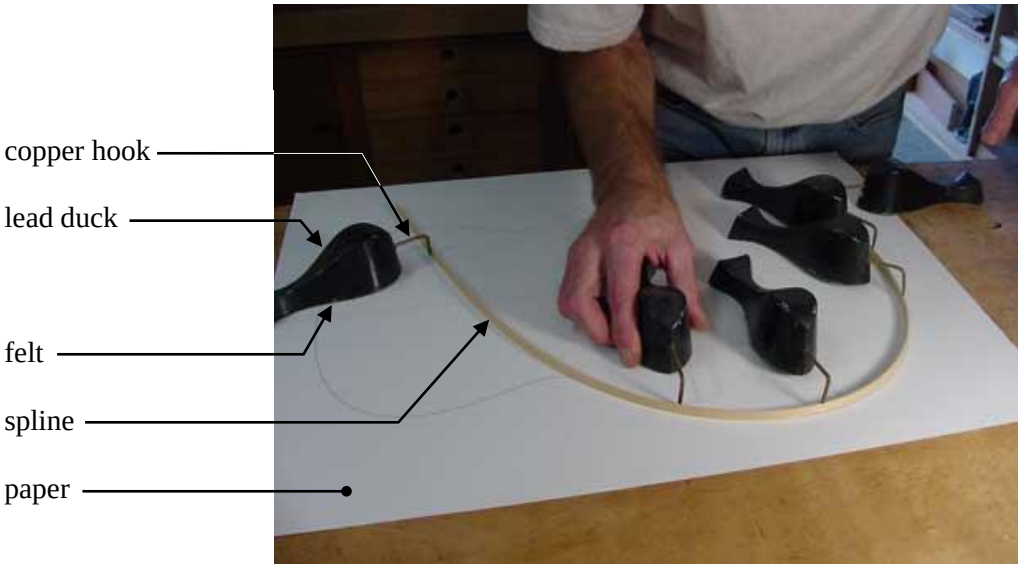

Figure 12. Spline and ducks for drawing smooth lines [Rain Noe, www.core77.com]

B-spline
In the earliest CAD programs we could draw straight lines only.[4] Every line had a begin point and an end point. This was soon extended with poly lines (plines) which also had intermediate points. It is faster to enter one pline instead of many lines. This was extended with splines. A spline is a curved line that goes smoothly through a number of points (see drafting spline p. 9). The problem with mathematically produced splines is that often loops occur which is not what we want (fig. 13). Therefore, a new line was introduced called basis spline (B-spline). Its mathematical definition is a number of smooth curves that are added. A B-spline goes through a begin point and an end point but it does not go through the intermediate points (fig. 13). The intermediate points are called control points. We can move these points on the computer screen and the B-spline follows smoothly. It acts as attached to the control points by invisible rubber bands.

NURBS
NURBS stands for Non Uniform Rational B-Spline. It is a mathematical way of defining surfaces. It was developed in the sixties to model car bodies (fig. 14). NURBS surfaces are generalizations of B-splines (p. 9). A NURBS surface is determined by an order, weighted control points and knots. We can see it as a black box in which the just mentioned data is input and any 3D point of the surface is output. Our software uses this black box to plot a surface. NURBSes are always deformed squares. They are organised in square patches which can be deformed and attached to each other (fig. 15). We can change the shape by moving the control points on the computer screen.

[4] The first version of AutoCAD was released in 1982. It run on the IBM Personal Computer which was developed in 1981. The IBM Personal Computer was one of the first computers that ordinary people could afford. It was priced at $1565 [Wikipedia]. Assuming 2.5% inflation, to date it would cost $1565 \times 1.025^{(2023-1981)} = \$4415$.

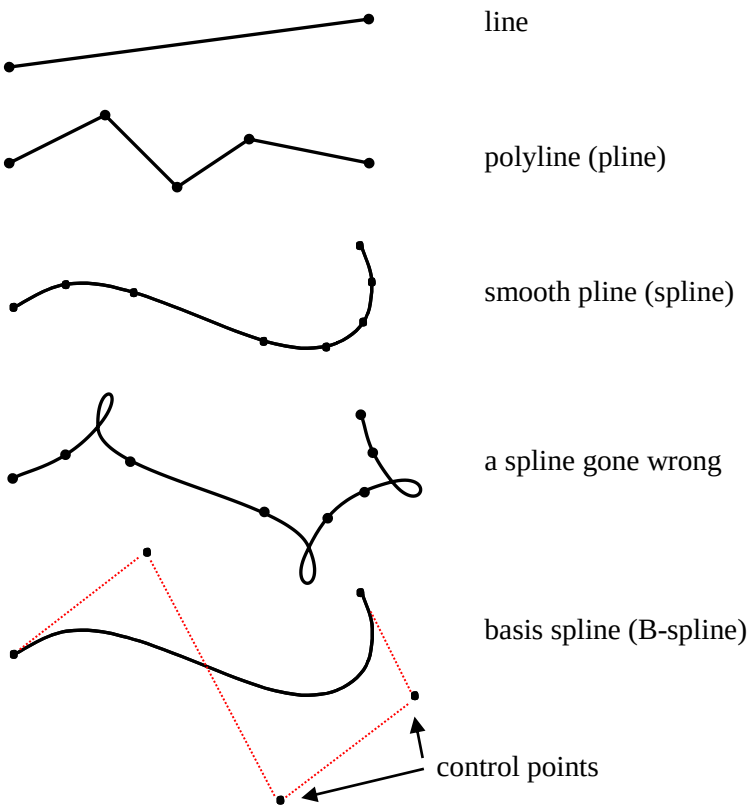

Figure 13. Types of line



Figure 14. Chrysler 1960 [www.carnut.com]

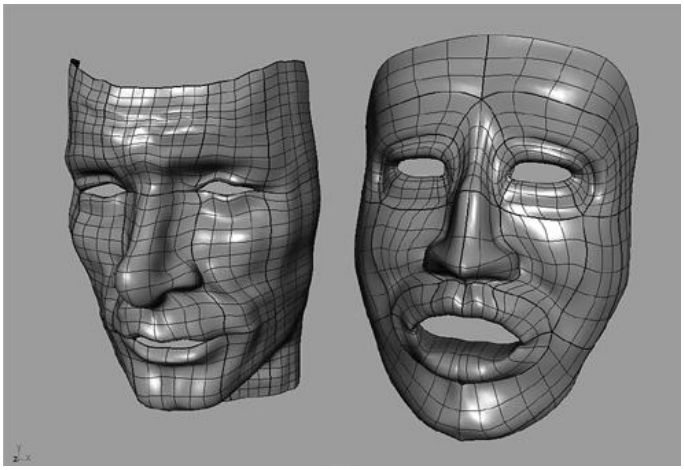

Figure 15. Faces made of NURBSes. The thin lines are NURBS edges. The thick lines are patch edges. Control points are not shown. [www.maya.com]

Continuity
Surfaces can be connected with different levels of continuity: C_0 continuity means that the surfaces are just connected, C_1 continuity means that also the tangents of the two surfaces at the connection line are the same. It can be recognized as not kinky. C_2 continuity means that also the curvatures of the two surfaces are the same at the connection line. It can be visually recognized as very smooth.
Higher orders of continuity are also possible. C_3 continuity means that also the third derivative of the surface shape in the direction perpendicular to the connection line is the same at either side of the connection line. If a shell has less than C_2 continuity then stress concentrations will occur at the connection line. Such a stress concentration is called edge disturbance (p. 14, 72).

Exercise: What is the level of continuity of the shape of a drafting spline? (p. 9)

Zebra analysis
People look fat in a convex mirror and slim in a concave mirror. Apparently, the curvature determines the width that we see. A neon light ceiling consists of parallel lines of neon light tubes. This light reflects of a car that is parked underneath. The car surface curvature determines the width of the tubes that we see. Car designers use this to inspect the continuity of a prototype car body. Any abrupt change in curvature will show as an abrupt change in tube width. The computer equivalent of this inspection is called *zebra analysis*.

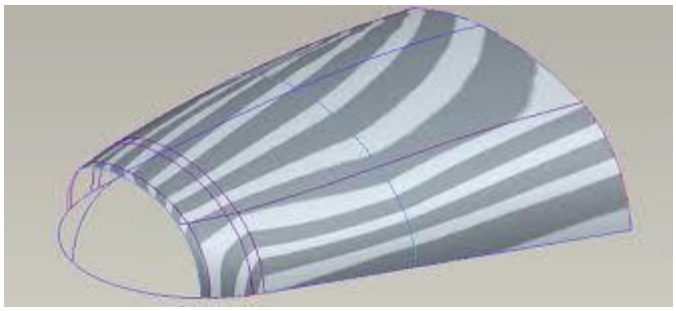
Figure 16. Simulated reflection of neon light tubes […]

Finite element mesh
A complicated shell structure needs to be analysed using a finite element program (ANSYS, DIANA, Mark, etc.). To this end the shell surface needs to be subdivided in shell finite elements (p. 82) which are triangular or quadrilateral. This subdivision is called finite element mesh. CAD software (Maya, Rhinoceros, etc) can transform a NURBS (p. 9) mesh into a finite element mesh and export it to a file. The finite element program can read this file.
The size of the finite elements is very important for the accuracy of the analyses. We need to carefully determine and adjust the element size in each part of a shell.

NURBS finite elements
Scientists are developing finite elements that look like NURBSes (p. 9). The advantage of these elements is that there is no need to transform CAD model meshes into finite element meshes (p. 11). Both meshes are the same. In the future this can save us a lot of time. However, it seems that this development is overtaken by another development. CAD programs start using polygon meshes (p. 11) instead of NURBSes. These meshes may be used directly in finite element analyses.

Polygon meshes
The problem with NURBSes (p. 9) is that they have so many control points. For example, if we have modeled Mickey Mouse and we want to make him smile we need to move more than 20 control points. This is especially impractical for animations. Therefore, CAD programs

also provide polygon meshes (fig. 17). Every part of a polygon mesh consist of a polygon, for example, a triangle, a square, a pentagon. The advantage is that we can work quickly with a rough polygon model. The mesh is automatically smoothened during rendering to any level of continuity (p. 11).

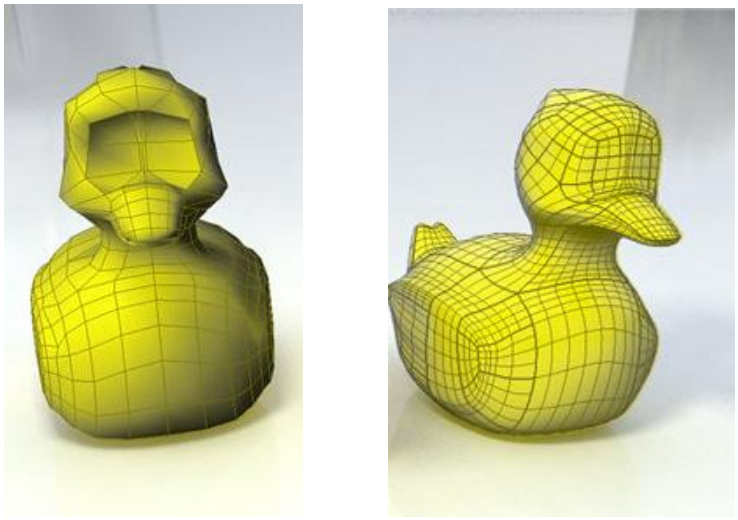

Figure 17. Polygon mesh and NURBS mesh […]

Section forces and moments

Consider a small part of a shell structure and cut away the rest. If there were stresses in the cuts they are replaced by forces per unit length [N/m] and moments per unit length [Nm/m] (fig. 18). The membrane forces are n_{xx}, n_{yy} and $\frac{1}{2}(n_{xy}+n_{yx})$. The first two are the normal forces and the third is the in-plane shear force. The moments are m_{xx}, m_{yy} and m_{xy}. The first two are the bending moments and the third is the torsion moment. The out-of plane shear forces are v_x and v_y.

In a tent structure only membrane forces occur. Therefore, $m_{xx}=m_{yy}=m_{xy}=v_x=v_y=0$. In addition, the tent fabric can only be tensioned. Therefore, $n_1 \geq 0,\ n_2 \geq 0$, where n_1 and n_2 are the principal membrane forces (p. 98).

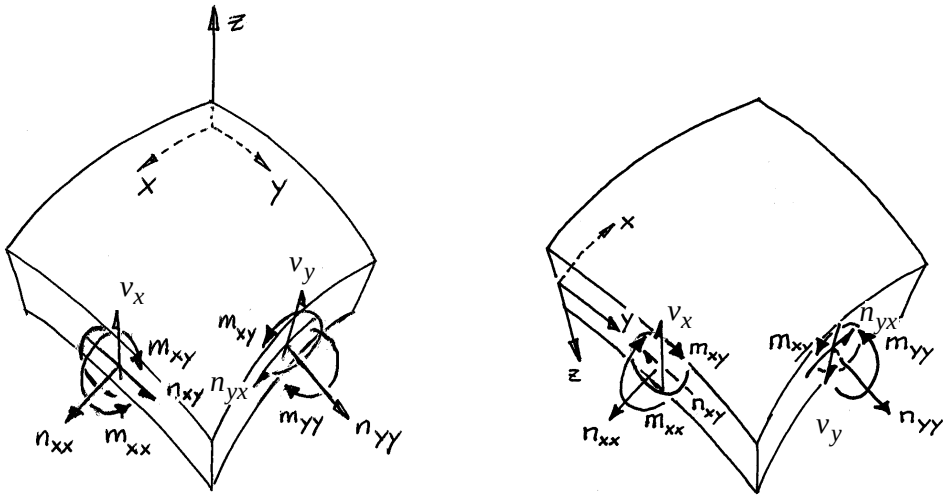

Figure 18. Positive section forces and moments in shell parts

Definition of membrane forces, moments and shear forces

In thin shells the membrane forces, the moments and the shear forces are defined in the same way as in plates.

$$n_{xx} = \int_{-\frac{1}{2}t}^{\frac{1}{2}t} \sigma_{xx}\,dz \qquad n_{yy} = \int_{-\frac{1}{2}t}^{\frac{1}{2}t} \sigma_{yy}\,dz \qquad \tfrac{1}{2}(n_{xy} + n_{yx}) = \int_{-\frac{1}{2}t}^{\frac{1}{2}t} \sigma_{xy}\,dz$$

$$m_{xx} = \int_{-\frac{1}{2}t}^{\frac{1}{2}t} \sigma_{xx}\,z\,dz \qquad m_{yy} = \int_{-\frac{1}{2}t}^{\frac{1}{2}t} \sigma_{yy}\,z\,dz \qquad m_{xy} = \int_{-\frac{1}{2}t}^{\frac{1}{2}t} \sigma_{xy}\,z\,dz$$

$$v_x = \int_{-\frac{1}{2}t}^{\frac{1}{2}t} \sigma_{xz}\,dz \qquad v_y = \int_{-\frac{1}{2}t}^{\frac{1}{2}t} \sigma_{yz}\,dz$$

For thick shells the definitions are somewhat different (appendix p. 203).

Thickness

A shell has a small thickness t compared to other dimensions such as width, span and radius a. The following classification is used.

- *Very thick shell* ($a / t < 5$): needs to be modelled three-dimensionally; structurally it is not a shell
- *Thick shell* ($5 < a / t < 30$): membrane forces, out of plane moments and out of plane shear forces occur; all associated deformations need to be included in modelling its structural behaviour
- *Thin shell* ($30 < a / t < 4000$): membrane forces and out of plane bending moments occur; out of plane shear forces occur, however, shear deformation is negligible; bending stresses vary linearly over the shell thickness
- *Membrane* ($4000 < a / t$): membrane forces carry all loading; out of plane bending moments and compressive forces are negligible; for example a tent

Shell force flow

Brick or stone arches are thick (p. 13) because the pressure line (p. 6) needs to go through the middle third (p. 7) for all load combinations. Shell structures are often thin. This is possible due to *hoop forces* (fig. 19). The hoop forces push and pull the pressure line into the middle third for any distributed loading. In other words, a well-designed shell does not need moments to carry load.

In the bottom of a spherical dome the hoop forces are tension (for quantification see p. 38). If this dome is made of brick or stone it needs horizontal steel reinforcement, but not much.

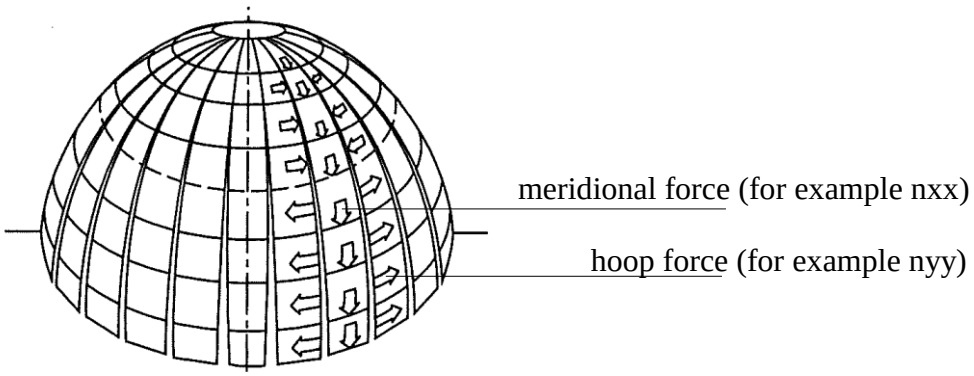

Figure 19. Forces in a spherical dome due to self-weight

Exercise: The designer of the *Hagia Sophia* found an even better solution for the tension hoop forces: He put windows at the locations where tension would have occurred. Which part of the Hagia Sophia dome can be classified as a shell and which part as arches?

Pantheon

The pantheon has been built in the year 126 AD in Rome as a Roman temple (fig. 20). Since the year 609 it is a Catholic church. The concrete of the dome top is made of light weight aggregate called pumice (fig. 21). The hole in the roof is called oculus. The name of the designer is unknown. The construction method is unknown. It has been well maintained through the centuries, which shows that people have always considered it a very special structure. You should go there one day and see it with your own eyes.

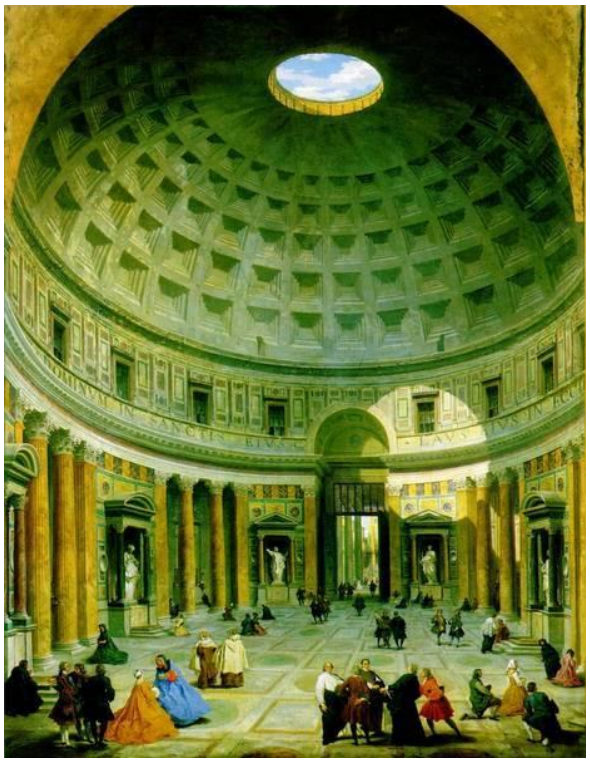

Figure 20. Pantheon painting by Panini in 1734 [National Gallery of Art, Washington D.C.]

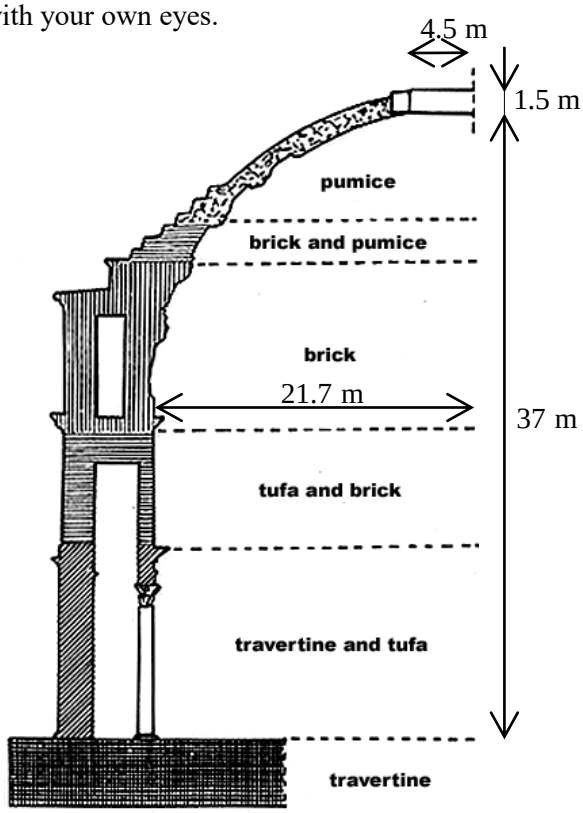

Figure 21. Pantheon cross-section [engineeringrome.org]

Edge disturbance

In a well-designed shell with distributed loads and roller supports the moments are very small (see shell force flow p. 13). However, rollers are expensive and do not resist wind, therefore, shell edges are often fixed. This causes a phenomena typical for thin shell structures: the *edge disturbance*.

Let's explain it by an experiment of thought. A dome loaded is by self-weight and supported by rollers. The membrane forces change the shape of the dome (fig. 22). This deformation is small – much smaller than the deformation of a similar size plate, truss or frame structure – but it does occur. Subsequently, we remove the rollers, push the dome edge back and fix it to the foundation (fig 23). In the process we have curved the shell wall. This curving occurs over a small width because the thin shell wall has little bending stiffness.

From the curvature we deduce that moments occur. The moment is large in the edge. The moment moves into the shell like a wave that dampens quickly. Of course, *wave* is not the right word because this wave does not move. It is called *edge disturbance*. It occurs where

ever a shell edge is fixed or pinned to something solid. (see also generalised edge disturbance p. 72)

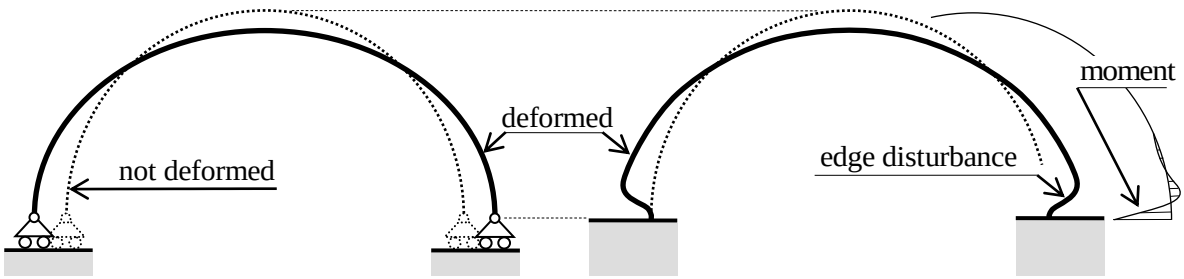

Figure 22. Dome with roller support

Figure 23. Dome with fixed support

Compatibility moment
The moments in a well-designed thin shell do not carry load. All load in the shell is carried by the membrane forces (see shell force flow p. 13). The shell moment is caused by the deformation necessary for the parts to stay connected (see edge disturbance p. 14). Such a moment is called *compatibility moment*.

Comparison of an arch and a dome
Figure 24 shows two moment distributions. On the left-hand side is shown an arch shaped as a horse shoe fixed at the foundation and loaded by self-weight. On the right-hand side is shown a cross-section of a spherical dome also fixed at the foundation and also loaded by self-weight. (This dome could protect an airport radar from rain and wind.) The left hand distribution has been obtained by solving the differential equation. The right hand distribution has been obtained by linear elastic finite element analysis. The left and right moment distributions are in the same directions and can be compared.

We observe that the arch has moments everywhere and the dome has moments in its edge only. The shell moment demonstrates the shell force flow (p. 13) and the edge disturbance (p. 14). The arch and the shell behave very differently.

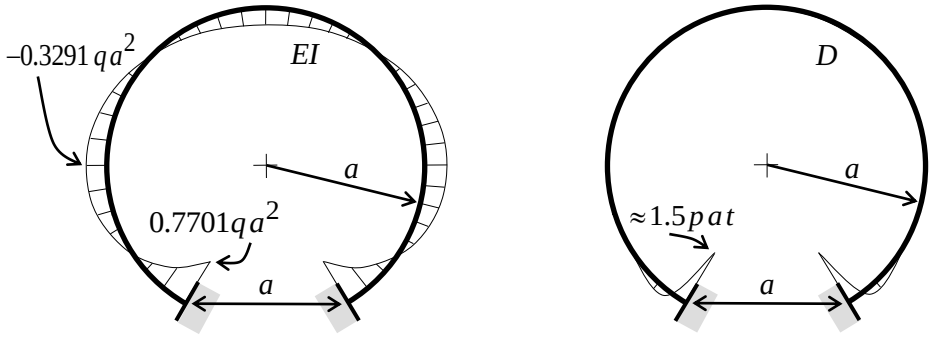

Figure 24. Linear elastic moment distributions due to self-weight in (left) a circular arch and (right) a spherical dome. Symbol a is the radius, t is the thickness, q [N/m] and p [N/m²] are self-weight. The dome result is computed for a = 20 m, t = 0.05 m, E = 3·10¹⁰ N/m², ν = 0, p = 1500 N/m². The plotted dome moment is in the same direction as that of the arch.

Exercise: If you plot the arch moment in figure 24 upside down you see the pressure line (p. 6). Can you explain this?

Plastic deformation in shell edges
Figure 24 left shows the equation of the arch peak moment. The thickness t does not occur in this equation, while it does occur in the equation of the dome moment. When we double the thickness, self-weight will double, the arch moment will double and the dome moment will increase by a factor four. When we divide moment by section modulus we obtain stress. Doubling the thickness halves the arch bending stress but the dome bending stress stays the same.

For shell design this means that we often have to accept plastic deformation in supported shell edges. Steel edges yield. Reinforced concrete edges crack. Extra attention is required for fatigue and durability of shell edges.

Exercise: Consider live load instead of self-weight. What happens if we make a dome thicker? Do the stresses become larger, smaller or do they stay the same? Compare this to a plate.

Form finding
A tent needs to be in tension everywhere otherwise the fabric would wrinkle. Therefore, the first step in tent design is to determine a shape that satisfies this condition. This is called form finding. The designer specifies the support points and prestressing and the computer determines a tent shape that is in equilibrium everywhere.

Some architects would like to reverse this procedure and directly specify the shape while the computer would find the required prestress. In theory this is possible, however, it is not supported by any software because the optimisation to find a suitable prestressing is very time consuming [4].

In contrast, shells do not need form finding. They can be designed as any frame structure: 1) choose shape, thickness, supports and loading, 2) compute the stresses, 3) check the stresses and improve the design. Repeat this until satisfied.

Fully stressed dome
Consider a dome loaded by self-weight only. The shape and thickness are such that everywhere in the dome the maximum compressive stress occurs (fig. 25). The compressive stress is both in the meridional direction and in the hoop direction (p. 13). This dome is called a fully stressed dome because everywhere the material is loaded to its full capacity.

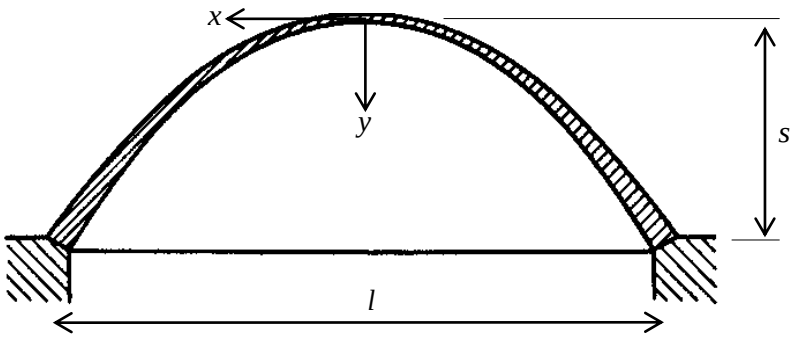

Figure 25. Cross-section of a fully stressed dome [5] (The proportions are exaggerated)

The shape of a fully stressed dome cannot be described by any mathematical function [5]. The following program can be used for calculating the dome shape. The thickness of a fully stressed dome is undetermined. (Any extra thickness gives both more load and more strength which compensate each other.) The program starts at the dome top with a specified thickness and stress. For every step in x a value y and a new thickness are determined.

```
t:=200:        # mm     top thickness
f:=4:          # N/mm2  compressive stress
rho:=2350e-9:  # kg/mm3 specific mass
g:=9.8:        # m/s2   gravitational acceleration
dx:=1:         # mm     horizontal step size
alpha:=0.1:    # rad    horizontal angle, has no influence on the results

x:=0: y:=0: V:=t*1/2*dx/2*alpha*dx/2*rho*g: H:=f*t*dx/2*alpha:
for i from 1 to 200000 do
  N:=sqrt(V^2+H^2):
  t:=N/(f*alpha*(x+dx/2)):
  dy:=V/H*dx:
  ds:=sqrt(dx^2+dy^2):
  x:=x+dx:
  y:=y+dy:
  V:=V+t*ds*alpha*x*rho*g:
  H:=H+f*t*ds*alpha:
end do:
```

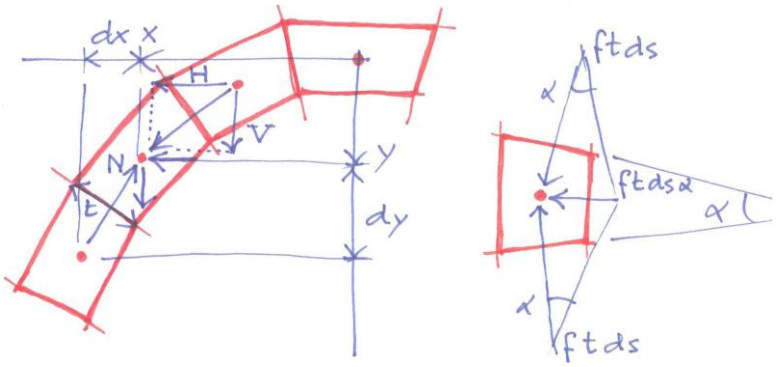

Figure 26. Derivation of the fully stressed dome program

Approximation of the fully stressed dome
For realistic material values the computed shape of a fully stressed dome (p. 16) can be approximated accurately by the formula

$$y = \frac{\rho g x^2}{4\sigma},$$

where ρ is the mass density, g is the gravitational acceleration and σ is the stress.
For example, a fully stressed masonry dome with a compressive strength of 4 N/mm² and a span of 100 m has a sagitta (p. 1) of

$$y = \frac{2000 \times 10 \times 50^2}{4 \times 4 \cdot 10^6} = 3.13 \text{ m}$$

Note that this is a very shallow dome. The above program also shows that the dome thickness is everywhere almost the same.

Buckling of the fully stressed dome
Buckling of a dome occurs at a stress of $0.1Et/a$, therefore, $\sigma \le 0.1Et/a$ (see buckling p. 140). The radius of curvature of the fully stressed dome top is (see line curvature p. 20)

$$a = \frac{1}{\frac{d^2y}{dx^2}} = \frac{2\sigma}{\rho g}$$

Substitution of a in the buckling stress equation gives a condition for the dome thickness

$$t \geq \frac{20\sigma^2}{\rho g E}.$$

For example, the fully stressed masonry dome with Young's modulus 10000 N/mm² needs a thickness

$$t \geq \frac{20\times(4\cdot 10^6)^2}{2000\times 10\times 10000\cdot 10^6} = 1.6 \text{ m}$$

$$\frac{a}{t} = \frac{E}{10\sigma} = \frac{10000}{10\times 4} = 250$$

Optimal dome

Suppose we want to build a dome with a span l that carries its weight with as little material as possible. We call this an *optimal dome*. An optimal dome is not a fully stressed dome (p. 16). The cause is that a larger sagitta (p. 1) will give smaller stresses and a much smaller thickness, which results in less material.

The sagitta of an optimal dome is about 30% of its span. To be exact, a spherical cap of constant thickness has the optimal ratio sagitta to span of $\sqrt{3}$ to 6 (fig. 27) (derivation in appendix 2). [5]

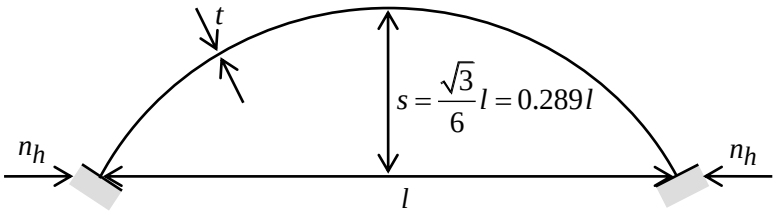

Figure 27. Proportions of an optimal spherical dome

The thickness of the spherical optimal dome is

$$t = \frac{20}{9}\frac{\rho g l^2}{E}$$

Applied to the masonry dome example above we find,

$$t = \frac{20}{9}\frac{2000\times 10\times 100^2}{10000\cdot 10^6} = 0.044 \text{ m}$$

[5] Kris Riemens showed in his bachelor project at Delft University that other shapes can be more optimal than the spherical cap [6]. In addition, a varying thickness can reduce the amount of material by 15% compared to a constant thickness dome. Therefore, the exact optimal dome has not been found as yet.

This is much thinner than the fully stressed dome. A 44 mm thick masonry dome with a span of 100 m has never been build. We need to keep in mind that this dome would just carry its self-weight. Nonetheless, the equations show that great shell structures are possible.

$$a = \tfrac{1}{2} s + \tfrac{1}{8} \frac{l^2}{s} = \frac{0.3 \times 100}{2} + \frac{100^2}{8 \times 0.3 \times 100} = 57 \text{ m} \qquad \frac{a}{t} = \frac{57}{0.044} = 1295$$

Exercise: Consider a glass dome covering a city. What thickness is needed? What thickness is needed on the Moon? Can this Moon dome be pressurised with Earth atmosphere?

Global coordinate system
Shell shapes can be described in a global Cartesian coordinate system $\bar{x}$, $\bar{y}$, $\bar{z}$. For example half a sphere is described by

$$\bar{z} = \sqrt{a^2 - \bar{x}^2 - \bar{y}^2}, \quad -\sqrt{a^2 - \bar{x}^2} \le \bar{y} \le \sqrt{a^2 - \bar{x}^2}, \quad -a \le \bar{x} \le a .$$

Local coordinate system
Consider a point on a shell surface. We introduce a positive Cartesian coordinate system in this point (fig. 28). The *z* direction is perpendicular to the surface. The *x* and *y* direction are tangent to the surface. The right-hand-rule is used to determine which axis is *x* and which is *y* (fig. 29).

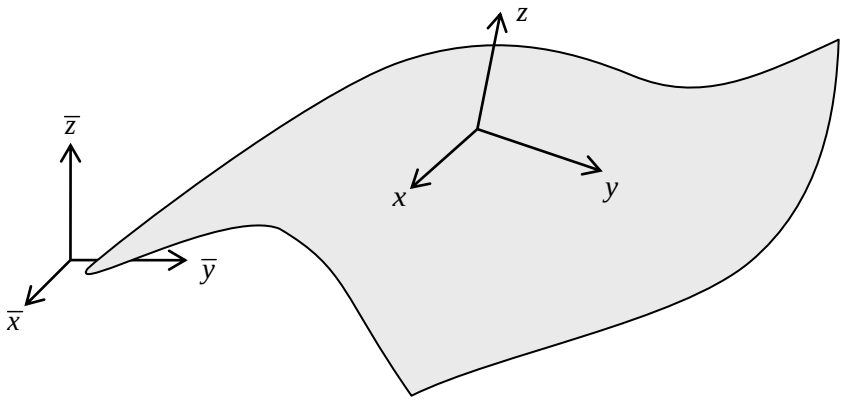

Figure 28. Global and local coordinate system

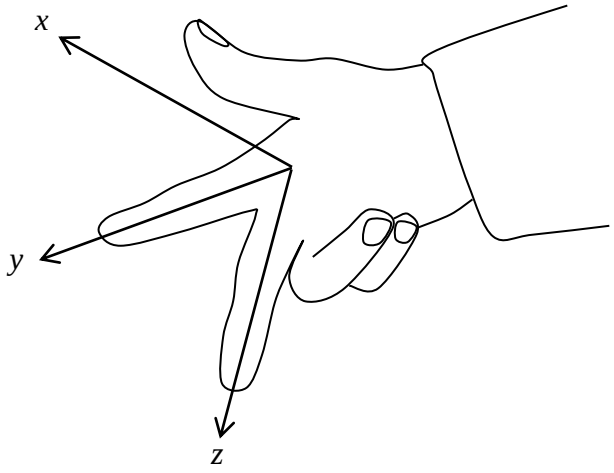

Figure 29. Right-hand-rule for remembering the Cartesian coordinate system

Line curvature
Consider a curved line on a flat sheet of paper (fig. 30). At any point of the curve there is a best approximating circle that touches the curve. The middle point of this circle is constructed by drawing two lines perpendicular to the curve at either side of the considered point. The reciprocal of the circle radius *a* is the curvature *k* at this point of the curve. The circle may lie above the curve or below the curve. We can choose to give the curvature a positive sign if the circle lies above the curve and negative sign if the circle lies below the curve. This is known as *signed curvature*. The Latin name of a best approximating circle is *circulus osculans*, which can be translated as *kissing circle*.

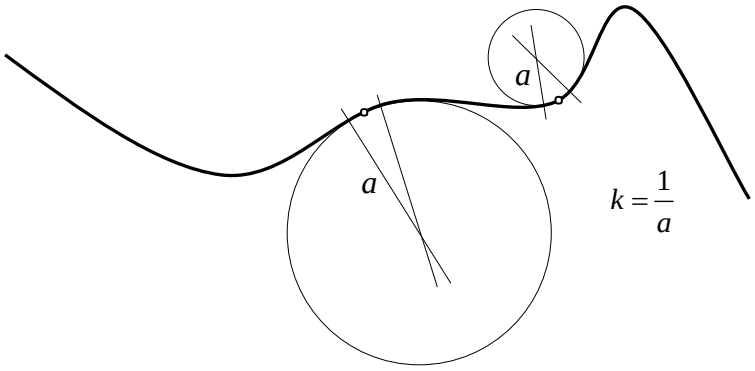

Figure 30. Curvature of a line

Exercise: Choose a local coordinate system *x*, *y* on a curve and show that $k = \pm \frac{d^2 y}{dx^2}$

Surface curvature
Curvature is also defined for surfaces. We start with a point on the surface and draw in this point a vector *z* that is normal to the surface (fig. 31). Subsequently, we draw any plane through this normal vector. This normal plane intersects the surface in a curved line. The curvature of this line is referred to as normal section curvature *k*. If the circle lies at the positive side of the *z* axis the normal section curvature is positive. If the circle lies at the negative side of the *z* axis the normal section curvature is negative. The direction of the *z* axis can be chosen freely (pointing inward or outward).

The *z* axis is part of a local coordinate system (p. 19). When the normal plane includes the *x* direction vector the curvature is k_{xx}. When the plane includes the *y* direction vector the curvature is k_{yy}. These curvatures can be calculated by

$$k_{xx} = \frac{\partial^2 z}{\partial x^2}, \qquad k_{yy} = \frac{\partial^2 z}{\partial y^2}.$$

The twist of the surface k_{xy} is defined as

$$k_{xy} = \frac{\partial^2 z}{\partial x \partial y}.$$

These formulas are valid for the local coordinate system. In the global coordinate system (p. 19) the formulas for the curvature are

$$k_{\overline{xx}} = \frac{\frac{\partial^2 \overline{z}}{\partial \overline{x}^2}}{(1+\frac{\partial \overline{z}}{\partial \overline{x}}^2)^{\frac{3}{2}}}, \qquad k_{\overline{yy}} = \frac{\frac{\partial^2 \overline{z}}{\partial \overline{y}^2}}{(1+\frac{\partial \overline{z}}{\partial \overline{y}}^2)^{\frac{3}{2}}}.$$

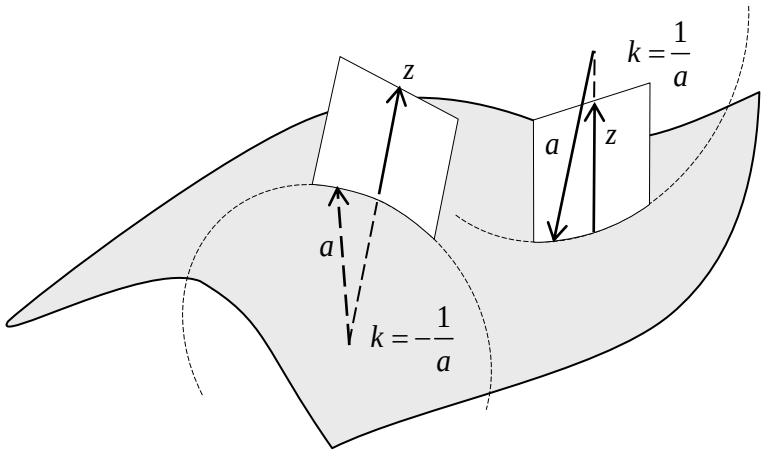

Figure 31. Normal section curvature

Note that these curvatures are not the same as the curvatures of the deformation of a flat plate. The latter curvatures are defined as

$$\kappa_{xx} = -\frac{\partial^2 w}{\partial x^2}, \qquad \kappa_{yy} = -\frac{\partial^2 w}{\partial y^2}, \qquad \rho_{xy} = -2\frac{\partial^2 w}{\partial x \partial y},$$

where *w* is the deflection perpendicular to the plate.

Paraboloid
A surface can be approximated around a point on the surface by

$$z = \tfrac{1}{2} k_{xx} x^2 + k_{xy} xy + \tfrac{1}{2} k_{yy} y^2.$$

Exercise: Check this approximation by substitution in the definitions of curvature and twist.

The above function is called paraboloid. If the principal curvatures (p. 22) have opposite signs it is a hyperbolical paraboloid (hypar). If the principal curvatures have the same sign it is an elliptical paraboloid (elpar). If the principal curvatures are the same, it is a circular paraboloid (fig. 32).

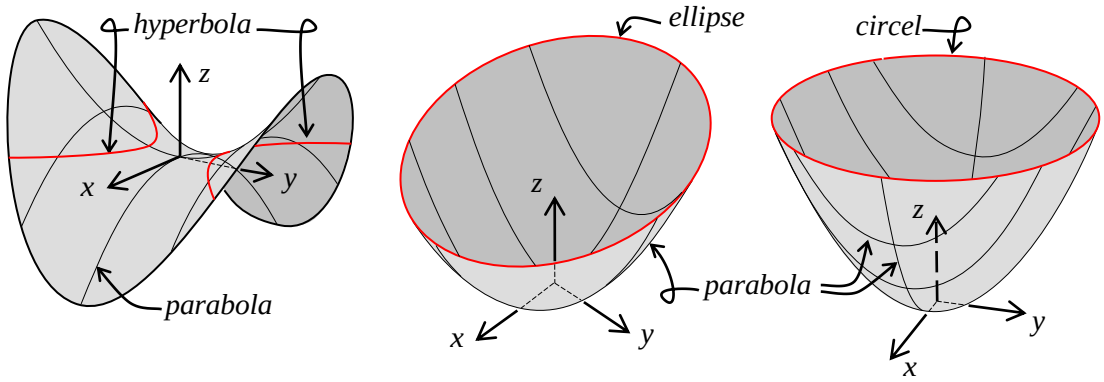

Hyperbolical paraboloid (hypar) *Elliptical paraboloid (elpar)* *Circular paraboloid*
Figure 32. Types of paraboloid

Principal curvatures
In a point of a surface many normal planes are possible. If we consider all of them and compute the normal section curvatures then there will be a minimum value k_2 and a maximum value k_1. These minimum and maximum values are the *principal curvatures* at this point.

$$k_1 = \tfrac{1}{2}(k_{xx} + k_{yy}) + \sqrt{\tfrac{1}{4}\left(k_{xx} - k_{yy}\right)^2 + k_{xy}^2}$$

$$k_2 = \tfrac{1}{2}(k_{xx} + k_{yy}) - \sqrt{\tfrac{1}{4}\left(k_{xx} - k_{yy}\right)^2 + k_{xy}^2}$$

The directions in which the minimum and maximum occur are perpendicular. In fact, curvature is a second order tensor (p. 97) and can be plotted using Mohr's circle (proof in appendix p. 196).

Savill building
Savill garden is close to Windsor castle in England. Its visitors centre has a *timber grid shell* roof (fig. 33). The roof was built in 2005 using timber from the forest of Winsor castle. The roof dimensions are; length 98 m, width 24 m, height 10 m. The structural thickness is 300 mm.

$$a = \tfrac{1}{2}s + \tfrac{1}{8}\frac{l^2}{s} = \frac{10}{2} + \frac{24^2}{8 \times 10} = 12.2 \qquad \frac{a}{t} = \frac{12.2}{0.3} = 41$$

The laths are made of larch with a strength of 24 N/mm^2. The roof is closed by two layers of plywood panels each 12 mm thick (fig. 34). This plywood is part of the load carrying system. The weather proofing consist of aluminium plates. On top of this, a cladding of oak has been applied. The roof has a steel tubular edge beam. Next to the edge beam the laths are strengthened by laminated veneer lumber (LVL), which is bolted to the edge beam (fig. 33). The roof is expected to deflect 200 mm under extreme snow and wind loading [8].

Project manager:	Ridge & Partners LLP
Architect:	Glenn Howells Architects
Structural engineers:	Engineers Haskins Robinson Waters
	Buro Happold
Main contractor:	William Verry LLP
Carpenters:	The Green Oak Carpentry Co Ltd
Falsework supplier:	PERI
Owner:	Crown Estate
Costs:	£ 5.3 million

The building won several awards including one from the Institution of Structural Engineers in the United Kingdom. Before construction of Savill building the garden had approximately 80 000 visitors a year. After construction the garden attracts approximately 400 000 visitors a year.[6]





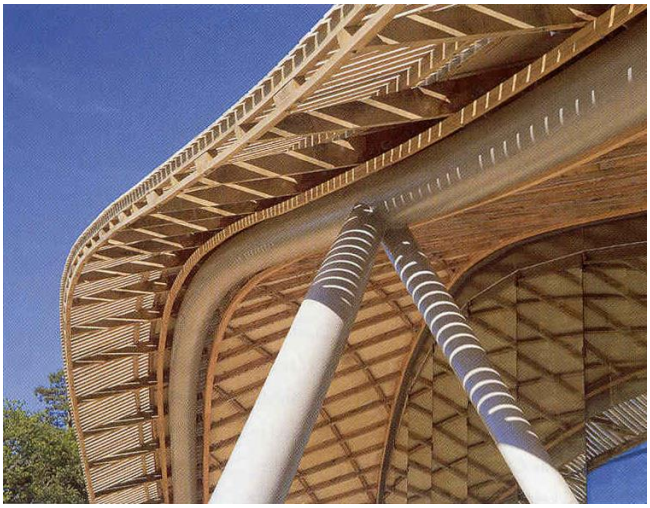

Figure 33. Savill building [ ]

Gaussian curvature

The Gaussian[7] curvature of a surface in a point is the product of the principal curvatures in this point $k_G = k_1 k_2$. It can be shown that also $k_G = k_{xx} k_{yy} - k_{xy}^2$. The Gaussian curvature is independent of how we choose the directions of the local coordinate system (p. 19). A positive value means the surface is bowl-like (fig. 35). A negative value means the surface is saddle-like. A zero value means the surface is flat in at least one direction (plates, cylinders, and cones have zero Gaussian curvature).

[6] Statement by deputy ranger P. Everett in a Youtube movie of 22 September 2007: http://www.youtube.com/watch?v=3xNdVDAoI5U

[7] Carl Gauß (1777-1855) was director of the observatory of Göttingen, Germany … and a brilliant mathematician. The German letter "ß" is pronounced "s".

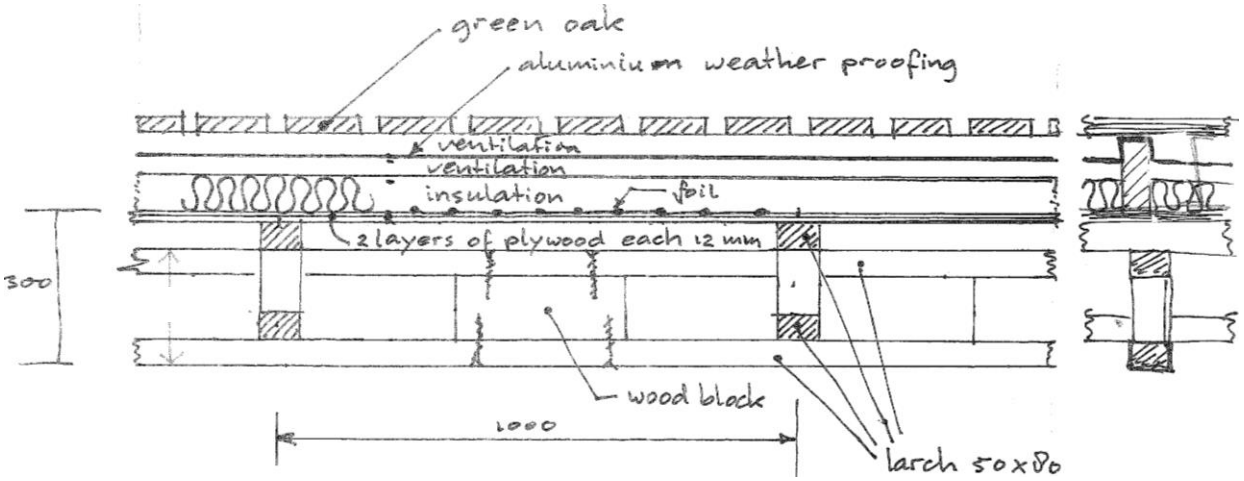

Figure 34. Cross-section of the Savill building roof

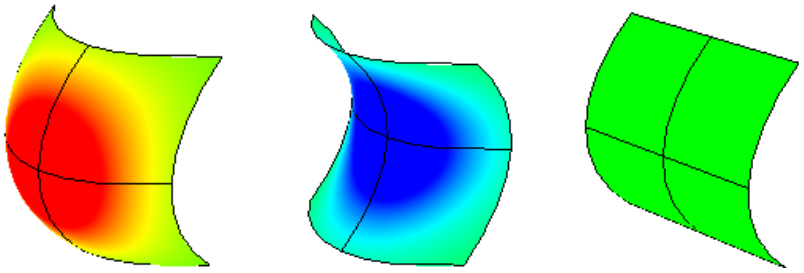

positive *negative* *zero*

Figure 35. Gaussian curvature (contour plot)

A surface having everywhere a positive Gaussian curvature is *synclastic*. A surface having everywhere a negative Gaussian curvature is *anticlastic*. Tents need to be anticlastic and pre-tensioned in order not to wrinkle. Some surfaces have a Gaussian curvature that is everywhere the same. Examples are a plane, a cylinder, a cone, a sphere, and a tractricoid (p. 26).

The Gaussian curvature is important for the deflection of a shell due to a point load. A large Gaussian curvature (in absolute value) gives a small deflection. The Gaussian curvature is also important for the membrane stresses in a shell. Membrane stresses occur when the Gaussian curvature changes during loading (see theorema egregium p. 113).

Mean curvature

The mean curvature of a surface in a point is half the sum of the principal curvatures in this point $k_m = \frac{1}{2}(k_1 + k_2)$. It can be shown that also $k_m = \frac{1}{2}(k_{xx} + k_{yy})$. The mean curvature is independent of how we choose the local coordinate system (p. 19) except for the direction of the *z* axis. If the direction of the *z* axis is changed from outward to inward then the sign of the mean curvature changes too. For this reason CAD programs often plot the absolute value of the mean curvature.

An example of a surface with zero mean curvature is a soap film (p. 46). In a soap film there is tension, which is the same in all directions and all positions, which makes it fully stressed (p. 16). This property is used in form finding (p. 16) of tent structures.

Exercise: A shell has a shape imperfection with magnitude *d*, length *l* and width *l*. Derive the following relations between the perfect and imperfect (′) curvatures. Assume that *d*, *s* □ *l*.

$$k_1' = k_1 - 8\frac{d}{l^2}$$

$$k_2' = k_2 - 8\frac{d}{l^2}$$

$$k_m' = k_m - 8\frac{d}{l^2}$$

$$k_G' = k_G - 16\frac{d}{l^2}k_m$$

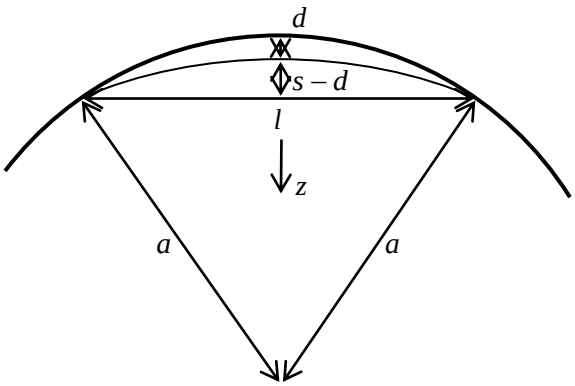

Note that the mean curvature is important for the change in the Gaussian curvature.
For example, adding a small imperfection to a shell that has zero mean curvature leads to no change in the Gaussian curvature.

Orthogonal parameterisation

A sphere can be described by $\bar{x}^2 + \bar{y}^2 + \bar{z}^2 = a^2$. Another way of describing a sphere is

$$\bar{x} = a\sin u\cos v$$
$$\bar{y} = a\sin u\sin v$$
$$\bar{z} = a\cos u \qquad 0 \le u \le \pi \qquad 0 < v \le 2\pi$$

This is called a *parameterisation*. The parameters are *u* and *v*. There are many ways to parameterise a sphere and this is just one of them. When *u* has some constant value and *v* is varied then a line is drawn on the surface (fig. 36). The other way around, when *v* has some constant value and *u* is varied then another line is drawn on the surface. In shell analysis we choose the lines *u* = constant and the lines *v* = constant perpendicular to each other. This is called an *orthogonal* parameterisation.

Other surfaces can be parameterised too, for example catenoids (p. 26) and tractricoids (p. 26). Unfortunately, for some surfaces an orthogonal parameterisation is not available, for example there is no orthogonal parameterisation available for a paraboloid (p. 21, 102, 129). It can be easily checked whether a parameterisation is orthogonal. In this case the following equation is true.

$$\frac{\partial\bar{x}}{\partial u}\frac{\partial\bar{x}}{\partial v} + \frac{\partial\bar{y}}{\partial u}\frac{\partial\bar{y}}{\partial v} + \frac{\partial\bar{z}}{\partial u}\frac{\partial\bar{z}}{\partial v} = 0$$

The proof is simple. If we change *u* a bit, then $\bar{x}$, $\bar{y}$ and $\bar{z}$ change a bit. These $\bar{x}$, $\bar{y}$, $\bar{z}$ bits form a small vector. If we change *v* a bit, another small vector is formed. These two vectors must be perpendicular, so their dot product must be zero. Q.E.D.

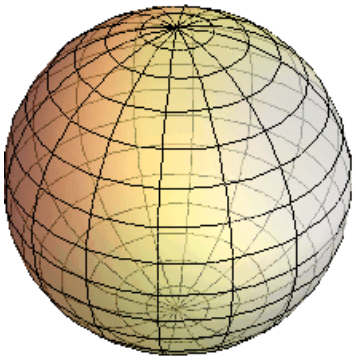

$$k_{xx} = \frac{-1}{a}$$
$$k_{yy} = \frac{-1}{a}$$
$$k_{xy} = 0$$
$$\alpha_x = a$$
$$\alpha_y = a \sin u$$

Figure 36. Parameter lines on a sphere. (α_x and α_y will be explained later.)

Exercise: I live at $u = 0.66029$, $v = 0.07995$. Where do you live?

Catenoid
A catenoid is formed by rotating a catenary (p. 5) around an axis (fig. 37). It can be parameterised by

$$\bar{x} = a u$$
$$\bar{y} = a \cosh u \sin v$$
$$\bar{z} = a \cosh u \cos v \qquad -\infty < u < \infty \qquad 0 \le v < 2\pi$$

The mean curvature (p. 24) is zero everywhere. The Gaussian curvature (p. 23) varies over the surface.

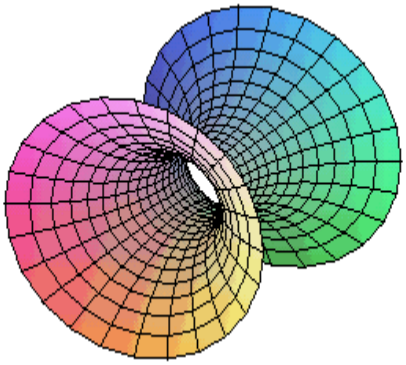

$$k_{xx} = \frac{1}{a \cosh^2 u}$$
$$k_{yy} = \frac{-1}{a \cosh^2 u}$$
$$k_{xy} = 0$$
$$\alpha_x = a \cosh u$$
$$\alpha_y = a \cosh u$$

Figure 37. Parameter lines on a catenoid

Tractricoid
A tractricoid (fig. 38) can be parameterised by

$$\bar{x} = a(\cos u + \ln \tan \frac{u}{2})$$
$$\bar{y} = a \sin u \sin v$$
$$\bar{z} = a \sin u \cos v \qquad 0 < u < \pi \qquad 0 \le v < 2\pi$$

Its volume is $\frac{4}{3}\pi a^3$ and its surface area is $4\pi a^2$, which are the same as those of a sphere. It has a constant negative Gaussian curvature $k_G = -a^{-2}$ (p. 23). Note that a sphere has a constant positive Gaussian curvature $k_G = a^{-2}$. The mean curvature (p. 24) varies over the surface of a tractricoid.

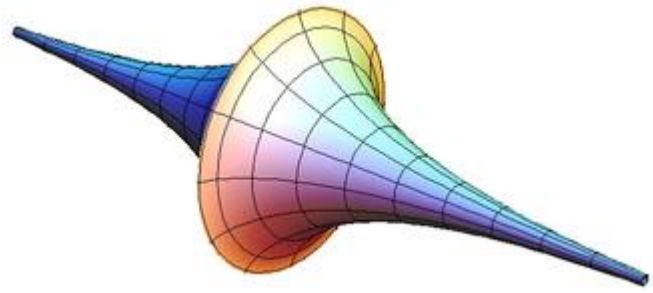

$$k_{xx} = \frac{|\tan u|}{a}$$

$$k_{yy} = \frac{-1}{a|\tan u|}$$

$$k_{xy} = 0$$

$$\alpha_x = \frac{a}{|\tan u|}$$

$$\alpha_y = a \sin u$$

Figure 38. Parameter lines on a tractricoid

Interpretation
We can interpret a parameterisation as the deformation of a rectangular sheet into a curved shell (fig. 39).

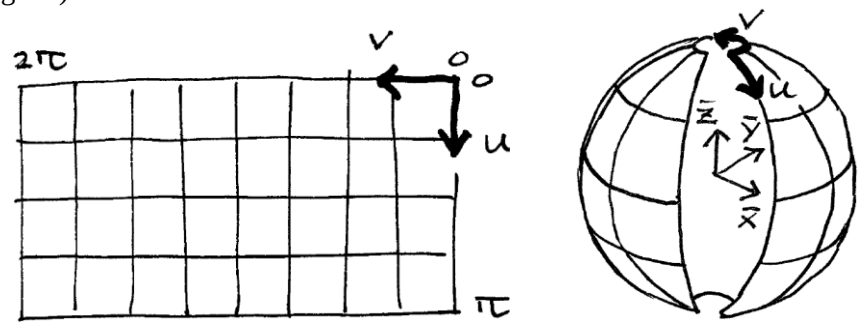

Figure 39. Deformation of a rectangular sheet

Exercise: In the above drawing, the local *z* axis is not shown. It can be deduced. In what direction is it? Into or out of the page? Inwards or outwards of the shell?

Sillogue water tower
Sillogue (pronounce silok) water tower stands close to Dublin airport in Ireland (fig. 40, 41, 42). Its shape is based on efficiency and aesthetics. (Water towers need a wide top diameter to obtain small fluctuations in water pressure when water is taken out and refilled.) It received the 2007 Irish Concrete Award for the best infrastructural project. It was honourably mentioned in the European Concrete Award 2008.

Height: 39 m
Top diameter: 38 m
Thickness: 786 mm
Steel formwork: 6300 m²
Reinforcing steel: 580 tonnes
Concrete volume: 4950 m³
External painting: 3700 m²
Capacity: 5000 m³
Engineers: McCarthy Hyder Consultants
Architects: Michael Collins and Associates
Contractor: John Cradock Ltd.
Formwork: Rund-Stahl-Bau, Austria



Figure 40. Sillogue water tower [Dublin City Council Image Gallery]

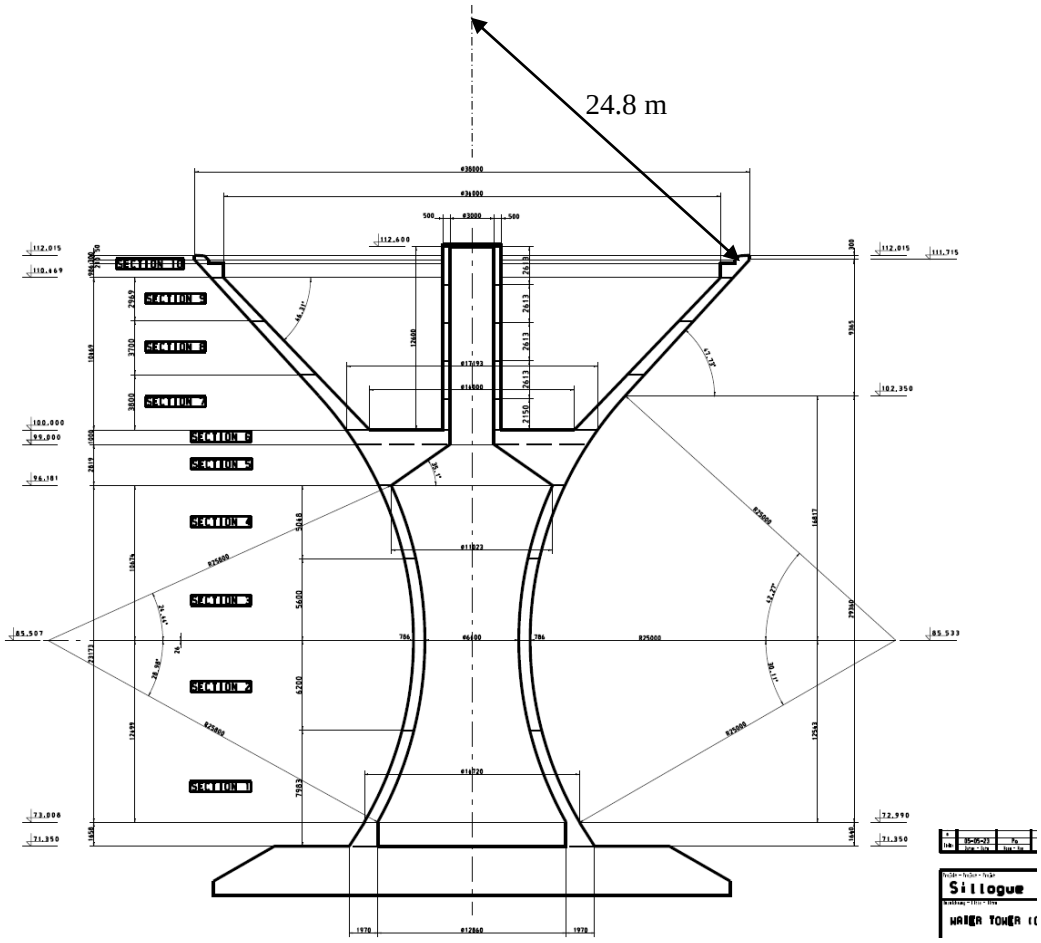

Figure 41. Cross-section of Sillogue water tower [Rund-Stahl-Bau]



Figure 42. Sillogue water tower under construction [Rund-Stahl-Bau]

To calculate the slenderness we measure the radius of curvature from the drawing. This is a line from the centre line of the tower perpendicular to the cone edge (fig. 41). The shell thickness is 0.786 m. Consequently, the slenderness is $a / t = 24.8 / 0.786 = 32$. This is a very small value in comparison to other shell structures (see table 1 p. 2). This suggests that the shell of Sillogue water tower could have been much thinner.

Exercise: Explain the radius of curvature of the water tower. Make a paper model or use your visual imagination. Note that the latter is a very powerful tool.

Differential geometry
Surfaces are studied in a branch of mathematics called *differential geometry*. The mathematicians study perfectly rigid surfaces and surfaces with no stiffness at all (topology) which is rather restrictive from our point of view. Nonetheless, several formulas in these notes are copied from books on differential geometry. Here are three useful formulas [7].

If an orthogonal parameterisation (p. 25) is available then the shell curvatures can be calculated with

$$k_{xx} = \left((\frac{\partial \bar{y}}{\partial u}\frac{\partial \bar{z}}{\partial v} - \frac{\partial \bar{z}}{\partial u}\frac{\partial \bar{y}}{\partial v})\frac{\partial^2 \bar{x}}{\partial u^2} + (\frac{\partial \bar{z}}{\partial u}\frac{\partial \bar{x}}{\partial v} - \frac{\partial \bar{x}}{\partial u}\frac{\partial \bar{z}}{\partial v})\frac{\partial^2 \bar{y}}{\partial u^2} + (\frac{\partial \bar{x}}{\partial u}\frac{\partial \bar{y}}{\partial v} - \frac{\partial \bar{y}}{\partial u}\frac{\partial \bar{x}}{\partial v})\frac{\partial^2 \bar{z}}{\partial u^2} \right) \frac{1}{\alpha_x^3 \alpha_y}$$

$$k_{yy} = \left((\frac{\partial \bar{y}}{\partial u}\frac{\partial \bar{z}}{\partial v} - \frac{\partial \bar{z}}{\partial u}\frac{\partial \bar{y}}{\partial v})\frac{\partial^2 \bar{x}}{\partial v^2} + (\frac{\partial \bar{z}}{\partial u}\frac{\partial \bar{x}}{\partial v} - \frac{\partial \bar{x}}{\partial u}\frac{\partial \bar{z}}{\partial v})\frac{\partial^2 \bar{y}}{\partial v^2} + (\frac{\partial \bar{x}}{\partial u}\frac{\partial \bar{y}}{\partial v} - \frac{\partial \bar{y}}{\partial u}\frac{\partial \bar{x}}{\partial v})\frac{\partial^2 \bar{z}}{\partial v^2} \right) \frac{1}{\alpha_x \alpha_y^3}$$

$$k_{xy} = \left((\frac{\partial \bar{y}}{\partial u}\frac{\partial \bar{z}}{\partial v} - \frac{\partial \bar{z}}{\partial u}\frac{\partial \bar{y}}{\partial v})\frac{\partial^2 \bar{x}}{\partial u \partial v} + (\frac{\partial \bar{z}}{\partial u}\frac{\partial \bar{x}}{\partial v} - \frac{\partial \bar{x}}{\partial u}\frac{\partial \bar{z}}{\partial v})\frac{\partial^2 \bar{y}}{\partial u \partial v} + (\frac{\partial \bar{x}}{\partial u}\frac{\partial \bar{y}}{\partial v} - \frac{\partial \bar{y}}{\partial u}\frac{\partial \bar{x}}{\partial v})\frac{\partial^2 \bar{z}}{\partial u \partial v} \right) \frac{1}{\alpha_x^2 \alpha_y^2}$$

where α_x and α_y are the Lamé parameters (p. 32).

Curvilinear coordinate system
In shell analysis three coordinate systems are used (fig. 43); 1) a global coordinate system (p. 19) to describe the shape of the shell, 2) a local coordinate system (p. 19) to define curvature, displacements, membrane forces, moments and loading, 3) a *curvilinear coordinate system* to derive and solve the shell equations.
The axis of the curvilinear coordinate system are *u* and *v*. They are plotted onto the shell middle surface. All lines of this coordinate system cross perpendicularly. It looks like a timber grid shell (see Savill building p. 22). The *x* direction in a point is tangent to the local *u* direction and the *y* direction in a point is tangent to the local *v* direction.

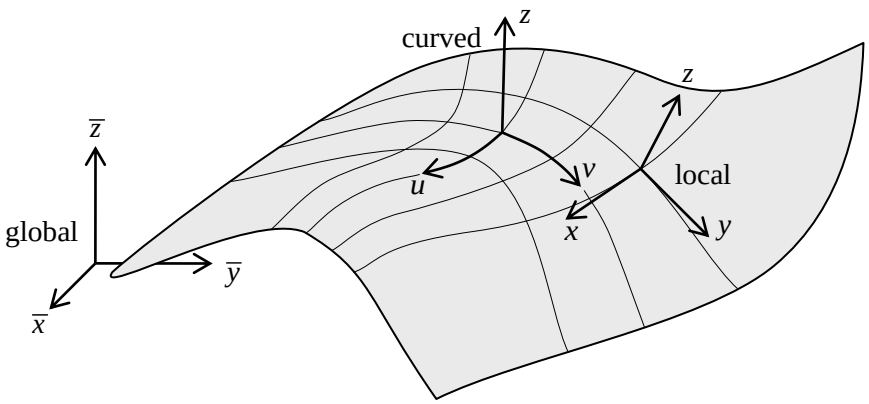

Figure 43. Coordinate systems

In the curvilinear coordinate system it is simple to locate any point (*u*, *v*) on the shell surface. Also, the positive directions of the membrane forces and moments are clear in any point. For example, consider the torus in figure 44. There is nothing unclear about the statement:
"At the location $(u, v) = (\frac{3}{2}\pi b, \frac{1}{2}\pi a)$ the membrane shear force is $n_{xy} = 10$ kN/m ".

$$\bar{x} = (b + a\sin\frac{v}{a})\sin\frac{u}{b}$$

$$\bar{y} = (b + a\sin\frac{v}{a})\cos\frac{u}{b}$$

$$\bar{z} = a\cos\frac{v}{a}$$

$$0 < v < 2\pi a$$

$$0 < u < 2\pi b$$

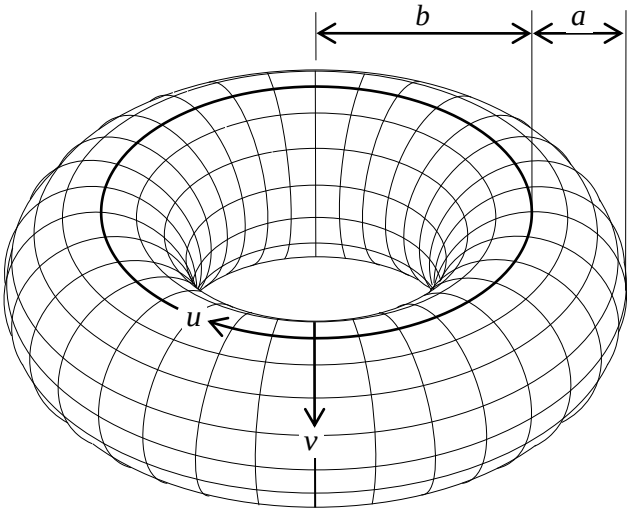

$$k_{xx} = \frac{-1}{a + \frac{b}{\sin\frac{v}{a}}}$$

$$k_{yy} = -\frac{1}{a}$$

$$k_{xy} = 0$$

$$\alpha_x = 1 + \frac{a}{b}\sin\frac{v}{a}$$

$$\alpha_y = 1$$

Figure 44. Curved coordinate system on a torus

Shell displacement and load

Every point of the shell middle surface has a local Cartesian coordinate system *x, y, z* (fig. 45). Every point has displacements u_x, u_y, u_z. Every point is loaded by distributed forces p_x, p_y, p_z [kN/m²].

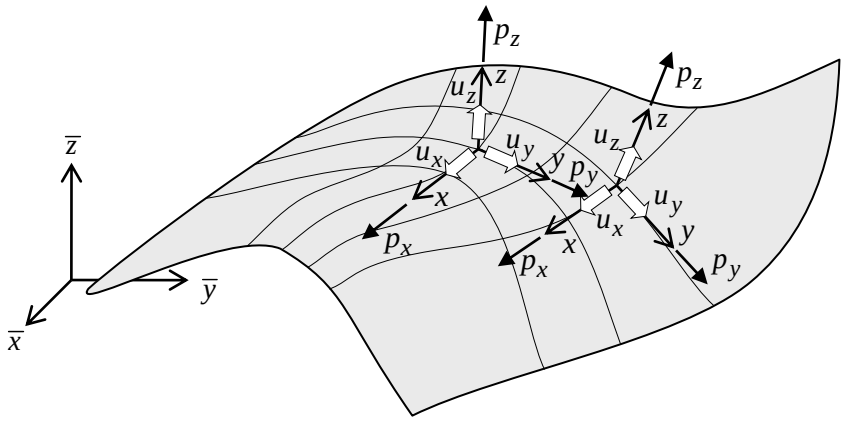

Figure 45. Displacements and loads

Lamé parameters

A complication of the curved coordinate system is that the distance between two grid lines varies from point to point. Therefore, a small length *dx* is often not the same as a small length *du*. For the torus in figure 44 we can derive

$$\begin{bmatrix} dx \\ dy \end{bmatrix} = \begin{bmatrix} 1 + \frac{a}{b}\sin\frac{v}{a} & 0 \\ 0 & 1 \end{bmatrix} \begin{bmatrix} du \\ dv \end{bmatrix}.$$

Exercise: Derive these equations by inspection of the torus curved coordinate system.

In general we write

$$\begin{bmatrix} dx \\ dy \end{bmatrix} = \begin{bmatrix} \alpha_x & 0 \\ 0 & \alpha_y \end{bmatrix} \begin{bmatrix} du \\ dv \end{bmatrix},$$

where α_x and α_y are called *Lamé parameters*.[1] The inverse of the later equations is simply

$$\begin{bmatrix} du \\ dv \end{bmatrix} = \begin{bmatrix} \frac{1}{\alpha_x} & 0 \\ 0 & \frac{1}{\alpha_y} \end{bmatrix} \begin{bmatrix} dx \\ dy \end{bmatrix}.$$

Therefore, $\frac{\partial u}{\partial x} = \frac{1}{\alpha_x}$, $\frac{\partial v}{\partial y} = \frac{1}{\alpha_y}$, $\frac{\partial u}{\partial y} = 0$, $\frac{\partial v}{\partial x} = 0$. The Lamé parameters are important when differentiating. For example, if we differentiate the membrane shear force $n_{xy}(u,v)$ to x we need to use the chain rule

$$\frac{\partial n_{xy}}{\partial x} = \frac{\partial n_{xy}}{\partial u}\frac{\partial u}{\partial x} + \frac{\partial n_{xy}}{\partial v}\frac{\partial v}{\partial x} = \frac{\partial n_{xy}}{\partial u}\frac{1}{\alpha_x}.$$

If an orthogonal parameterisation (p. 25) is available then the Lamé parameters can be calculated with

$$\alpha_x = \sqrt{\frac{\partial \bar{x}^2}{\partial u} + \frac{\partial \bar{y}^2}{\partial u} + \frac{\partial \bar{z}^2}{\partial u}},$$
$$\alpha_y = \sqrt{\frac{\partial \bar{x}^2}{\partial v} + \frac{\partial \bar{y}^2}{\partial v} + \frac{\partial \bar{z}^2}{\partial v}}.$$

The proof is simple. If we change u a bit then $\bar{x}$, $\bar{y}$ and $\bar{z}$ change a bit and the length of the latter bit follows from Pythagoras' theorem. Q.E.D.

Equation of Gauß
The Lamé parameters (p. 32) can be used to calculate Gaussian curvature (p. 23).

$$k_G = -\frac{1}{\alpha_y}\frac{\partial^2 \alpha_y}{\partial x^2} - \frac{1}{\alpha_x}\frac{\partial^2 \alpha_x}{\partial y^2}$$

This is called the *equation of Gauß* [for a derivation see 8 p. 175]. Applying the chain rule this can be written as

$$k_G = -\frac{1}{\alpha_x \alpha_y}\left[\frac{\partial}{\partial u}\left(\frac{1}{\alpha_x}\frac{\partial \alpha_y}{\partial u}\right) + \frac{\partial}{\partial v}\left(\frac{1}{\alpha_y}\frac{\partial \alpha_x}{\partial v}\right)\right].$$

For example, the torus of figure 44 has a Gaussian curvature of

[1] Gabriel Lamé (1795–1870) was a French mathematician who taught at universities in Saint Petersburg and in Paris [Wikipedia]

$$k_G = -\frac{1}{1+\frac{a}{b}\sin\frac{v}{a}}\left[0+\frac{\partial}{\partial v}\left(1\frac{\partial}{\partial v}(1+\frac{a}{b}\sin\frac{v}{a})\right)\right] = \frac{1}{a^2+\frac{ab}{\sin\frac{v}{a}}}.$$

Table 2. Examples of Lamé parameters (p. 32) that produce uniform Gaussian curvatures (p. 23)
(Uniform means not a function of u and not a function of v.)

$\alpha_x = 1$	$\alpha_y = \sin\frac{u}{a}$	$k_G = \frac{1}{a^2}$	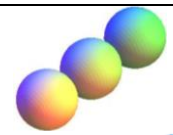
$\alpha_x = 1$	$\alpha_y = \cos\frac{u}{a}$	$k_G = \frac{1}{a^2}$	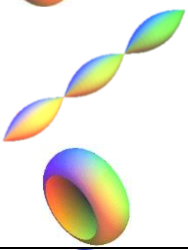
$\alpha_x = 1$	$\alpha_y = \cosh\frac{u}{a}$	$k_G = -\frac{1}{a^2}$	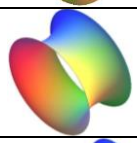
$\alpha_x = 1$	$\alpha_y = \sinh\frac{u}{a}$	$k_G = -\frac{1}{a^2}$	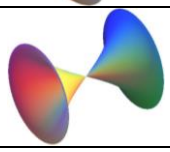
$\alpha_x = 1$	$\alpha_y = \exp\frac{u}{a}$	$k_G = -\frac{1}{a^2}$	
$\alpha_x = 1$	$\alpha_y = 1-\frac{Cu^2}{2}+\frac{C^2u^4}{4!}-\frac{C^3u^6}{6!}+\frac{C^4u^8}{8!}-\ldots$	$k_G = C$	
$\alpha_x = 1-C(\frac{1}{4}v^2-\frac{3}{20}u^2)$	$\alpha_y = 1-C(\frac{1}{4}u^2-\frac{3}{20}v^2)$	$k_G \approx C$	

Exercise: Are the shapes in table 2 completely determined?

Intrinsic property
Consider the sticker shown in figure 46. It has a length and width of 20 cm. The sticker material is very flexible. Subsequently, it is carefully glued onto a curved surface without wrinkles and cracks. The angles between the lines remain 90°. Figure 47 shows the stretched lengths of the sticker lines.

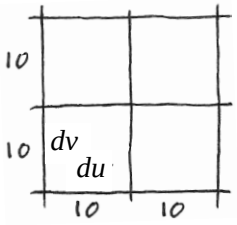

Figure 46. Sticker printed on a flexible material surface

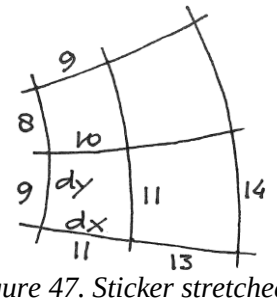

Figure 47. Sticker stretched onto a

The Lamé parameters (p. 32) are

$$\alpha_x = \frac{11\,\text{cm}}{10\,\text{cm}} = 1.1 \qquad \alpha_y = \frac{9\,\text{cm}}{10\,\text{cm}} = 0.9$$

$$\frac{\partial \alpha_x}{\partial v} = \frac{1.0 - 1.1}{10\,\text{cm}} = \frac{-0.01}{\text{cm}} \qquad \frac{\partial \alpha_y}{\partial u} = \frac{1.1 - 0.9}{10\,\text{cm}} = \frac{0.02}{\text{cm}}$$

Substitution in the equation of Gauß (p. 33) gives

$$k_G = -\frac{1}{1.1 \times 0.9}\left[\frac{\partial}{\partial u}\left(\frac{1}{1.1}\frac{0.02}{\text{cm}}\right) + \frac{\partial}{\partial v}\left(\frac{1}{0.9}\frac{-0.01}{\text{cm}}\right)\right]$$

$$= -\frac{1}{1.1 \times 0.9}\left[\frac{\frac{1}{1.3}\frac{0.03}{\text{cm}} - \frac{1}{1.1}\frac{0.02}{\text{cm}}}{10\,\text{cm}} + \frac{\frac{1}{0.8}\frac{-0.01}{\text{cm}} - \frac{1}{0.9}\frac{-0.01}{\text{cm}}}{10\,\text{cm}}\right] = -0.00035\,\frac{1}{\text{cm}^2}$$

Only surface measurements were used. Apparently, for calculating Gaussian curvature we need not measure the shell shape in three-dimensional space. For this reason, Gaussian curvature (p. 23) is called an *intrinsic* property. Mean curvature (p. 24) is not intrinsic.

Exercise: Do the sticker calculation with $k_G = -\frac{1}{\alpha_y}\frac{\partial^2 \alpha_y}{\partial x^2} - \frac{1}{\alpha_x}\frac{\partial^2 \alpha_x}{\partial y^2}$. It should produce the same result.

Curved roofs with tiles

Modern tile roofs are always flat. However, the length that tiles overlap can vary, which can be used to build curved roofs (fig. 48). Clearly, tiles should divert rain and stay on the roof in a storm. This imposes constraints to the slope of tiles. The particle-spring method (p. 105) can be used to determine a suitable grid.



Figure 48. Queens palace in Silinduang Bulan, Indonesia [9]
The curved roofs are made of flat tiles.

Equations of Codazzi
The equations of Codazzi are [7] [2]

$$\frac{\partial \alpha_x k_{xx}}{\partial y} = k_{yy}\frac{\partial \alpha_x}{\partial y}, \qquad \frac{\partial \alpha_y k_{yy}}{\partial x} = k_{xx}\frac{\partial \alpha_y}{\partial x}.$$

They are valid if *x* and *y* are the principal curvature directions, so $k_{xy} = 0$.

Apparently, we cannot create a shell by just choosing functions $k_{xx} = \ldots$, $k_{yy} = \ldots$, $k_{xy} = \ldots, \alpha_x = \ldots$ and $\alpha_y = \ldots$. Our choice must fulfil the equation of Gauß and the equations of Codazzi.

Helicoid
A helicoid (fig. 49) can be described by

$$\bar{x} = a\,v\cos u \qquad \bar{y} = a\,v\sin u \qquad \bar{z} = a\,u$$

and by

$$\bar{x} = a\sinh(u-v)\cos(u+v) \qquad \bar{y} = a\sinh(u-v)\sin(u+v) \qquad \bar{z} = a(u+v)$$

Its mean curvature (p. 24) is zero everywhere, therefore, it is a minimal surface.

[2] Delfino Codazzi (1824–1873) was a mathematics professor at the University of Pavia, Italy. The Codazzi equations were also discovered by Gaspare Mainardi (1800–1879) and by Karl Mikhailovich Peterson (1828–1881). The latter seems to have been the first [Wikipedia].

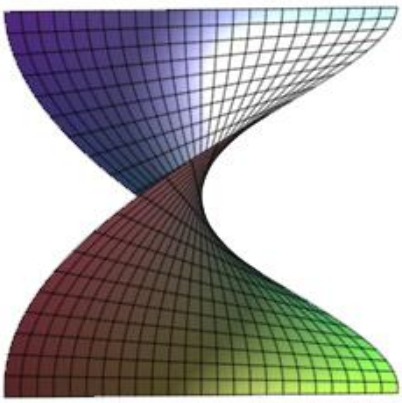

$k_{xx} = 0$

$k_{yy} = 0$

$k_{xy} = \dfrac{1}{a(1+v^2)}$

$\alpha_x = a\sqrt{1+v^2}$

$\alpha_y = a$

$-\pi/2 < u < \pi/2 \qquad -\pi/2 < v < \pi/2$

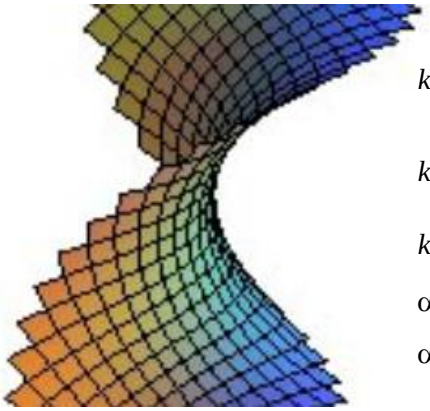

$k_{xx} = \dfrac{-1}{a\cosh^2(u-v)}$

$k_{yy} = \dfrac{1}{a\cosh^2(u-v)}$

$k_{xy} = 0$

$\alpha_x = a\sqrt{2}\cosh(u-v)$

$\alpha_y = a\sqrt{2}\cosh(u-v)$

$-\pi/2 < u+v < \pi/2 \qquad -\pi/2 < u-v < \pi/2$

Figure 49. Helicoid

Exercise: Check the equation of Gauß (p. 33) and the equations of Codazzi (p. 36) for a helicoid.

Challenge: It should be possible to generalise the equations of Codazzi to one equation that is valid for $k_{xy} \neq 0$ too.

In plane curvature

Figure 50 shows curved parameter lines on a curved surface. The lines have a radius of curvature r_y in the plane that is tangent to the shell middle surface. This radius can be expressed in the Lamé parameter α_x (p. 32). The proportions in the figure show that

$$\frac{\alpha_x\, du}{r_y} = \frac{\dfrac{\partial \alpha_x}{\partial y}\, du\, dy}{dy}. \qquad \Rightarrow \qquad \frac{1}{r_y} = \frac{1}{\alpha_x}\frac{\partial \alpha_x}{\partial y}$$

We define $k_x = \dfrac{1}{r_y}$, therefore, $\quad k_x = \dfrac{1}{\alpha_x}\dfrac{\partial \alpha_x}{\partial y}$

In the same way can be defined $\quad k_y = \dfrac{1}{\alpha_y}\dfrac{\partial \alpha_y}{\partial x}$.

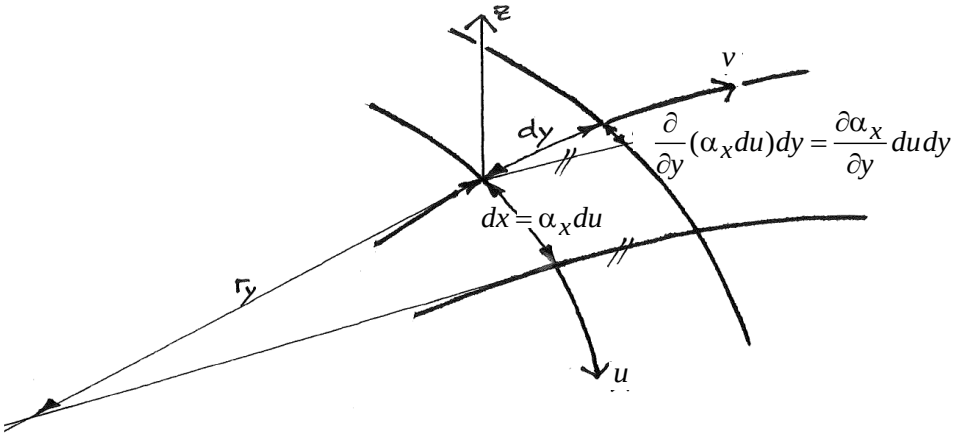

Figure 50. Radius r_y of the parameter line v = constant

Exercise: Derive that $k_G = -\dfrac{\partial k_x}{\partial y} - \dfrac{\partial k_y}{\partial x} - k_x^2 - k_y^2$

Challenge: Suppose we have two orthogonal parameterisations of a shell.

The local coordinate systems in a shell point are *x*–*y*–*z* and *r*–*s*–*z*. Proof or disproof that

$k_r = k_x \cos\varphi - k_y \sin\varphi$

$k_s = k_x \sin\varphi + k_y \cos\varphi$

where φ is the angle between the *r* axis and the *x* axis (appendix p. 196).

Shell membrane equations

The shell membrane equations are shown in table 3. These equations describe the behaviour of thin shell structures, however, all moments have been neglected. Nonetheless, they are useful because for many shells the moments have little influence on their global behaviour. The shell equations that do include moments are called Sanders-Koiter equations (p. 54).

In these notes only the equilibrium equations and the kinematic equations are derived. The constitutive equations are the same as for flat plates loaded in plane. For their derivations see a course on plates.

Table 3. Shell membrane equations

kinematic equations	$\varepsilon_{xx} = \frac{\partial u_x}{\partial x} - k_{xx} u_z + k_x u_y$	1
	$\varepsilon_{yy} = \frac{\partial u_y}{\partial y} - k_{yy} u_z + k_y u_x$	2
	$\gamma_{xy} = \frac{\partial u_x}{\partial y} + \frac{\partial u_y}{\partial x} - 2k_{xy} u_z - k_x u_x - k_y u_y$	3
constitutive equations	$\varepsilon_{xx} = \frac{1}{E\,t}(n_{xx} - \nu n_{yy})$	4
	$\varepsilon_{yy} = \frac{1}{E\,t}(n_{yy} - \nu n_{xx})$	5
	$\gamma_{xy} = \frac{2(1+\nu)}{E\,t} n_{xy}$	6
equilibrium equations	$\frac{\partial n_{xx}}{\partial x} + \frac{\partial n_{xy}}{\partial y} + k_y(n_{xx} - n_{yy}) + 2k_x n_{xy} + p_x = 0$	7
	$\frac{\partial n_{yy}}{\partial y} + \frac{\partial n_{xy}}{\partial x} + k_x(n_{yy} - n_{xx}) + 2k_y n_{xy} + p_y = 0$	8
	$k_{xx} n_{xx} + 2k_{xy} n_{xy} + k_{yy} n_{yy} + p_z = 0$	9

Membrane forces in a spherical dome

The forces in a spherical dome can be computed by maple using the shell membrane equations (p. 38). The dome is loaded by self-weight *p* only. The result is shown in figure 52. For example, a dome with a radius a = 12 m and self-weight p = 2 kN/m² will give a hoop force in the bottom edge of $n = p\,a = 2 \times 12 = 24$ kN/m tension.

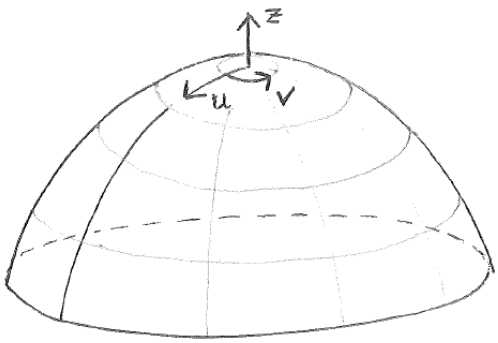

Figure 51. Curved coordinates on a spherical dome

```
> restart:
> kxx:=-1/a: kyy:=-1/a: kxy:=0: ax:=1: ay:=sin(u/a):
> ky:=diff(ay,u)/ax/ay: kx:=diff(ax,v)/ay/ax:
> px:=p*sin(u/a): py:=0: pz:=-p*cos(u/a): # p:=t*rho*g:
> nxx:=f1(u): nyy:=f2(u): nxy:=0:
> eq1:= kxx*nxx + kyy*nyy + 2*kxy*nxy + pz = 0:
> eq2:= diff(nxx,u)/ax + diff(nxy,v)/ay + (nxx-nyy)*ky + 2*nxy*kx + px = 0:
> eq3:= diff(nyy,v)/ay + diff(nxy,u)/ax + (nyy-nxx)*kx + 2*nxy*ky + py = 0:
> dsolve({eq1,eq2});
```

$$\left\{ f1(xs) = -\frac{2\left(p\cos\left(\frac{xs}{a}\right)a + _C1\right)}{-1+\cos\left(\frac{2\,xs}{a}\right)},\ f2(xs) = \frac{1}{2}\frac{5\,p\cos\left(\frac{xs}{a}\right)a + 4\,_C1 - p\,a\cos\left(\frac{3\,xs}{a}\right)}{-1+\cos\left(\frac{2\,xs}{a}\right)} \right\}$$

```
> # boudary condition nxx(0)=nyy(0)
> f1:=-2*(p*cos(u/a)*a+_C1)/(-1+cos(2*u/a)):
> f2:=1/2*(5*p*cos(u/a)*a+4*_C1-p*a*cos(3*u/a))/(-1+cos(2*u/a)):
> solve(f1=f2,_C1):
> _C1:=-p*a:
>
> nxx:= -p*a/(1+cos(u/a)):                    # meridional force, pressure line
> nyy:= -p*a*( cos(u/a) - 1/(1+cos(u/a)) ): # hoop force
> nxy:= 0:
> p:=1:       # self-weight [kN/m2]
> a:=10:      # radius [m]
> um:=Pi/2*a: # maximum u value [m]
> f:=-0.3:    # plot factor -
> plot({[ a       *sin(u/a), a       *cos(u/a),u=-um..um],
        [(a+f*nxx)*sin(u/a),(a+f*nxx)*cos(u/a),u=-um..um],
        [(a+f*nyy)*sin(u/a),(a+f*nyy)*cos(u/a),u=-um..um]},
color=[black,red,green],thickness=[3,1,1]);
```

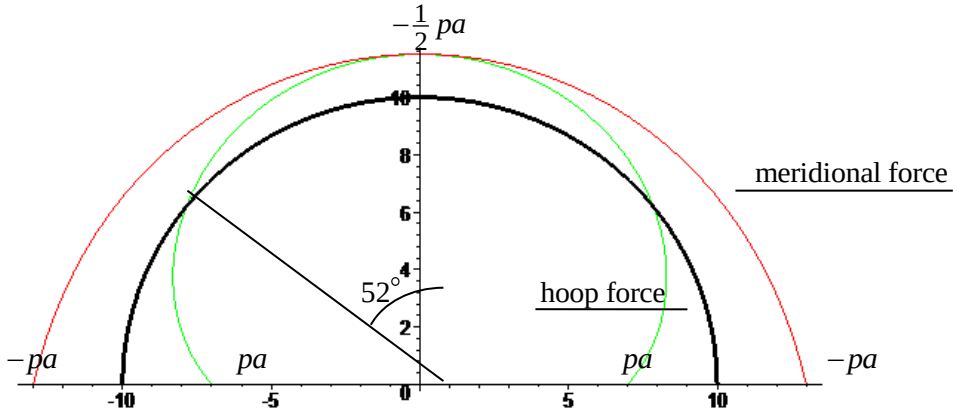

Figure 52. Membrane forces in a spherical dome

Derivation of membrane equation 1

An imaginary fibre in the x direction will elongate with du_x (fig. 53). Strain is elongation over length, therefore,

$$\varepsilon_{xx1} = \frac{du_x}{dx}.$$

The fibre will shorten due to u_z (fig. 53). The new fibre length is angle times radius

$$\frac{s}{\frac{1}{k_{xx}}} \times (\frac{1}{k_{xx}} - u_z) = s(1 - u_z k_{xx}),$$

therefore,

$$\varepsilon_{xx2} = \frac{s - s(1 - u_z k_{xx})}{s} = u_z k_{xx}.$$

The fibre will elongate due to displacement u_y (fig. 53). The fibre strain is

$$\varepsilon_{xx3} = \frac{\frac{s}{r_y}(r_y + u_y) - s}{s} = \frac{u_y}{r_y} = u_y k_x.$$

The total strain is $\varepsilon_{xx} = \varepsilon_{xx1} - \varepsilon_{xx2} + \varepsilon_{xx3} = \frac{\partial u_x}{\partial x} - k_{xx} u_z + k_x u_y$.

Q.E.D.

Shell membrane equation 2 can be derived in the same way.

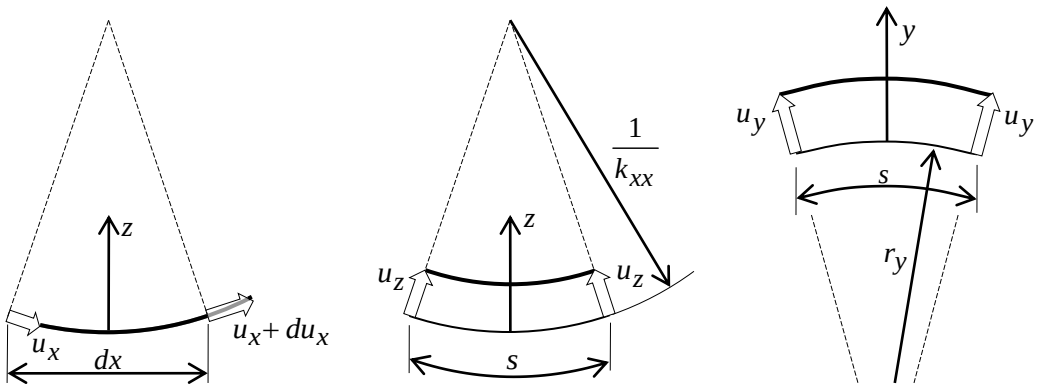

Figure 53. Deformation in the x direction; in the z direction; in the y direction

Derivation of membrane equation 3
The first two terms of equation 3 are the same as for plates (fig. 54).

$$\gamma_{xy,1} = \frac{du_x}{dy} + \frac{du_y}{dx}$$

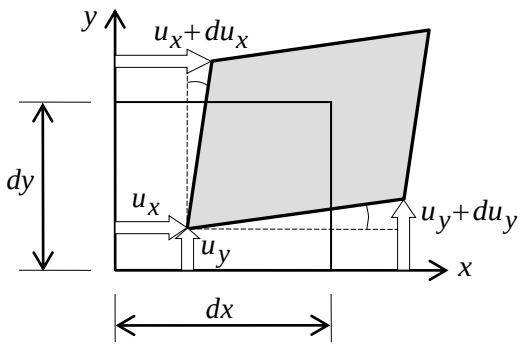

Figure 54. Deformation in the x and y direction

Since u_z is perpendicular to the surface, a uniform u_z causes shear in the panel (fig. 55).

$$\gamma_{xy,2} = \frac{u_z \dfrac{k_{xy}\,dx\,dy}{dx}}{dy} + \frac{u_z \dfrac{k_{xy}\,dx\,dy}{dy}}{dx} = 2k_{xy}u_z\,.$$

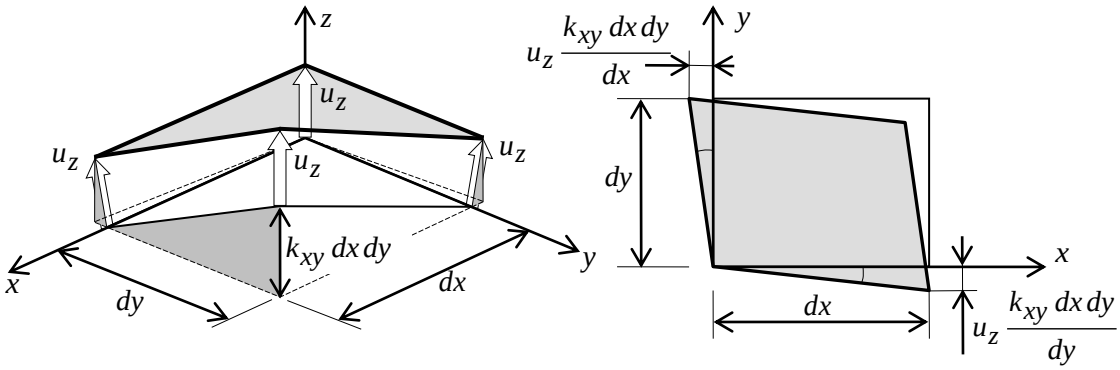

Figure 55. Deformation due to displacement in the z direction

In a curved coordinate system, a uniform deformation u_x produces a shear strain (fig. 56).

$$\gamma_{xy3} = k_x u_x$$

In the same way can be derived $\gamma_{xy4} = k_y u_y$.

The total shear deformation is

$$\gamma_{xy} = \gamma_{xy1} - \gamma_{xy2} - \gamma_{xy3} - \gamma_{xy4} = \frac{\partial u_x}{\partial y} + \frac{\partial u_y}{\partial x} - 2k_{xy}u_z - k_x u_x - k_y u_y\,.$$

Q.E.D.

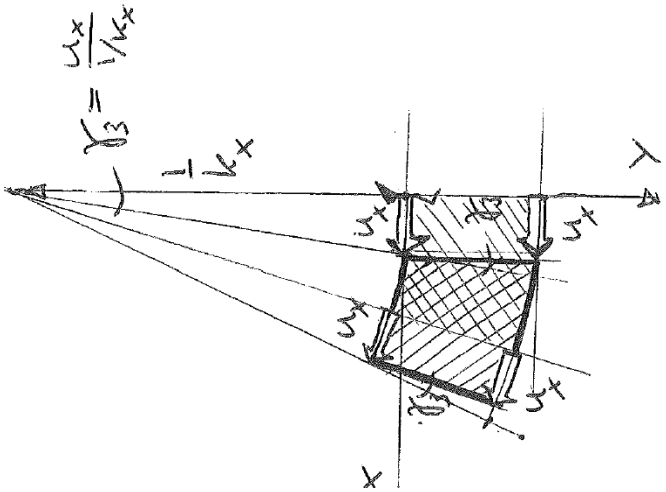

Figure 56. Shear deformation due to uniform x displacement in a curved coordinate system

Duomo di Firenze

The Cathedral of Firenze (Florence, Italy) has a dome with a span of 44 m (fig. 57). The builder of the dome was Filippo Brunelleschi. As far as we know he had only two examples, the Pantheon (p. 14) and the *Hagia Sophia*. The Pantheon has a span of 43.4 m and is made of concrete. However, it had been built 1500 years before and the recipe for making concrete had been forgotten. The Hagia Sophia has a span of 31 m and is made of brick. However, it has large buttresses which the people of Firenze thought were ugly. Brunelleschi made a brick design with an inner and an outer shell (fig. 58). Construction of the dome started in 1420 and took 16 years. Many historians see this dome as the end of the middle ages and the start of the renaissance.[3]



Figure 57. Duomo di Firenze, Italy

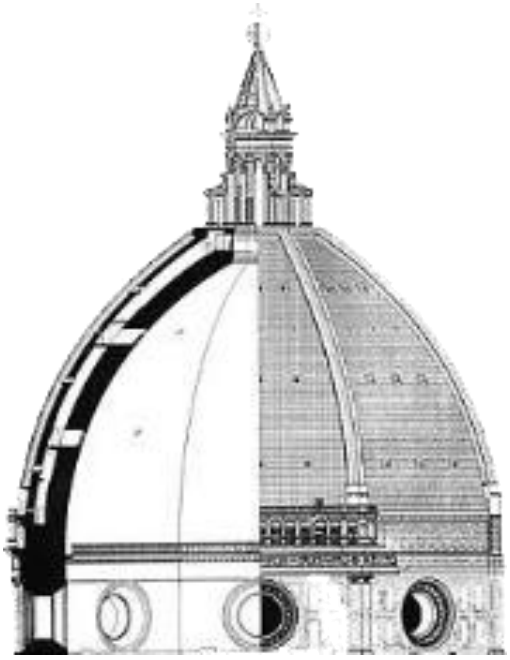

Figure 58. Cross-section of the dome

In the lower part of the dome the hoop forces are tension. This is carried by stone blocks connected by iron bars. Without this the dome would crack and collapse. Fortunately, the iron

[3] Time frame: In 1505 Leonardo da Vinci painted his Mona Lisa.

did not corrode away in the more than 570 years that the dome exists. Humidity in the masonry is carefully monitored.

Saint Paul's Cathedral

Saint Paul's cathedral in London was built from 1675 until 1711.[4] The design has been made by Christopher Wren who also supervised construction (see cables and arches p. 5). The outside dome is made of timber (fig. 59, 60). The inside dome is made of bricks and has an oculus. In between is a third dome. This dome is cone shaped and made of bricks. It carries the stone lantern and supports the outside dome. Note that the pressure line (p. 6) in the domes and the cathedral walls is very clear. This designer knew exactly what he was doing. The dome spans approximately 35 m.

Under the dome is the famous whispering gallery. When you are at this gallery and whisper something it can be clearly heard by someone on the other side of the gallery. This is because sound waves are guided along the curved wall of the gallery. Clapping your hands produces no less than four echoes. The name "whispering gallery" is now generally used for this acoustical effect in physics.

[4] Time frame: In 1684 Isaac Newton discovered the laws of motion, with which we calculate trajectories of objects on earth and in space. In 1765 James Watt invented the steam engine with condenser, which marks the start of the industrial revolution. When you visit Saint Paul's Cathedral you can literally touch the civilization that made these big steps in human development. As a consequence we speak English today.

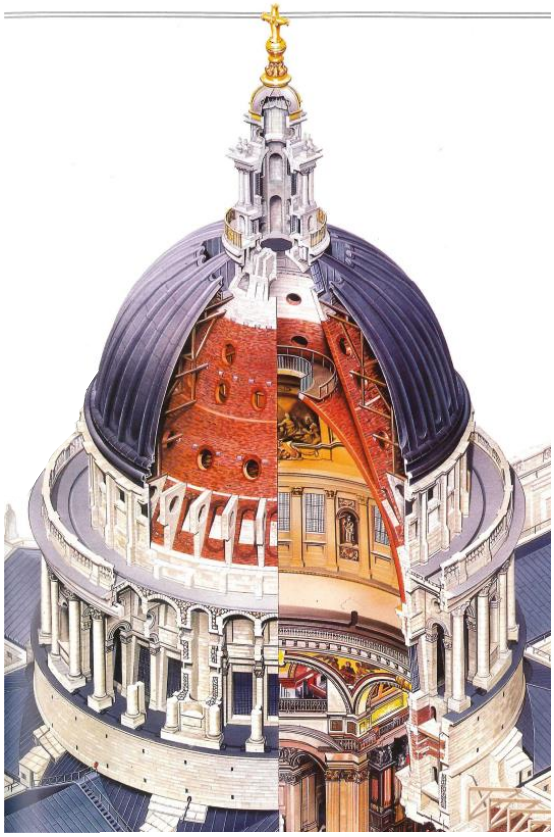

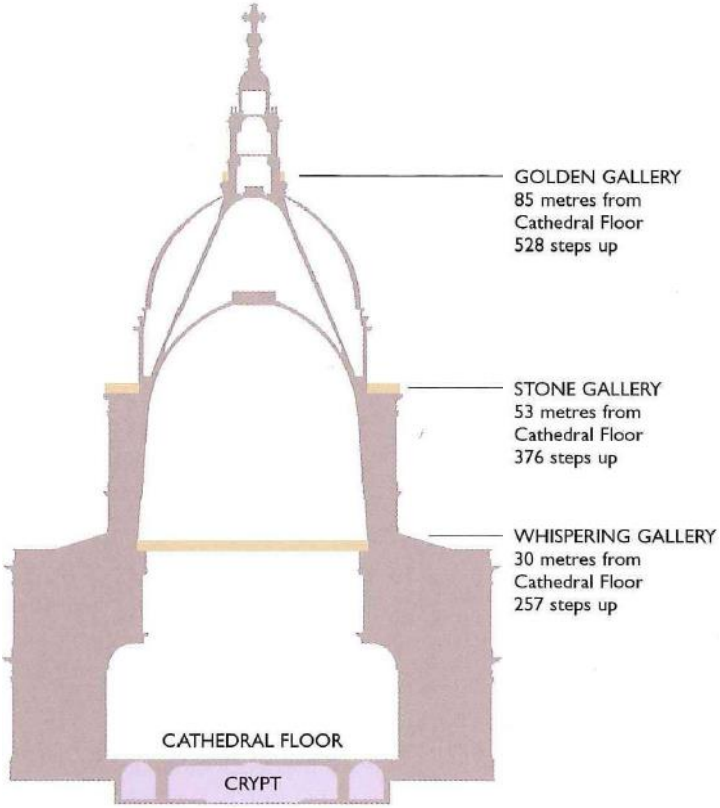

Figure 59. Dome of Saint Paul's Cathedral [10] Figure 60. Cross-section of the Cathedral [11]

Derivation of membrane equation 7

Figure 61 left top shows a small shell part with only normal force n_{xx}. Three forces act on this shell part. Equilibrium in the *x* direction gives

$$p_{x1}dxdy + (n_{xx} + \frac{\partial n_{xx}}{\partial x}\frac{dx}{2})\vartheta_1(\frac{1}{k_y} + \frac{dx}{2}) - (n_{xx} - \frac{\partial n_{xx}}{\partial x}\frac{dx}{2})\vartheta_1(\frac{1}{k_y} - \frac{dx}{2}) = 0$$

This can be simplified to $\frac{\partial n_{xx}}{\partial x} + k_y n_{xx} + p_{x1} = 0$.

Figure 61 left bottom shows a small shell part with only normal force n_{yy}. Three forces act on this shell part too. Equilibrium in the *x* direction gives

$$p_{x2}dxdy - n_{yy}dx\vartheta 1 = 0$$

This can be simplified to $-k_y n_{yy} + p_{x2} = 0$.

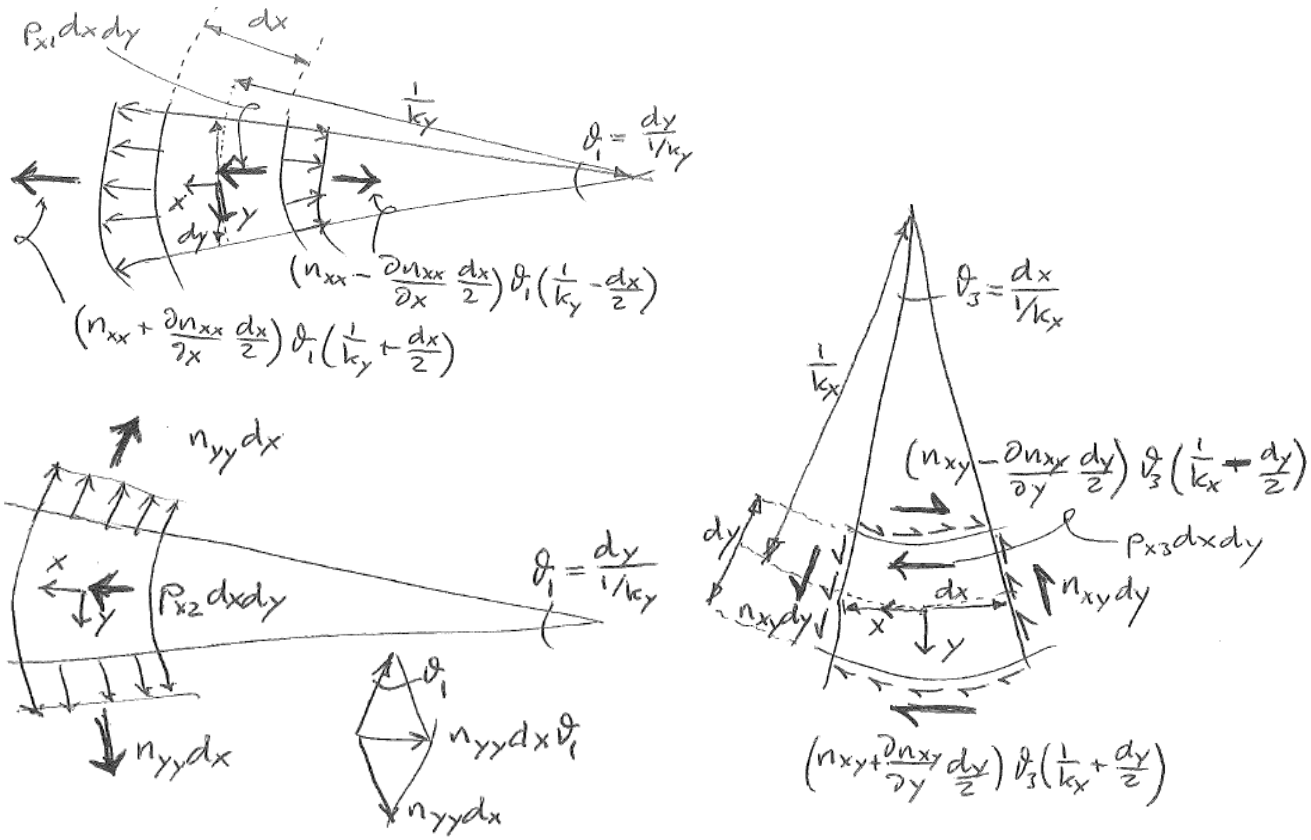

Figure 61. Equilibrium of a curved plate part in the x direction

Figure 61 right shows a small shell part with only shear force n_{xy}. Four forces act on this shell part. Equilibrium in the *x* direction gives

$$p_{x3}dxdy + (n_{xy} + \frac{\partial n_{xy}}{\partial y}\frac{dy}{2})\vartheta_3(\frac{1}{k_x} + \frac{dy}{2}) - (n_{xy} - \frac{\partial n_{xy}}{\partial y}\frac{dy}{2})\vartheta_3(\frac{1}{k_x} - \frac{dy}{2}) + n_{xy}dy\vartheta_3 = 0$$

This can be simplified to $\frac{\partial n_{xy}}{\partial y} + 2k_x n_{xy} + p_{x3} = 0$.

Substitution in $p_x = p_{x1} + p_{x2} + p_{x3}$ gives

$$\frac{\partial n_{xx}}{\partial x} + \frac{\partial n_{xy}}{\partial y} + k_y (n_{xx} - n_{yy}) + 2k_x n_{xy} + p_x = 0$$

Q.E.D.

Shell membrane equation 8 can be derived in the same way.

Derivation of membrane equation 9
A shell part can be curved in the *x* direction (fig. 62). It needs to be in equilibrium in the *z* direction. This is described by Barlow's formula (p. 8).

$$n_{xx} + p_{z1} \frac{1}{k_{xx}} = 0 .$$

A shell part that is curved in the *y* direction gives a similar equilibrium equation

$$n_{yy} + p_{z2} \frac{1}{k_{yy}} = 0 .$$

A shell part can also be twisted (fig. 63). Equilibrium in the *z* direction gives

$$n_{xy}\, dy \frac{k_{xy} dx dy}{dy} + n_{xy}\, dx \frac{k_{xy} dx dy}{dx} + p_{z3}\, dx\, dy = 0 ,$$

which can be simplified to

$$2 n_{xy} k_{xy} + p_{z3} = 0$$

For a shell part that is curved in all three ways k_{xx}, k_{yy} and k_{xy} the load p_z is obtained by summation.

$$p_{z1} + p_{z2} + p_{z3} = p_z$$

Substitution of the previous four equations gives

$$k_{xx} n_{xx} + k_{yy} n_{yy} + 2k_{xy} n_{xy} + p_z = 0$$

Q.E.D.

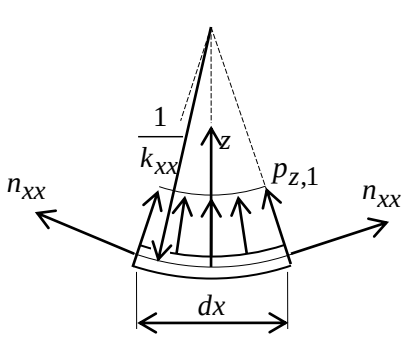

Figure 62. Equilibrium of a curved shell part

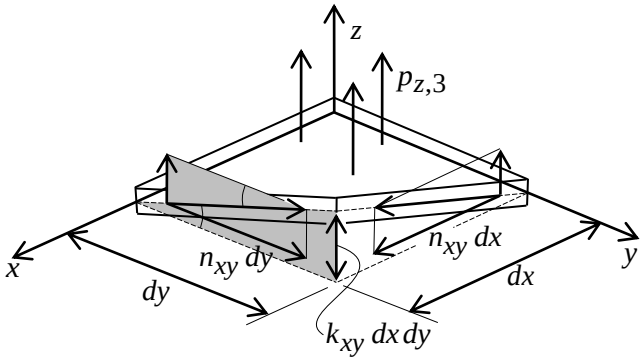

Figure 63. Equilibrium of a twisted shell part

Soap bubbles and soap films

A free soap bubble is a sphere (fig. 64). When a bubble is attached to an object its shape is more difficult to describe. A step in the right direction is that for any bubble the mean curvature k_m (p. 24) is constant over the surface. This is proven here by applying shell membrane equation 9 (p. 38).

Soap has the properties of a liquid; there is no shear stress and the normal stress is the same in all directions. Therefore, $n_{xy} = 0$ and $n_{xx} = n_{yy} = n$. Substitution in equation 9 gives

$$\tfrac{1}{2}(k_{xx} + k_{yy}) = -\frac{p_z}{2n},$$

which is by definition equal to k_m. The air pressure in the bubble is a little larger than outside due to the stress in the soap membrane. The over pressure p_z is the same everywhere in the bubble and the force n is the same everywhere in the membrane. Consequently, the mean curvature is everywhere the same. Q.E.D.

A soap film in a wire loop is free to minimise its area (fig. 65). Therefore, it is called a minimal surface. It has equal air pressure on both sides. Therefore, $p_z = 0$, consequently, $k_m = 0$ everywhere in the film. This property is often used in form finding (p. 16) of tent structures.

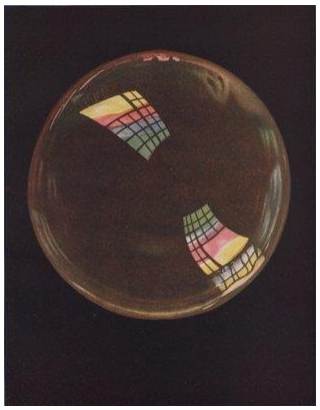

Figure 64. Free soap bubble

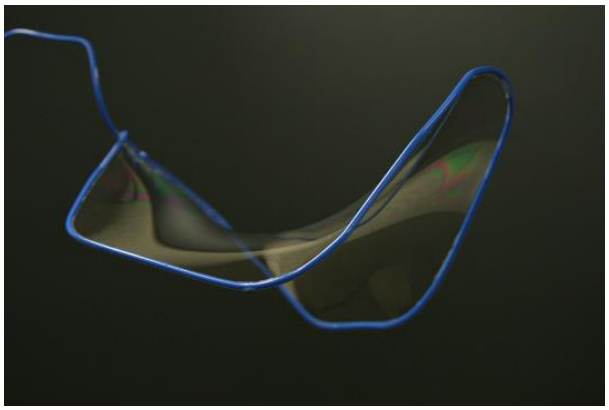

Figure 65. Soap film in a wire loop

Beam calculation of a simply supported tube

Consider a simply supported beam with an evenly distributed load (fig. 66). The cross-section of the beam is circular (fig. 67). The load is self-weight p [kN/m²].

In a handbook we find the moment of inertia $I = \pi a^3 t$.
From figure 67 we derive the distributed line load $q = 2\pi a\, p$ [kN/m].
Elementary mechanics gives us the moment in the middle $M = \frac{1}{8} q l^2$,
the stress at the bottom $\sigma = \frac{M\, a}{I}$,
and the deflection in the middle $w = \frac{5}{384} \frac{q l^4}{EI}$.
Substitution in the last two equations gives $\sigma = \frac{p l^2}{4 a t}$ and $w = \frac{5}{192} \frac{p l^4}{a^2 E t}$.

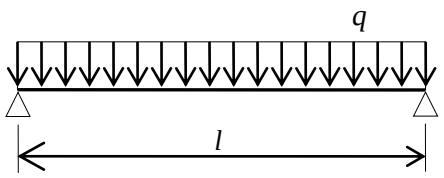

Figure 66. Simply supported beam

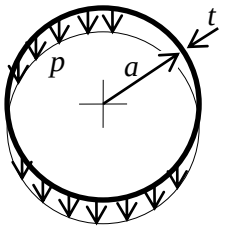

Figure 67. Cross-section of the beam

Shell calculation of a simply supported tube
Consider the simply supported beam (fig. 66). The coordinate system is shown in figure 68. We see that

$$k_{xx} = 0, \quad k_{yy} = -\frac{1}{a}, \quad k_{xy} = 0, \quad \alpha_x = 1, \quad \alpha_y = 1$$

$$p_x = 0, \quad p_y = p \sin\frac{v}{a}, \quad p_z = -p \cos\frac{v}{a}.$$

At both ends $u = \frac{1}{2} l$ and $u = -\frac{1}{2} l$ the tube is closed by a thin diaphragm. This diaphragm can carry membrane forces without buckling but it cannot carry bending moments. The middles of the diaphragms are fixed.

The boundary conditions are

$u = \frac{1}{2} l$	$u_z = 0$	1
	$u_y = 0$	2
	$n_{xx} = 0$	3
$u = 0$	$u_x = 0$	4
	$n_{xy} = 0$	5

Most boundary conditions are obvious. Only boundary condition 5 is explained (fig. 69). The shell and the loading are symmetrical. Symmetry and equilibrium have opposite requirements for the directions of the stresses at $u = 0$. Therefore, the only possible stress is zero stress.

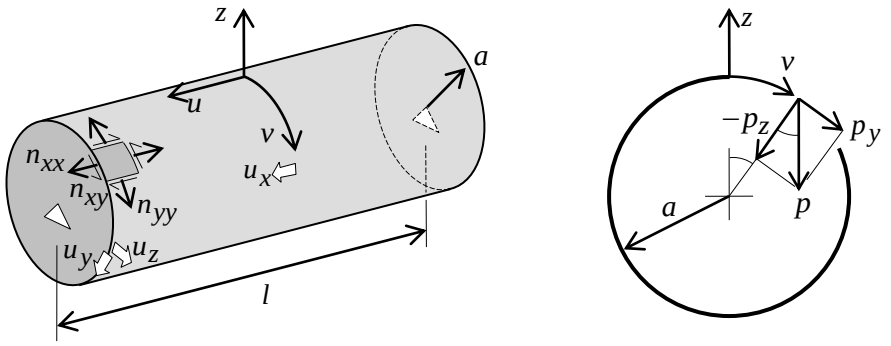

Figure 68. Local coordinate system of the tube

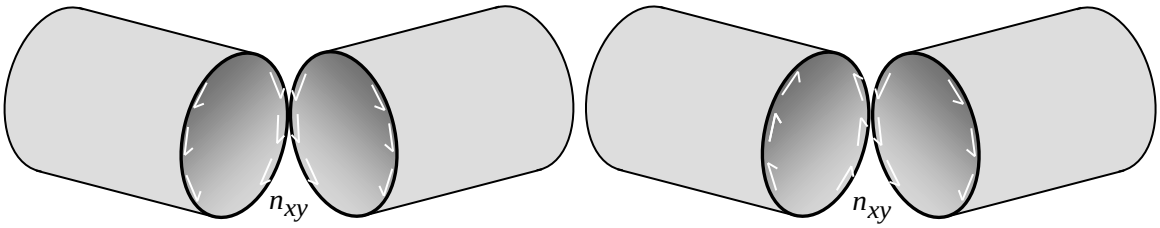

Figure 69. Shear stresses in the middle section due to symmetry (left) and equilibrium (right)

Shell calculation of the stresses

In this section the stresses in the tube are calculated using the shell membrane equations (p. 38).

Equation 9 simplifies to $-\frac{n_{yy}}{a} - p\cos\frac{v}{a} = 0$ from which we solve $n_{yy} = -p\,a\cos\frac{v}{a}$.

Equation 8 simplifies to $p\sin\frac{v}{a} + \frac{\partial n_{xy}}{\partial x} + p\sin\frac{v}{a} = 0$ from which we

solve $n_{xy} = -2\,p\,u\sin\frac{v}{a} + C_1$.

Boundary condition $n_{xy}(0,v) = 0$ gives $C_1 = 0$.

Equation 7 simplifies to $\frac{\partial n_{xx}}{\partial x} - \frac{2\,p\,u}{a}\cos\frac{v}{a} + 0 = 0$ from which we

solve $n_{xx} = \frac{p\,u^2}{a}\cos\frac{v}{a} + C_2$.

Boundary condition $n_{xx}(\frac{1}{2}l,v) = 0$ gives $C_2 = -\frac{p(\frac{1}{2}l)^2}{a}\cos\frac{v}{a}$.

For steel tubes the Von Mises stress (p. 101) in the middle bottom $(u,v) = (0,\pi a)$ is important.

$n_{VM} = \sqrt{n_{xx}^2 - n_{xx}n_{yy} + n_{yy}^2 + 3n_{xy}^2}$

Using $\sigma_{VM} = \frac{n_{VM}}{t}$, this can be evaluated to $\boxed{\sigma_{VM\,\max} = \frac{p\,l^2}{4\,a\,t}\sqrt{1 - 4\frac{a^2}{l^2} + 16\frac{a^4}{l^4}}}$.

We see that for long tubes $(l >> a)$ the shell result is the same as the beam result (see beam calculation p. 47). For a short tube of $l = 6a$ the shell result is 5% smaller than the beam result.

Exercise: What is the stress in the top of the beam?

Statically determinate
In the previous section, the stresses everywhere in the tube are calculated using the equilibrium equations only. Therefore, the tube is a statically determinate structure. This is typical for shell structures:

If the support is statically determinate, then the membrane stresses are statically determinate.[5]

Tube shear stress
The shear force V in the tube cross-section is (fig. 70)

$$V = \int_{v=0}^{2\pi a} n_{xy} \sin\frac{v}{a} dy = -2\pi a\, p u\,.$$

The largest shear stress in the tube cross-sections is

$$\tau_{\max} = \frac{n_{xy}(u, \frac{1}{2}\pi a)}{t} = \frac{-2pu}{t}.$$

Expressed in shear force V and cross-section area A it becomes[9]

$$\boxed{\tau_{\max} = \frac{V}{\frac{1}{2}A}}.$$

Shell calculation of the tube deformation
In this section the deformation of a simply supported tube is calculated using the shell membrane equations (p. 38). The solutions of n_{xx}, n_{yy} and n_{xy} are substituted in equations 4, 5 and 6.

Equation 1 simplifies to $\frac{p}{aEt}\left(u^2 - \frac{1}{4}l^2 + \nu a^2\right)\cos\frac{v}{a} = \frac{\partial u_x}{\partial x}$ from which we solve

$$u_x = \frac{pu}{aEt}\left(\frac{1}{3}u^2 - \frac{1}{4}l^2 + \nu a^2\right)\cos\frac{v}{a} + C_3\,.$$

Boundary condition 4 gives $C_3 = 0$.

Equation 3 simplifies to $-\frac{4pu}{Et}(1+\nu)\sin\frac{v}{a} = -\frac{pu}{a^2Et}\left(\frac{1}{3}u^2 - \frac{1}{4}l^2 + \nu a^2\right)\sin\frac{v}{a} + \frac{\partial u_y}{\partial x}$ from

which we solve $u_y = \frac{pu^2}{a^2Et}\left(\frac{1}{12}u^2 - \frac{1}{2}a^2(4+3\nu) - \frac{1}{8}l^2\right)\sin\frac{v}{a} + C_4$

Boundary condition 2 gives $C_4 = \frac{pl^2}{a^2Et}\left(\frac{5}{192}l^2 + \frac{1}{2}a^2 + \frac{3}{8}\nu a^2\right)\sin\frac{v}{a}$.

Equation 2 simplifies to

$$\frac{p}{aEt}\left(-\nu u^2 - a^2 + \frac{1}{4}\nu l^2\right)\cos\frac{v}{a} = \frac{pu^2}{a^3Et}\left(\frac{1}{12}u^2 - \frac{1}{2}a^2(4+3\nu) - \frac{1}{8}l^2\right)\cos\frac{v}{a} +$$

[5] Statically determinate is a model property. A more advanced model of the same structure can be statically indetermined.

$$+\frac{p l^2}{a^3 E t}\left(\frac{5}{192}l^2+\frac{1}{2}a^2+\frac{3}{8}\nu a^2\right)\cos\frac{v}{a}+\frac{u_z}{a}$$ from which we solve

$$u_z=\frac{p}{a^2 E t}\left(-\frac{1}{12}u^4+\frac{1}{8}a^2(4u^2-l^2)(4+\nu)+\frac{1}{8}u^2l^2-a^4-\frac{5}{192}l^4\right)\cos\frac{v}{a}$$

The deflection of the middle bottom $(u,v)=(0,\pi a)$ is important.

$$\boxed{u_{z\max}=\frac{p l^4}{a^2 E t}\left(\frac{5}{192}+\frac{\nu+4}{8}\frac{a^2}{l^2}+\frac{a^4}{l^4}\right)}$$

For long tubes $(l >> a)$ the shell result is the same as the beam result (see beam calculation of a simply supported tube p. 47). The second term is caused by shear deformation. The last term is caused by ovalization of the cross-section. For a tube of $l=20a$ the shell result is 5% larger than the beam result. For a short tube of $l=6a$ the shell result is 61% larger than the beam result.

Bernoulli's hypothesis

Jacob Bernoulli's hypothesis is: *Plane cross-sections remain plane during bending.*[6] It is the starting point for deriving section moments in beams, plates and shells. We can test this hypothesis for tubes using the shell solution.[7] The deformation in the *x* direction is

$$u_x=\frac{p u}{a E t}\left(\frac{1}{3}u^2-\frac{1}{4}l^2+\nu a^2\right)\cos\frac{v}{a}.$$

This can be written as

$$u_x=C d,$$

where $C=\frac{p u}{a^2 E t}\left(\frac{1}{3}u^2-\frac{1}{4}l^2+\nu a^2\right)$ and $d=a\cos\frac{v}{a}$.

Factor *d* is the distance of the considered material point to the neutral axis. It is a function of *v*. Please note the difference between ν (Poisson's ratio) and *v* (curvilinear coordinate). Factor *C* is not a function of *v* and it depends on the considered cross-section. Therefore, u_x is linear in *d* and Bernoulli's hypothesis is true for tubular sections despite the presence of shear forces. For tubular sections it should be called Bernoulli's theorem.[8]

Shear stiffness

Shear stiffness is defined as

[6] Jacob Bernoulli (1654-1705) was a professor of mathematics at the University of Basel in Switzerland.

[7] Note that in this section Bernoulli's hypothesis is applied to a beam with a thin-wall circular cross-section. Here, it is not applied to the thin shell wall.

[8] For other cross-section shapes Bernoulli's hypothesis is not true due to shear and torsion deformation. Fortunately, the linear distribution of normal stresses due to bending – which follows from Bernoulli's hypothesis – is true for all cross-sections of slender beams.

$$GA_S = \frac{V}{\gamma},$$

where V is the shear force and γ is the shear deformation of a slice of a beam (fig. 70). For the considered tube we obtain

$$V = \int_{v=0}^{2\pi a} n_{xy} \sin\frac{v}{a} dy = -2\pi a\, p u$$

$$\gamma = \frac{\partial u_y}{\partial x}(u, \tfrac{1}{2}\pi a) + \frac{u_x(u,\pi a) - u_x(u,0)}{2a} = \frac{-4 p u (1+\nu)}{E t}$$

$$\frac{V}{\gamma} = \frac{-2\pi a\, p u}{\frac{-4 p u (1+\nu)}{E t}} = \frac{E}{2(1+\nu)} \frac{1}{2} 2\pi a t = \frac{1}{2} GA$$

So,

$$\boxed{GA_S = \tfrac{1}{2} GA}.$$[9]

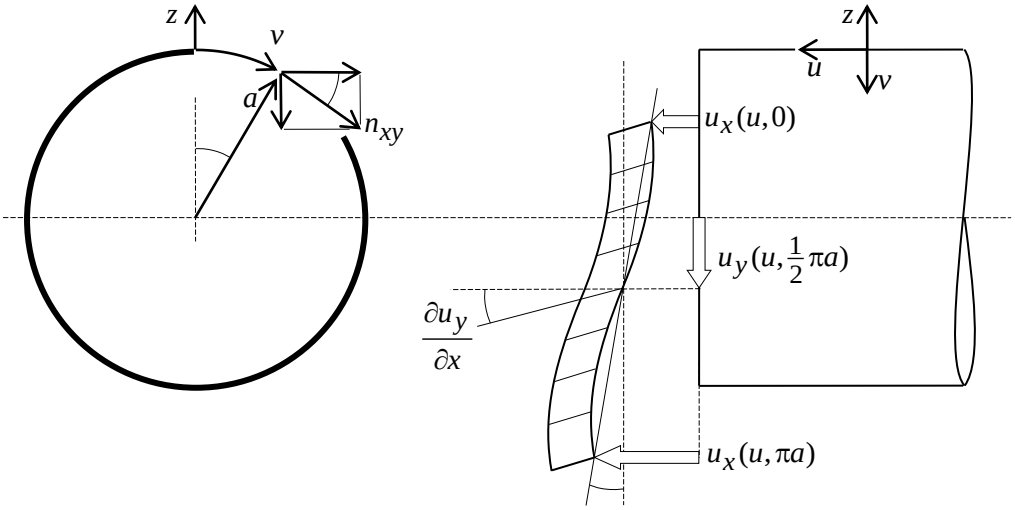

Figure 70. Shear deformation of a tube slice. Bernoulli's hypothesis (p. 50) has not been used.

Gap

Boundary condition 1 has not been used. Here it is checked if this boundary condition is fulfilled.

The displacement in the radial direction is

$$u_z = \frac{p}{a^2 E t}\left(-\frac{1}{12}u^4 + \frac{1}{8}a^2(4u^2 - l^2)(4+\nu) + \frac{1}{8}u^2 l^2 - a^4 - \frac{5}{192}l^4\right)\cos\frac{v}{a}$$

At $u = \pm\frac{1}{2}l$ this simplifies to $u_z = \frac{-a^2 p}{E t}\cos\frac{v}{a}$ which is not zero.

[9] For thick wall tubes the shear stiffness is $GA_s = (\frac{1}{2} + \frac{3}{4}\frac{t}{a})GA$ and the largest shear stress is $\tau_{max} = (2 + \frac{t}{a})\frac{V}{A}$. This has been derived from finite element analysis using volume elements [12].

Therefore, boundary condition 1 is not fulfilled. There is a gap between the diaphragm and the shell (fig. 71). To close the gap the shell needs to bend. This deformation is not part of the membrane equations. To fulfil all boundary conditions the membrane equations need to be extended with bending (see Sanders-Koiter equations p. 54). The phenomenon of strong bending close to edges is called edge disturbance (p. 14, p. 72). It is typical for thin shell structures.

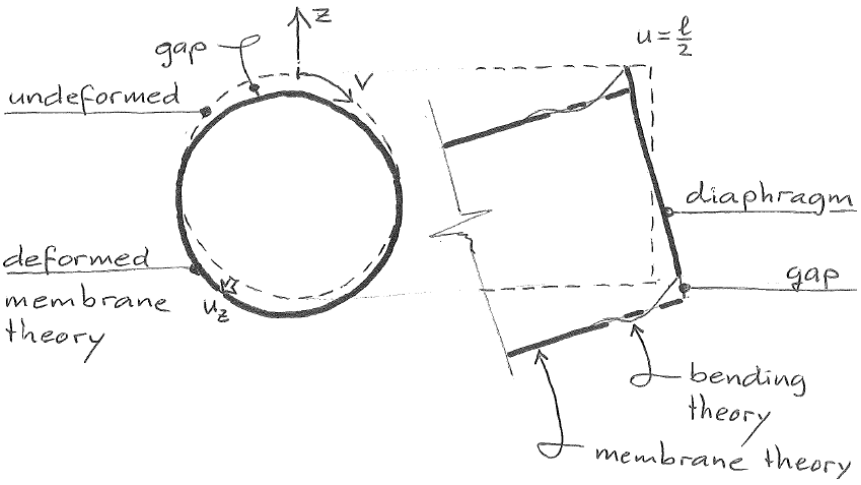

Figure 71. Boundary condition 1 is not fulfilled

Monocoque

The first airplane structures were a frame of wood or steel covered with a skin of cotton fabric. In 1912 a racing plane was built with a skin of three glued layers of wood veneer in total 4 mm thick (fig. 72, 73). This skin was also the load bearing structure, so a frame was not applied. The French company that build these planes was founded by Armand Deperdussin.[10] The plane was called the Deperdussin monocoque (Pronounce mo-no-cock without emphasis. Monos is alone in Greek; coquille is shell in French) [Wikipedia]. To us it looks like a normal plane but in those days its shape was different from any other plane, for example, it had one set of main wings instead of two above each other. The plane won several races and set the world speed record. Ever since, the word monocoque is used for structures that are fast and derive a large part of their strength from their skin. Examples are racing cars, rockets and army tanks.

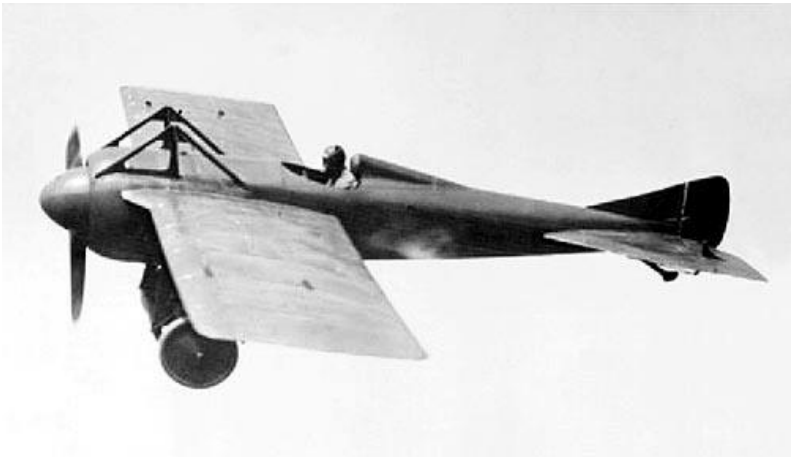

Figure 72. Deperdussin monocoque airplane [1913 Musée de l'Air et de l'Space, Paris]

[10] Armand Deperdussin (1860–1924) was a French business man [Wikipedia].



Figure 73. Fuselage of the Deperdussin monocoque
[G. Printamp 1912, Smithsonian's National Air and Space Museum, Washington]

Structural models overview
In scientific literature often the following names are used for structural idealisations.

structural element	name	deformation included
beams	Euler-Bernoulli beam	bending
	Timoshenko beam	bending and shear
plates loaded in plane	Navier equations	extension
plates loaded perpendicularly to their plane	Kirchhoff plate	bending
	Reissner-Mindlin plate (p. 61)	bending and shear
	Von Kármán-Föppl equations	extension, bending and large displacements
shells	Shell membrane equations (p. 38)	extension
	Sanders-Koiter equations (p. 54)	extension and bending
	several theories	extension, bending and shear

Shell theory
In 1888 Augustus Love [11] formulated the basic equations that govern the behaviour of thin elastic shells [13, 14]. He used Jacob Bernoulli's [12] hypothesis (p. 50), which was also used by Gustav Kirchhoff [13] in formulating the plate theory. In the years that followed there was much discussion on this shell theory. Some inconsistencies were found. Many scientists proposed other equations, such as Wilhelm Flügge [14] (1934) [15], Ralph Byrne [15] (1944) [16], Valentin Novozhilov [16] (1951) [17], Eric Reissner [17] (1952) [18] and Paul Naghdi [18] (1957)

[11] Augustus Love (1863–1940) was a mathematician and professor in Oxford. He presented his shell theory to the Royal Society at the age of 25 [Wikipedia].
[12] Jacob Bernoulli (1654–1705) was a professor of mathematics in Bazel [Wikipedia].
[13] Gustav Kirchhoff (1824–1887) was a German physicist and professor in Berlin, Breslau and Heidelberg. He is also well-known in physics for discoveries such as Kirchhoff's laws on electrical current [Wikipedia].
[14] Wilhelm Flügge (1904–1990) was professor of civil engineering in Göttingen. After the second world war he and his wife moved to the USA and became professors in Stanford [Wikipedia].
[15] Ralph Byrne (1912–1948) was associate professor of applied mechanics in Caltech, Pasadena. [27, 28]
[16] Valentin Novozhilov (1910–1987) was born in Lublin, Poland. He studied in Saint Petersburg and became a professor there [www.shellbuckling.com].

[19]. Also Love himself proposed improved equations [20]. Lyell Sanders [19] was the first to remove all inconsistencies from Love's first equations [21]. Independently, Warner Koiter [20] proved that Love's initial assumptions were correct after all and he also derived the correct shell equations [22, 23]. In 1959 there was a conference in the aula of Delft University where Sanders presented the correct shell equations and Koiter presented the correct shell equations. One of Koiter's papers on the subject has the clear title "All you need is Love" [24].

Love's first equations are called the first approximation theory. Including improvements they are referred to as the Sanders-Koiter equations (p. 54). Other theories account for out-of-plane shear deformation and are called higher-order approximation theory. They are for thick shells (p. 13).

Before 1959, equations were developed for specific shell shapes. For example, equations for cylindrical shells were proposed by Lloyd Donnell [21] (1934) [25] and Leslie Morley [22] (1959) [26].

Sanders-Koiter equations
The following 21 equations describe membrane action and bending action in thin shell structures. Equation 18 is derived below (p. 66). The other equations are not derived in these notes but they can be obtained in the same way. The derivation of Sanders and that of Koiter can be found in literature [21] and [22, 23] respectively. The derivation of Koiter is based on tensor analysis and is most rigorous. The equations are valid for elastic material behaviour and small displacements. They correctly predict no stresses for rigid translations. The equations do not change when the local coordinate system is rotated around the *z* axis. The equations correctly produce symmetrical stiffness matrices (Betti's reciprocal theorem). The Sanders-Koiter equations include the equations for plates. In other words, with appropriate values for $k_{xx}, k_{yy}, k_{xy}, \alpha_x, \alpha_y$ the Sanders-Koiter equations simplify to the equations for plates loaded in plane, plates loaded perpendicular to their plane (Kirchhoff theory), circular plates and the shell membrane equations (p. 38). This is clearly a remarkable achievement of the 20th century scientists. The Sanders-Koiter equations are a scientific masterpiece. [23]

---

[17] Eric Reissner (1913–1996) was professor of applied mechanics in MIT and San Diego. His father, Hans Reißner (1874–1967) was an aircraft engineer and professor in Aachen and Berlin. The family moved from Berlin to the Illinois just before the second world war [Wikipedia].
[18] Paul Naghdi (1924–1994) was born in Tehran. He studied in the USA and became professor of mechanical engineering in Berkeley [Wikipedia].
[19] Lyell Sanders (1924–1998) was professor of structural mechanics in Harvard [German Wikipedia].
[20] Warner Koiter (1914–1997) was professor of applied mechanics in Delft [Wikipedia].
[21] Lloyd Donnell (1895–1997) was professor of mechanical engineering in Illinois [Wikipedia].
[22] Leslie Morley (1924–2011) was a scientist in the Royal Aircraft Establishment and a professor in Brunel University, London [Wikipedia].

[23] The following dates provide a time frame. In 1822, Claude-Louis Navier formulated the Navier-Stokes equations which describe the behaviour of fluids [Wikipedia]. In 1850, Gustav Kirchhoff completed the differential equation that describes the behaviour of plates [Wikipedia]. In 1865, James Clerk-Maxwell unified many laws into Maxwell's equations that describe electric and magnetic fields [Wikipedia]. In 1916, Albert Einstein found the Einstein field equations describing the structure of the universe [Wikipedia]. In 1926, Erwin Schrödinger derived the Schrödinger equation of quantum mechanics describing materials on a very small scale [Wikipedia].

Table 4. Sanders-Koiter equations

kinematic equations	$\varepsilon_{xx} = \frac{\partial u_x}{\partial x} - k_{xx}u_z + k_x u_y$	1
	$\varepsilon_{yy} = \frac{\partial u_y}{\partial y} - k_{yy}u_z + k_y u_x$	2
	$\gamma_{xy} = \frac{\partial u_x}{\partial y} + \frac{\partial u_y}{\partial x} - 2k_{xy}u_z - k_x u_x - k_y u_y$	3
	$\varphi_x = -\frac{\partial u_z}{\partial x} - k_{xx}u_x - k_{xy}u_y$	4
	$\varphi_y = -\frac{\partial u_z}{\partial y} - k_{yy}u_y - k_{xy}u_x$	5
	$\varphi_z = \frac{1}{2}(-\frac{\partial u_x}{\partial y} + \frac{\partial u_y}{\partial x} - k_x u_x + k_y u_y)$	6
	$\kappa_{xx} = \frac{\partial \varphi_x}{\partial x} - k_{xy}\varphi_z + k_x \varphi_y$	7
	$\kappa_{yy} = \frac{\partial \varphi_y}{\partial y} + k_{xy}\varphi_z + k_y \varphi_x$	8
	$\rho_{xy} = \frac{\partial \varphi_x}{\partial y} + \frac{\partial \varphi_y}{\partial x} + (k_{xx} - k_{yy})\varphi_z - k_x\varphi_x - k_y\varphi_y$	9
constitutive equations	$n_{xx} = \frac{Et}{1-\nu^2}(\varepsilon_{xx} + \nu\varepsilon_{yy})$	10
	$n_{yy} = \frac{Et}{1-\nu^2}(\varepsilon_{yy} + \nu\varepsilon_{xx})$	11
	$\frac{n_{xy} + n_{yx}}{2} = \frac{Et}{2(1+\nu)}\gamma_{xy}$	12
	$m_{xx} = \frac{Et^3}{12(1-\nu^2)}(\kappa_{xx} + \nu\kappa_{yy})$	13
	$m_{yy} = \frac{Et^3}{12(1-\nu^2)}(\kappa_{yy} + \nu\kappa_{xx})$	14
	$m_{xy} = \frac{Et^3}{24(1+\nu)}\rho_{xy}$	15
equilibrium equations	$v_x = \frac{\partial m_{xx}}{\partial x} + \frac{\partial m_{xy}}{\partial y} + k_y(m_{xx} - m_{yy}) + 2k_x m_{xy}$	16
	$v_y = \frac{\partial m_{yy}}{\partial y} + \frac{\partial m_{xy}}{\partial x} + k_x(m_{yy} - m_{xx}) + 2k_y m_{xy}$	17
	$n_{xy} - n_{yx} = -k_{xy}(m_{xx} - m_{yy}) + (k_{xx} - k_{yy})m_{xy}$	18
	$p_x = -\frac{\partial n_{xx}}{\partial x} - \frac{\partial n_{yx}}{\partial y} - k_y(n_{xx} - n_{yy}) - k_x(n_{xy} + n_{yx}) + k_{xx}v_x + k_{xy}v_y$	19
	$p_y = -\frac{\partial n_{yy}}{\partial y} - \frac{\partial n_{xy}}{\partial x} - k_x(n_{yy} - n_{xx}) - k_y(n_{xy} + n_{yx}) + k_{yy}v_y + k_{xy}v_x$	20

	$p_z = -k_{xx}n_{xx} - k_{xy}(n_{xy} + n_{yx}) - k_{yy}n_{yy} - \frac{\partial v_x}{\partial x} - \frac{\partial v_y}{\partial y} - k_y v_x - k_x v_y$	21

Exercise: Novozhilov writes $\gamma_{xy} = \frac{\alpha_y}{\alpha_x}\frac{\partial}{\partial u}\left(\frac{u_y}{\alpha_y}\right) + \frac{\alpha_x}{\alpha_y}\frac{\partial}{\partial v}\left(\frac{u_x}{\alpha_x}\right) - 2k_{xy}u_z$ [17 p. 24]. Show that this is just another way of writing Sanders-Koiter equation 3.

Ping pong ball

Consider a sphere that is deformed into an ellipsoid (fig. 74). Think of a ping pong ball that is squeezed by your hand. The code below shows the evaluation of the Sanders-Koiter equations (p. 56) by Maple. The deformation $u_z = b\cos\frac{2u}{a}$, $u_x = 0.49b\sin\frac{2u}{a}$ has been obtained by trial and error to minimize the load p_x. The code produces figure 75. Displacement u_y and distributed force p_y are zero and p_x is almost zero. Only p_z is needed to obtain this deformation.

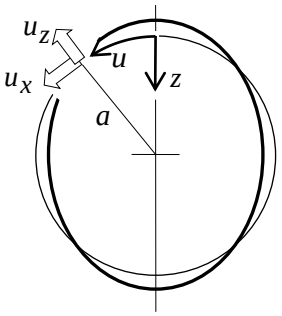

Figure 74. Deformation of a spherical ping pong ball into a prolate ellipsoid shape

```
> a:=20: t:=0.4: E:=1400: nu:=0.3: b:=1:
> kxx:=-1/a: kyy:=-1/a: kxy:=0: alphax:=1: alphay:=sin(u/a):
> ux:=-0.49*b*sin(2*u/a): uy:=0: uz:=b*cos(2*u/a):
>
> ky:=diff(alphay,u)/alphay/alphax: kx:=diff(alphax,v)/alphax/alphay:
> epsilonxx:=diff(ux,u)/alphax-kxx*uz+kx*uy:
> epsilonyy:=diff(uy,v)/alphay-kyy*uz+ky*ux:
> gammaxy:=diff(ux,v)/alphay+diff(uy,u)/alphax-2*kxy*uz-kx*ux-ky*uy:
> phix:=-diff(uz,u)/alphax-kxx*ux-kxy*uy:
> phiy:=-diff(uz,v)/alphay-kyy*uy-kxy*ux:
> phiz:=1/2*(-diff(ux,v)/alphay+diff(uy,u)/alphax-kx*ux+ky*uy):
> kappaxx:=diff(phix,u)/alphax-kxy*phiz+kx*phiy:
> kappayy:=diff(phiy,v)/alphay+kxy*phiz+ky*phix:
> rhoxy:=diff(phix,v)/alphay+diff(phiy,u)/alphax+(kxx-kyy)*phiz-kx*phix-ky*phiy:
> nxx:=E*t/(1-nu^2)*(epsilonxx+nu*epsilonyy):
> nyy:=E*t/(1-nu^2)*(epsilonyy+nu*epsilonxx):
> nxym:=E*t/(2*(1+nu))*gammaxy:
> mxx:=E*t^3/(12*(1-nu^2))*(kappaxx+nu*kappayy):
> myy:=E*t^3/(12*(1-nu^2))*(kappayy+nu*kappaxx):
> mxy:=E*t^3/(24*(1+nu))*rhoxy:
> vx:=diff(mxx,u)/alphax+diff(mxy,v)/alphay+ky*(mxx-myy)+2*kx*mxy:
> vy:=diff(myy,v)/alphay+diff(mxy,u)/alphax+kx*(myy-mxx)+2*ky*mxy:
> tmp:=kxy*(mxx-myy)-(kxx-kyy)*mxy:
> nxy:=nxym-tmp/2:
> nyx:=nxym+tmp/2:
> px:=-(diff(nxx,u)/alphax+diff(nyx,v)/alphay+ky*(nxx-nyy)+kx*(nxy+nyx)-kxx*vx-kxy*vy):
> py:=-(diff(nyy,v)/alphay+diff(nxy,u)/alphax+kx*(nyy-nxx)+ky*(nxy+nyx)-kyy*vy-kxy*vx):
> pz:=-(kxx*nxx+kxy*(nxy+nyx)+kyy*nyy+diff(vx,u)/alphax+diff(vy,v)/alphay+ky*vx+kx*vy):
>
> plot({ux,uy,uz,px/1.5,py/1.5,pz/1.5},u=0..Pi*a-1);
```

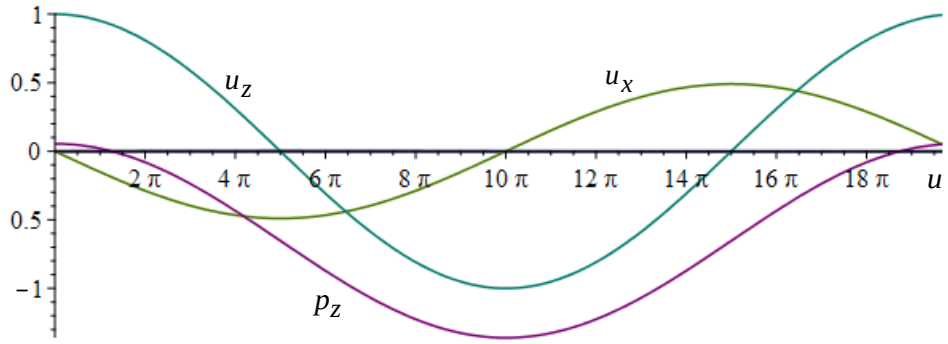

Figure 75. Loading p_z and deformation u_x, u_z of a ping pong ball computed by Maple

Compatibility equation

Sanders-Koiter equations 1 to 9 (p. 54) can be combined, resulting in the following equation.

$$-\frac{\partial^2 \varepsilon_{xx}}{\partial y^2}+\frac{\partial^2 \gamma_{xy}}{\partial x \partial y}-\frac{\partial^2 \varepsilon_{yy}}{\partial x^2}=-k_{yy}\kappa_{xx}+k_{xy}\rho_{xy}-k_{xx}\kappa_{yy}$$

In the derivation is used that k_x, k_y and k_G are small (appendix p. 199). This equation shows that the strains of the middle surface are connected to the bending deformation. So, we cannot randomly choose functions for the strains $\varepsilon_{xx}, \gamma_{xy}, \varepsilon_{yy}$ and randomly choose functions for bending curvatures $\kappa_{xx}, \rho_{xy}, \kappa_{yy}$ and expect this could happen in a specific shell with curvatures k_{xx}, k_{xy}, k_{yy}. Therefore, this equation is called the *compatibility equation*. See Shell behaving like a plate (p. 114).

Rigid translation

The Sanders-Koiter equations (p. 54) are accurate for small displacements. However, for large rigid translations they are accurate too. For example, consider a reinforced concrete industrial chimney with a height of 70 m, a radius a = 2.6 m and a wall thickness t = 0.1 m. During a storm the chimney top moves b = 1.0 m which is not exceptional for a chimney of this height.

A rigid translation of the whole chimney (fig. 76) can be described exactly by the displacements

$$u_x=0, \quad u_y=b\cos\frac{v}{a}, \quad u_z=b\sin\frac{v}{a}\ .$$

Obviously, this translation should not produce strains.

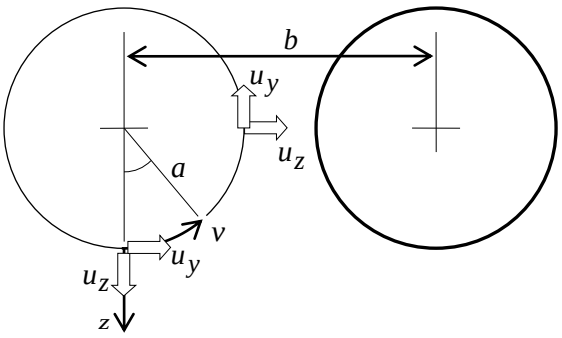

Figure 76. Rigid translation of a cylinder cross-section

From the chimney geometry it follows that $k_{xx}=0,\quad k_{yy}=-\frac{1}{a},\quad k_{xy}=0,\quad \alpha_x=1,\quad \alpha_y=1.$

Substitution of these in the kinematic equations 1 to 9 gives

$$\varepsilon_{xx}=0,\quad \varepsilon_{yy}=0,\quad \gamma_{xy}=0,\quad \kappa_{xx}=0,\quad \kappa_{yy}=0,\quad \rho_{xy}=0,$$

which is the correct result. Consequently, the large deflection of the chimney top can be described by the Sanders-Koiter equations.

Exercise: Large rigid rotations do produce unrealistic strains and stresses. Check the Sanders-Koiter equations for this.

Shell differential equations

When the Sanders-Koiter equations (p. 54) are substituted into each other, the following two coupled partial differential equations are obtained (assuming $p_x=p_y=0$ and v_x, v_y, $n_{xy}-n_{yx}$ are small).

$$-\Gamma\phi+\frac{Et^3}{12(1-\nu^2)}\nabla^2\nabla^2 u_z=p_z$$

and

$$\nabla^2\nabla^2\phi+Et\Gamma u_z=0,$$

where,

$$\Gamma(.)=k_{xx}\frac{\partial^2(.)}{\partial y^2}-2k_{xy}\frac{\partial^2(.)}{\partial x\partial y}+k_{yy}\frac{\partial^2(.)}{\partial x^2},$$

$$\nabla^2(.)=\frac{\partial^2(.)}{\partial x^2}+\frac{\partial^2(.)}{\partial y^2}.$$

ϕ is the Airy stress function,[24] which is related to the membrane forces

$$n_{xx}=\frac{\partial^2\phi}{\partial y^2},\qquad n_{yy}=\frac{\partial^2\phi}{\partial x^2},\qquad n_{xy}=n_{yx}=-\frac{\partial^2\phi}{\partial x\partial y}.$$

[24] George Airy (1801–1892) was an astronomy professor in Cambridge, England [Wikipedia]

Differential equation type
Linear partial differential equations of the second order are subdivided in three types; elliptic, parabolic and hyperbolic [Wikipedia]. Physicists use this to predict the nature of the solution and select a solution method. The membrane part of the shell differential equations (p. 58) is

$$-\Gamma\phi = p_z$$

In a well-designed thin shell, this part dominates the behaviour. It can be shown that the type of this differential equation depends on the Gaussian curvature k_G (p. 23).

$k_G > 0 \quad \Rightarrow$ elliptic, the solution is local
$k_G = 0 \quad \Rightarrow$ parabolic, the solution extends along one straight line
$k_G < 0 \quad \Rightarrow$ hyperbolic, the solution extends along two straight lines, which are called *characteristics*

Shallow shell differential equation
For cylinders and spheres k_{xx}, k_{yy}, k_{xy} are uniform. This reduces the shell differential equations (p. 58) to

$$\frac{E\,t^3}{12(1-\nu^2)}\nabla^2\nabla^2\nabla^2\nabla^2 u_z + E\,t\,\Gamma\Gamma u_z = \nabla^2\nabla^2 p_z\,.$$

This is a linear eight order partial differential equation in curvilinear coordinates *u* and *v* (p. 31).

A *shallow shell* is a shell with a sagitta (p. 1) that is small compared to its span. For such shells the curvatures do not change much over the surface and the above differential equation can be a good approximation.

A limitation of the shallow shell differential equation is that we cannot fix u_x or u_y on boundaries. This leads to inextensional deformation of shells with negative Gaussian curvatures.

Plate boundary conditions
In general, the solution to an eight order partial differential equation has 8 constants in the *u* direction and 8 constants in the *v* direction. The constants can be solved by 4 boundary conditions on each edge. Figure 77 shows the boundary conditions of a canopy that is fixed on one edge. Note that there are too many boundary conditions. So, some boundary conditions cannot be fulfilled.

This problem also occurs in plates. It was solved by Gustav Kirchhoff [3] in 1850 [29]. He derived the correct boundary conditions of plates from virtual work. Others interpreted his solution as that the stresses due to the torsion moment m_{xy} go round in the edge (fig. 78-1). Therefore, m_{xy} on the edge needs be replaced by a *concentrated shear force V* in the edge (fig. 78-2).

$$m_{xy}dx = Vdx \quad \Rightarrow \quad \boxed{V = m_{xy}}$$

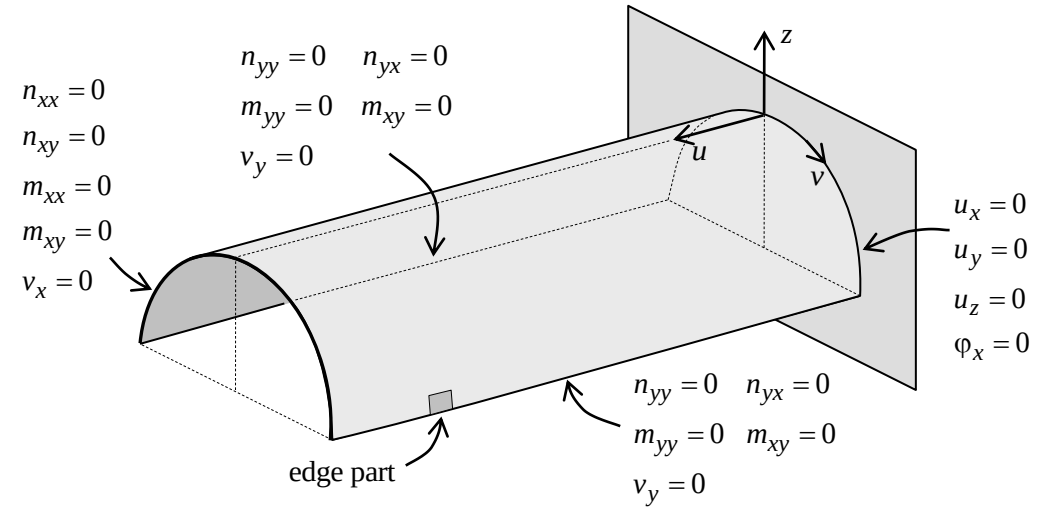

Figure 77. Boundary conditions of a canopy

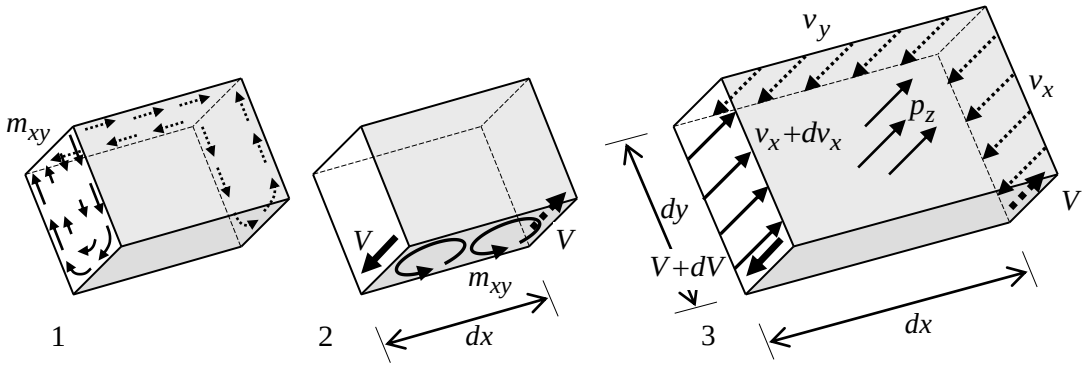

Figure 78. Forces on an edge part

From equilibrium of a somewhat larger edge part (fig. 78-3) it follows that

$$p_z dxdy - v_y dx + (v_x + dv_x)dy - (V + dV) + V - v_x dy = 0\,.$$

This can be simplified to

$$p_z dy - v_y + \frac{dv_x}{dx}dy - \frac{dV}{dx} = 0\,.$$

When $dy \downarrow 0$ then $-v_y - \frac{dV}{dx} = 0$ which can be written as

$$v_y = -\frac{\partial V}{\partial x}\,.$$

Now we have 4 boundary conditions per edge and the differential equation can be solved (fig. 79).

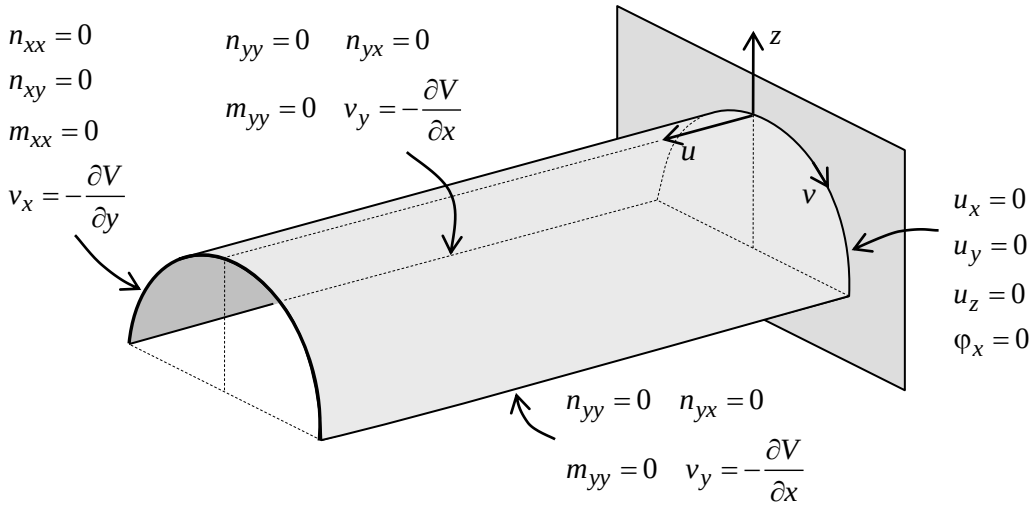

Figure 79. Boundary conditions according to Kirchhoff (plates)

Thus, according to Kirchhoff, m_{xy} need not be zero on a plate or shell edge in the *x* or *y* direction. Also v_x need not be zero on an edge in the *y* direction, and v_y need not be zero on an edge in the *x* direction. Clearly, in reality they are zero.

We need to interpret m_{xy} on an edge as a concentrated shear force V in the edge.

We need to interpret v on an edge as a change in the concentrated shear force V.

However, the plate boundary conditions are not entirely correct for shells (see shell boundary conditions p. 68).

Exercise: In Kirchhoff plates $m_{xy} = 0$ in a fixed edge along the *x* or *y* direction. In shells this can be observed too, however, there are exceptions. Can we show this with the Sanders-Koiter equations?

Reissner-Mindlin plate theory[25]

It is possible to come up with a new shell theory that does not have interpretation problems of the boundary conditions? In fact, the *Reissner-Mindlin theory* [29] for thick plates predicts m_{xy}, v_x and v_y on edges realistically without interpretations (fig. 77). However, to compute these values accurately we need to use very small finite elements on the edges. For example, when a plate is 180 mm thick we need to use finite elements that are less than 20 mm wide. This is impractical due to large computation time and therefore almost never applied. A practical element for a 180 mm plate is more than 250 mm wide. For this mesh m_{xy} will not be zero on the edges also not when the Reissner-Mindlin theory is used. Therefore, also in the Reissner-Mindlin theory we need to interpret the torsion moment on an edge as a concentrated shear force in the edge.

[25] The name of this theory refers to Eric Reissner and Raymond Mindlin. Eric Reissner (1913–1996) was a professor of applied mechanics at MIT and the University of California San Diego [Wikipedia]. Raymond Mindlin (1906–1987) was a professor of applied science at Columbia University, USA [Wikipedia]. From our point of view they were very skilled in mathematics. They had to be because they did not have computers.

Edge shear stresses
The shear stress in a plate edge or shell edge is [26]

$$\sigma_{xz} = \frac{3}{2}\frac{v_x}{t} - \frac{3}{2}\sqrt{10}\frac{V}{t^2}.$$

The formula is valid when the local *x* axis points in the direction of the edge and the local *y* axis points outwards (fig. 80). Unfortunately, finite element programs using shell elements do not compute this stress. If important, we need to calculate and check this stress by hand.

The concentrated shear force produces a local stress peak. In many structures a local stress peak is not important because the stress will redistribute (steel yields, reinforced concrete cracks). However, a stress peak is important for materials that do not yield such as glass. A stress peak is also important for fatigue.

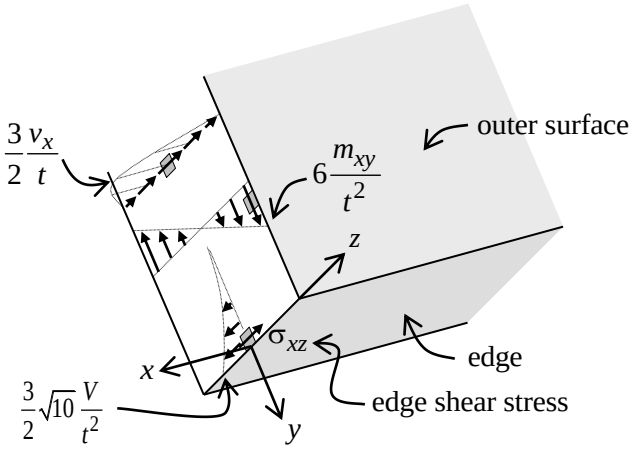

Figure 80. Shear stresses in a free shell edge

Reinforced concrete plate edges
In reinforced concrete plates it is common practice to put hairpins in the edges (fig. 81). A hairpin is a reinforcing bar that is bend in the shape of a U. The hairpins have the same diameter and spacing as the bars perpendicular to the edge. There is a good reason for these hairpins. They carry the concentrated shear force (fig. 82).

[26] In 2010, Johan Blaauwendraad (professor of structural mechanics at Delft University) used Reissner's plate theory (p. 62) to derive the stresses in plate edges. He showed that the shear stress distribution is exponential and the factor of the peak stress is $\frac{3}{2}\sqrt{10}$ [29]. In 2013, Rutger Zwennis (at that time a student at Delft University) modelled a plate loaded in torsion using volume finite elements [30]. He showed that the peak stress due to *V* includes the factor 4.48 instead of $\frac{3}{2}\sqrt{10}$ = 4.74. Who is right? The Reissner plate theory is not exact because Reissner made several assumptions in the derivation. The finite element analyses is not exact either because the number of elements is restricted. In these notes the safe choice of $\frac{3}{2}\sqrt{10}$ has been made. Future computers will be able to determine the factor accurately.

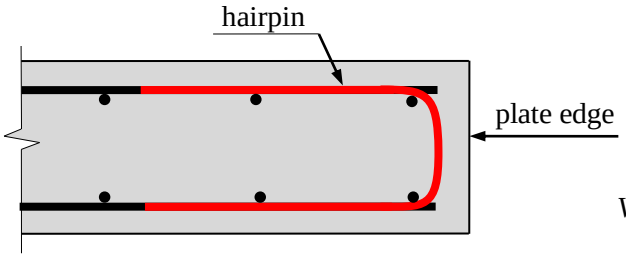

Figure 81. Reinforcement in a cross-section of a concrete plate edge

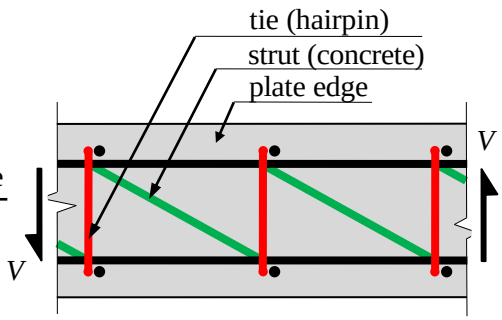

Figure 82. Strut-and-tie model of a reinforced concrete plate edge

Edges that are not in the *x* or *y* direction

If an edge is not in the *x* direction or *y* direction, the shear force v_x and the torsion moment m_{xy} need to be transformed to the edge direction. For this we need to rotate the local coordinate systems of the edge finite elements such that one of the axes is in the direction of the edge. The obtained concentrated shear force on a free or simply supported edge can be easily checked because it is equal to $V = \pm\sqrt{m_{xy}^2 - m_{xx}m_{yy}}$, where m_{xy}, m_{xx} and m_{yy} are the moments before rotation.

Proof: Plate moments are a tensor (p. 97). m_1 and m_2 are the principal values (p. 98). The product $m_1 m_2$ is an invariant (p. 23) of this tensor. Therefore, $m_1 m_2 = m_{xx}m_{yy} - m_{xy}^2 = m_{ss}m_{tt} - m_{st}^2$. Suppose that the *s* axis is perpendicular to the shell edge. Since the edge is free or simply supported $m_{ss} = 0$. Therefore, $m_{xx}m_{yy} - m_{xy}^2 = -m_{st}^2 = -V^2$. Q.E.D.

Palazzetto dello sport [31]

The palazzetto dello sport (p. 1) was built for the 1960 summer Olympics in Rome (fig. 1). It hosted basketball. Nowadays, it is a sports and community centre.

The buttresses are made of prefab concrete. The shell and ribs are made of reinforced concrete that was cast in situ. The formwork of the shell consisted of 1620 cassettes supported by steel tube scaffolding. The cassettes were made of 25 mm thick ferrocement (fig. 83). Ferrocement is a thin layer of mortar with a steel wire mesh inside.

Construction sequence of the dome	*Completed*
- Placing the buttresses - Building the scaffolding for the cassettes. The scaffolding included circular rings made of curved rails of an old railway track. These rings were horizontally elevated onto temporary columns of steel tubes.	
- Building a timber template of a large part of the shell internal surface - Drawing the grid onto the template	August 1956
- Fabrication of moulds for the cassettes. First, onto the timber template the inside shape of one cassette was made of bricks and plaster (fig. 84). Second, a cassette was made onto this inside shape. Third, this cassette was moved down and several moulds were made of this cassette. Etc. - Prefabrication of 30 cassettes a day - Placing the cassettes onto the scaffolding (fig. 85, 86)	December 1956
- Placing reinforcing bars in and on the cassettes - Pouring concrete (fig. 87)	February 1957

architect:	Annibale Vitellozzi (1903-1990)
engineer:	Pier Luigi Nervi (1891-1979)
contractor:	Bartoli

Computer analyses were not performed. Structural calculations were done by hand and checked by scale model tests.

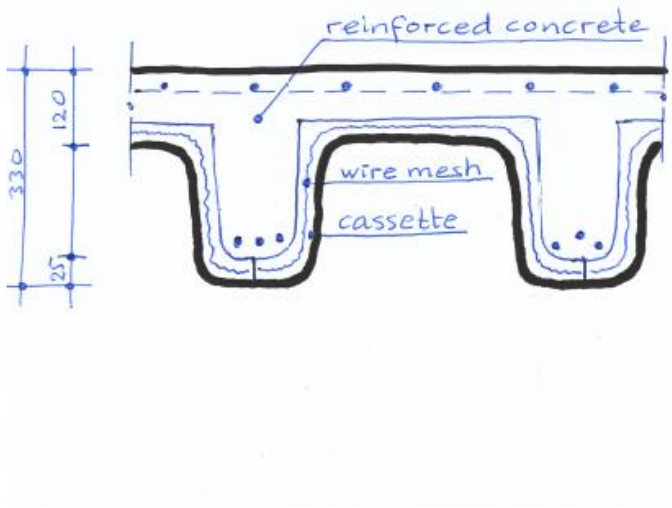

Figure 83. Cross-section of the shell and ribs

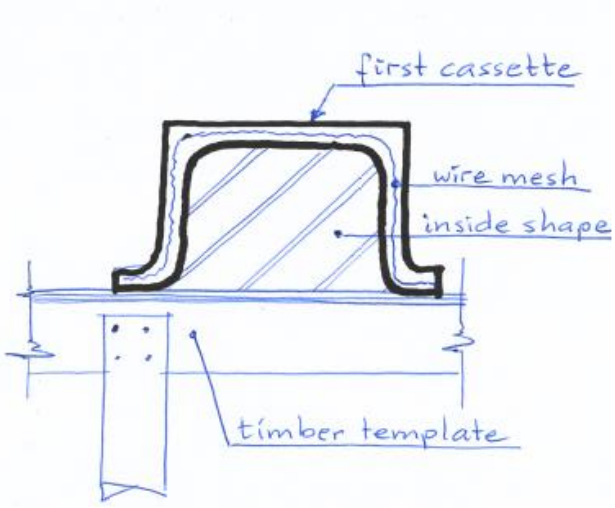

Figure 84. Mould fabrication



Figure 85. A cassette […, 1957]



Figure 86. Scaffolding and cassettes [..., 1957]



Figure 87. Construction site during concrete pouring [..., 1957]

$n_{xy} \neq n_{yx}$

Sanders and Koiter independently derived that for shells $n_{xy} \neq n_{yx}$. This is a very strange result because shear stresses on perpendicular faces of an infinitesimal cube have the same magnitude $\sigma_{xy} = \sigma_{yx}$ (fig. 88). If the shear stresses are the same, the shear membrane forces must be the same. Nevertheless, Sanders and Koiter are right. This strange results follows from moment equilibrium around the *z* axis of an elementary shell part (see derivation of equation 18 p. 67). It can also be seen in the definition of membrane forces for thick shells in the appendix on p. 201.

Finite element programs plot the mean membrane shear force $\frac{1}{2}(n_{xy} + n_{yx})$. It would be interesting to plot the quantity $\frac{1}{2}(n_{xy} - n_{yx})$ too, however, finite element programs do not have this option. It can be shown that $\frac{1}{2}(n_{xy} - n_{yx})$ does not change when the local coordinate system rotates around the *z* axis (it is an invariant). When $\frac{1}{2}(n_{xy} - n_{yx})$ is large compared

to $\frac{1}{2}(n_{xy}+n_{yx})$ then the shell is very thick and should be modelled by volume elements instead of shell elements (see shell thickness p. 13).

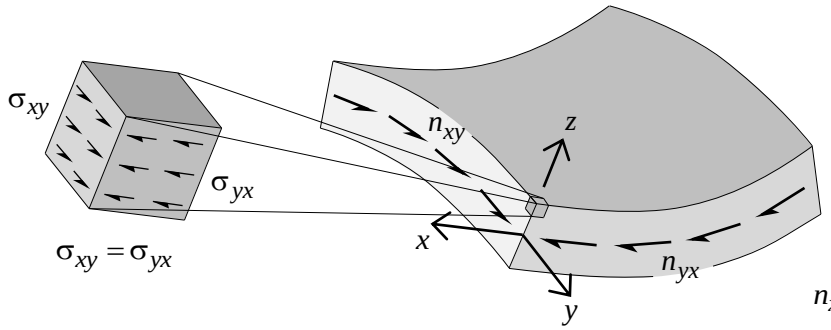

Figure 88. Shear stresses on a small cube

Figure 89. In plane shear forces on a shell part

Challenge: The tensor $\begin{bmatrix} n_{xx} & n_{xy} \\ n_{yx} & n_{yy} \end{bmatrix}$ is not symmetrical. Are the principal directions perpendicular? In what situation are the principal values complex numbers?

Derivation of equation 18

In this note the eighteenth Sanders-Koiter equation (p. 54) is derived. Consider moment equilibrium of a small shell part around the *z* axis (fig. 90). When the part is only twisted, the bending moments can produce a resulting moment around the *z* axis.

$$M_{z1} = m_{xx}\,dy\;\; k_{xy}\,dx - m_{yy}\,dx\;\; k_{xy}\,dy$$

When the part is curved but not twisted the torsion moment can produce a resulting moment around the *z* axis.

$$M_{z2} = m_{xy}\,dx\;\; k_{yy}\,dy - m_{xy}\,dy\;\; k_{xx}\,dx$$

The in plane shear forces can also produce a moment around the *z* axis.

$$M_{z3} = n_{xy}\,dy\,dx - n_{yx}\,dx\,dy$$

The total moment around the *z* axis must be zero.

$$M_{z1} + M_{z2} + M_{z3} = 0$$

This evaluates to

$$k_{xy}(m_{xx} - m_{yy}) - (k_{xx} - k_{yy})m_{xy} + n_{xy} - n_{yx} = 0\,.$$

Q.E.D.

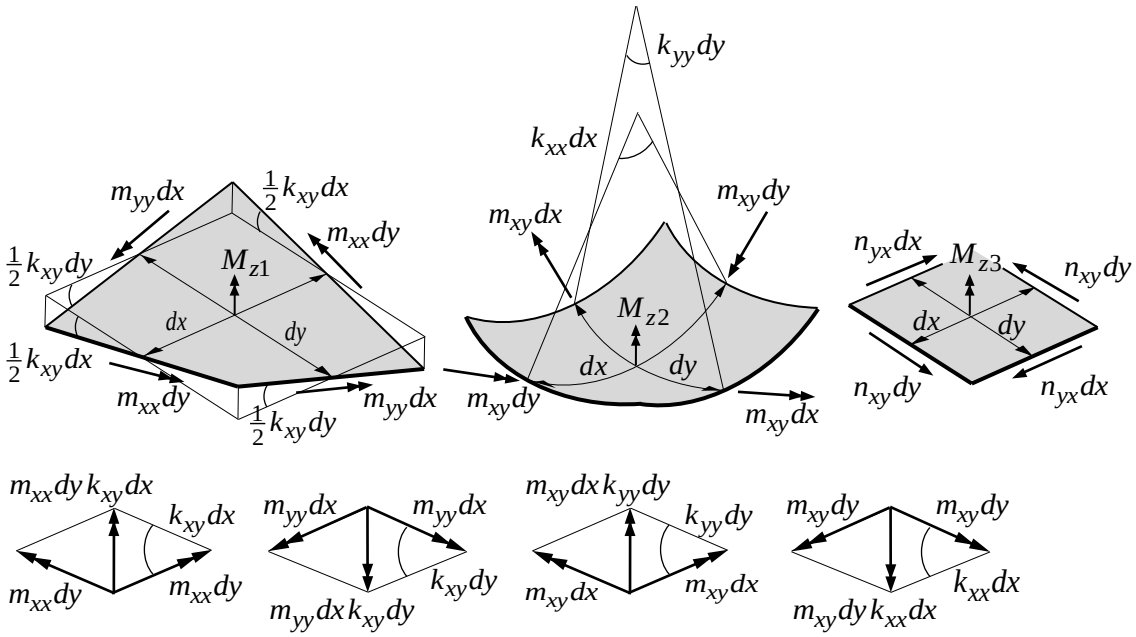

Figure 90. Moment equilibrium around the z axis

Shell boundary conditions

The plate boundary conditions (p. 60) are not completely correct for shells. A shell edge has 3 displacements and 1 rotation. If a value is imposed to one of these a support reaction occurs. Table 5 shows the formulas for computing the support reactions. They are derived from equilibrium of small edge parts (fig. 91 and 92). The table is valid for an edge in the *x* direction and the *y* axis pointing outwards. Clearly, instead of imposing a displacement, a distributed edge load can be applied. The table can also be used for formulating these boundary conditions.

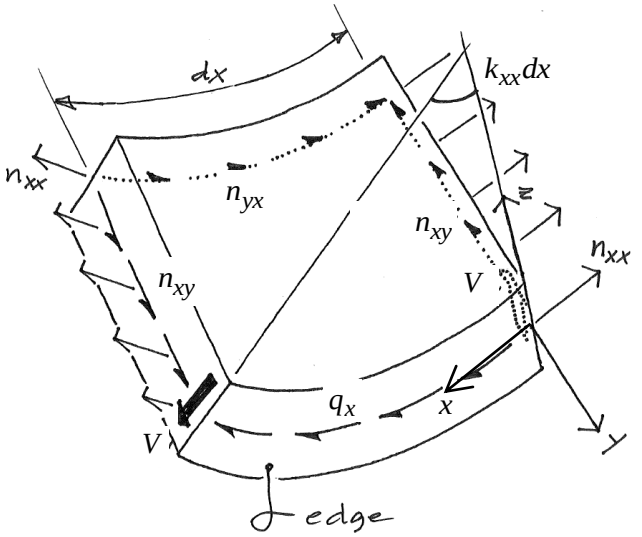

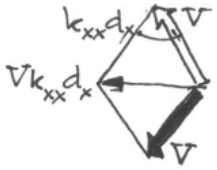

$$q_x dx + V\,k_{xx}dx - n_{yx}dx = 0$$

Figure 91. Equilibrium of a shell edge loaded by a distributed shear force q_x

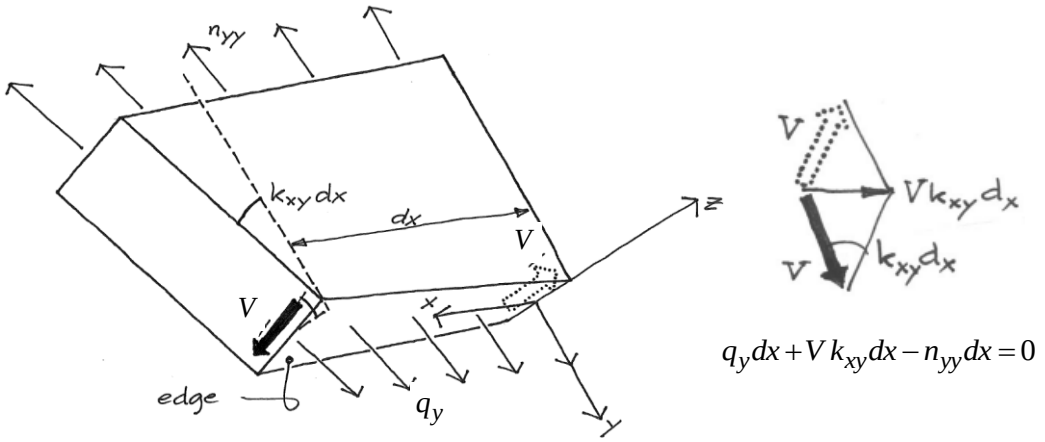

Figure 92. Equilibrium of a shell edge loaded by a distributed normal force q_y

Table 5. Boundary conditions for an edge in the x direction and the y axis pointing outwards

Kinematic (K)			Dynamic (D)	
Impose displacement	u_x	or apply line load	$q_x = n_{yx} - k_{xx}V$.	1
Impose displacement	u_y	or apply line load	$q_y = n_{yy} - k_{xy}V$.	2
Impose displacement	u_z	or apply line load	$q_z = v_y + \frac{\partial V}{\partial x}$.	3
Impose rotation	$-\varphi_y$	or apply line moment	$-m_{yy}$.	4

Table 6. Boundary conditions for an edge in the x direction and the y axis pointing inwards

Impose displacement	u_x	or apply line load	$q_x = -n_{yx} + k_{xx}V$.	5
Impose displacement	u_y	or apply line load	$q_y = -n_{yy} + k_{xy}V$.	6
Impose displacement	u_z	or apply line load	$q_z = -v_y - \frac{\partial V}{\partial x}$.	7
Impose rotation	$-\varphi_y$	or apply line moment	m_{yy} .	8

Table 7. Boundary conditions for an edge in the y direction and the x axis pointing outwards

Impose displacement	u_x	or apply line load	$q_x = n_{xx} - k_{xy}V$.	9
Impose displacement	u_y	or apply line load	$q_y = n_{xy} - k_{yy}V$.	10
Impose displacement	u_z	or apply line load	$q_z = v_x + \frac{\partial V}{\partial y}$.	11
Impose rotation	φ_x	or apply line moment	m_{xx} .	12

Table 8. Boundary conditions for an edge in the y direction and the x axis pointing inwards

Impose displacement	u_x	or apply line load	$q_x = -n_{xx} + k_{xy}V$.	13
Impose displacement	u_y	or apply line load	$q_y = -n_{xy} + k_{yy}V$.	14
Impose displacement	u_z	or apply line load	$q_z = -v_x - \frac{\partial V}{\partial y}$.	15
Impose rotation	φ_x	or apply line moment	$-m_{xx}$.	16

Exercise: Proof that $m_{xy} = 0$ in a free corner.

Canopy example, shell boundary conditions

The canopy in figure 93 has curvatures $k_{xx} = k_{xy} = 0,\ k_{yy} = -\frac{1}{a}$. Substitution of these curvatures in the shell boundary conditions (p. 68) gives the canopy boundary conditions.

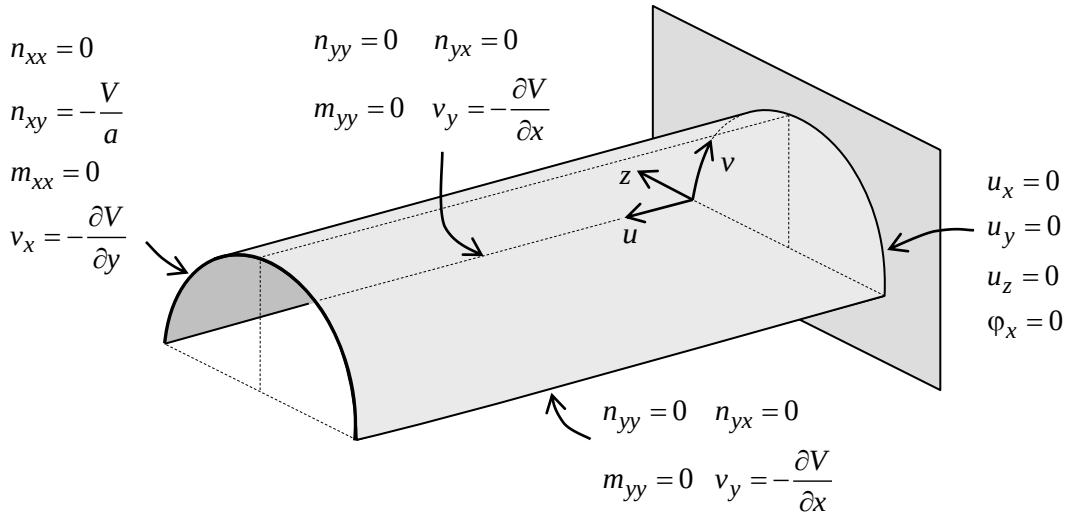

Figure 93. Shell boundary conditions of the canopy. (Compare with fig. 79)

Diaphragm boundary condition

A tube is often closed by a thin wall, called *diaphragm* (fig. 94). The diaphragm can be bend easily out of its plane but it resists deformation in its plane. Therefore, the diaphragm prevents displacement of the tube edge perpendicular to the tube. It also prevents displacement of the tube edge in the direction of the edge. The other displacements are free. This is called a *diaphragm boundary condition*. It is often applied in shell analysis. (Examples on p. 47 and p. 163)

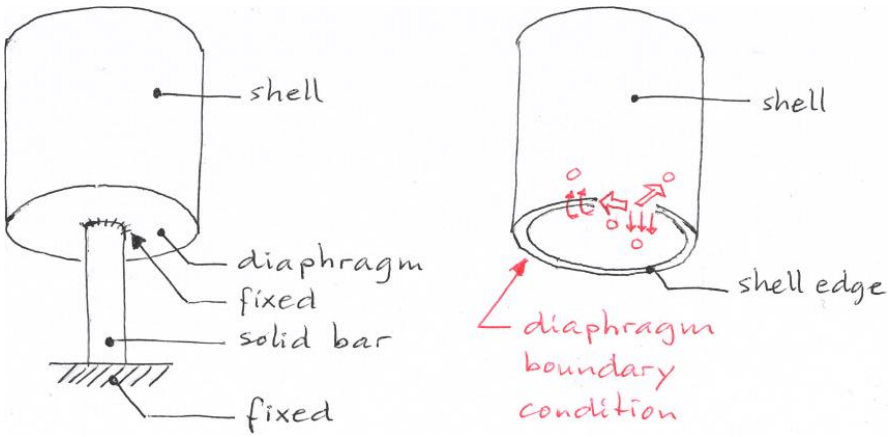

Figure 94. The diaphragm boundary condition can replace a diaphragm.

Edge in the *y* direction	Edge in the *x* direction
$n_{xx} - k_{xy}V = 0$	$u_x = 0$
$u_y = 0$	$n_{yy} - k_{xy}V = 0$
$u_z = 0$	$u_z = 0$
$m_{xx} = 0$	$m_{yy} = 0$

Overview of the shell variables

The table below gives an overview of the variables in the Sanders-Koiter equations (p. 54). The variables that need solving are green. They are called *dependent variables*. Note that there are 21 dependent variables and 21 Sanders-Koiter equations. Boundary conditions (p. 68) are imposed on the red edges.

material, thickness

curvature

Lamé parameters

in plane curvature of the parameter lines

displacement

strain of the middle surface

slope

deformation curvature

membrane force

moment

shear force, out of plane

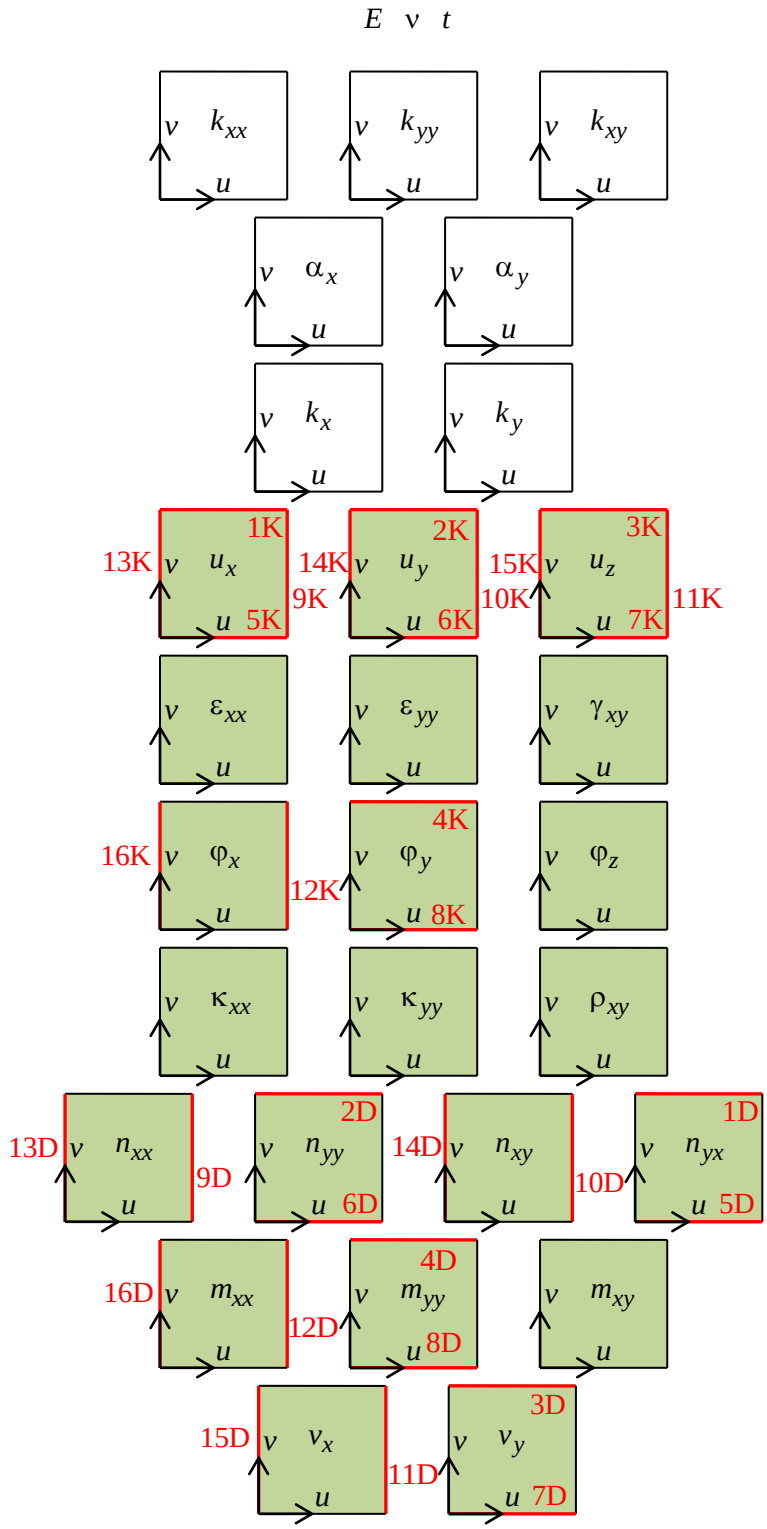

load

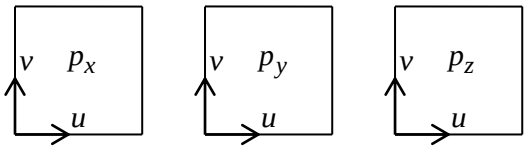

Generalised edge disturbance
An edge disturbance is a large moment at a discontinuity in a shell. This moment is local and at some distance of the discontinuity it is much smaller. Examples of discontinuities are

- Fixed edge or pinned edge
- Point load or line load
- Discontinuity in the distributed load
- Discontinuity in the derivative of the distributed load
- Discontinuity in the middle surface
- Discontinuity in the slope of the middle surface (C_0 continuity p. 11)
- Discontinuity in the curvature of the middle surface (C_1 continuity)
- Change in sign of the Gaussian curvature (p. 23, see differential equation type p. 59)
- Discontinuity in the material stiffness
- Discontinuity in the shell thickness

Exercise: Which of the above discontinuities occur in a torus?

Beam supported by springs
A long beam is supported by uniformly distributed springs (fig. 95). The bending stiffness of the beam is EI [Nm²]. The stiffness of the distributed springs is k [N/m²]. The differential equation that describes this beam is

$$EI\,\frac{d^4w}{dx^4} + k\,w = 0\,.$$

At the left beam end a displacement is imposed and the slope is zero. The right beam end is far away. The boundary conditions are

$$\text{if}\quad x=0\quad\text{then}\quad w=w_0\quad\text{and}\quad \frac{\partial w}{\partial x}=0$$

$$\text{if}\quad x\to\infty\quad\text{then}\quad w=0\quad\text{and}\quad \frac{\partial w}{\partial x}=0$$

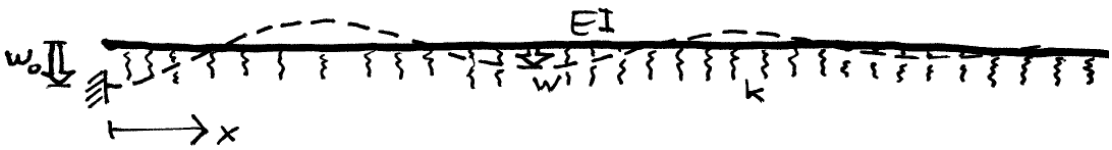

Figure 95. Beam supported by distributed springs and loaded by an imposed displacement w_0

The solution is

$$w = w_0\,(\sin\frac{\pi x}{l_i} + \cos\frac{\pi x}{l_i})\exp\frac{-\pi x}{l_i},$$

where

$$l_i = \sqrt{2}\,\pi \sqrt[4]{\frac{EI}{k}}$$

is the halve wave length.

Figure 96 shows displacement *w*, moment $M = -EI\,\frac{\partial^2 w}{\partial x^2}$ and shear force $V = \frac{\partial M}{\partial x}$.

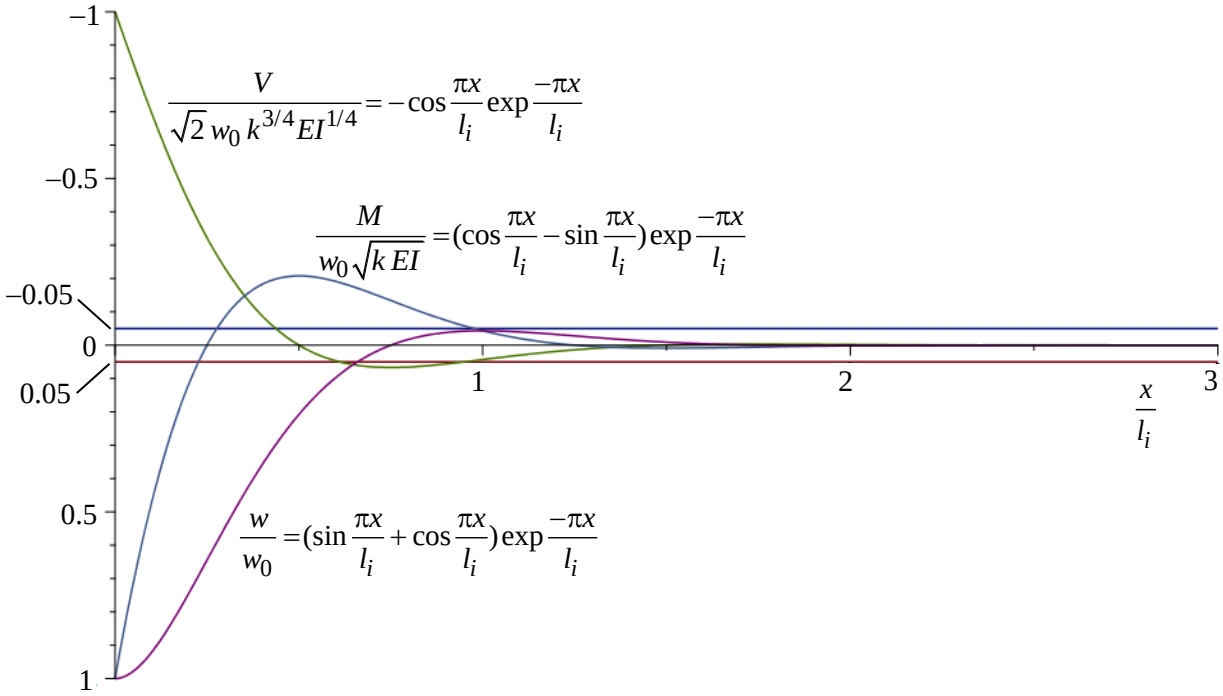

Figure 96. Displacement w, moment M and shear force V in the beam

Exercise: Suppose that the beam end is not fixed but pinned. What is the ratio of the pinned largest moment and the fixed largest moment?

Exercise: Suppose that the imposed displacement is removed, the left beam end is fixed and a uniformly distributed load *q* is applied to the beam. What changes to the differential equation, boundary conditions and solution?

Influence length

In figure 96 we see that the peak values occur at the left beam end. At some distance from the end the values are much smaller. At a distance $x = l_i$, all values are a bit smaller than 5% of the peak values (ignoring the signs). This distance is called the influence length. The influence length happens to be the same as the halve wave length l_i.

Exercise: What is the exact value of "a bit smaller than 5%" ?

Influence length of a cylinder edge

Consider a circular cylinder (fig. 97).

$$k_{xx} = 0 \qquad k_{yy} = \frac{-1}{a} \qquad k_{xy} = 0 \qquad \alpha_x = 1 \qquad \alpha_y = 1$$

An axial symmetric displacement is described by

$$u_x = -\frac{\nu}{a}\int w(u)du \qquad u_y = 0 \qquad u_z = w(u) \qquad p_z = 0$$

Please note the difference between ν (Poisson's ratio) and *v* (curvilinear coordinate). Surface load is not applied $p_z = 0$. These 9 equations have been substituted in the Sanders-Koiter equations (p. 54). The result is (see derivation in appendix p. 200)

$$\frac{Et^3}{12(1-\nu^2)}\frac{d^4w}{du^4} + \frac{Et}{a^2}w = 0$$

This is the same differential equation as that of a beam supported by springs (p. 71). Apparently we can make the following interpretation.

$$\frac{Et^3}{12(1-\nu^2)} = EI \qquad \frac{Et}{a^2} = k$$

Using the analogy, the influence length of a cylinder edge is

$$l_i = \sqrt{2}\,\pi\sqrt[4]{\frac{EI}{k}} = \frac{\pi}{\sqrt[4]{3(1-\nu^2)}}\sqrt{at} \qquad \boxed{l_i \approx 2.4\sqrt{at}}$$

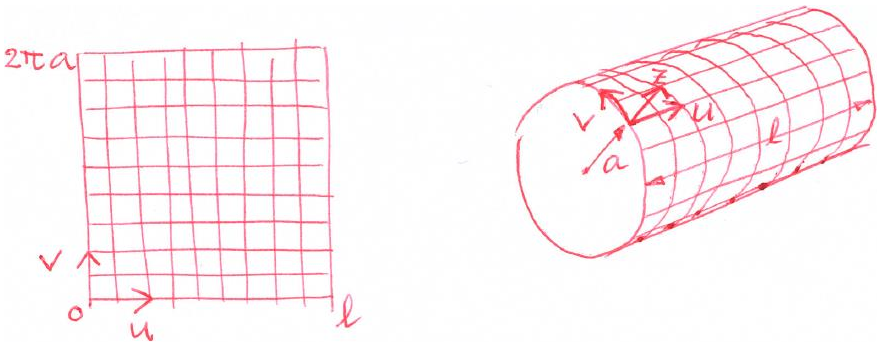

Figure 97. Cylinder parameterisation and dimensions

Exercise: Apparently, a shell can be sometimes interpreted as a beam supported by uniformly distributed springs. Which shell part is the beam and which shell part are the springs?

Influence lengths of all shells

Figure 98 gives influence lengths of edges of elementary shells. In more complicated shells the influence length of edge disturbances (p. 14, 72) can be estimated by comparing to the elementary shell shapes.

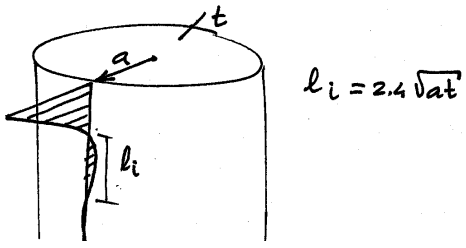

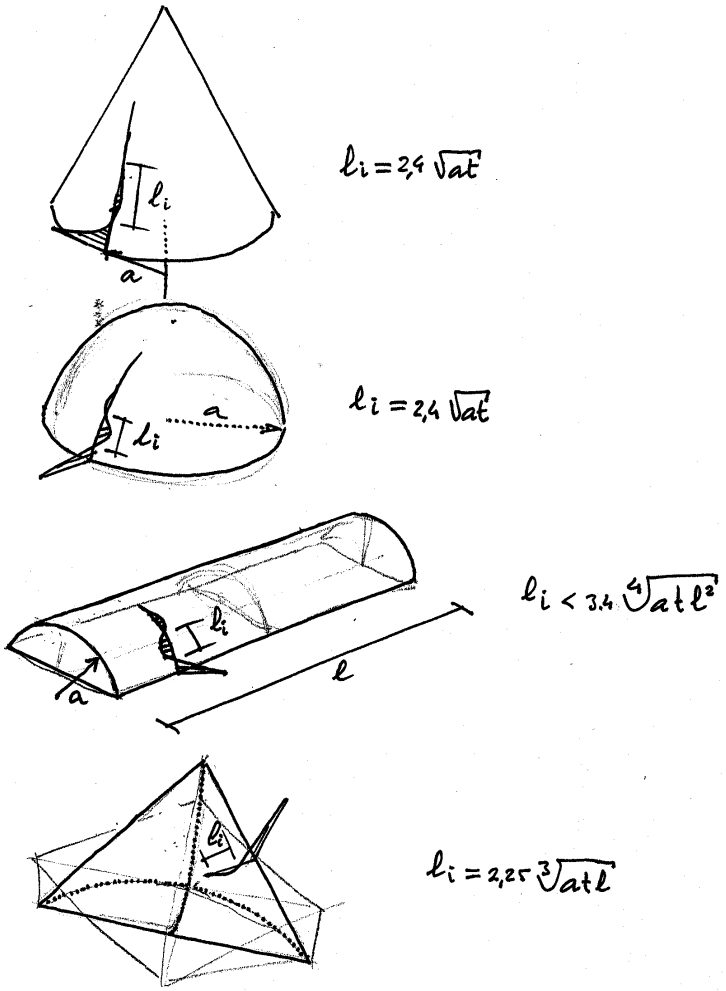

Figure 98. Influence lengths of elementary shell shapes [32]

Finite element mesh

The influence length can be used to choose a finite element mesh (p. 11, 84). If we use elements that approximate a solution linearly we need at least 6 elements in a length l_i in order to obtain solutions with some accuracy (fig. 99). This provides a rule for the finite element length perpendicular to a shell discontinuity. Clearly, smaller elements will improve the accuracy.

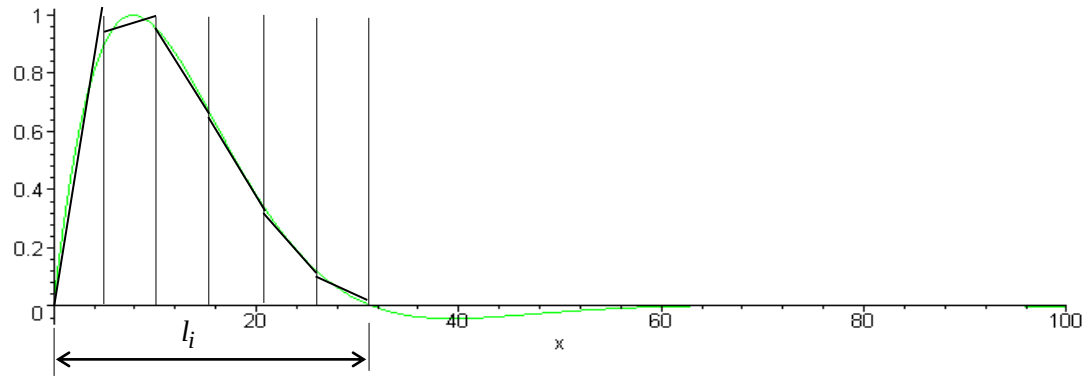

Figure 99. Piece-wise linear approximation of a solution

Exercise: For plates the recommended element size is 2*t*. Do thin shells need smaller or larger elements than 2*t* ?

Boiler drums

Cylindrical boiler drums are made to contain pressurised water. The connection between the cylinder and a cap is an edge disturbance (p. 72). This edge disturbance can be analysed manually due to the axial symmetry in geometry and loading [32]. Figure 100 and 101 show results for different cap shapes. Figure 100 shows C_1 continuity (p. 11). Figure 101 shows C_0 continuity. The displayed membrane stresses are in the hoop direction. The displayed moments are in the meridional direction. In figure 100 the stress due to the maximum moment is approximately 30% of the stress due to the membrane force in the same direction. In figure 101 the stress due to the maximum moment is approximately 11 times the stress due to the membrane force in the same direction. Consequently, the drum in figure 101 is likely to yield when pressurised. This does not result in failure because the membrane forces continue to carry the load. For repeated loading fatigue will be a problem. Therefore, drum caps as in figure 101 are rarely applied.

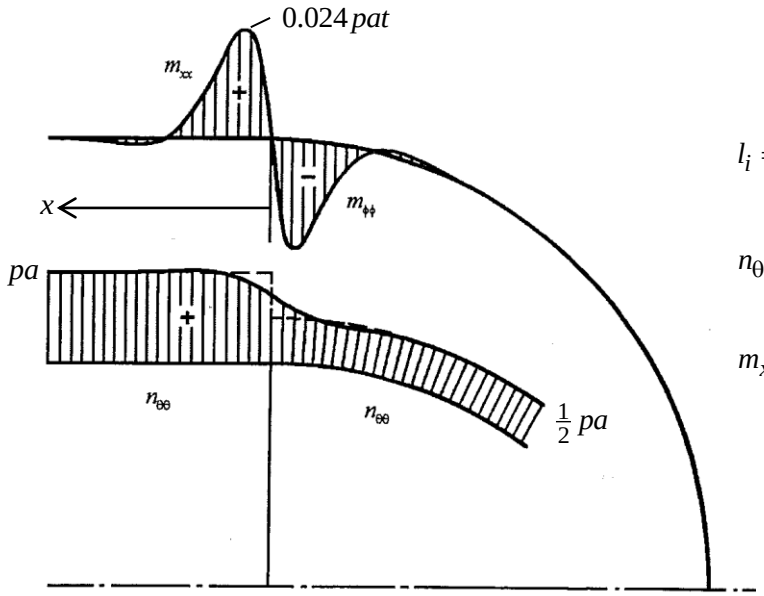

$$l_i = \frac{\pi}{\sqrt[4]{3(1-\nu^2)}}\sqrt{at}$$

$$n_{\theta\theta} = pa\left(1-\frac{1}{4}\sin\frac{\pi x}{l_i}\exp\frac{-\pi x}{l_i}\right)$$

$$m_{xx} = \frac{pl_i^2}{8\pi^2}\sin\frac{\pi x}{l_i}\exp\frac{-\pi x}{l_i}$$

Figure 100. Membrane forces and moments in a hemispherical drum cap (v = 1/3 and a / t = 100) [32 p. 175]

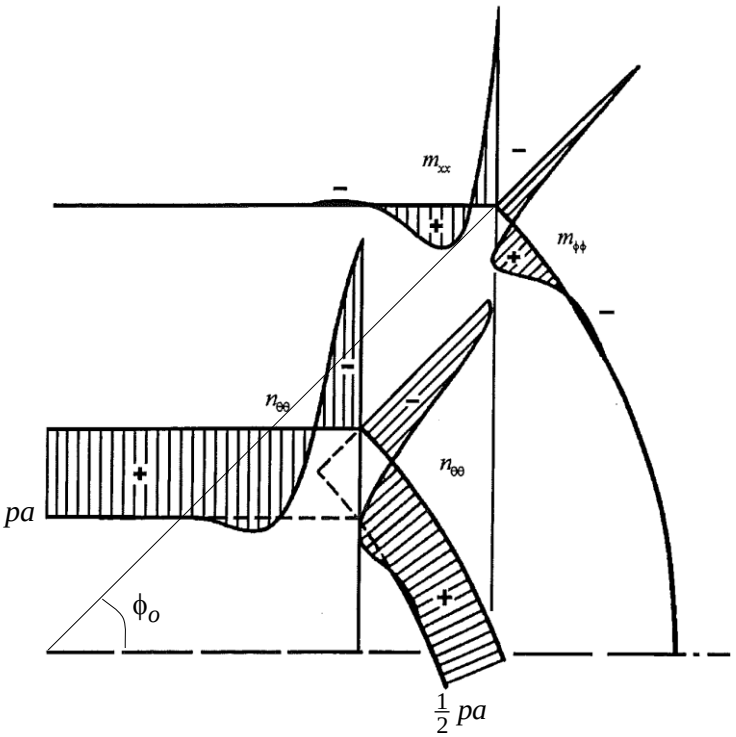

$$l_i = \frac{\pi}{\sqrt[4]{3(1-\nu^2)}}\sqrt{\frac{at}{\sin\phi_o}}$$

$$m_{xx(x=0)} = \frac{-\cos\phi_o}{1+\sqrt{\sin\phi_o}}\frac{pal_i}{4\pi}$$

Figure 101. Membrane forces and moments in a shallow drum cap (ν = 1/3, a / t = 100 and ϕ_o = p / 4*) [32 p. 182]*

Fatigue

Repeated loading can cause fatigue in a stress concentration. The stress range *S* is the largest stress minus the smallest stress in a stress concentration during a load cycle. It can be determined by two static linear elastic finite element analyses. Figure 102 gives examples of the number of load cycles that cause a crack. Graphs can be found for many of materials and many joints.

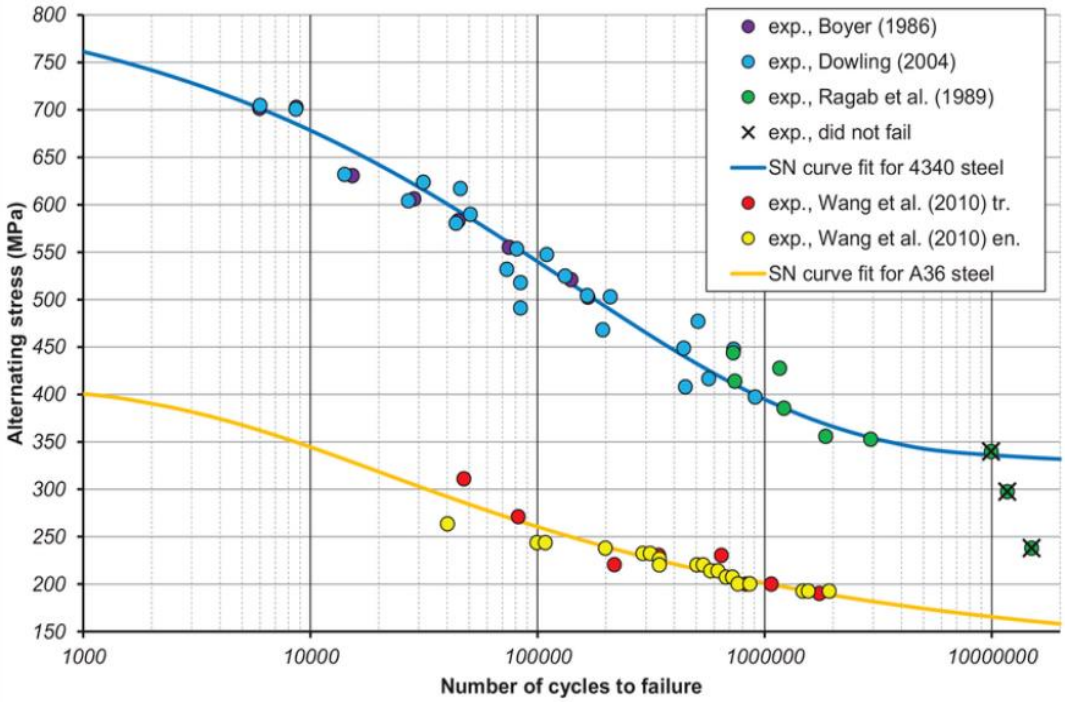

Figure 102. S-N curves of ASTM A36 steel and AISI 4340 steel [32b]

Saturn V

The rocket that brought people to the moon and back was called Saturn V (pronounce Saturn five). More than 20 Saturn Vs were built between 1965 and 1975. The parts were made by American aircraft companies. The Douglas Aircraft Company made an important part called S-IVB (pronounce S4B). It consisted of 8 shells and an engine (figs 103, 104). Note that the wall of the fuel tank is also the wall of the rocket. NASA made a rough design of S-IVB and specified the loads. The loads included an acceleration of 5 m/s^2, a fuel pressure of 6 bar and a fuel temperature of -253 ^{o}C. The engineers of Douglas designed the details and did a lot of testing [33, 34].

Exercise: The Saturn V rockets were not reusable. The cost of each launch was 185 10^6 dollar [Wikipedia]. Suppose that all costs in the end are labour cost. Suppose that all people make approximately the same hourly salary. What percentage of the USA population was working to launch Saturn Vs?

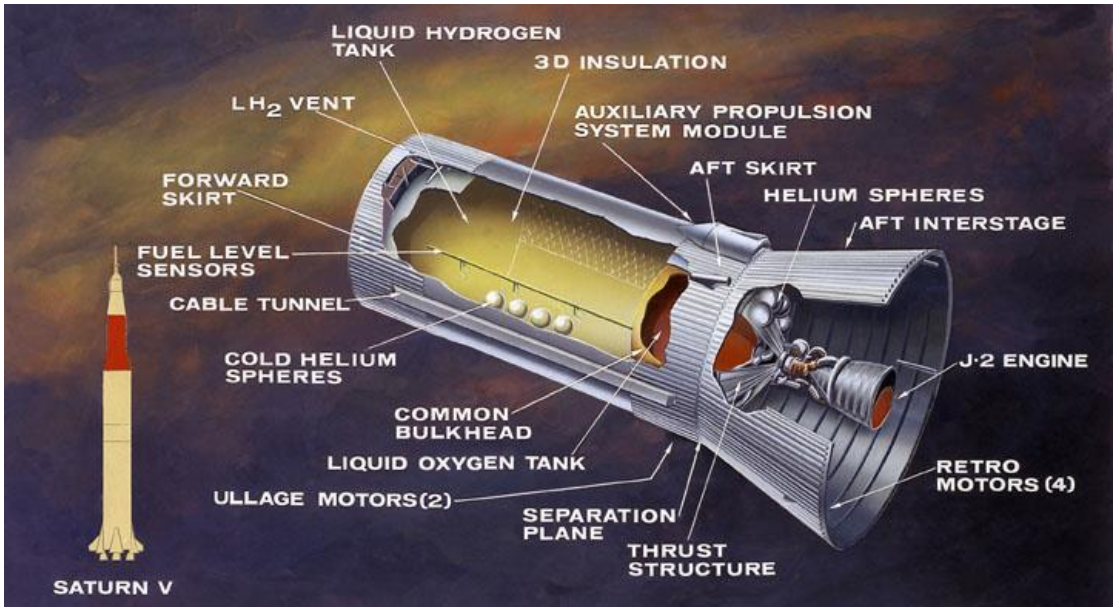

Figure 103. The S-IVB part of the Saturn V [Wikipedia]

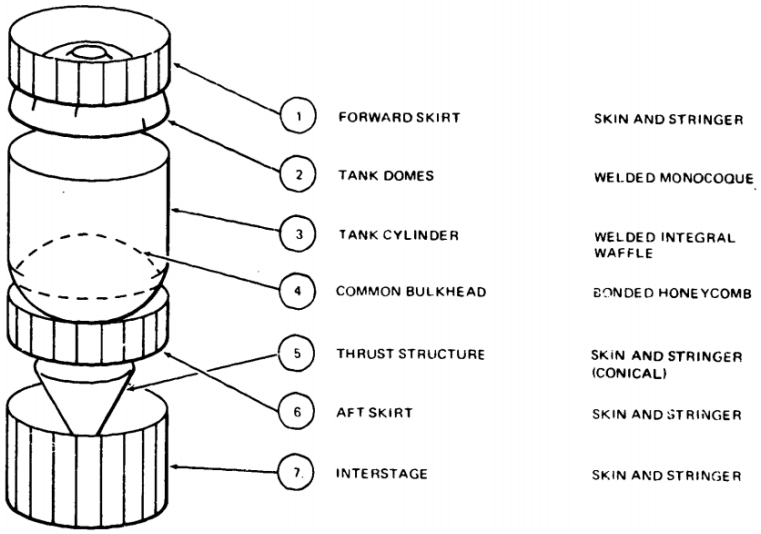

Figure 104. Shell components of S-IVB [33]

Finite difference method

One way of solving the Sanders-Koiter equations (p. 54) is the *finite difference method*. This is a method for computing approximate solutions to differential equations. The method uses a grid of points, for example 100×100 points (fig. 104). In the points, the values of the 21 dependent variables (p. 71) are computed. In total this is approximately 210 000 variables. For the computation we need as many equations. The 21 Sander-Koiter equations are discretised around the points. For example, equation 4

$$\varphi_x = -\frac{\partial u_z}{\partial x} - k_{xx}u_x - k_{xy}u_y$$

is discretised around point 307 as.

$$0 = -\varphi_{x,307} - \frac{u_{z,304} - u_{z,303}}{\frac{1}{99}\alpha_x(\frac{3.5}{99},\frac{3}{99})} - k_{xx}(\frac{3.5}{99},\frac{3}{99})\frac{u_{x,303}+u_{x,304}}{2} - k_{xy}(\frac{3.5}{99},\frac{3}{99})\frac{u_{y,303}+u_{y,304}}{2}$$

Some grid points are outside the shell. These are solved with the boundary conditions (p. 68), for example, boundary condition 16K

$$\varphi_x = 0$$

gives

$$\varphi_{x,303} = -\varphi_{x,304}$$

All equations are written in a large square matrix and the dependent variables are solved and plotted. This method uses much computer memory and much computation time but it is easy to program. A bit of python code is shown below. A complete program can be downloaded from http://phoogenboom.nl/b17_code.txt

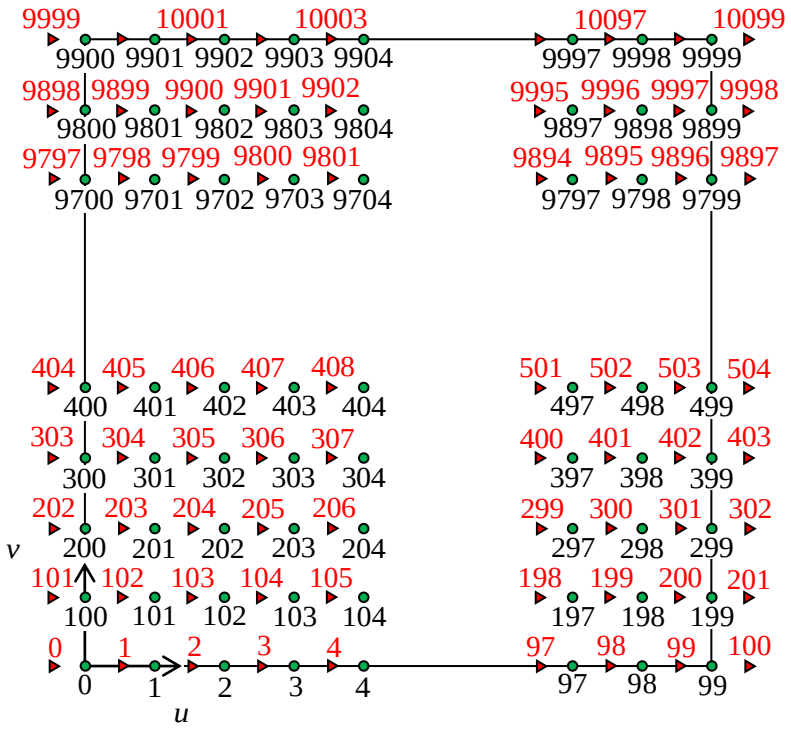

Figure 104. Finite difference grid. Green dots ● are locations of discrete displacements u_x, u_y, u_z. Red triangles ▸ are locations of discrete rotations φ_x. The red triangles outside the shell are eliminated by boundary conditions.

```
for j in range(100) # Add Sanders-Koiter equation 4 to the matrix
   for i in range(99)
      row=row+1
      M[row,p[phix]+j*101+i+1]=-1
      M[row,p[uz  ]+j*100+i+1]=-99/alphax((i+0.5)/99,j/99)
      M[row,p[uz  ]+j*100+i  ]= 99/alphax((i+0.5)/99,j/99)
      M[row,p[ux  ]+j*100+i+1]=-0.5*kxx  ((i+0.5)/99,j/99)
      M[row,p[ux  ]+j*100+i  ]=-0.5*kxx  ((i+0.5)/99,j/99)
      M[row,p[uy  ]+j*100+i+1]=-0.5*kxy  ((i+0.5)/99,j/99)
      M[row,p[uy  ]+j*100+i  ]=-0.5*kxy  ((i+0.5)/99,j/99)
```

Exercise: The above code uses 100×100 grid points. Upgrade it to *m*×*n* grid points.

Canopy example, finite difference solution

The finite difference method (p. 79) has been applied to the canopy example (p. 70). The numbers are $E = 10^7$ kN/m^2, ν = 0.15 (reinforced concrete), length l = 12 m, width = 4 m, radius a = 2 m, shell thickness t = 0.060 m (a / t = 33), no self-weight, point load F = 100 kN in corner. In other words: in node 9999, $q_y \frac{1}{2}\frac{1}{99} l = 100$ kN.

$k_{xx} = 0,\ \ k_{yy} = -1/a,\ \ k_{xy} = 0,\ \ \alpha_x = l,\ \ \alpha_y = \pi a,\ \ 0 \le u \le 1,\ \ 0 \le v \le 1$

The result is shown in figures 105 to 111. The horizontal axis shows u and the vertical axis shows v.

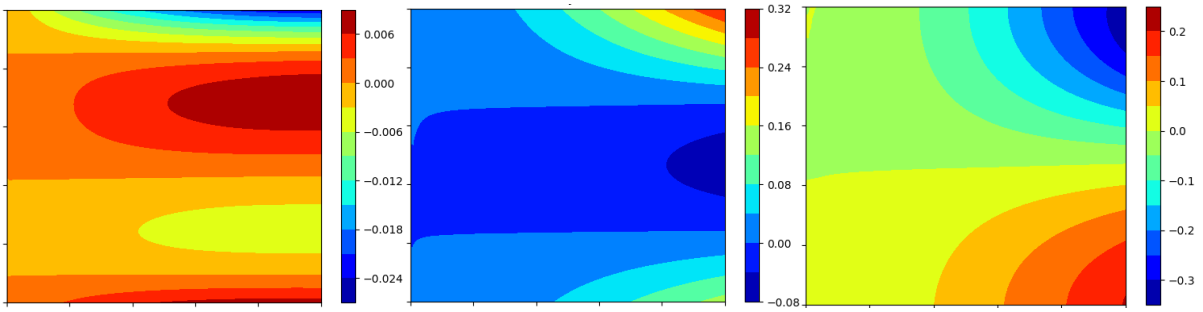

Figure 105. Canopy u_x, u_y *and* u_z [m]

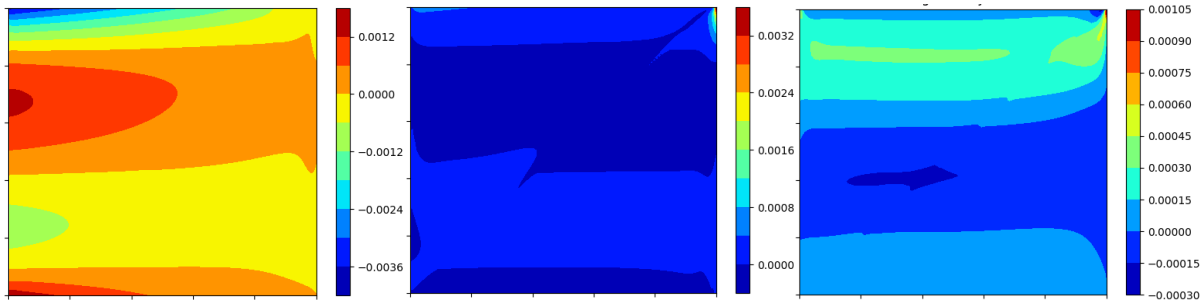

Figure 106. Canopy $\varepsilon_{xx}, \varepsilon_{yy}$ *and* γ_{xy}

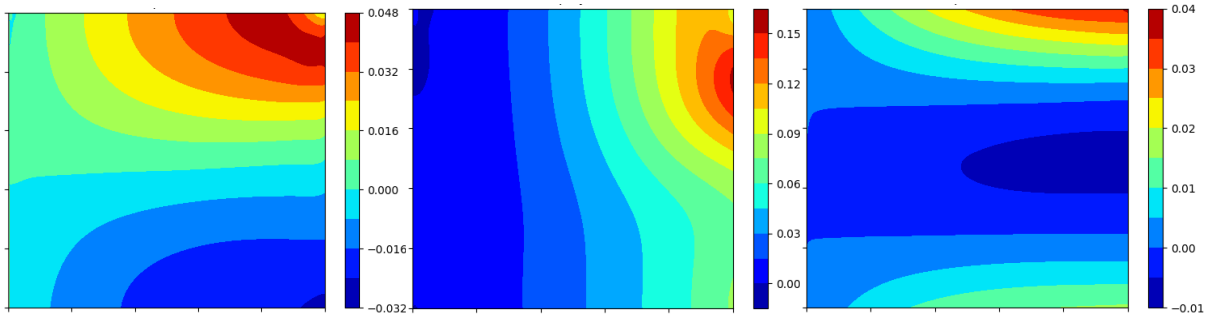

Figure 107. Canopy φ_x, φ_y *and* φ_z [rad]

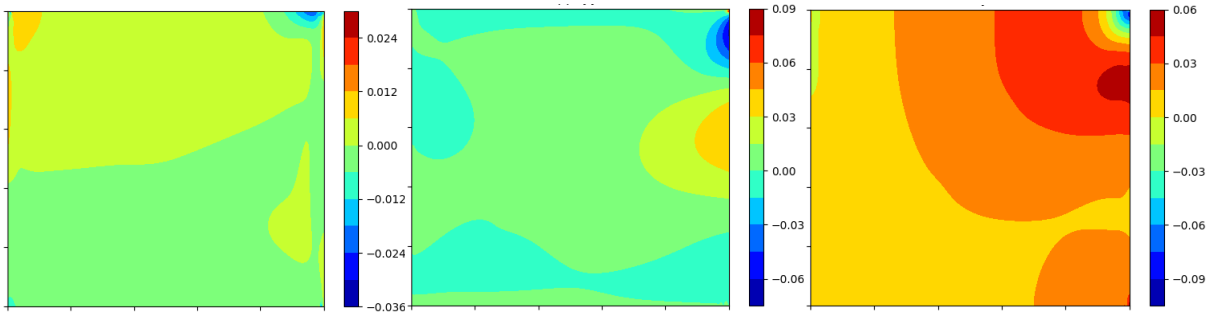

Figure 108. Canopy κ_{xx}, κ_{yy} *and* ρ_{xy} [1/m]

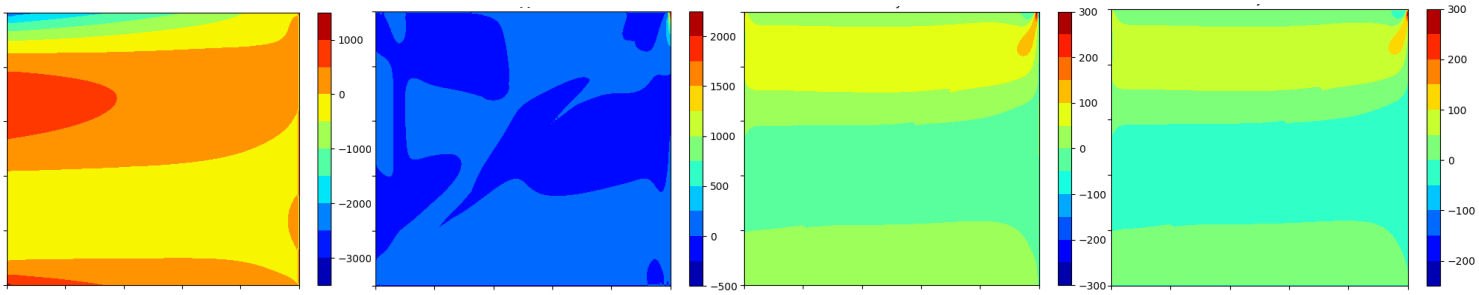

Figure 109. Canopy n_{xx}, n_{yy}, n_{xy} *and* n_{yx} [kN/m]

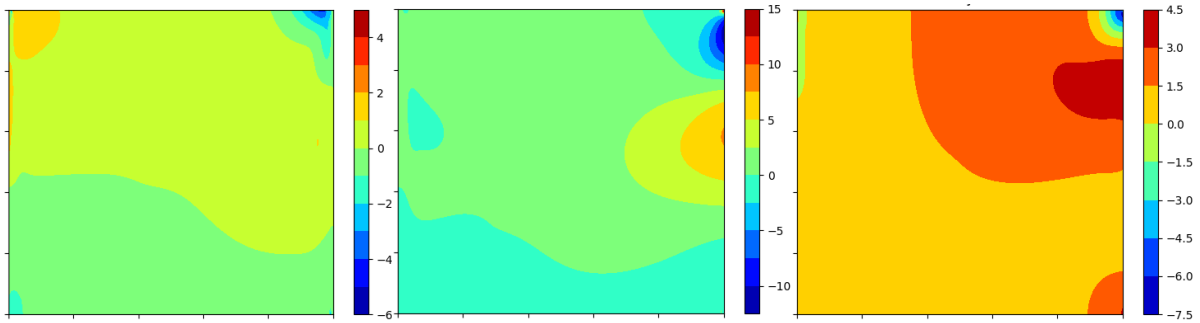

Figure 110. Canopy m_{xx}, m_{yy} *and* m_{xy} [kNm/m]

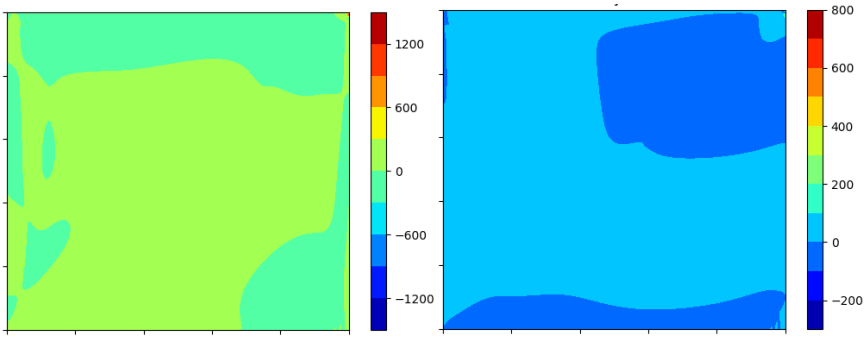

Figure 111. Canopy v_x *and* v_y [kN/m]

Exercise: Do figure 105 to 111 show all dependent variables?

Exercise: When we know the displacement functions u_x, u_y, u_z, we can use the Sanders-Koiter equations to calculate all other dependent variables easily. This is demonstrated in the ping pong ball example (p. 56). From this point of view we need to solve only 3 dependent variables: u_x, u_y and u_z. When we have solved these we know all. Nonetheless, in the finite difference method we solve 21

dependent variables. Why is this? In other words, what is so special about a ping pong ball that it is an exception?

Challenge: Use the program b17_code to study influence length (p. 75) as a function of k_{xx}, k_{yy}, k_{xy} and k_x. Are the equations on page 74 correct?

Shell finite elements

There are three types of shell finite element; 1) flat elements, 2) elements based on the Sanders-Koiter equations (p. 54) and 3) elements based on reduction of a solid element.

Flat elements are triangles or quadrilaterals. A flat element is based on a simple combination of an element for plates loaded in plane (walls) and an element for plates loaded perpendicularly (floors). Each node has six degrees of freedom (dofs) (fig. 112, 113, 114). The red dofs do not really contribute to the element accuracy. They are added to make the element fit in a general purpose finite element program. Flat elements have two requirements for the mesh: 1) the elements need to be small due to their low accuracy [43] and 2) each quadrilateral really needs to be flat and cannot have a twisted shape.

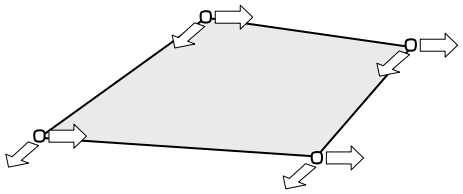

Figure 112.
Element for plates loaded in plane

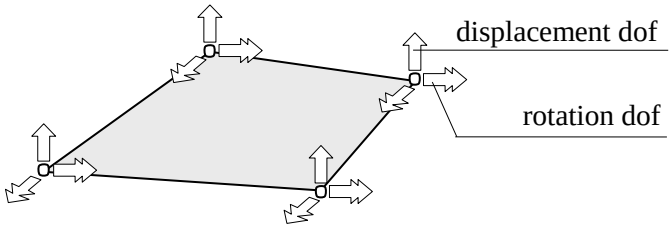

Figure 113.
Element for plates loaded perpendicularly

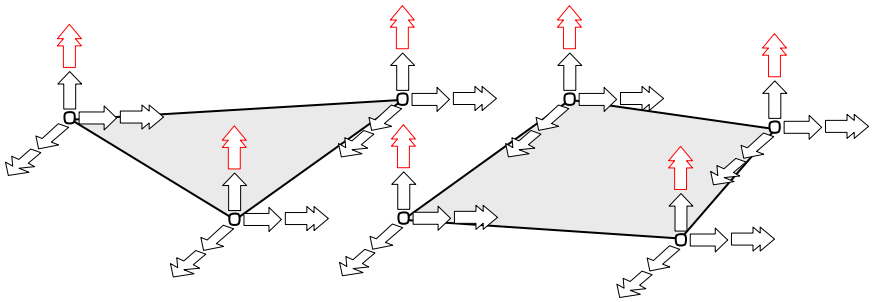

Figure 114. Degrees of freedom of flat shell elements

Exercise: Suppose that a finite element mesh is in the principal curvature directions. Can flat quadrilateral elements be used?

Curved elements can be derived from the Sanders-Koiter equations. A well known element of this type is the semiloof element [44]. It has been derived by Bruce Irons based on discussions with Henk Loof.[1] The element has 3 degrees of freedom in 8 nodes and 1 rotational degree of freedom in 8, so

[1] Bruce Irons (1924–1983) was professor at Swansea and Calgary. He was specialised in programming finite elements. He made important contributions to this field and wrote three books on computational analysis. He suffered from multiple sclerosis and committed suicide, together with his wife, at the age of 59 [Wikipedia].

Henk Loof (1929–1988) was professor at Delft University of Technology, Faculty of Civil Engineering. He was very skilful in the mathematics of shell structures. He was not married and lived in the city of Den Haag together with his sister [source Johan Blaauwendraad and Coen Hartsuijker]. The “oo” in Loof is pronounced as the “o” in go.

called, Loof nodes (fig. 115). This thin shell element has high accuracy, however, it is difficult to implement in a finite element program. Therefore, it is not much used.

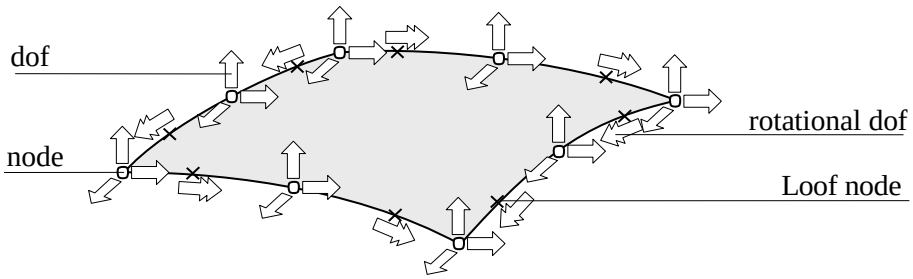

Figure 115. Degrees of freedom of a semiloof element

Shell elements can also be derived from *solid elements*. In the process some degrees of freedom are replaced by others and the constitutive equations are simplified (fig. 116). These elements have 3, 4, 6 or 8 nodes with each 6 degrees of freedom and can be implemented conveniently. The elements with 4 nodes can be twisted. The elements with 6 and 8 nodes can be curved as well (fig. 117) [45]. Most finite element programs use shell elements derived from solids.

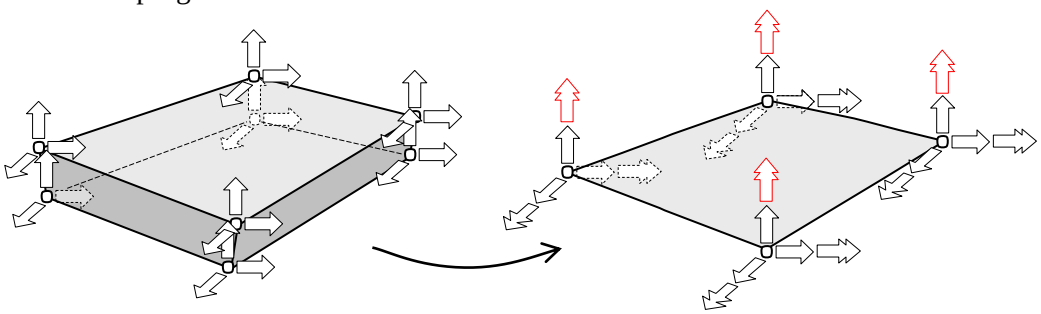

Figure 116. Eight node volume element reduced to a four node shell element

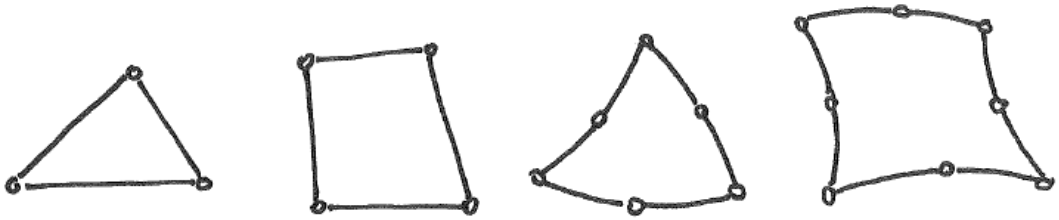

Figure 117. Shell elements with 3, 4, 6 and 8 nodes

Element aspect ratio

The aspect ratio of a rectangular shell element is defined as length over width. Many finite element programs have a restriction on the aspect ratio. For example

$$\frac{1}{20} < \frac{\text{length}}{\text{width}} < 20$$

The development of the semiloof element can be described shortly. Irons met Loof at a conference in Newcastle in 1966. Irons presented a paper on integration rules and Loof presented a paper on shell finite element analysis [46]. In an informal setting they must have talked at length about shell behaviour and shell mathematics. In the years that followed Irons derived a finite element with rotation degrees of freedom in unusual points at the edges. He referred to these points as Loof nodes after his good friend Henk Loof. When he presented his element at a conference in 1974 he modestly called it the SemiLoof element [44]. Surely a better name for the element is the Irons-Loof element but this name change did not take place. The semiloof element is regarded by specialists a scientific master piece [48].

The reason for this restriction is that if the element stiffness in two directions is very different, the structural stiffness matrix has both very large numbers and almost zero numbers on the main diagonal. As a consequence the computed displacements and stresses may have little arithmetic accuracy (p. 94). However, in modern software this is not a problem because high accuracy number representations are used. Sometimes, we need to use an aspect ratio of 1000 and this does not need to give accuracy problems.

Mesh refinement
Like all finite elements, a shell element is accurate when it is small. An engineer who is experienced in finite element analysis can just see whether the elements in a model are sufficiently small. However, when in doubt, the following procedure is used. 1) Do the analysis with any mesh. 2) Halve the element size. 3) Repeat the analysis. 4) If the important results do not change significantly, the last mesh is sufficient. If the important results change significantly, continue at step 2.

For example, the first analysis gives a deflection of 24 mm. The second analysis, with half size elements, gives a deflection of 26 mm. If you think that 2 mm is sufficient accuracy than you are done. We can estimate the exact result that would be obtained by an extremely fine mesh. For this add the difference to the last result. In this example the exact result is approximately 26 + 2 = 28 mm.

Refining a shell mesh to half element size, requires approximately 4 times as many nodes, 16 times as much memory plus computer hard disk space and 64 times as much computation time.

Model accuracy
The accuracy of an element depends on the situation in which it is used. Therefore, accuracy cannot be expressed as a fixed percentage. What we do know is the smaller the elements, the smaller the error. For example, the model deformation can have an error of O(h). (pronounce order h). This means that the error is proportional to the element size h. It is the smallest finite element accuracy possible. Other errors are O(h^2) and O(h^3). The table below gives the errors of shell finite element models [49, 50].

	deflection	membrane forces	moments	shear forces
flat elements	O(h^3)	O(h)	O(h^2)	O(h)
semiloof elements	?	?	?	?
reduced solid elements without mid-side nodes	O(h^2)	O(h^2)	O(h^2)	O(h^2)
reduced solid elements with mid-side nodes	O(h^2)	O(h^2)	O(h^2)	O(h^2)

Model accuracy can be determined by performing three analysis; the second with half element size and the third with one-fourth element size. This gives three equations

```
> eq1:= u=u1+C*h^b:
> eq2:= u=u2+C*(h/2)^b:
> eq3:= u=u3+C*(h/4)^b:
> solve({eq1,eq2,eq3},{b,u,h});
```

from which the order of the error can be solved. $b = \log_2 \frac{u_2 - u_1}{u_3 - u_2}$

Result extrapolation
In the example on mesh refinement (p. 84) it is assumed that the deformation has an error O(h), which is conservative. The table below shows more formulas for estimating the exact result from two computation results.

	O(h)	O(h^2)	O(h^3)
$h_2 = 0.500\ h_1$	$u = u_2 + (u_2 - u_1)$	$u = u_2 + (u_2 - u_1)/3$	$u = u_2 + (u_2 - u_1)/7$
$h_2 = 0.707\ h_1$	$u = u_2 + 2.41(u_2 - u_1)$	$u = u_2 + (u_2 - u_1)$	$u = u_2 + 0.547(u_2 - u_1)$
$h_2 = 0.794\ h_1$	$u = u_2 + 3.85(u_2 - u_1)$	$u = u_2 + 1.70(u_2 - u_1)$	$u = u_2 + (u_2 - u_1)$

The table results have been obtained from two equations. For example

```
> eq1:= u=u1+C*h^2:
> eq2:= u=u2+C*(0.500*h)^2:
> solve({eq1,eq2},{u,C});
```

Exercise: A finite element type approximates the membrane force n_{xx} as uniform over the element surface (see figure). We want to compute the membrane force in the shell edge at $y = 0$. What is the order of the error?

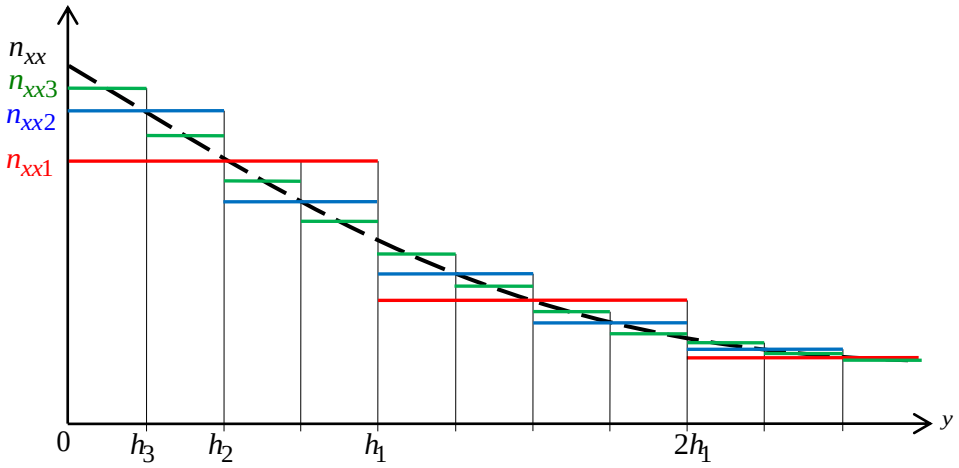

Bohemian dome
A Bohemian dome consist of identical circle segments. A parameterisation that follows these circles is convenient for construction (fig. 118). [2]

$$\bar{x} = a\cos u$$
$$\bar{y} = a\cos v$$
$$\bar{z} = a\sin u + a\sin v$$

However, this parameterisation is not orthogonal. An orthogonal parameterisation (p. 25) of a Bohemian dome is

$$\bar{x} = a\cos(u+v)$$
$$\bar{y} = a\cos(u-v)$$
$$\bar{z} = a[\sin(u+v) + \sin(u-v)]$$

$$k_{xx} = \frac{\sin u \cos v}{a\,A\sqrt{AB}} \qquad \alpha_x = a\sqrt{2A} \qquad A = 1 + \cos(u+v)\cos(u-v)$$

$$k_{yy} = \frac{\sin u \cos v}{a\,B\sqrt{AB}} \qquad \alpha_y = a\sqrt{2B} \qquad B = 1 - \cos(u+v)\cos(u-v)$$

$$k_{xy} = -\frac{\cos u \sin v}{a\,AB}$$

Exercise: Neither of the Bohemian dome parameterisations are in the principal curvature directions (p. 22). How do we know?

[2] The Bohemian dome was first studied by Antonín Sucharda (1854–1907), who was a mathematics professor at Brno University, Czech Republic [Wikipedia]. The Czech Republic consist of several parts, of which one is the old Kingdom of Bohemia.

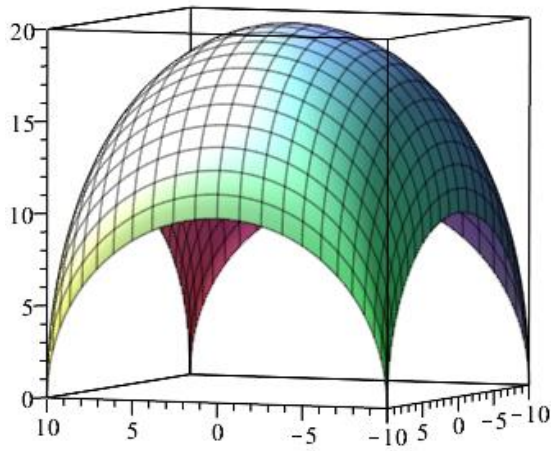

Parameterisation along circles

$0 < u < \pi \quad 0 < v < \pi$

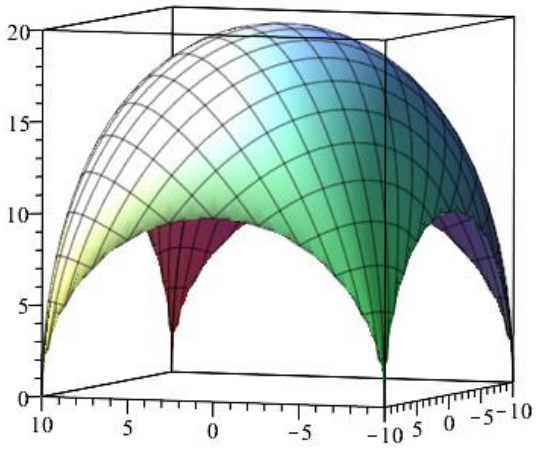

Orthogonal parameterisation

$0 < u < \frac{1}{2}\pi \quad -u \le v < u$

$\frac{1}{2}\pi < u < \pi \quad -\pi + u < v < \pi - u$

Figure 118. Bohemian dome (a = 10 m)

Selecting the element type

Suppose we can do an analysis with four node elements or eight node elements. Which element type is best? Of course, we want accurate results and a fast computation. Figure 119 shows some computation result as a function of the number of nodes. This graph is typical for complicated structures. If we are satisfied with an error of 10% or larger then O(h) elements require the least number of nodes and the least computation time. If we need a smaller error then the O(h^2) elements need the least computation time. From this we conclude,

Choose the most accurate element that is available, unless you are just testing.

Also the shape of the elements is important. Quadrilaterals are more accurate than triangles of the same order.

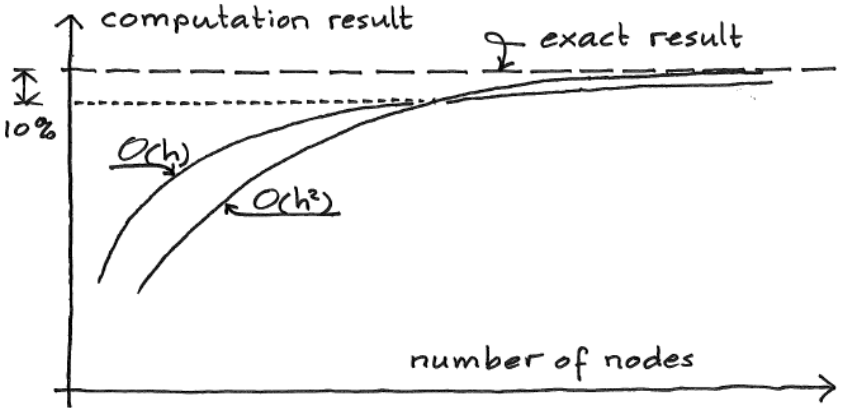

Figure 119. Typical convergence of a finite element result for O(h) *and* O(h^2) *elements*

Integration points

In finite elements the material behaviour (stresses, stains, yielding, cracks, et cetera) is computed in a number of points (fig. 120). These points are called *integration points* or *Gauss points*. The stresses et cetera in other points of the element are computed by interpolation and extrapolation.

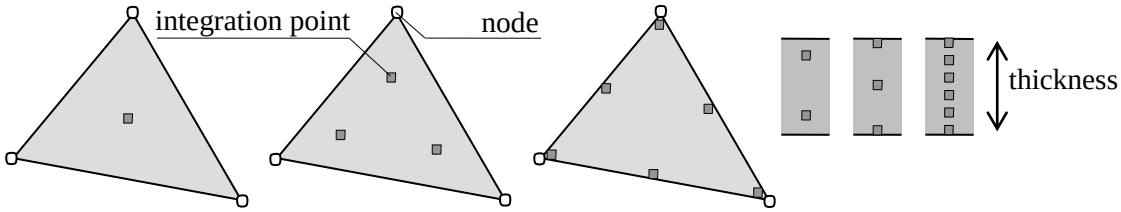

Figure 120. Possible locations of integration points in triangular elements

Locking
In some element types the in plane or out of plane bending stiffness is too large. This is called *shear locking*. Some element types are too stiff for extensional deformation (p. 109). This is called *membrane locking*. These locking problems can be solved in two ways; 1) very fine mesh 2) reduced integrations. In reduced integrations specific integration points that are needed for exact computation of the element stiffness are omitted. This can be an effective trick to improve the element accuracy. Most finite element programs use reduced integration. It can be switched off but it is not wise to do so.

Hourglass mode
Due to reduced integration the elements may have no stiffness at all for particular deformations. Consequently, the elements can deform in a pattern that looks like hourglasses (fig. 122). This deformation is called an *hourglass mode* or a *zero energy mode*. Clearly, this is not what we want and all handbooks give warnings for the phenomenon. However, an hourglass mode can only occur in a perfectly regular mesh with special boundary conditions. In a practical finite element model these hourglass modes are extremely rare. The author has observed few despite many years of experience. If you would ever see an hourglass mode in a finite element model, please make a picture of the screen and send it to me.

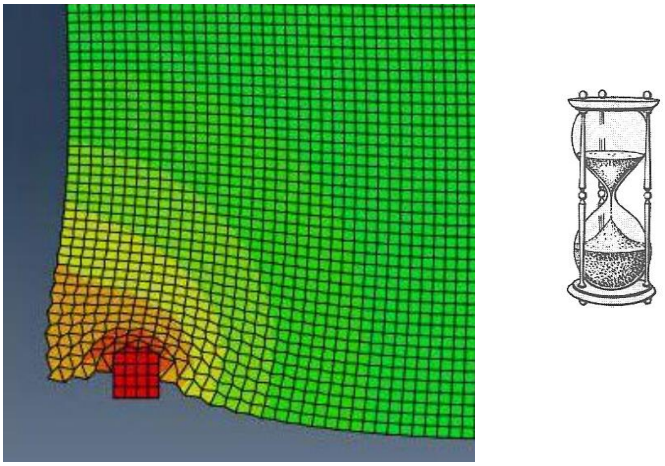

Figure 122: Hourglass mode at the left support of a deep beam finite element model (Abaqus, 4 node constant shear elements)
[Curtesy of A. Al-Sharqi, CIE4180 course, assignment 1, November 2023]

Finite element boundary conditions
Boundary conditions on displacement or slope are called *kinematic* boundary conditions. Boundary conditions on membrane forces, shear forces or moments are called *dynamic* boundary conditions. In the finite element method we only specify the kinematic boundary conditions. The dynamic boundary conditions are fulfilled automatically, however, not very accurately. Only for small finite elements the dynamic boundary conditions are fulfilled accurately. [3]

[3] The dynamic boundary conditions are fulfilled automatically because they are used in deriving the weak formulation or the virtual work equation, which is used in deriving finite elements. Some scientist do not agree

Canopy finite element boundary conditions

A complication is that the finite element method computes $\frac{1}{2}(n_{xy}+n_{yx})$ instead of n_{xy} and n_{yx}. If we want to check the finite element results at boundaries we need to rewrite the shell boundary conditions (p. 68).

The canopy in figure 123 has curvatures $k_{xx}=k_{xy}=0,\ k_{yy}=-\frac{1}{a}$. Substitution in Sanders-Koiter equation 18 (p. 54) gives $-\frac{V}{a}+n_{xy}-n_{yx}=0$, in which is used that $V=m_{xy}$ (see plate boundary conditions p. 61). On the front straight edge the shell boundary conditions is $n_{yx}-k_{xx}V=0$ or $n_{yx}=0$. From these two equations it follows that $\frac{n_{xy}+n_{yx}}{2}=\frac{V}{2a}$. On the free curved edge the shell boundary condition is $n_{xy}-k_{yy}V=0$ or $n_{xy}=-\frac{V}{a}$. From this and Sanders-Koiter equation 18 it follows that $\frac{n_{xy}+n_{yx}}{2}=-\frac{3}{2}\frac{V}{a}$. In one shell corner both boundary conditions on $\frac{n_{xy}+n_{yx}}{2}$ meet. The only solution that fulfils both equations is $\frac{n_{xy}+n_{yx}}{2}=0$ and $V=0$.

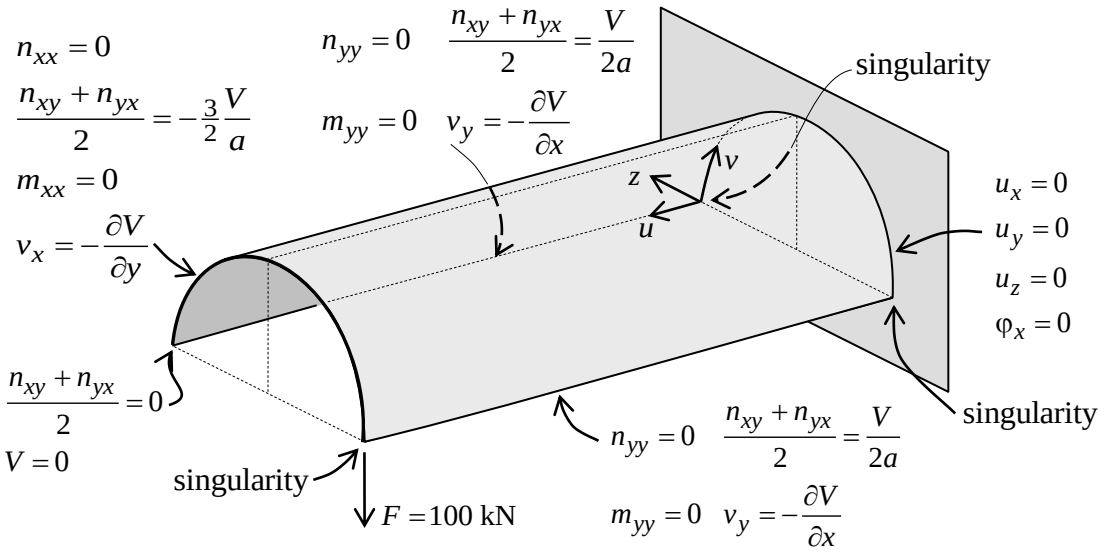

Figure 123. Finite element boundary conditions
(*The only boundary conditions we enter into the program are* $u_x=u_y=u_z=\varphi_x=0$ *and* $F=100$ kN.)

Canopy finite element analysis

A linear elastic finite element analysis has been performed of the canopy. The numbers are $E = 10^7$ kN/m^2, $\nu = 0.15$ (reinforced concrete), length = 12 m, width = 4 m, radius a = 2 m, shell thickness t = 0.060 m, point load F = 100 kN in corner, no self-weight. The boundary conditions on the fixed curved edge have been specified. The boundary conditions on the free edges are a result of the finite element computation. The analysis has been performed by SCIA Engineer 16 (2019) with 4 node quadrilateral elements. Out of plane shear deformation was switched off.

---

with this statement. They say it is the other way around; boundary conditions are derived from the virtual work equation. It is a chicken or the egg problem.

The results are shown in figure 124 to 133. Table 9 shows the forces and moments in four points in the edges. The following conclusion can be drawn from the point of view of finite element analyses. *Some variables are small on shell edges but not zero; also not for very small finite elements.* This is caused by the boundary conditions (p. 88).

Note that this shell is almost thick (see thickness p. 13).

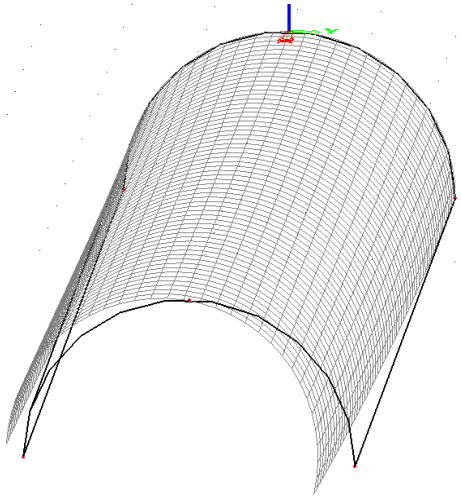

Figure 124. Deformation of the canopy due to just the point load

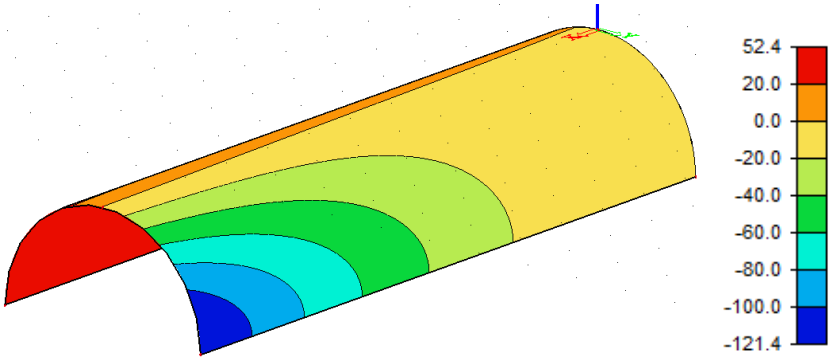

Figure 125. Deflection due to the point load in the global $\bar{z}$ direction [mm] *(positive is up and negative is down)*

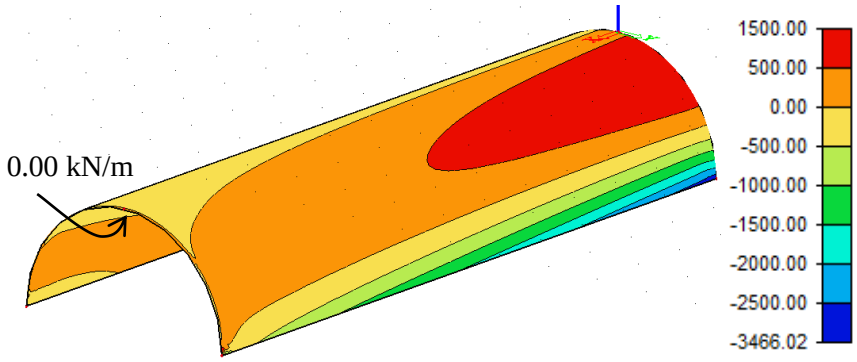

Figure 126. Normal force n_{xx} [kN/m]

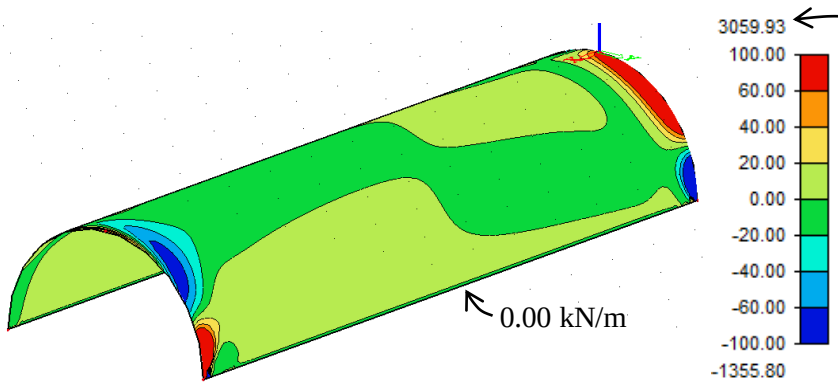

Figure 127. Normal force n_{yy} [kN/m]

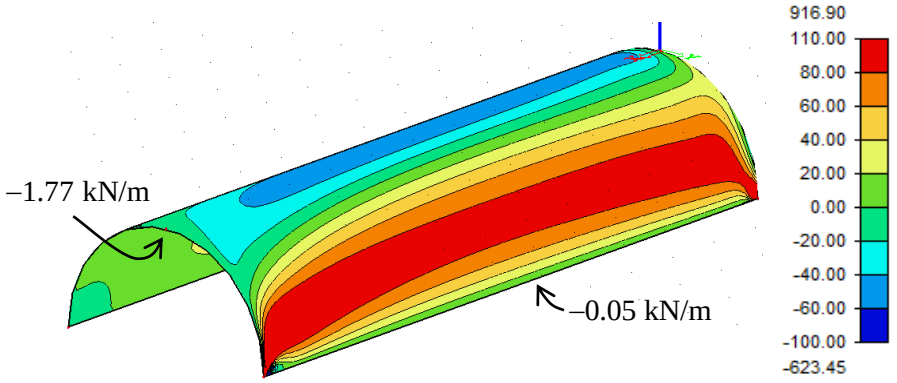

Figure 128. In plane shear force $\frac{n_{xy} + n_{yx}}{2}$ [kN/m]

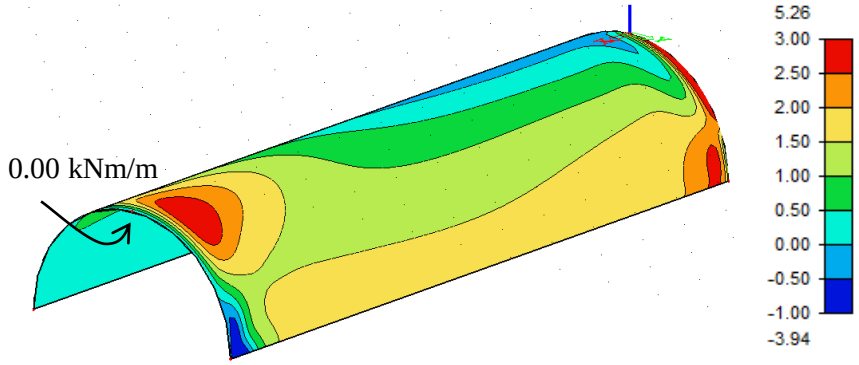

Figure 129. Bending moment m_{xx} [kNm/m]

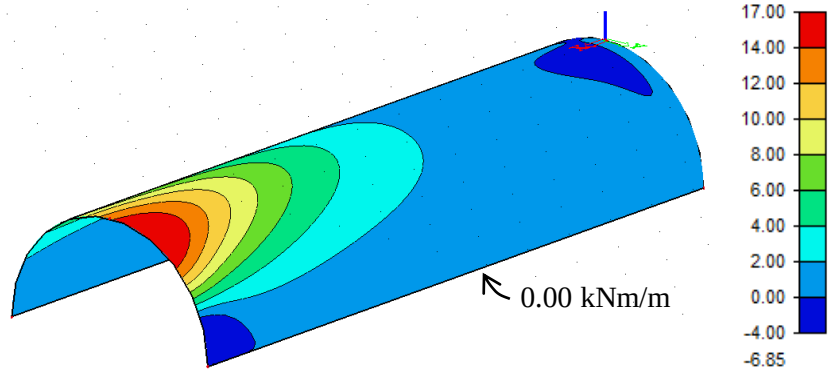

Figure 130. Bending moment m_{yy} [kNm/m]

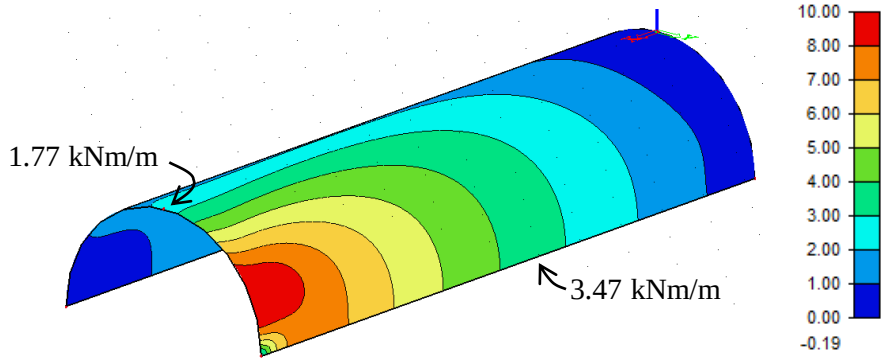

Figure 131. Torsion moment m_{xy} [kNm/m]

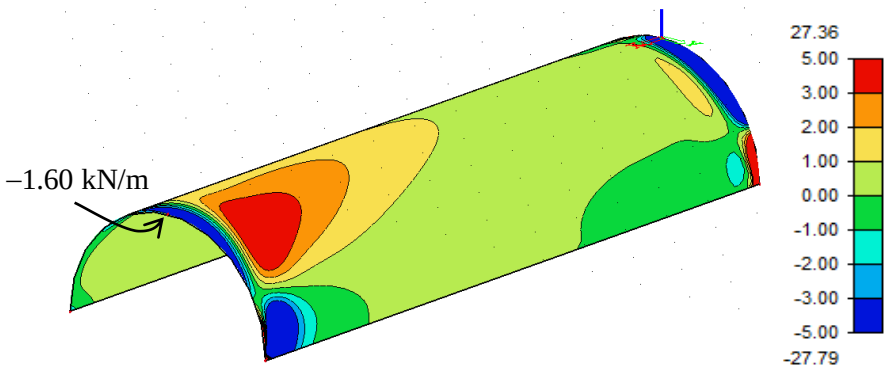

Figure 132. Out of plane shear force v_x [kN/m]

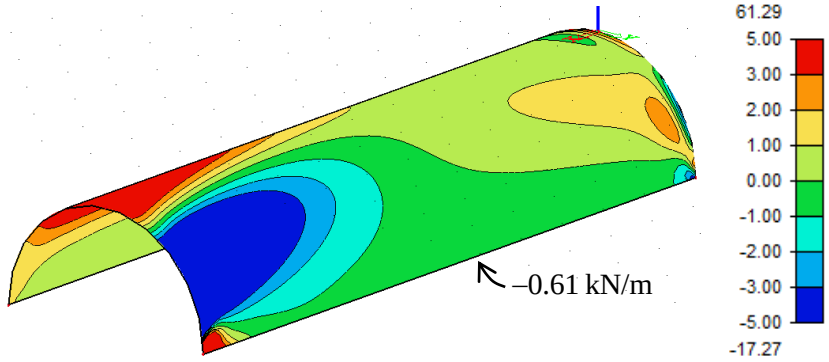

Figure 133. Out of plane shear force v_y [kN/m]

Exercise: What element size follows from the influence length? (p. 75) Is the element size in figure 124 okay?

Table 9. Computation results at four edge locations for five element sizes [51]

element size	n_{xx} kN/m	n_{yy} kN/m	$\frac{1}{2}(n_{xy}+n_{yx})$ kN/m	m_{xx} kN	m_{yy} kN	m_{xy} kN	v_x kN/m	v_y kN/m
edge location $(u, v) = (0, ½)$								
400 mm	315.03	56.31	-6.961	-0.942	-0.1715	0.1136	-4.289	1.125
200 mm	310.21	51.05	-3.784	-1.191	-0.2061	0.0539	-6.797	2.256
100 mm	309.32	47.75	-2.860	-1.252	-0.1939	0.0191	-7.485	2.909
50 mm	309.28	46.72	-2.689	-1.262	-0.1902	0.0046	-7.590	3.161
25 mm	309.30	46.47	-2.654	-1.264	-0.1897	0.0005	-7.600	3.251

edge location (*u*, *v*) = (0, 1)								
400 mm	-3065	-460.56	230.29	-1.452	0.079	0.3110	3.8521	-1.0232
200 mm	-3238	-500.50	332.82	-1.417	-0.069	0.1121	3.9945	-0.3229
100 mm	-3475	-563.62	421.55	-1.501	-0.118	0.0141	3.0948	-0.6421
50 mm	-3781	-640.10	502.97	-1.483	-0.130	-0.031	3.2192	-2.2137
25 mm	-4162	-726.31	585.39	-1.343	-0.121	-0.051	8.6338	-6.4897
edge location (*u*, *v*) = (½, 1)								
400 mm	-1638.4	-12.55	1.8226	-1.4533	-0.0302	3.5035	0.0577	-0.6357
200 mm	-1654.7	-3.276	-0.0439	-1.4203	-0.0180	3.4789	0.0563	-0.6179
100 mm	-1658.7	-0.832	-0.3383	-1.4064	-0.0097	3.4716	0.0532	-0.6141
50 mm	-1659.7	-0.216	-0.2564	-1.4002	-0.0051	3.4693	0.0518	-0.6133
25 mm	-1660.0	-0.054	-0.1493	-1.3972	-0.0026	3.4684	0.0511	-0.6131
edge location (*u*, *v*) = (1, ½)								
400 mm	4.415	19.91	0.5417	0.0329	-12.8505	1.8623	-4.288	6.765
200 mm	3.058	46.57	-0.8098	0.0644	-12.8053	1.7954	-3.864	6.473
100 mm	1.143	55.31	-1.4361	0.0147	-12.8041	1.7755	-2.504	6.355
50 mm	0.336	57.52	-1.6548	0.0022	-12.8038	1.7712	-1.863	6.320
25 mm	0.090	58.06	-1.7299	0.0002	-12.8035	1.7703	-1.659	6.307

Exercise: Do the computed edge forces and moments comply with the canopy finite element boundary conditions? (p. 88)

Exercise: What model accuracy (p. 84) follows from table 9?

Singularities

A singularity in a linear elastic model is a point with very large membrane forces, moments, shear forces or stresses. If the stress in a singularity were determined exactly, its magnitude would be infinite. Singularities can be expected at point loads, at point supports, at re-entrant corners and where line supports stop (fig. 134).

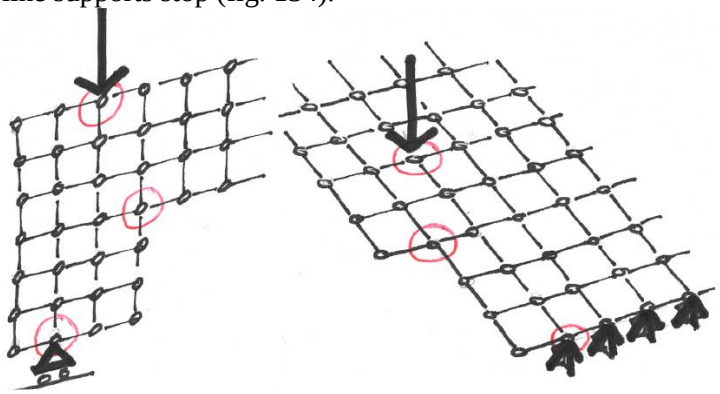

Figure 134. Locations of singularities

Singularities can be removed from a model. The singularity under a point force can be removed by replacing the force by a stress on a realistic area. The singularity in a re-entrant corner can be removed by rounding the corner with realistic radius and allowing the material to yield at a realistic stress. The singularity at a point support can be removed by contact elements and geometrical nonlinear analysis. However, adding details to a model is extra work. In addition, a finer mesh and nonlinear analyses cost extra computation time. Most engineers choose not to remove singularities and instead interpret the computation results. For example, we know that the peak stress at a point support is unrealistic, so we ignore it and calculate the real support stress by hand; $\sigma = F / A$.

Typical of singularities is that smaller elements give larger stresses. Therefore, do not apply the rule of halving the element size (p. 84) to a singularity.

Almost all models with shell finite elements have singularities. Please keep this in mind when reading contour plots of finite element results. Often the computed peak value needs to be ignored because it occurs in a singularity.

Exercise: What type of singularities occur in the canopy? (p. 88)

Exercise: A finite element analysis is performed. Every time we half the element size, the stress peak increases by 7 N/mm^2. Clearly, this stress peak goes to infinity. Which function describes this? Show that the integral of this function from zero to some value is finite. In other words; the linear elastic stress peak is infinite but the resultant force is not.

Largest model that your PC can process
Modern computer programs for numerical analysis use numbers with double precision. This means that each number is stored in 8 bytes of memory. One byte is equal to 8 bits. A bit is represented by an electrical switch with can assume either of two voltage levels.

The most important operation that a finite element program performs is solving a very large system of equations that is represented in a matrix. This matrix has a length and width equal to the number of degrees of freedom (dofs) of the finite element model. This matrix needs to be stored in the memory of the PC. For example, if a model with 15000 dofs is analysed the computer needs $15000 \times 15000 \times 8 = 1.8\ 10^9$ bytes of memory. This is 1.8 GB (gigabyte). A powerful new PC (2019) has approximately 32 GB memory of which about 3 GB is used by Windows. Therefore, the model of this example can be analysed in memory. The linear elastic computation can be performed within a minute.

If the matrix does not fit in memory, then the software can move most of the matrix to the hard disk. This computation is called out-of-core. For example, if a model has 10^5 dofs the required hard disk space is $10^5 \times 10^5 \times 8 = 80$ GB. A partition on a hard disk might have 460 GB (2019), of which 300 GB might be free for performing the analysis. This is more than sufficient for analysing this example. The linear elastic computation can take half an hour or more. If you listen carefully, you can hear the hard disk becoming active. Then you know that the computation will take more than a minute.

Many finite element programs use smart methods to optimise the computation. 1) The matrix is often symmetrical so only half of it needs be stored. 2) Most of the numbers in the matrix are just zero. The non-zero numbers occur around the matrix diagonal. Therefore, only the numbers within some distance from the diagonal need be stored. 3) This distance is called band width. The band width can be reduced by sorting the node numbers of the finite element model. 4) Some programs have an iterative solver that does not need any matrix for solving the system of equations.
Therefore, the largest model that can be analysed depends strongly on efforts of the software engineers. For example, the finite element program Ansys can analyse a model of 10^6 dofs in half an hour on a normal PC (2007). The largest model also depends on the analyses choices that the software user makes, for example, yes or no node sorting.

Moore's law
Moore's law is [52]

Computation power doubles every two years.

This law describes the development of computation power since 1971. It is expected to be valid in the near future too. So, if your current PC cannot analyse a particular model, it is not difficult to calculate when your future PC can do this job.

Arithmetic accuracy
A double precision number has approximately 16 significant digits and a magnitude range of approximately 10^{-308} to 10^{+308}. Some accuracy is lost in every addition, subtraction, multiplication and

division. This is inevitable. After solving a large matrix the result can have just 3 significant digits. This is sufficient for most applications. The software should give a warning if the calculation is not accurate but some programs do not.

Arithmetic accuracy can be checked in a simple way. Add all loads and add all support reactions. If these are not in equilibrium, the equations have not been solved accurately.

Exercise: The accuracy of a finite element model depends on model accuracy and arithmetic accuracy. Suppose that we have a model and we reduce the element size. Which accuracy increases and which reduces?

Exercise: Show that 3 significant digits means an error of at most 1%.

Finite element benchmarks

Shell elements need to be tested to determine their accuracy. Three tests are often applied; a cylinder (fig. 135), a hemisphere (fig. 136) and a hemisphere with an opening (fig. 137). The cylinder is closed on both ends by a diaphragm, therefore, the edge nodes are fixed in the $\overline{x}$ and $\overline{y}$ directions. Note that due to symmetry just part of the shells needs to be modelled. A finite element program can be checked by comparing the displacement under the forces with the results of others. The reference displacement of the cylinder directly under the force is 1.8248 mm [53]. The displayed mesh is too course for most applications. Approximately 1000 elements will be needed to obtain 1% error. The reference displacement of the hemisphere is 0.0924 m directly under the forces. Approximately 200 elements will be needed to obtain 1% error. The reference displacement of the hemisphere with an opening is 0.0935 m directly under the forces. Approximately 100 elements will be needed to obtain 1% error.

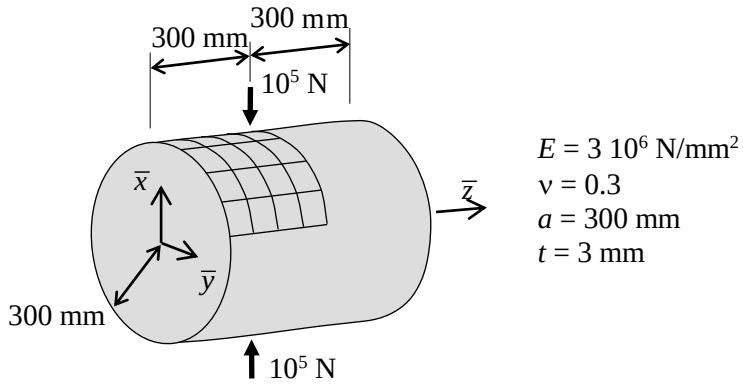

Figure 135. Cylinder loaded by opposite forces

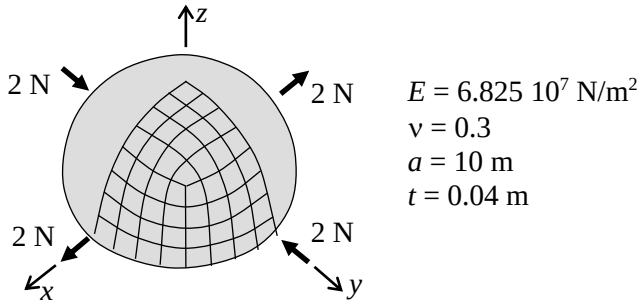

Figure 136. Hemisphere loaded by opposite forces

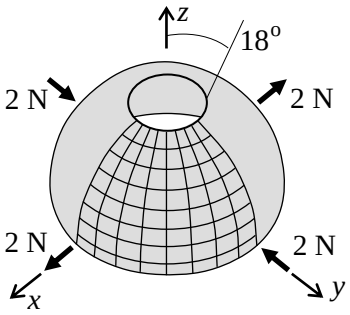

E = 6.825 10^7 N/m^2
ν = 0.3
a = 10 m
t = 0.04 m

Figure 137. Hemisphere with an opening loaded by opposite forces

Exercise: Which benchmark deforms extensionally and which in-extensionally? (see inextensional deformation p. 109)

Modelling thick shells
In a thick shell (p. 13) the shear deformation can be important compared to bending deformation. Shear deformation is included in Mindlin-Reissner elements (p. 62). These elements can be necessary to obtain sufficient accuracy.

In a very thick shell the normal stress is not distributed linearly over the thickness and the shear stress is not a parabola over the thickness. Volume elements can be necessary to compute the stresses accurately. The element mesh needs to have several volume elements in the shell thickness. Volume elements are also called solids, bricks or tets. The latter is short for tetrahedrons.

Averaging at nodes
In the finite element method, all elements in the model are in equilibrium. However, the stresses et cetera on either side of element edges can be different. This is a result of approximations in the element formulation. Many programs can average the computation results at the nodes to make the stresses on either side of the element edges the same. This improves the accuracy and produces smooth contour plots (fig. 138). It needs to be kept in mind that this also removes real jumps in the results. For example, a real jump in the stresses occurs when adjacent shell elements have different thicknesses.

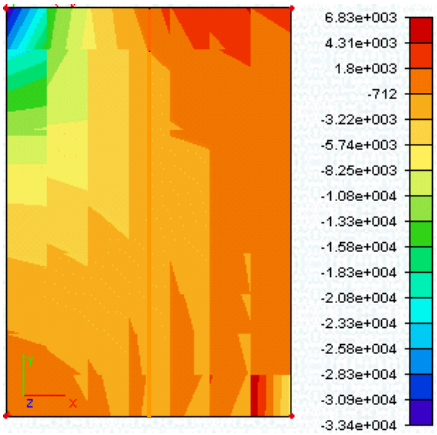

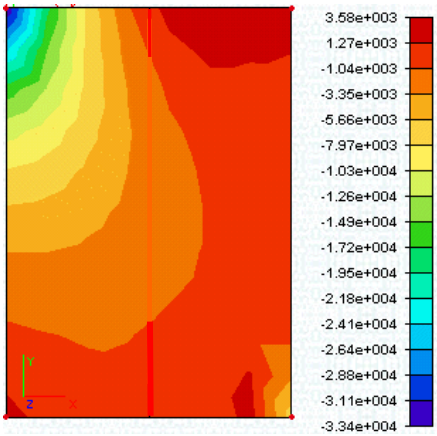

Not averaged *Averaged at nodes*
Figure 138. Contour plots of a finite element result

Influence of coordinate system on the FEM results
When a finite element program plots membrane forces or moments the result can be a mosaic of colours that does not make sense (fig. 140). This is because every finite element has a different local coordinate system *x*-*y*-*z* (p. 19). Most programs align the element coordinate systems in some direction, for example in the hoop direction and the meridional direction (see shell force flow p. 13). For a complicated shell structure the program probably does not put the local coordinate systems in the directions you would like them to be. For example, at the edges of a shell the coordinate system needs to be in the direction of the edge to determine the concentrated shear force (p. 60). Another example is that for a reinforced concrete shell the local coordinate system needs to be in the directions of the reinforcement (see designing reinforcement p. 104). The directions of the local coordinate systems can be changed by hand (click on the elements) but this can be a lot of work.

Fortunately, some finite element results do not depend on the coordinate system, for example principal stresses (p. 101) and Von Mises stress (p. 101). Some finite element results do not depend on the coordinate system, except that the sign depends on the direction of the *z* axis (inwards or outwards), for example the principal moments m_1, m_2 and the principal out of plane shear force v (see principal values p. 98)

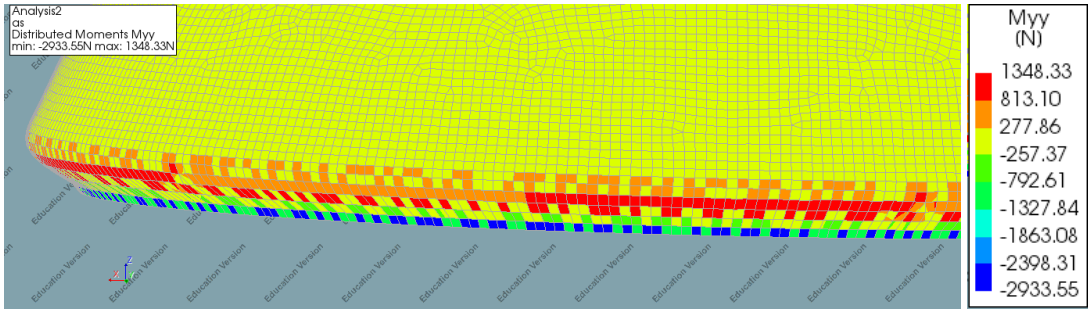

Figure 140. Bending moment m_{yy} in the fixed edge of a deformed semispherical dome.
The colors make no sense because the element coordinate systems are not aligned.
(Tobias Blankenstein 2019)

Tensors
A tensor is a physical quantity that transforms in a particular way when the coordinate system rotates. For example, moment in a shell is a second order tensor. It transforms in the following way when the local coordinate system rotates around the *z* axis from *x*–*y*–*z* to *r*–*s*–*z*.

$$\begin{bmatrix} m_{rr} & m_{rs} \\ m_{rs} & m_{ss} \end{bmatrix} = R \begin{bmatrix} m_{xx} & m_{xy} \\ m_{xy} & m_{yy} \end{bmatrix} R^{\mathrm{T}} \qquad R = \begin{bmatrix} \cos\theta & \sin\theta \\ -\sin\theta & \cos\theta \end{bmatrix}$$

In this, θ is the angle between the *s* axis and the *x* axis.

When the coordinate system changes the tensor numbers change too. However, every tensor has a core that does not change with coordinate system changes. This core consists of the principal values (p. 98) and *Mohr's circle*. When you think about it, anything physical cannot depend on the choice of a coordinate system. This must be the cause of most quantities in these notes being tensors.

The other tensors in shells are

$$\begin{bmatrix} k_{xx} & k_{xy} \\ k_{xy} & k_{yy} \end{bmatrix} \qquad \begin{bmatrix} n_{xx} & n_{xy} \\ n_{yx} & n_{yy} \end{bmatrix} \qquad \begin{bmatrix} \varepsilon_{xx} & \frac{1}{2}\gamma_{xy} \\ \frac{1}{2}\gamma_{xy} & \varepsilon_{yy} \end{bmatrix} \qquad \begin{bmatrix} \kappa_{xx} & \frac{1}{2}\rho_{xy} \\ \frac{1}{2}\rho_{xy} & \kappa_{yy} \end{bmatrix}$$

Principal directions
The principal directions of a moment tensor (p. 97) are defined as the directions in which $m_{xy} = 0$. They are computed by

$$\theta_1 = \tfrac{1}{2}\arctan\frac{2m_{xy}}{m_{xx} - m_{yy}}$$

$$\theta_2 = \theta_1 + \tfrac{1}{2}\pi$$

Computed with similar equations are the principal directions of other tensors. As the equations show, they are perpendicular, except in umbilics (p. 124).

The direction of the principal shear force is computed by

$$\theta = \arctan\frac{v_y}{v_x}.$$

Principal values
The moments in the principal directions (p. 98) are called *principal values*. They are also the largest and smallest moments that can be found by rotating the local coordinate system. They are computed by

$$m_1 = \tfrac{1}{2}\left(m_{xx} + m_{yy}\right) + \sqrt{\tfrac{1}{4}\left(m_{xx} - m_{yy}\right)^2 + m_{xy}^2}$$

$$m_2 = \tfrac{1}{2}\left(m_{xx} + m_{yy}\right) - \sqrt{\tfrac{1}{4}\left(m_{xx} - m_{yy}\right)^2 + m_{xy}^2}.$$

The principal values of other tensors (p. 97) are computed with similar equations. The principal shear force is computed with

$$v = \sqrt{v_x^2 + v_y^2}.$$

Trajectories
Software can plot principal directions (p. 98) in every finite element of a shell. By hand we can draw lines that follow the principal directions (fig. 141). We call these lines *trajectories*. Shells have many trajectories, for example curvatures k_1, k_2, normal forces n_1, n_2, shear force v, moments m_1, m_2 and stresses σ_1, σ_2 in the bottom, middle and top surface. These trajectories do not need to coincide. In other courses other words are used for trajectories, for example hydraulic engineers call them flow lines, electro engineers call them field lines and mathematicians call them integral curves. (See also umbilics p. 123.)

Membrane forces around a square opening
Consider a large wall with a square opening, for example a window in a castle. A finite element analysis shows how the membrane forces go around the opening (fig. 141). It is tempting to expect that the trajectories (p. 98) form an optimal arch (p. 7) above the opening. Note that reality is different.

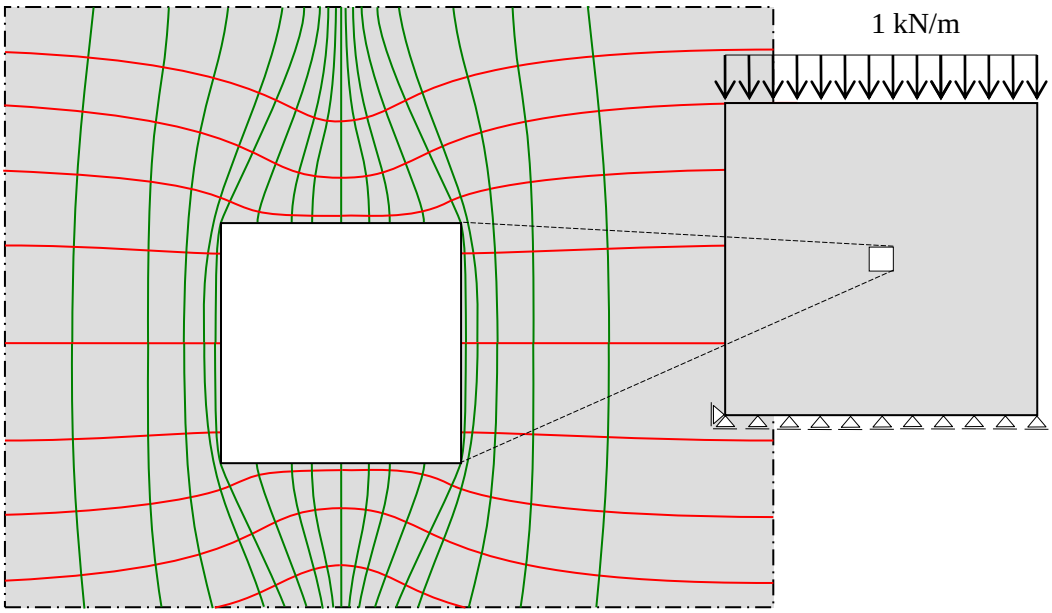

Figure 141. Membrane force trajectories around a square opening in a large wall (Linear elastic, ν = 0.2, no self-weight, vertical evenly distributed load, no horizontal load) Red is tension, green is compression.

Exercise: Are there singularities (p. 92) in the wall membrane forces?

Ellipsoid

An ellipsoid can be described by $\frac{x^2}{a^2}+\frac{y^2}{b^2}+\frac{z^2}{c^2}=1$.

It can be also described by an orthogonal parameterisation (fig. 142).

$$\bar{x}=a\sqrt{\frac{a^2-B}{a^2-c^2}}\cos u \qquad A=a^2\sin^2 u+b^2\cos^2 u$$

$$\bar{y}=b\cos v\,\sin u \qquad B=b^2\sin^2 v+c^2\cos^2 v$$

$$\bar{z}=c\sqrt{\frac{A-c^2}{a^2-c^2}}\sin v \qquad a\geq b\geq c>0$$

In this parameterisation $k_{xy}=0$, consequently, the parameter lines are also the curvature trajectories (p. 98).

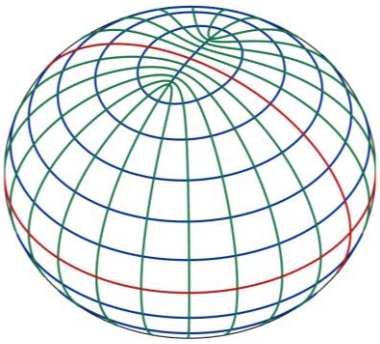

Figure 142. Curvature trajectories on an ellipsoid

$$k_{xx}=\frac{-abc}{\sqrt{BA^3}}$$

$$k_{yy}=\frac{-abc}{\sqrt{AB^3}}$$

$$k_{xy}=0$$

$$\alpha_x=\sqrt{\frac{A(A-B)}{A-c^2}}$$

$$\alpha_y=\sqrt{\frac{B(B-A)}{B-a^2}}$$

Exercise: What is the Gaussian curvature of an ellipsoid at $u = v = 0$?

Stresses
The stresses in a shell are computed in both surfaces and in the imaginary middle surface (fig. 143). For this we consider three small cubes which each have 6 stress components (fig. 144). We use Bernoulli's hypothesis (p. 50) to derive the stresses. The result for thin shells (p. 13) is shown in table 10. The result for thick shells is shown in appendix p. 203. The derivation for both thick and thin shells is in appendices p. 201 and p. 203.

Please note that the stress formulas for thin shells are the same as those for slender beams and columns with rectangular cross-sections. For example, the stress in a beam is moment over section modulus $\sigma_{xx} = M/S$. In a shell the moment is per unit width and the section modulus is per unit width, therefore $\sigma_{xx} = (m_{xx} w)/(\frac{1}{6} w t^2) = 6 m_{xx}/t^2$.

Some finite element programs plot the stresses in the global coordinate system $\bar{x}$ - $\bar{y}$ - $\bar{z}$ (p. 19), which is useless for shell structures.

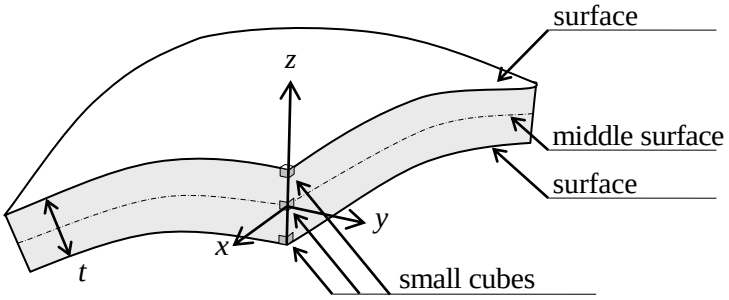

Figure 143. Small cubes in a shell

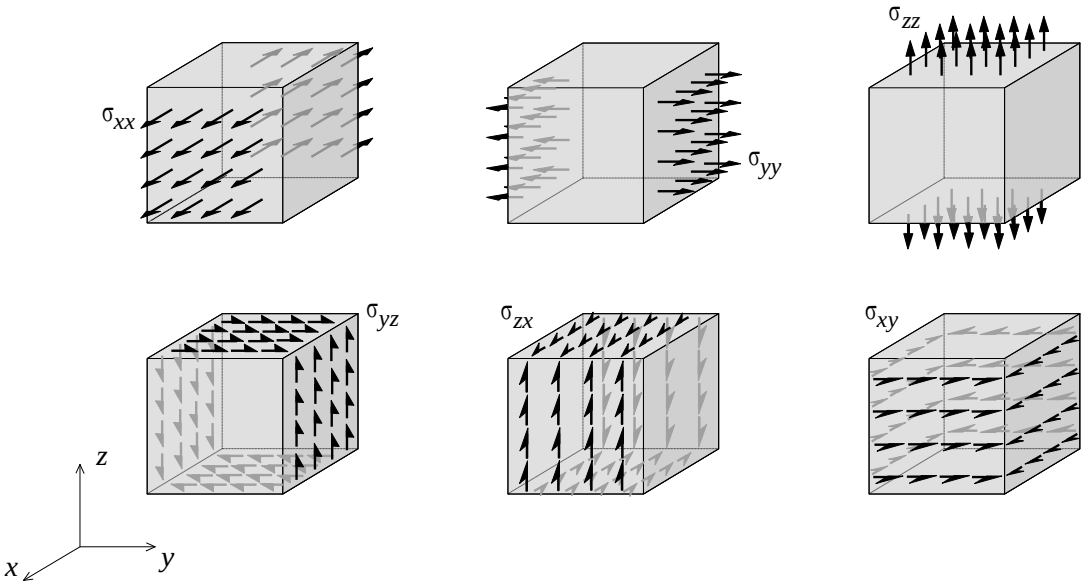

Figure 144. A small cube has six stress components.

Table 10. Stresses in thin shells

surface, $z = -\frac{1}{2}t$	middle surface, $z = 0$	surface, $z = \frac{1}{2}t$
$\sigma_{xx} = \frac{n_{xx}}{t} - 6\frac{m_{xx}}{t^2}$	$\sigma_{xx} = \frac{n_{xx}}{t}$	$\sigma_{xx} = \frac{n_{xx}}{t} + 6\frac{m_{xx}}{t^2}$
$\sigma_{yy} = \frac{n_{yy}}{t} - 6\frac{m_{yy}}{t^2}$	$\sigma_{yy} = \frac{n_{yy}}{t}$	$\sigma_{yy} = \frac{n_{yy}}{t} + 6\frac{m_{yy}}{t^2}$
$\sigma_{zz} \approx 0$	$\sigma_{zz} \approx 0$	$\sigma_{zz} \approx 0$
$\sigma_{yz} = 0$	$\sigma_{yz} = \frac{3}{2}\frac{v_y}{t}$	$\sigma_{yz} = 0$
$\sigma_{xz} = 0$	$\sigma_{xz} = \frac{3}{2}\frac{v_x}{t}$	$\sigma_{xz} = 0$
$\sigma_{xy} = \frac{n_{xy} + n_{yx}}{2t} - 6\frac{m_{xy}}{t^2}$	$\sigma_{xy} = \frac{n_{xy} + n_{yx}}{2t}$	$\sigma_{xy} = \frac{n_{xy} + n_{yx}}{2t} + 6\frac{m_{xy}}{t^2}$

Von Mises stress

For metals the equivalent stress according to Von Mises is important. If this stress is larger than the yield stress then the material would have yielded.

$$\sigma_{VM} = \sqrt{\frac{1}{2}\left((\sigma_{xx} - \sigma_{yy})^2 + (\sigma_{yy} - \sigma_{zz})^2 + (\sigma_{zz} - \sigma_{xx})^2\right) + 3\left(\sigma_{xy}^2 + \sigma_{xz}^2 + \sigma_{yz}^2\right)}$$

Local yielding does not mean that the structure collapses. Collapse occurs only when one or more yield lines form a failure mechanism. The Von Mises criterion is not suitable to check stresses in concrete, masonry or timber. It seems that the Von Mises criterion can be used for plastics, but there is little experimental evidence to confirm this.

Principal stresses

The principal stresses σ_1, σ_2, σ_3 are the eigenvalues of the stress tensor.

$$\begin{bmatrix} \sigma_{xx} & \sigma_{xy} & \sigma_{xz} \\ \sigma_{xy} & \sigma_{yy} & \sigma_{yz} \\ \sigma_{xz} & \sigma_{yz} & \sigma_{zz} \end{bmatrix}$$

The principal directions are directions of the eigenvectors. For hand calculations, Python can be used to calculate eigenvalues and eigenvectors quickly. Below is an example. For numerical implementation, the Jacobi algorithm is recommended [54].

```
>>> import numpy as np
>>> sigma = np.mat("1.12 30.4 -9.65; 30.4 76.5 3.14; -9.65 3.14 -10.3")
>>> print(sigma)
[[  1.12 30.4   -9.65 ]
 [ 30.4  76.5    3.14 ]
 [ -9.65  3.14 -10.3  ]]
>>> eigenvalues, eigenvectors = np.linalg.eig(sigma)
>>> print(eigenvalues)
[ 87.2327 0.1943 -20.1071 ]
```

Top and bottom surface principal stresses

At the top or bottom surface $\sigma_{zz} = p_z$ and $\sigma_{xz} = \sigma_{yz} = 0$. In this case the eigenvalues can be computed by

$$s_1 = \tfrac{1}{2}\left(\sigma_{xx} + \sigma_{yy}\right) + \sqrt{\tfrac{1}{4}\left(\sigma_{xx} - \sigma_{yy}\right)^2 + \sigma_{xy}^2}$$

$$s_2 = \tfrac{1}{2}\left(\sigma_{xx} + \sigma_{yy}\right) - \sqrt{\tfrac{1}{4}\left(\sigma_{xx} - \sigma_{yy}\right)^2 + \sigma_{xy}^2}$$

$$s_3 = p_z$$

Usually the principal values are ordered from large to small

$\sigma_1 = \max(s_1, s_2, s_3)$

$\sigma_3 = \min(s_1, s_2, s_3)$

σ_2 is the value that is left.

Hypar curvature
Consider a shell defined by the function (fig. 145)

$$\bar{z} = h\frac{\bar{x}}{b}\frac{\bar{y}}{c}$$

This shape is called a *hypar*, which is short for hyperbolical paraboloid (p. 21). An orthogonal parameterisation (p. 25) is not available for this shape. The radius of curvature in the origin is.

$$a = \frac{bc}{h}$$

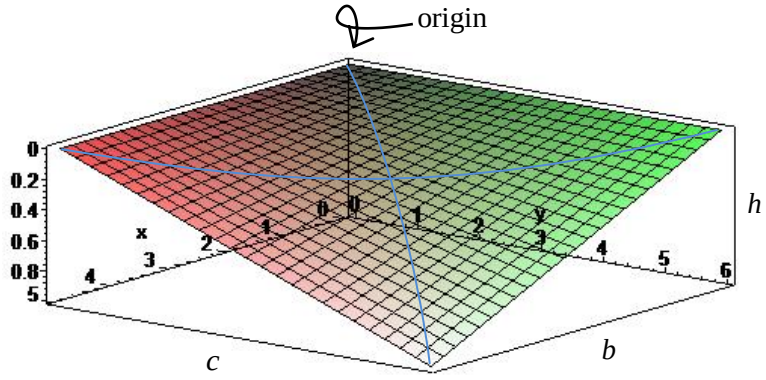

Figure 145. Hypar, b = 5, *c* = 6, *h* = 1, *Maple script:* > plot3d(h*x/b*y/c, x=0..b, y=0..c)

Exercise: Derive that in the origin $k_{xx} = k_{yy} = 0$, $k_{xy} = \frac{1}{a}$ and $k_1 = -k_2$.

Challenge: Find the orthogonal parameterisation of a hypar.
(Not in the principal curvature directions. See p. 129).

Zeckendorf plaza
Hypars (p. 102) are very suitable for reinforced concrete roofs (fig. 146). The formwork is not difficult. It can constist of steel struts, straight parallel timber beams and slightly twisted plywood plates (see plate twisting p. 120). Hypar shells can be very thin, for example 70 mm, which provides just enough cover on the reinforcing bars.



Figure 146. Zeckendorf Plaza, Denver, USA

Zeckendorf Plaza, Denver, USA [55, 56]
Built for the firm Webb & Knapp which was owned by William Zeckendorf
Architects: Ieoh Ming Pei, Henry Cobb
Engineer: Anton Tedesko
Build in 1958, demolished in 1996.
Shell span 132' x 112', shell height 28', thickness 3"
It won an award from the American Institute of Architects.

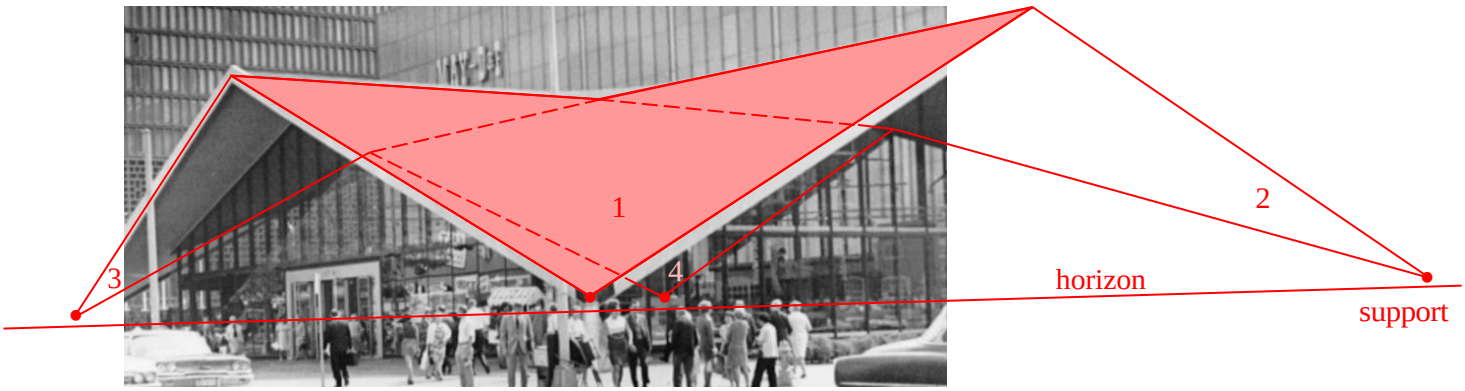

Figure 147. A thin shell roof consisting of four hypars

Exercise: Calculate the *a/t* ratio of Zeckendorf Plaza.

Hypar membrane forces
The membrane forces in a hypar roof (p. 102) are approximately

$$n_{xx} = 0, \quad n_{yy} = 0, \quad n_{xy} = -\frac{1}{2} a\, p_z, \quad n_{yx} = -\frac{1}{2} a\, p_z\,.$$

This follows from shell membrane equation 7, 8 and 9 (p. 38). The *x* and *y* directions are along the edges. In the derivation is assumed that $p_x = p_y = 0$ and that the edge beams have little bending stiffness and do not carry n_{xx} or n_{yy} at the shell edges.

Checking membrane reinforcement
Suppose that somebody has designed reinforcement for a concrete shell. The bars in the *x* direction yield at a membrane force n_{sx} [kN/m]. The bars in the *y* direction yield at a membrane force n_{sy}. In other directions there are no bars. Clearly, we need to check whether $n_{xx} \le n_{sx}$ and $n_{yy} \le n_{sy}$. How can we check n_{xy} and n_{yx}? Equilibrium of a small shell part shows that

$$n_{xy} n_{yx} \le (n_{sx} - n_{xx})(n_{sy} - n_{yy})$$

Perhaps you prefer to write the latter with an utilisation factor. For this, solve μ from

$$n_{xy} n_{yx} = (\mu n_{sx} - n_{xx})(\mu n_{sy} - n_{yy}) \qquad \mu \le 1$$

The result is

$$\tfrac{1}{2}\left(\frac{n_{xx}}{n_{sx}} + \frac{n_{yy}}{n_{sy}}\right) + \sqrt{\tfrac{1}{4}\left(\frac{n_{xx}}{n_{sx}} - \frac{n_{yy}}{n_{sy}}\right)^2 + \frac{n_{xy} n_{yx}}{n_{sx} n_{sy}}} \le 1$$

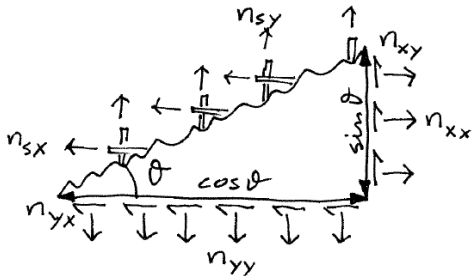

Exercise: Derive that $n_{xy} n_{yx} \le (n_{sx} - n_{xx})(n_{sy} - n_{yy})$.

Exercise: The equation $\ldots \le 1$ is similar to the equation of the first principal value (p. 98) of a tensor. Would utilisation be a tensor too?

Designing membrane reinforcement
Suppose that we want to design the least amount of reinforcement that can carry the load. We assume there is just one load combination, which belongs to the ultimate limit state. We assume that the reinforcing bars are in the local *x* and *y* directions. At some shell location, the bars in the *x* direction yield at a membrane force n_{sx} [kN/m]. The bars in the *y* direction yield at a membrane force n_{sy}. The amount of reinforcement is proportional to $n_{sx} + n_{sy}$. This is to be minimised. The constraints are specified in the above note (checking membrane reinforcement p. 104). There are four solutions, which are shown in table 11. The first row contains the conditions for a solution to be valid. The second row shows the membrane forces that the reinforcement needs to carry. It also shows the stress in the concrete σ_c.

Finite element computer programs can plot these bar membrane forces n_{sx}, n_{sy} as a contour plot over the shell surface. We need to rotate the reference system *x*–*y*–*z* of each finite element in the reinforcement directions.

Exercise: The reinforcement in a hypar (p. 102) can be directed along the hypar edges or along the hypar diagonals. Which direction gives the smallest amount of reinforcement?

Table 11. Membrane forces n_{sx} and n_{sy} for designing shell reinforcement

$n_{xx} \geq -\sqrt{n_{xy}n_{yx}}$	$n_{xx} < -\sqrt{n_{xy}n_{yx}}$	$n_{xx} \geq \frac{n_{xy}n_{yx}}{n_{yy}}$	$n_{xx} < \frac{n_{xy}n_{yx}}{n_{yy}}$
$n_{yy} \geq -\sqrt{n_{xy}n_{yx}}$	$n_{yy} \geq \frac{n_{xy}n_{yx}}{n_{xx}}$	$n_{yy} < -\sqrt{n_{xy}n_{yx}}$	$n_{yy} < \frac{n_{xy}n_{yx}}{n_{xx}}$
$n_{sx} = n_{xx} + \sqrt{n_{xy}n_{yx}}$	$n_{sx} = 0$	$n_{sx} = n_{xx} - \frac{n_{xy}n_{yx}}{n_{yy}}$	$n_{sx} = 0$
$n_{sy} = n_{yy} + \sqrt{n_{xy}n_{yx}}$	$n_{sy} = n_{yy} - \frac{n_{xy}n_{yx}}{n_{xx}}$	$n_{sy} = 0$	$n_{sy} = 0$
$\sigma_c = \frac{-2\sqrt{n_{xy}n_{yx}}}{t}$	$\sigma_{c=} \frac{n_{xx}}{t} + \frac{n_{xy}n_{yx}}{n_{xx}t}$	$\sigma_{c=} \frac{n_{yy}}{t} + \frac{n_{xy}n_{yx}}{n_{yy}t}$	$\sigma_{c=} \frac{n_2}{t}$

Timber grid shell design

A timber grid shell consists of many laths that are bent into a curved shape and subsequently connected together (see Savill building p. 22). Suppose that a lath is in the local x direction. The largest normal stress due to bending is $\sigma_{xx} = \frac{1}{2} E t k_{xx}$, where t is the lath thickness. The lath can also be twisted. The largest shear stress due to twisting is $\sigma_{xy} = \frac{1}{2} E t k_{xy}$. These stresses occur in the same material cube and can be checked by $(\frac{\sigma_{xx}}{f_t})^2 + (\frac{\sigma_{xy}}{f_s})^2 \leq 1$, where f_t is the wood tensile strength and f_s is the wood shear strength. The utilisation value can be plotted as a function of the direction of the x axis. This shows that for any grid shell shape it is best to point the laths in the principal curvature directions (p. 98).

Consequently, for the laths not to break during construction, the architect needs to make sure that the principal curvatures (p. 98) of the grid shell surface are nowhere too large.

$$-\frac{2 f_t}{Et} \leq k_2, \qquad k_1 \leq \frac{2 f_t}{Et}$$

The architect's software – for example Rino – can display the principal curvatures with contour plots on the shell surface.

Exercise: Derive the latter formulas yourself.

Particle-spring method

Determining the grid of a grid shell cannot be done by hand. It would be too much work. A suitable grid can be found by a computer algorithm called particle-spring method [58]. In this method, particles are connected by five types of spring (table 12). At the start of the computation the grid of particles and springs is flat. During the computation the grid is pushed onto an object. The result is a curved grid (fig. 148). The spring stiffnesses can be adjusted to improve the grid.

Table 12. Types of spring in the particle-spring method

spacing	orthogonality	in-plane curvature	out-of-plane curvature	twist
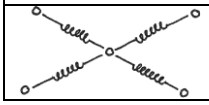	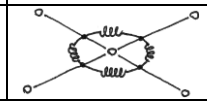	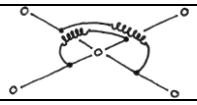	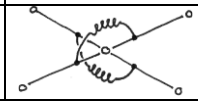	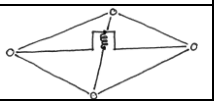

$\frac{Et}{1-\nu^2}\begin{bmatrix} \frac{\alpha_y}{\alpha_x} & \nu \\ \nu & \frac{\alpha_x}{\alpha_y} \end{bmatrix}$	$\frac{1}{8}\frac{Et}{1+\nu}\alpha_x\alpha_y$	$\frac{1}{12}Et\frac{\alpha_y^3}{\alpha_x}$ $\frac{1}{12}Et\frac{\alpha_x^3}{\alpha_y}$	$\frac{Et^3}{12(1-\nu^2)}\begin{bmatrix} \frac{\alpha_y}{\alpha_x} & \nu \\ \nu & \frac{\alpha_x}{\alpha_y} \end{bmatrix}$	$\frac{4}{3}\frac{Et^3}{1+\nu}\frac{1}{\alpha_x\alpha_y}$

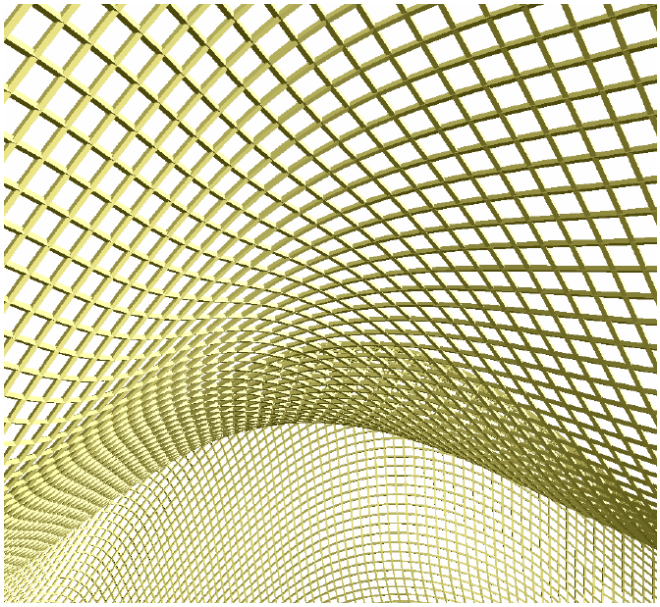

Figure 148. A computed grid using the particle-spring method [58]

The particle-spring method can be used to represent continuous shells too. To this end, deform the grid in the desired shape. Use a small particle spacing and a large stiffness of the orthogonality springs to make the grid directions almost perpendicular (see orthogonal parameterisation p. 25). Redefine the spring deformations as zero and apply the spring stiffnesses of table 12. Finally, apply supports and loads. In the table, α_x and α_y are the particle spacings in the local *x* and *y* directions.

Exercise: Derive one of the spring stiffnesses in table 12.

Spring back analysis

The shape that the architect designed for a timber grid shell is probably not in equilibrium. This is explained with a thought experiment, in which we have many giants at our disposal. The giants push the laths of a grid shell into the shape that the architect designed.[4] Subsequently, construction workers make the connections between the laths. The giants feel the forces that they exert on the laths. The connections did not change these forces because nothing moved. When the giants let go of the grid shell it springs to its equilibrium shape. Suppose that the giants do not let go and keep exerting forces to the lath connections to maintain the architect's shape. These forces can be calculated from the curvatures of the laths. To remove the giants' forces we apply opposite forces on all lath connections. We assemble all the latter forces in a load case called "spring back". Wood creeps strongly, therefore, in time the forces will be reduced to about half the initial value.

Timber grid shell analysis

A timber grid shell can be analysed with a three dimensional frame program. The structure is idealised with many straight frame elements following the shape that the architect designed. The elements do not have an initial stress. (Clearly, in reality the bend laths have large initial stresses but most frame programs are not able to process this.) The first load case that is applied to the structure is spring back

[4] In reality, contractors use scaffolding instead of giants.

(p. 107) with a load factor of 0.5 to determine the equilibrium shape of the structure. The "0.5" accounts for relaxation. Subsequently, the other load cases are applied, such as self-weight, wind and snow. Probably, all analyses can be linear because only small displacements are obtained. (Large displacements would not be acceptable). When checking the stresses we need to manually add half the stress due to bending into the architect's shape.

Exercise: To compute the forces of the giants we consider a continuous beam over five pinned supports. Check the following matrix by computing the value of F_3 with a frame analysis program.

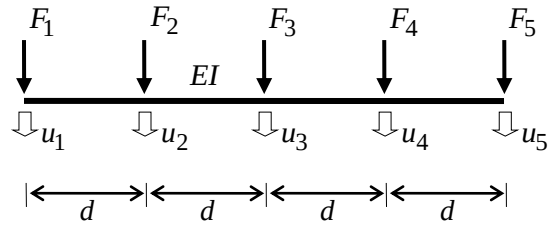

$$\begin{bmatrix} F_1 \\ F_2 \\ F_3 \\ F_4 \\ F_5 \end{bmatrix} = \frac{EI}{28d^3} \begin{bmatrix} 45 & -102 & 72 & -18 & 3 \\ -102 & 276 & -264 & 108 & -18 \\ 72 & -264 & 384 & -264 & 72 \\ -18 & 108 & -264 & 276 & -102 \\ 3 & -18 & 72 & -102 & 45 \end{bmatrix} \begin{bmatrix} u_1 \\ u_2 \\ u_3 \\ u_4 \\ u_5 \end{bmatrix}$$

Challenge: A beam continues over an infinite number of pinned supports.

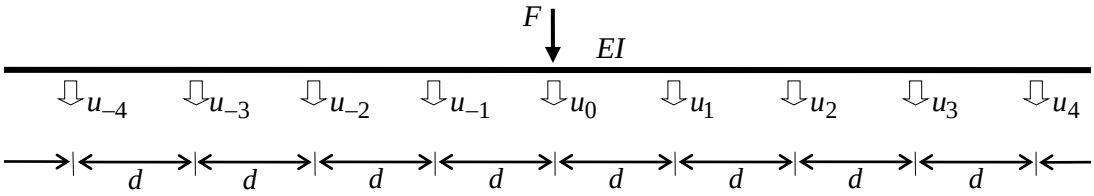

Derive the following equation.

$$\frac{Fd^3}{EI} = ... + (36\sqrt{3} - 48)u_0 - (72\sqrt{3} - 114)u_1 + (252\sqrt{3} - 432)u_2 - (936\sqrt{3} - 1620)u_3 + (3492\sqrt{3} - 6048)u_4 - ...$$

The next factor can be obtained by multiplying the last factor by $\sqrt{3} - 2$ et cetera.
The factors evaluate to

$$\frac{Fd^3}{EI} = ... + 4.48u_{-2} - 10.71u_{-1} + 14.35u_0 - 10.71u_1 + 4.48u_2 - 1.20u_3 + 0.32u_4 - 0.09u_5 + ...$$

Inextensional deformation
Figure 149 shows a very thin plastic spherical cap. The cap is simply supported and loaded by a force. The person applying the force feels that the shell is quite stiff. We see bending deformation but we know that the shell middle surface is stretching too. Otherwise this thin shell would not be stiff. This deformation is called *extensional deformation* because the shell middle surface is stretching. The loading is carried mostly by membrane forces and only a little by bending moments.

Figure 150 shows the same spherical cap but now free from its supports. The person applying the load feels that the shell is not stiff at all. This deformation is called *inextensional deformation* because it does not involve stretching or shrinking of the middle surface. The loading is carried mostly by bending and only a little by membrane forces.


Figure 149. Extensional deformation

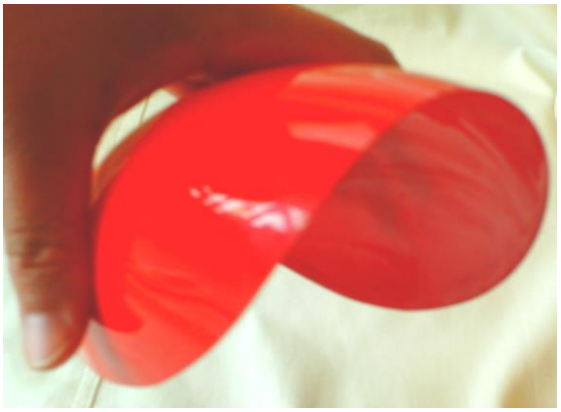
Figure 150. Inextensional deformation

In general, suppose that a shell roof is loaded by snow. If it deforms inextensionally the displacements are very large and the bending stresses are very large. Clearly, thin shells need to be designed such that inextensional deformation does not occur for any applied force.

However, inextensional deformation gives small stresses when a displacement is imposed, for example a foundation settlement. If the response to a foundation settlement would be extensional the stresses would be very large. Therefore, shells need to be designed such that inextensional deformations occur for imposed displacements.

Viking ship Oseberg
Viking ships (fig. 151) are known to be very flexible [59]. This has two causes.
1) The planks of a Viking ship are joint by iron rivets (fig. 152). The planks form an open shell which can move inextensionally (p. 109). The motion is somewhat controlled by curved members (ribs and knees) and horizontal members (beams and thwarts) (fig. 153).
2) The Vikings had no saws to cut timbers. (In those days, manufacturing thin steel plate was difficult.) They used axes for cutting timber. To make ship members they split the timber along the grain. Timber cut along the grain (by axe) is much stronger than timber cut through the grain (by saw). Therefore, each Viking ship member was strong, light and flexible.
It is not clear whether the Vikings liked their ships to be very flexible. The flexibility was just a consequence of planks joint into an open shell and light timber cut along the grain. Note that steel ships cannot be flexible. They would suffer from fatigue.



Figure 151. Viking longship Oseberg, Norway, 800 AD, 21.58 m long 5.10 m wide



Figure 152. Rivets next to an oar hole

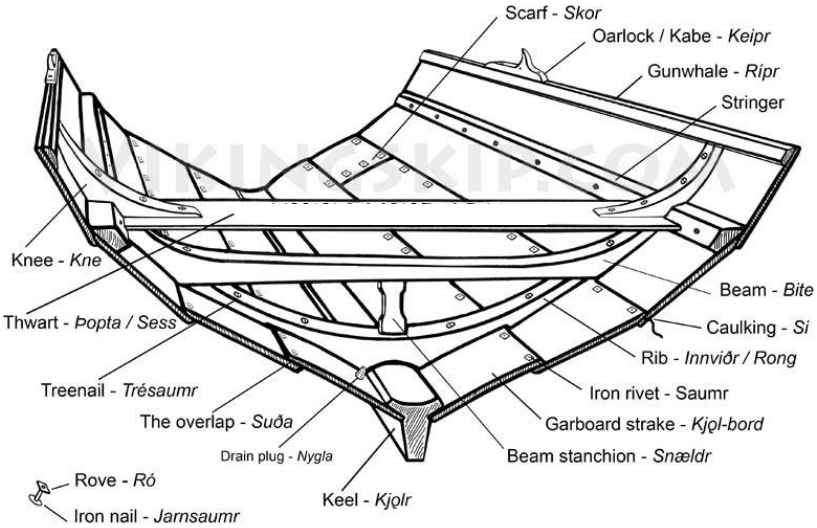

Figure 153. Parts of a Viking ship (words in English and old Norwegian) (www.vikingskip.com)

Liquid storage tanks
In Rotterdam port there are many liquid storage tanks. The tanks are welded out of 10 mm thick steel plates. The bottom steel plate is supported by square concrete plates that are simply placed onto compacted sand. Some of these tanks have a roof that floats onto the liquid. This is to prevent build-up of explosive gases in half filled tanks. Unfortunately, many tank roofs get stuck against the tank walls after just a few years of operation.

It appeared that some concrete plates settle more than at others. Therefore, the steel bottom plate curves and the tank wall deforms (fig. 154). Small settlements can cause surprisingly large wall deformations. This deformation is inextensional (p. 109). For the tank itself this is good because the steel stresses are small despite the large deformations. Unfortunately, as a consequence the floating roof gets stuck. Clearly, a floating tank roof needs be designed with a large clearance to the tank wall.

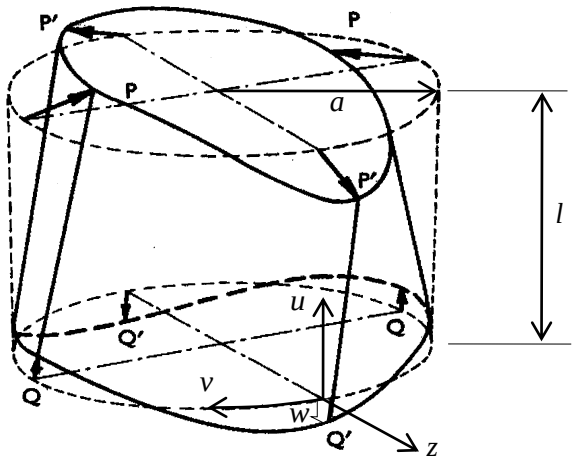

Figure 154. Inextensional deformation of a storage tank without roof [60]

Analysis of the liquid storage tank
The inextensional deformation of a liquid storage tank can be analysed by hand. Someone found out that the deformation is described by [60]

$$u_x = -w\cos\frac{2v}{a},$$
$$u_y = -2w\frac{u}{a}\sin\frac{2v}{a},$$
$$u_z = 4w\frac{u}{a}\cos\frac{2v}{a},$$

where a is the tank radius and w is the vertical displacement of Q'.This can be checked by substituting these equations in the shell membrane equations (p. 38).

$$\varepsilon_{xx} = \frac{\partial u_x}{\partial x} - k_{xx}u_z + k_x u_y = 0$$
$$\varepsilon_{yy} = \frac{\partial u_y}{\partial y} - k_{yy}u_z + k_y u_x = 0$$
$$\gamma_{xy} = \frac{\partial u_x}{\partial y} + \frac{\partial u_y}{\partial x} - 2k_{xy}u_z - k_x u_x - k_y u_y = 0$$

where has been used that $k_{xx} = k_{xy} = 0$, $k_{yy} = -\frac{1}{a}$ and $\alpha_x = \alpha_y = 1$. Apparently, all strains of the middle surface are zero, therefore, the described deformation is inextensional.

The horizontal displacement at P' ($u = l$, $v = 0$) is $u_z = \frac{4wl}{a}$.

Rijswijk shell roof [1]

In the city of Rijswijk (ZH) in the Netherlands a reinforced concrete shell roof was built for a factory. The shell consisted of several half cylinders that continued over three supports (fig. 155). Due to the heavy materials stored in the factory, the foundation started settling and some columns were pulled down more than others. In the lateral direction the shell followed the deformations beautifully in an inextensional way. However, in the axial direction the shell deformation was extensional (p. 109) and stiff. Apparently large membrane stresses occurred because large cracks were clearly visible in the shell near the settled columns. After a few years already, the building was demolished due to excessive maintenance costs. The conclusion is that cylinder shell roofs should not span over more than two supports.

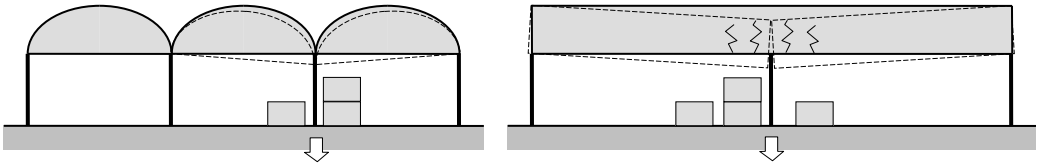

lateral cross-section axial cross-section

Figure 155. Extensional deformation of a shell roof in the city of Rijswijk

Spotting inextensional deformation

Inextensional deformation and extensional deformation can occur together. For example, a cylinder that is loaded in the axial direction (fig. 156). This loading will compress the middle surface and cause extensional deformation. On the other hand, a lateral loading on this cylinder will cause mainly bending and the deformation will be inextensional. When the loads are applied together, the combined deformation will be extensional.

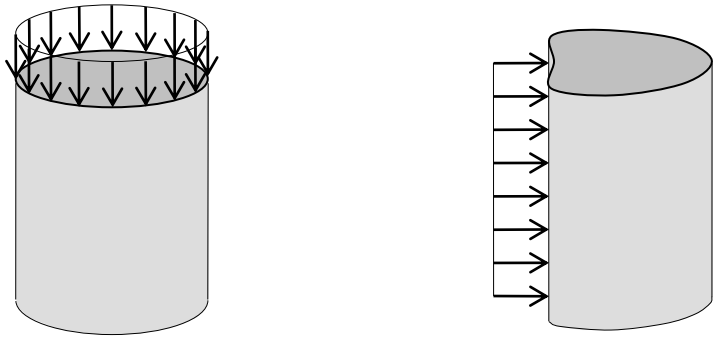

Figure 156. Extensional and inextensional deformation of an open cylinder

Vibration mode shapes

One way of spotting inextensional deformation (p. 109) is to compute the natural frequencies (p. 156) of a shell structure. If inextensional deformation is possible, this mode will have the smallest natural frequency. In most well designed shells the modes shapes are local deformations. Inextensional deformations, on the other hand, are typically deformations that

[1] Told by Henk van Koten in a lecture in May 2007. Henk van Koten (1929 – ....) was a teacher at Delft University.

involve a large part of a shell. This approach does not work for spotting extensional deformation due to support settlements.

Strain energy
Another way of spotting inextensional deformation (p. 109) is observing the strain energy in a shell. The membrane strain energy in a small shell part is

$$E_{sm} = \tfrac{1}{2} n_{xx}\varepsilon_{xx} + \tfrac{1}{2} n_{xy}\gamma_{xy} + \tfrac{1}{2} n_{yy}\varepsilon_{yy}\,.$$

The bending strain energy is

$$E_{sb} = \tfrac{1}{2} m_{xx}\kappa_{xx} + \tfrac{1}{2} m_{xy}\rho_{xy} + \tfrac{1}{2} m_{yy}\kappa_{yy} + \tfrac{1}{2} v_x\gamma_{xz} + \tfrac{1}{2} v_y\gamma_{yz}\,.$$

In this it is assumed that the material behaviour is elastic. The strains and curvatures are those of the middle surface. Note that strain energy does not have a direction and is always positive. A ratio α can be defined as

$$\alpha = \frac{E_{sm} - E_{sb}}{E_{sm} + E_{sb}}$$

A contour plot of α over the shell shows where membrane action is dominant ($0 < \alpha < 1$) and where bending action is dominant ($-1 < \alpha < 0$). Dominant bending action is a sign of inextensional deformation. Unfortunately, most structural analysis programs cannot plot this quantity.

Theorema egregium
The shell compatibility equation (p. 57) reads

$$-\frac{\partial^2\varepsilon_{xx}}{\partial y^2} + \frac{\partial^2\gamma_{xy}}{\partial x\partial y} - \frac{\partial^2\varepsilon_{yy}}{\partial x^2} = -k_{yy}\kappa_{xx} + k_{xy}\rho_{xy} - k_{xx}\kappa_{yy}$$

The left hand side represents membrane deformation. The right hand side represents bending deformation. Both sides are equal to the increase of the Gaussian curvature k_G (p. 23) during loading. This is proved in appendix p. 205. Studying the compatibility equation we see the following.

If the deformation is inextensional ($\varepsilon_{xx} = \gamma_{xy} = \varepsilon_{yy} = 0$) then the Gaussian curvature does not change.

This property was discovered by the mathematician Carl Gauß in 1827. Gauß called it *theorema egregium*, which is Latin for "remarkable theorem". He formulated it as "*If a curved surface is developed upon any other surface, the measure of curvature in each point remains unchanged.*" (translated from Latin) It is true for small, large and very large deformations [61].

Exercise: How do we call "*developed upon*"? How do we call "*measure of curvature*"?

Studying the compatibility equation we see that there are more situations in which the Gaussian curvature does not change due to the load, for example $\varepsilon_{xx} = \gamma_{xy} = \varepsilon_{yy} = 1$ everywhere. So, inextensional deformation is a special case of no-change-in-Gaussian-curvature (fig. 157).

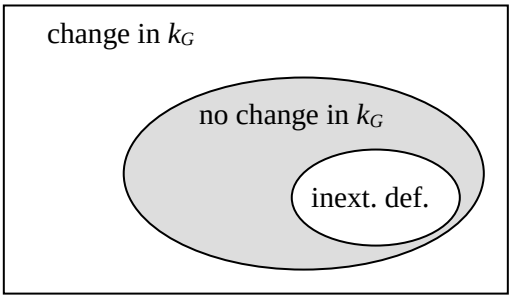

Figure 157: Venn diagram of local shell behaviour

Shells behaving like a plate

If the Gaussian curvature does not change by a load perpendicular to the surface, then this load is carried in bending only.

Proof: The increase of the Gaussian curvature can be written as (appendix p. 205.)

$$\Gamma u_z = k_{yy}\frac{\partial^2 u_z}{\partial x^2} - 2k_{xy}\frac{\partial^2 u_z}{\partial x \partial y} + k_{xx}\frac{\partial^2 u_z}{\partial y^2}.$$

The shallow shell differential equation (p. 59) is

$$\frac{E t^3}{12(1-\nu^2)}\nabla^2\nabla^2\nabla^2\nabla^2 u_z + E t \Gamma\Gamma u_z = \nabla^2\nabla^2 p_z .$$

When the Gaussian curvature does not change then

$$\Gamma u_z = 0 .$$

If this condition is fulfilled over some shell area then the differential equation in this area reduces to

$$\frac{E t^3}{12(1-\nu^2)}\nabla^2\nabla^2 u_z = p_z$$

which is the differential equation of plates loaded in bending. Though the shell is curved, the load p_z is carried by bending moments and not by membrane forces. Q.E.D.

Shell design

Suppose we are designing a thin shell and part of its area has very large stresses (1). We increase the thickness and this reduces the stresses. However, we find that for acceptable stresses the thickness needs to be large (2). The large stresses seem to be caused by large bending moments and not by normal forces (3). Now we have observed three symptoms of inextensional deformation (p. 109) and we think that this might be the problem. We plot the increase of the Gaussian curvature for each load case. It appears that for one of the load cases the increase of the Gaussian curvature is almost zero in the problem area. Now we know for sure that our shell suffers from inextensional deformation. A solution can be to add a stiff beam to the shell edge.

Plotting Gaussian curvature
Unfortunately, most finite element programs cannot make a contour plot of the Gaussian curvature or the increase of the Gaussian curvature. Programmers need to implement this, which is not an easy task. Only for high accuracy elements the Gaussian curvature can be computed from information available within an element (see shell finite elements p. 82).

Kresge Auditorium
Kresge Auditorium is a building at MIT campus in Cambridge (close to Boston, USA) (fig. 158). It was completed in 1955. Its shape is spherical with three edge beams and three point supports. The reinforced concrete edge-beams prevent inextensional deformation (p. 109) of the reinforced concrete shell. The edge beams cause edge disturbances (p. 14) in the shell. The height is 15 m. The span between two supports is 48 m. The shell thickness is 90 mm. The architect is Eero Saarinen. The engineering firm is Ammann & Whitney. The contractor is the George A. Fuller Company. The money was donated by Sebastian Kresge ($1.5 million).
In the original design the curtain walls were horizontally supported by the edge beams. In the vertical direction the curtain walls were self-supporting with an expansion joint to the edge beam. However, after removal of the timber formwork much creep occurred in the concrete (more than 130 mm deflection). Therefore, the curtain walls were quickly redesigned to also vertically support the edge beams [62].

The current roof cover dates from 1980. It consists of copper sheets. Earlier roof covers were made of plastic applied as a liquid (lasted 8 years) and soldered lead sheets (lasted 15 years). They cracked due to temperature deformation of the roof. (In the Boston climate half a roof can be covered in snow while the other half is heated by the sun.) The cracks and lack of ventilation made the concrete wet. Corrosion and freezing severely damaged the concrete. Extensive and costly repairs have taken place, including replacing large parts of the edge beams. If the building were not architecturally important, it would have been replaced a long time ago. Fortunately, the problems seem to be solved now [62].

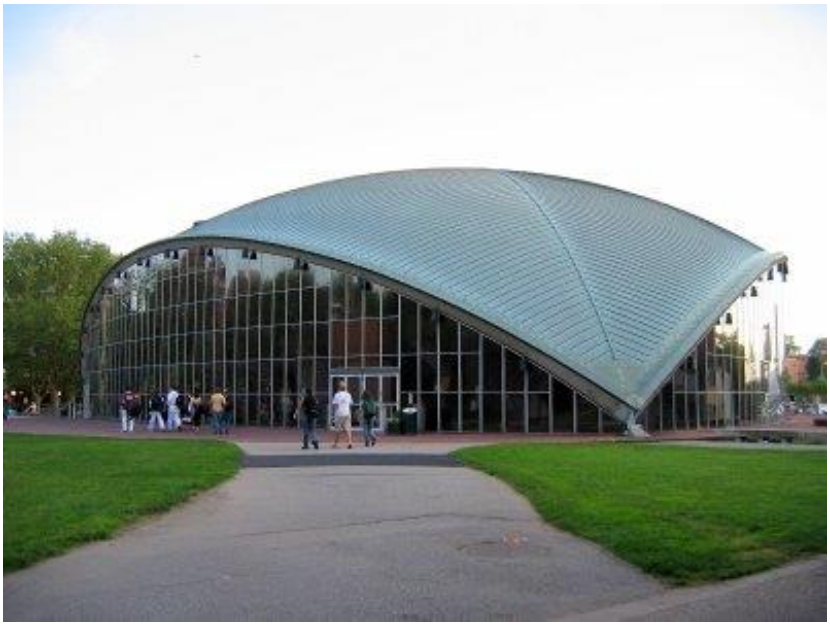
Figure 158. Kresge Auditorium (MIT, Cambridge USA)

Kresge auditorium has whispering galleries (p. 43). Nevertheless, the acoustic properties are quite good and it is often used as a concert hall.

Exercise: The radius of curvature of Kresge Auditorium can be calculated by $a = \frac{1}{2}s + \frac{1}{6}\frac{l^2}{s}$, where s is the sagitta and l is the distance between the supports. Derive this formula.

Deitingen petrol station

In Switzerland next to highway A1 is Deitingen petrol station (fig. 159). It has two reinforced concrete canopies that have been designed by Heinz Isler.[2] They have been built by Willi Bösiger AG in 1968. Note that this shell does not have edge beams. It can deform inextensional but apparently this does not give problems. The span is 31.6 m. The smallest thickness is 90 mm. The radius of curvature is 52 m. The ratio a/t = 580.

The formwork of this shell consisted of steel scaffolding, curved glulam beams (approximately 180 x 50 mm spaced 800 mm) and wood floor boards. The formwork parts were reused on other projects. The concrete is watertight and a roof cover has not been applied. The surface is just painted [63, 64, 65].



Figure 159. Deitingen petrol station

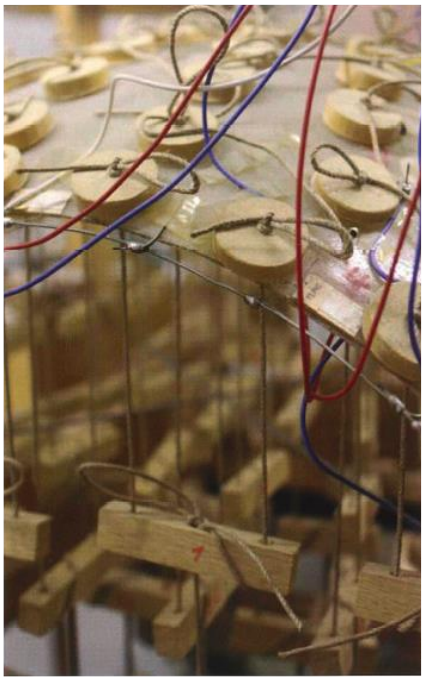

Figure 160. Model of a shell structure made by Heinz Isler [64]

Gauß-Bonnet theorem

A sphere has in every point a Gaussian curvature of $k_G = k_1 k_2 = (-\frac{1}{a})(-\frac{1}{a}) = \frac{1}{a^2}$.

It has a surface area of $A = 4\pi a^2$.

The total Gaussian curvature of a sphere is $\int_A k_G dA = k_G A = \frac{1}{a^2} 4\pi a^2 = 4\pi$.

When this calculation is repeated for an ellipsoid, a tractricoid or a brick the results are also 4π. The total Gaussian curvature of the surface of any object without holes is 4π. If the object has one hole then the total Gaussian curvature is 0. If the object has two holes the total

[2] Heinz Isler (1926–2009) was a Swiss engineer. He designed more than 1200 reinforced concrete shell roofs. Most were built between 1955 and 1979. He did not use computers for structural analysis. Instead, he used plastic models and strain gauges to determine deflections, stresses and buckling loads (fig. 160) [64].

Gaussian curvature is -4π. This is the *Gauß-Bonnet theorem* which was published by the mathematician Pierre Bonnet in 1848 [Wikipedia].

Table 13. Total Gaussian curvature of 10 objects

	4π
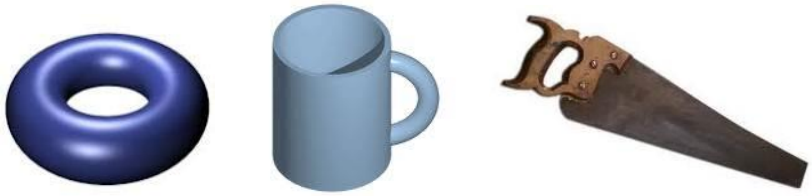	0
	– 4π

Exercise: Which are the two holes in a teapot?

Exercise: The total Gaussian curvature of a brick is 4π. A brick has 6 faces, 8 edges and 8 corners. Which part contributes most to the 4π ?

Corollary
Consider a point load perpendicular to the surface of a shell. Under the point load the Gaussian curvature has decreased (or increased). According to the Gauß-Bonnet theorem (p. 116) the total Gaussian curvature does not change. So somewhere else the Gaussian curvature must have increased (or decreased). Apparently, shells carry load by moving around Gaussian curvature.

Force on a sphere
In 1946, Eric Reissner solved a simplified version of the Sanders-Koiter equations (p. 54) for a spherical cap loaded by a force perpendicular to the surface. The solution consists of Kelvin functions [67]. The deflection u_z under the point load P is

$$u_z = \frac{\sqrt{3}}{4}\frac{Pa}{Et^2}\sqrt{1-\nu^2}\ .$$

The membrane forces under the point load are

$$n_1 = n_2 = -\frac{\sqrt{3}}{8}\frac{P}{t}\sqrt{1-\nu^2}\ .$$

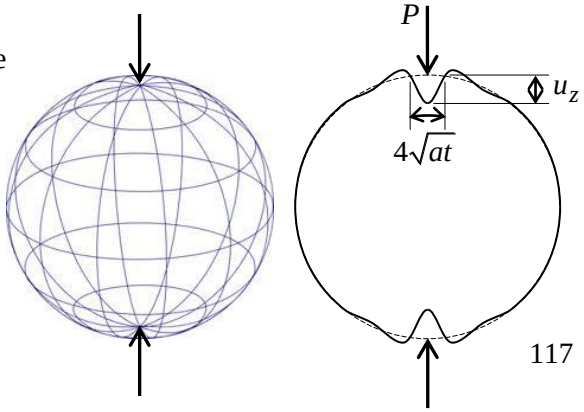

Force on a shell of positive Gaussian curvature

In 1963, He Guang Qian (何广乾 pronounce ho kwang tsien) and Chen Fu (陈伏) derived the solution to a force perpendicular to a shell of any positive Gaussian curvature [68]. [3]

$$u_z = \frac{\sqrt{3}}{4}\frac{P}{Et^2\sqrt{k_G}}\sqrt{1-\nu^2}\ .$$

The formula is accurate when the deformation is extensional and the distance from the point load to the shell edges is large. The membrane forces under the point load are the same as for a force on a sphere (p. 117)

Force on a cylinder

In 1977, Chris Calladine studied circular cylindrical shells loaded by point loads (fig. 161) [69 p. 305]. [4] He found a difference between long cylinders and short cylinders.

long cylinder $l > \frac{a}{t}\sqrt{at}$		$u_z = 2^{-\frac{1}{3}}\frac{P}{Et}\left(\frac{a}{t}\sqrt{1-\nu^2}\right)^{\frac{3}{2}}$
short cylinder $\sqrt{at} < l < \frac{a}{t}\sqrt{at}$	with fixed ends	$u_z = \frac{1}{4}\sqrt{2}\frac{P}{Et}\left(\frac{a}{t}\sqrt{1-\nu^2}\right)^{\frac{5}{4}}\left(\frac{l}{a}\right)^{\frac{1}{2}}$
	with diaphragm ends	$u_z = \frac{1}{2}\frac{P}{Et}\left(\frac{a}{t}\sqrt{1-\nu^2}\right)^{\frac{5}{4}}\left(\frac{l}{a}\right)^{\frac{1}{2}}$
	with free ends	$u_z = \frac{1}{2}\frac{P}{Et}\left(\frac{a}{t}\sqrt{1-\nu^2}\right)^{2}\frac{a}{l}$

where l is half the cylinder length. The membrane forces under a point load are

$$n_1 = 0, \quad n_2 = -\frac{\sqrt{3}}{8}\frac{P}{t}\sqrt{1-\nu^2}\ .$$ [5]

The principal normal force directions are the principal curvature directions.

The cylinder formulas are not accurate at the transition between long and short. The accurate deflection can be read from the graphs in figure 161b. These graphs were computed by representing the point loads as a summation of sine line loads (Fourier series p. 166). The formulas were derived as straight line curve fits of the graphs.

---

[3] He and Chen worked at Ministry of Building Construction in China. Their formula was confirmed by Russian, European and American scientists a few years after it was discovered. Unfortunately, by then the cultural revolution (1966–1975) had destroyed Chinese science.

In 2012, Amir Semiari made finite element models of surfaces of varying curvature for his bachelor end project in Delft University [70]. He did not know of He and Chen's solution. He also found that Reissner's solution of a point load on a sphere can be adapted to shells of any positive Gaussian curvature by replacing the radius a by $1/\sqrt{k_G}$.

[4] C.R. Calladine (1935–…) was professor of structural mechanics at the University of Cambridge [Wikipedia].

[5] The formulas are also valid for a negative load P. In that case, exchange n_1 and n_2 .

Exercise: Which of the cylinder formulas describes inextensional deformation?

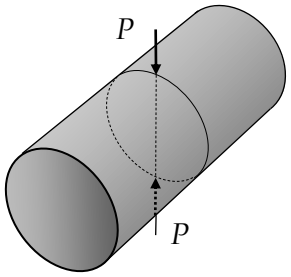

Figure 161. Two point loads on a circular cylindrical shell

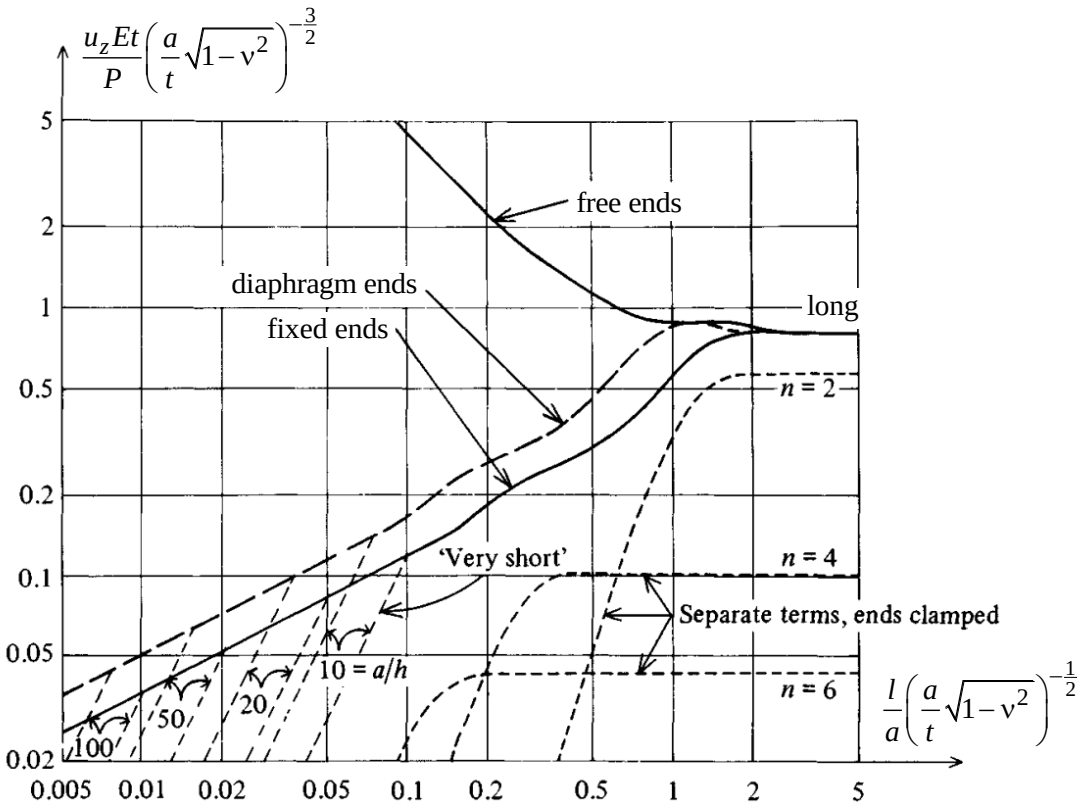

Figure 161b. Deflection at one of the point loads in figure 161 [69 p. 305]

Force on a shell of negative Gaussian curvature

In 2013, Nathalie Ramos studied anticlastic shells loaded by perpendicular forces. From many finite element results she derived the following formulas [73]. The deflection u_z under the force *P* is

$$u_z = 0.92\frac{P}{Et^2\sqrt{-k_G}}\sqrt{1-\nu^2}\ .$$

The membrane forces under the force are

$$n_1 = -0.13\frac{k_1}{\sqrt{-k_G}}\frac{P}{t}\sqrt{1-\nu^2}, \quad n_2 = -0.13\frac{k_2}{\sqrt{-k_G}}\frac{P}{t}\sqrt{1-\nu^2}\ .$$

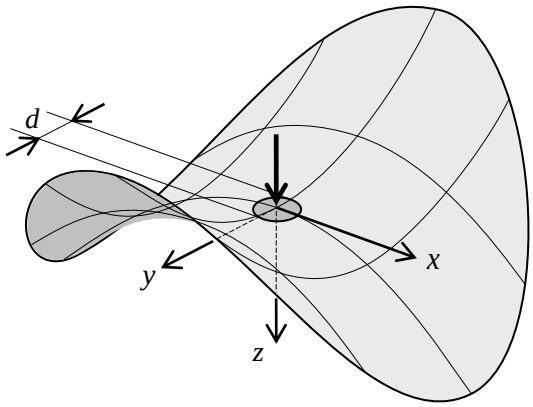

Figure 162. Point load on a hypar shell

Moments due to a force
In 2016 formulas were developed for moments due to perpendicular forces on shells of any curvature [74].

$$m_1 = 0.0388(1+\nu)P\ln\frac{t}{\tilde{k}_2 d^2}$$

$$m_2 = 0.0388(1+\nu)P\ln\frac{t}{\tilde{k}_1 d^2}$$

where

$$\tilde{k}_2 = |0.00725k_1 + 0.199k_2| + |0.0529k_1 + 0.0298k_2|$$
$$\tilde{k}_1 = |0.00725k_2 + 0.199k_1| + |0.0529k_2 + 0.0298k_1|$$

Symbol d represents the diameter of the circular area over which the load is distributed (fig. 162). The moments m_1 and m_2 are the local peaks, which occur directly under the force. They are in the principal curvature directions; m_1 is in the direction of k_1 and m_2 is in the direction of k_2. The formulas are also valid for $P < 0$, however, then m_1 is not larger than m_2. This can be simply solved by exchanging the names m_1 and m_2.

Plate twisting
A flat plate has zero Gaussian curvature. When the plate is twisted it has a negative Gaussian curvature. Since the Gaussian curvature has changed, membrane forces develop (see Theorema egregium p. 113). The phenomenon can be observed in a towel (fig. 163). Ask someone to hold two corners of the towel and hold the other two corners yourself. Stretch the towel firmly. Slowly move one of the corners out of plane. You will observe that the middle of the towel becomes floppy. If the towel were a plate, the middle would be compressed and the edges would be tensioned.

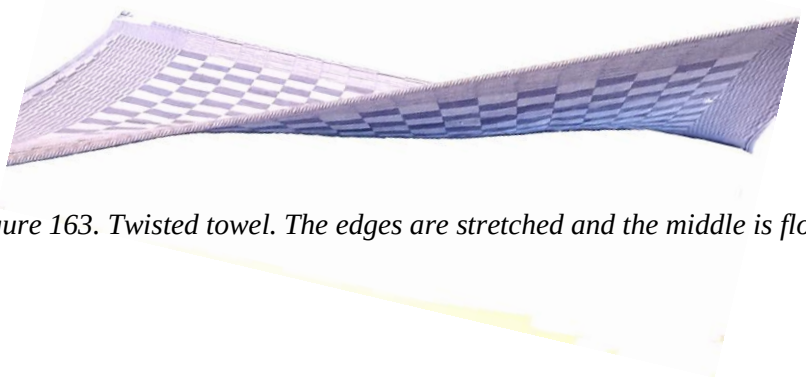

Figure 163. Twisted towel. The edges are stretched and the middle is floppy.

Due to compression in the middle, a twisted plate can buckle. The shape changes from a hypar to a cylinder and the Gaussian curvature disappears. Buckling occurs at an out of plane corner displacement $u = 16.8t$. This has been discovered by Dries Staaks in his 2003 graduation project [75]. In the plate middle the membrane forces are

$$n_1 = n_2 = \tfrac{1}{107} E t b^2 k_G ,$$

where b is the plate length and width [75b]. In the plate edge the membrane forces are

$$n_1 = -\tfrac{1}{26} E t b^2 k_G \qquad n_2 = 0 .^{6}$$

Before buckling the Gaussian curvature is $k_G = -u^2 / b^4$. The latter equation can be derived in the same way as hypar curvature (p. 102) The previous formulas are for square panels. Unfortunately, for rectangular panels no formula is available. Important applications are glass façades and glass roofs (fig. 165).



Figure 165. Canopy of twisted glass panels at a bus stop in Delft, the Netherlands

Exercise: A reinforced concrete hypar (a = 140 m) will be cast on a timber formwork. The formwork will consist of straight beams in parallel to the hypar edges and multiplex plates. The plates will be twisted. Clearly, we do not want them to buckle. The factory dimensions of the plates are 2440 x 1220 x 18 mm. Do the plates need to be cut to a smaller size?

Gaussian curvature of boats
Steel boats are made of plates that have zero Gaussian curvature both before assembling and after assembling (fig. 166). An edge where the plates are connected is called chime.

[6] These formulas are also valid for positive Gaussian curvatures. In that case, exchange $n1$ and $n2$.

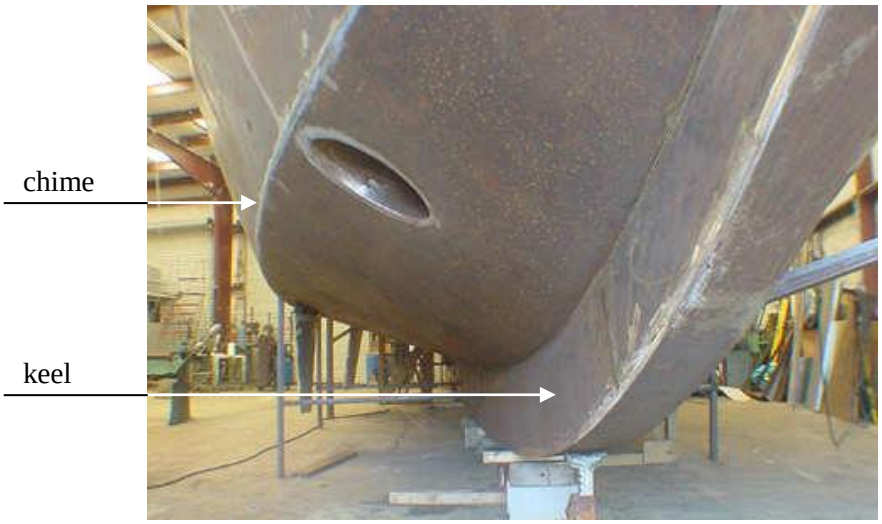

Figure 166. Curved plates at the bow of a steel boat (zero Gaussian curvature)

Prestressing tents

Tents are made of fabric parts that are sewed together. The Gaussian curvature of the fabric is zero (It leaves the factory on a role). Therefore, in a traditional circus tent every fabric part has zero Gaussian curvature (fig. 167). However, architects like smooth shapes which do have Gaussian curvature (fig. 168). If we impose a Gaussian curvature to a fabric it wrinkles, unless it is prestressed. In the direction of the seams the required prestress is

$$n_{xx} = -\frac{1}{24} E t b^2 k_G ,$$

where b is the fabric width. Perpendicular to the seams the required prestress is

$$n_{yy} = \frac{1}{6144} \frac{E t b^4 |k_G k_{xx}|}{z} ,$$

where z is accepted maximum distance from the theoretical smooth surface to the tent fabric [76].



Figure 167. Traditional circus tent (zero Gaussian curvature)

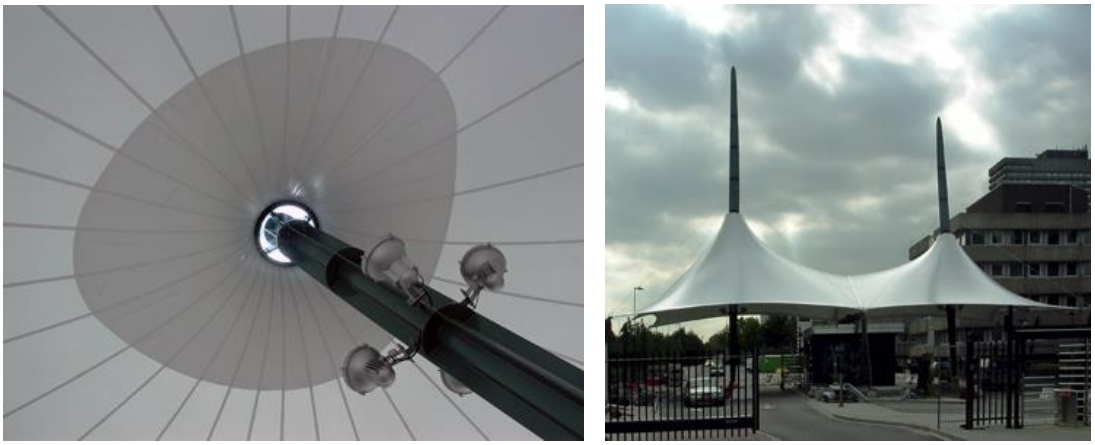

Figure 168. Canopy at the European patent office in Rijswijk, Netherlands (negative Gaussian curvature) architect Lewis X Associates, consultant Tentech, contractor Poly-Ned

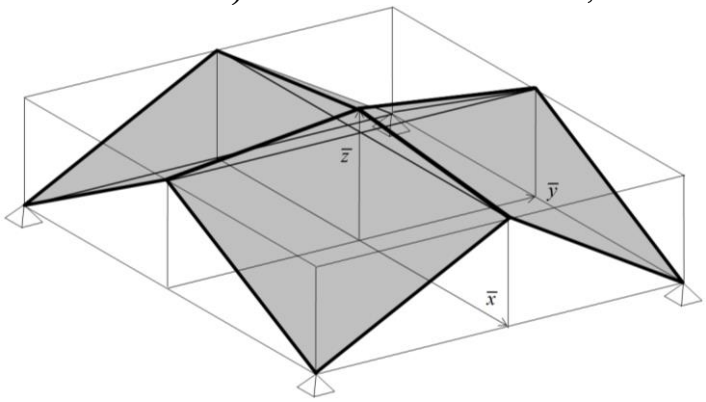

Figure 169. Four hypar shells

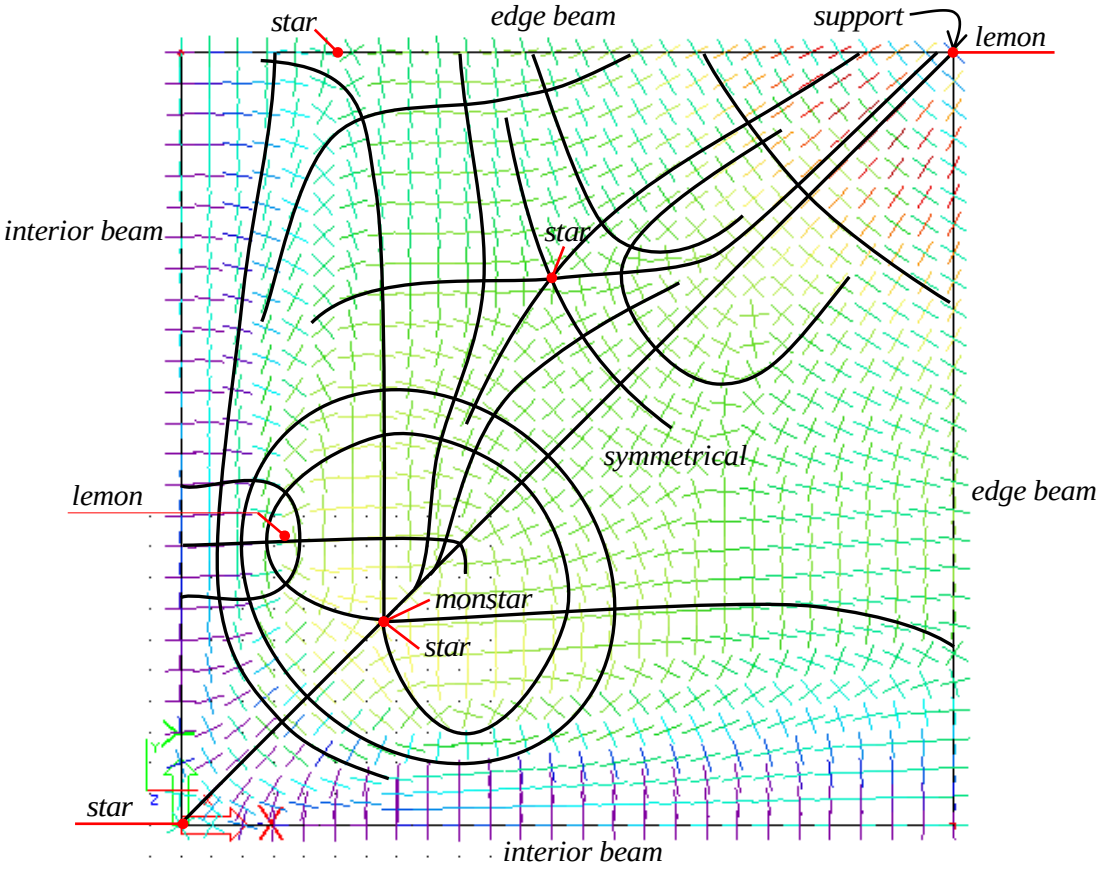

Figure 170. Moment trajectories in one of the hypar shells of figure 169 due to self-weight

Umbilics

An *umbilic* is a point in a tensor field where both principal values are the same. For example $m_{xx} = 40$ kNm/m, $m_{yy} = 40$, $m_{xy} = 0$. Consequently, $m_1 = 40$ and $m_2 = 40$ and Mohr's circle is just a point. Principal directions cannot be determined. The reason is that the principal directions are defined as the directions in which $m_{xy} = 0$. In an umbilic $m_{xy} = 0$ in any direction. Umbilics are also called *umbilical points* or *isotropic points*.

Umbilics draw attention to themselves, however, they are harmless. It seems that shells are less likely to fail in umbilics then in other locations.

Umbilical patterns

The trajectories (p. 98) around an umbilic (p. 124) have a particular pattern. If the tensor field is linear in *x* and *y* around the umbilic then either a *monstar* or a *star* occurs (fig. 171). Both patterns have three trajectories that go through the umbilic. These trajectories are called *ridges*. The ridges of a monstar are always within a 90º angle. The ridges of a star are always not within a 90º angle. When any two ridges have an angle of exactly 90º then the third ridge does not occur and the usual orthogonal pattern occurs.

When the three ridges of a monstar coincide a *lemon* occurs.[7] When two ridges of a monstar coincide a pattern occurs that does not have a name. Let us call it a *flame*.[8] Figure 172 shows the trajectory pattern as a function of the ridge angles (see appendix Umbilical patterns).

More patterns are possible if the tensor field around an umbilic is nonlinear in *x* and *y*. Then the number of ridges is unlimited, for example the moment trajectories around a point load on a shell. These are not studied in these notes.

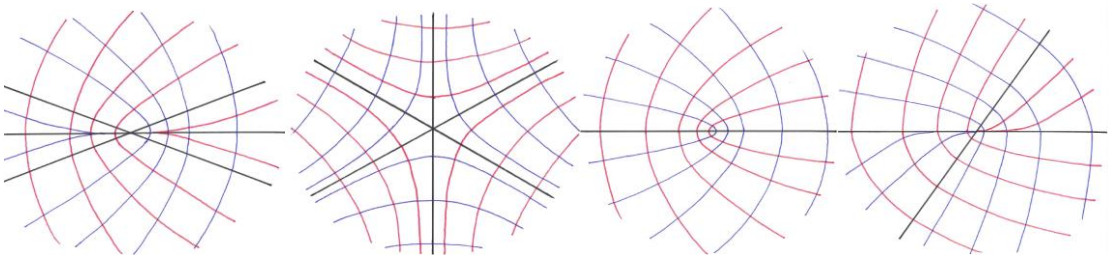

Figure 171. Trajectory patterns around an umbilic in case of a linear tensor field

[7] The name lemon is related to the fruit's shape that can be recognised in the trajectory pattern. The name monstar is derived from lemon-star.

[8] The theory of umbilics has been developed by mathematicians studying differential geometry [77]. They probably thought that the flame was not interesting and did not need mentioning. This has created confusion amongst engineers who observed trajectories in which two ridges crossed at angles different than 90º which they thought would not be possible. By giving it a name future confusion can be avoided.

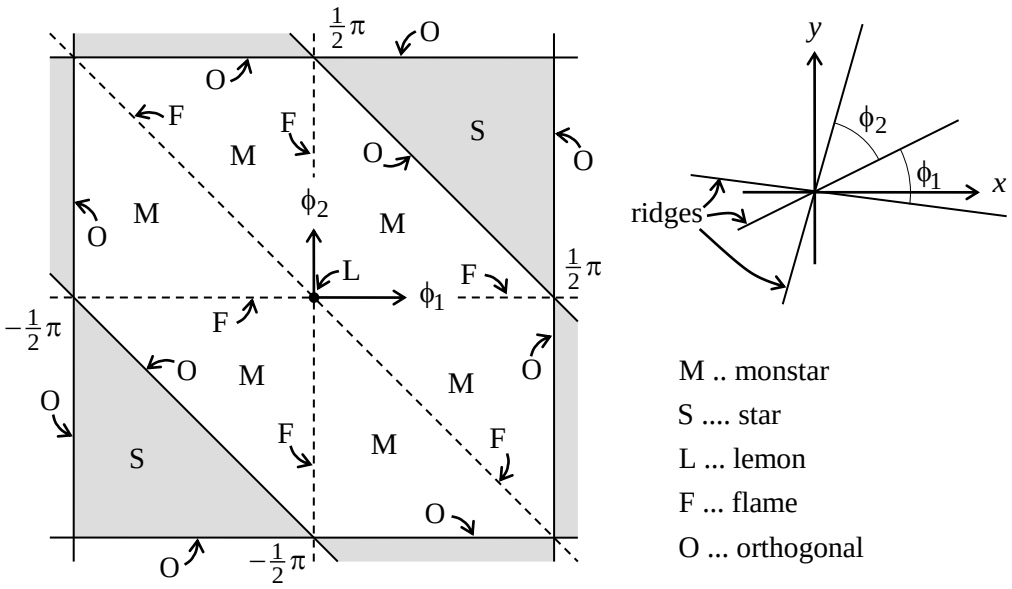

Figure 172. Umbilical patterns as a function of the ridge angles ϕ_1 and ϕ_2

Monkey saddle
A monkey saddle (fig. 173) is a surface described by the function

$$\bar{z} = \frac{\bar{x}^3 - 3\bar{x}\bar{y}^2}{6a^2}$$

An orthogonal parameterisation (p. 25) is not available. The origin is a point of zero Gaussian curvature (p. 23) in an area of negative Gaussian curvature. The curvature trajectories (p. 98) show a star umbilic (p. 124).

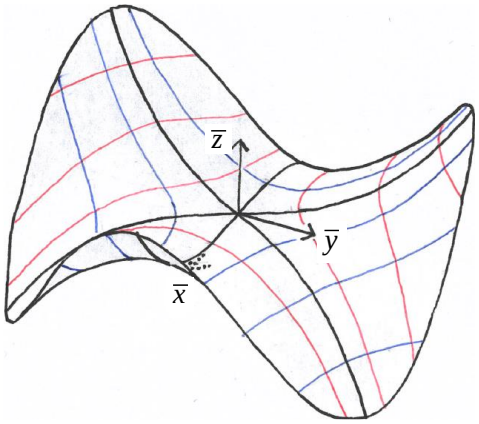

Figure 173. Curvature trajectories on a monkey saddle

Exercise: People in Switzerland use the words *Kammweg* and *Talweg*. These words are useful in geometry too. Can you apply these to the monkey saddle?



Figure 174. Sydney opera house

Architect: Jørn Utzon
Engineering: Ove Arup and partners
Contractor: Hornibrook Group Pty Ltd.
The building was designed in 1955 and completed in 1973.
The shell roofs are made of precast concrete panels supported by precast concrete ribs.
Cladding: white tiles
Costs: $102 million

Hypar edge moments

The edges of hypar shells are supported by edge beams. The edge beams help the shell by carrying normal forces but they also cause edge disturbances (p. 14). Figure 175 shows hypar bending moments for a hinged edge and a fixed edge. The loading p is perpendicular to the surface and evenly distributed. The hinged edge represents a small edge beam with little torsion stiffness. The fixed edge represents a strong edge beam or an interior beam which will not twist because it is loaded symmetrically. The graphs were made by Henk Loof in 1961 [78]. For example, in the graph we read that the largest moment at a non-twisting edge beam is

$$m_{xx} = -0.511 \frac{p}{l^2} (a t l)^{\frac{4}{3}},$$

where l is the length of the edge beam. The related shear force is (slope of the moment distribution)

$$v_x = 1.732 \frac{p a t}{l}.$$

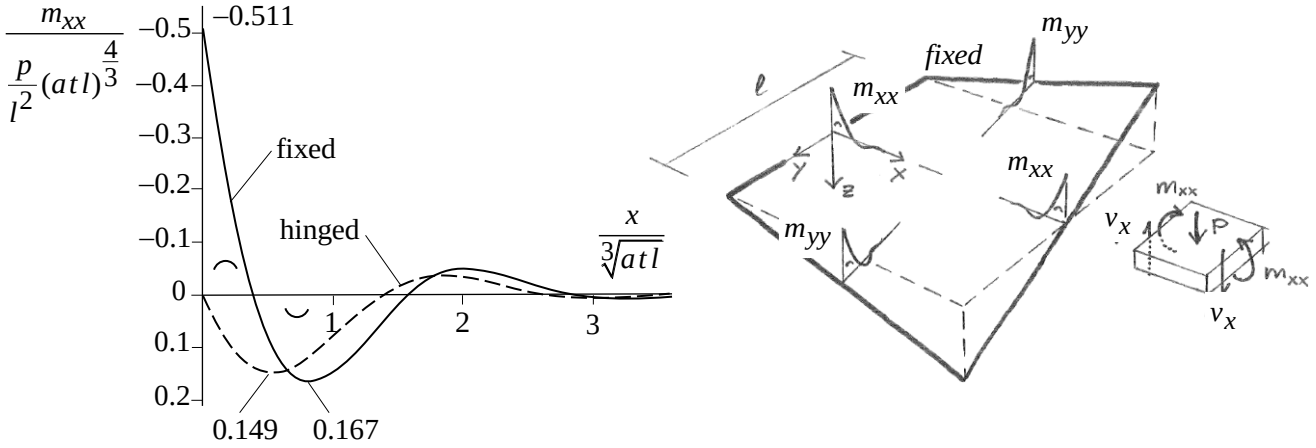

Figure 175. Bending moments in the edge of hypar shell

Unfortunately, the graphs are not accurate for all situations [79] and finite element analyses are necessary to check hypar designs.

Berenplaat hypar roof
In Spijkenisse, the Netherlands … Berenplaat water treatment facility,
Filter house, 107 x 133 m, consists of twenty reinforced concrete shells. Each shell consists of 4 hypars.
Architect: Wim Quist
Built from 1959 to 1964.
Not open to the public.

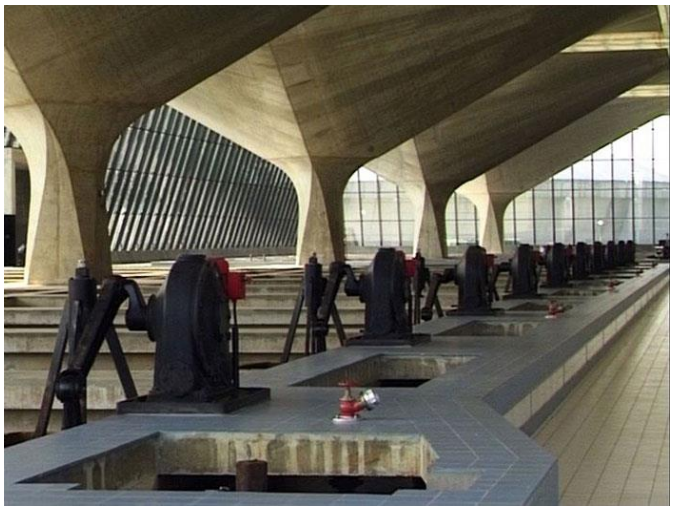

Figure 176. Berenplaat water treatment facility [Yoshito Isono]

Paaskerk hypar roof
The Paaskerk is a church in Amstelveen, the Netherlands.
Its roof consists of one thin hypar shell.
It was built in 1963.
Architect: Johan van Asbeck
Contractor: Woudenberg te Ameide
Plan 21.50 x 21.50 m, a = 31 m
Dutch national monument



Figure 177. Paaskerk

Surprising flexibility

Figure 178 shows a curved shell roof supported by brick walls. The twisting curvature k_{xy} is zero. The Gaussian curvature k_G is negative. The brick walls provide diaphragm boundary conditions (p. 70) to the shell. (In brick walls occur only normal forces and in plane shear forces. A significant abutment force from the shell to a wall would not be resisted; the wall would just crack and bend.) The shell length l_x and shell width l_y are special; they have the ratio

$$\frac{l_x}{l_y} = \sqrt{-\frac{k_{yy}}{k_{xx}}}\,.$$

This particular shell and boundary conditions is surprisingly flexible; it suffers from inextensional deformation (p. 109) [80]. The deformation is described by

$$u_x = \frac{l_x k_{xx}}{\pi} \sin\frac{\pi u}{l_x} \cos\frac{\pi v}{l_y}, \qquad u_y = \frac{l_y k_{yy}}{\pi} \cos\frac{\pi u}{l_x} \sin\frac{\pi v}{l_y}, \qquad u_z = \cos\frac{\pi u}{l_x} \cos\frac{\pi v}{l_y}.$$

The problem can be solved by a significant change to the shell length, width, curvatures or boundary conditions. However, if the length or the width is doubled, the inextensional deformation still occurs. The deformation simply repeats itself.

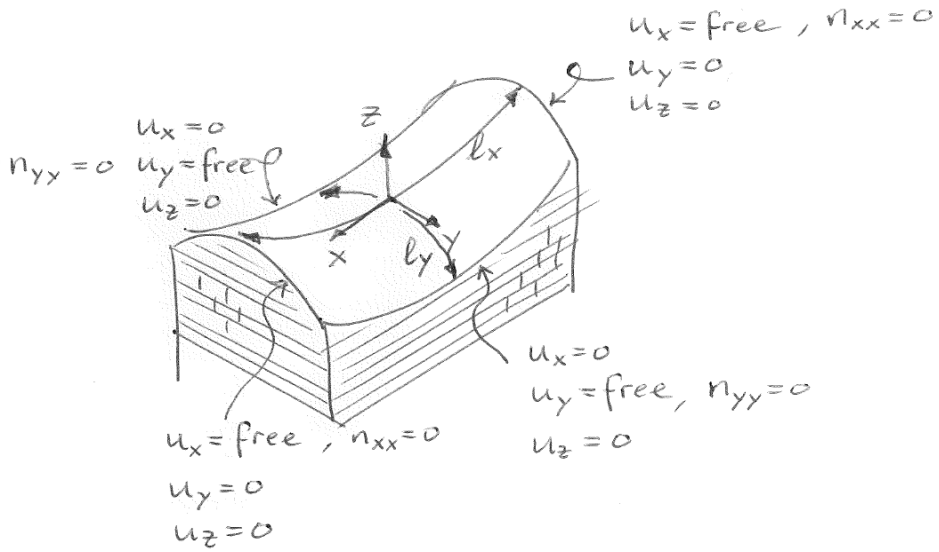

Figure 178. Curved shell roof supported by brick walls

Exercise: Proof that the above deformation is inextensional indeed. Assume that the shell is shallow. So, $u \approx x$, $v \approx y$, k_{xx} and k_{yy} are constant. Note that for positive Gaussian curvatures, this inextensional deformation is imaginary $(\sqrt{-1})$ and therefore does not exist.

Parameterisation of a paraboloid in the principal curvature directions

A paraboloid can be described by the following orthogonal parameterisation (p. 25) in the principal curvature directions (p. 22). In figure 179, the parameters a = 1 m and b = -1 m, produce a hypar (p. 21), which looks like Enneper's surface (p. 164). The curvilinear coordinates u and v (p. 31) have the dimension length. It is possible to change the parameterisation such that u and v have no dimension, however, this makes the equations of k_{xx}, k_{yy}, α_x, α_y a bit longer.

$$\bar{x} = u\left(1 + \frac{A}{1+\sqrt{1+A}}\right) \qquad A = \frac{v^2}{b(b-a)}$$

$$\bar{y} = v\left(1 + \frac{B}{1+\sqrt{1+B}}\right) \qquad B = \frac{u^2}{a(a-b)}$$

$$\bar{z} = \frac{\bar{x}^2}{2a} + \frac{\bar{y}^2}{2b} \qquad a \neq b$$

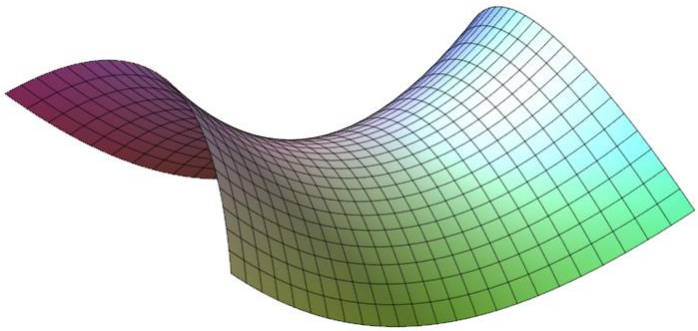

Figure 179. Parameter lines on a paraboloid
a = 1 m, b = –1 m, –1 m < u < 1 m, –1 m < v < 1 m

$$k_{xx} = \frac{1}{a}\left(1 - \frac{3u^2}{2a^2} - \frac{v^2}{2b^2} + \ldots\right)$$

$$k_{yy} = \frac{1}{b}\left(1 - \frac{3v^2}{2b^2} - \frac{u^2}{2a^2} + \ldots\right)$$

$$k_{xy} = 0$$

$$\alpha_x = 1 + \frac{u^2}{2a^2} + \frac{1}{2}A + \ldots$$

$$\alpha_y = 1 + \frac{v^2}{2b^2} + \frac{1}{2}B + \ldots$$

$$k_G = \frac{a^3 b^3}{(a^2+u^2)^2 (b^2+v^2)^2}$$

Sudden collapse
Shells are very efficient in carrying load. However, this efficiency comes at a price. If a shell buckles, it collapses with a bang. There will be no warning and it will collapse faster than we can run.
Truss, frame and plate structures do not have this problem. Usually, they slowly deform a lot before collapsing and therefore they give clear warnings to evacuate the area.
Consequently, shells need to be extra safe. In other words, for shells we often use larger load factors and material factors than for most structures. In the eurocode this is organised in consequence classes. Often, the highest consequence class is appropriate.

Tucker High School
On September 14, 1970, the gymnasium of The Tucker High School in, Henrico County, Virginia, collapsed completely [81]. Some school children were injured but fortunately there was no loss of life. The structure was a four element hypar (p. 102) with a plan of 47.2 m by 49.4 m (fig. 180). It had a sagitta (p. 1) of about 4.6 m, large inclined supporting ribs and centre ribs that were essentially concentric with the shell. The shell was 90 mm thick for the most part. Therefore, it had a ratio $\frac{a}{t} = \frac{47.2/2 \times 49.4/2}{4.6 \times 0.090} = 1400$.
The failure was due to progressive deflection. The lightweight concrete showed much creep. Three similar structures were subsequently demolished. One of these had a deflection of 460 mm at the centre. Research showed that the collapse could have been simply prevented by cambering upward the centre point of the shell [81].

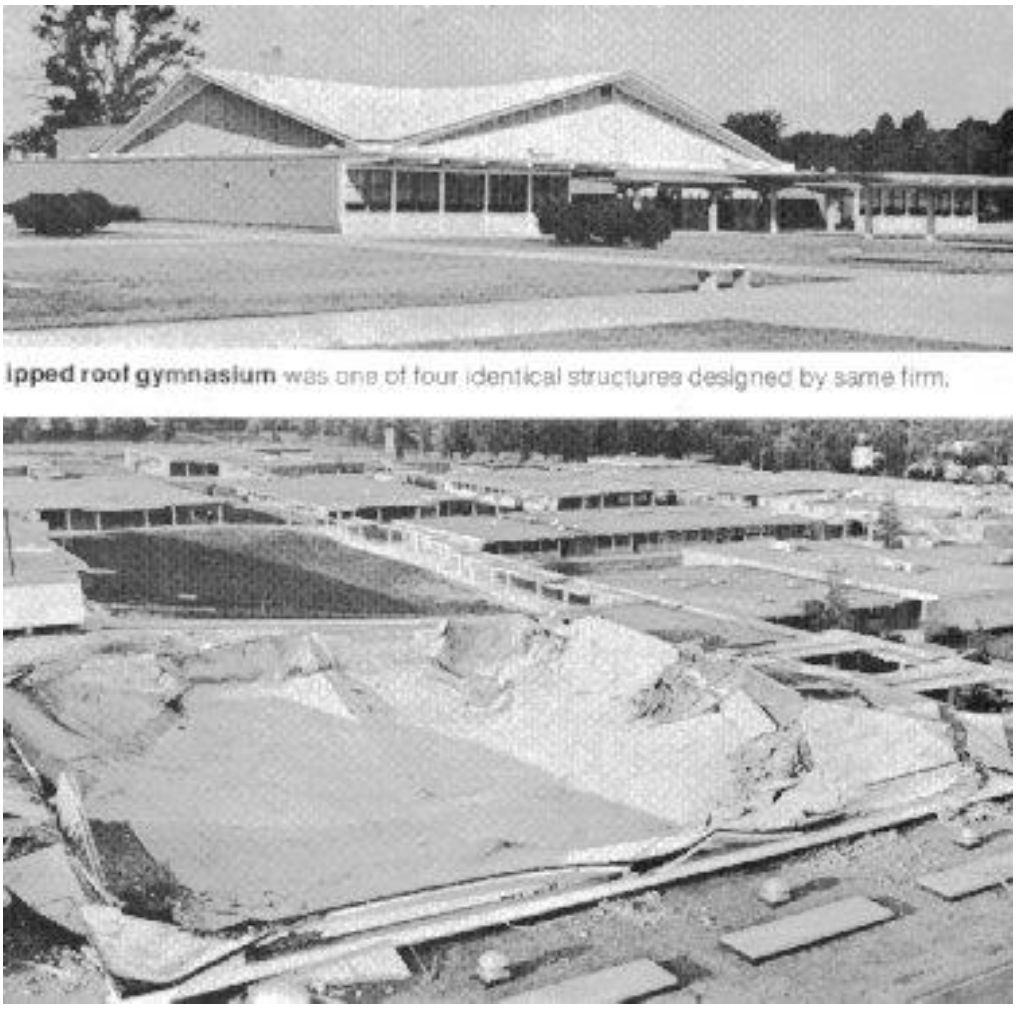

Figure 180. Newspaper photograph of the collapsed hypar shell [81]

Cylinder buckling shapes

The buckling shape of an axially loaded cylinder starts as ring mode or a chessboard mode (fig. 181). Which one occurs depends on the shell thickness and its radius. When buckling progresses the ring mode can transform into the chessboard mode. However, these deformations are very small and rarely visible. When the material starts to deform plastically the ring mode develops into an elephant foot (fig. 182); the chessboard mode develops into a Yoshimura[1] pattern (fig. 183), which are clearly visible.

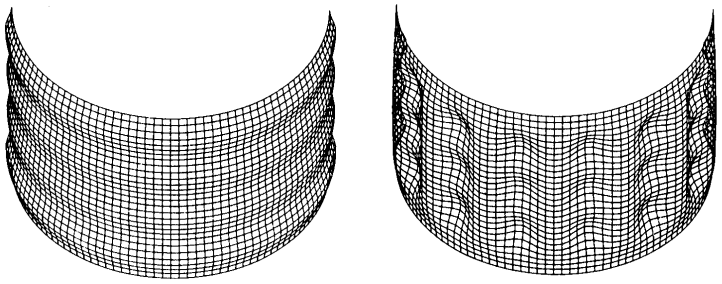

Ring mode *Chessboard mode*

Figure 181. Buckling modes of axially compressed cylinders computed by the finite element method (The deformation is enlarged to make it visible.)

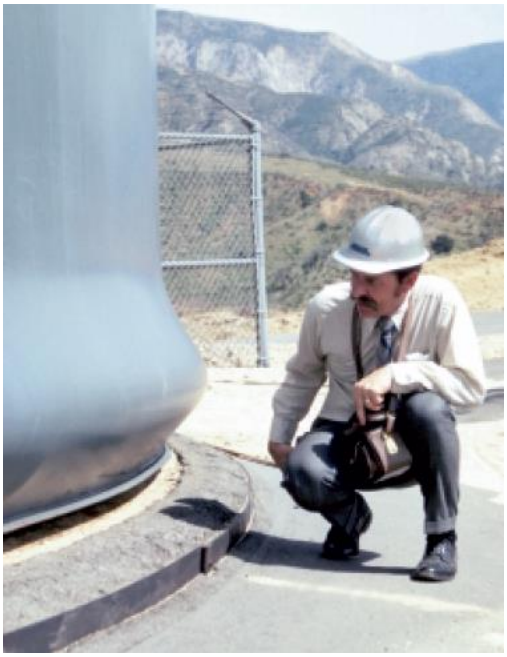

Figure 182. Elephant foot buckling of a tank wall [82]



Figure 183. Yoshimura buckling of an aluminium cylinder

Exercise: The Yoshimura pattern can be obtained as an origami exercise. Take a sheet of paper and draw the lines of figure 184 on it. Fold all horizontal lines towards you and all diagonal lines away from you. When all folds are made, the sheet tends to curve. Curve the sheet further and close it with sticky tape.

[1] Yoshimura Yoshimaru (吉村 慶丸) (approximately 1920-1964) was a professor of applied mechanics at Tokyo University of Technology. Nine years after the Second World War, he was invited to the USA to work on shell structures. There, he wrote a report [83] which explained the buckling shape that was often observed in cylinder experiments. Unfortunately for many of us, his other publications are in Japanese.

Remarkable about the Yoshimura pattern is that it is inextensional (p. 109). Fortunately, large extensions are needed to transform a cylinder directly into a Yoshimura pattern [83]. You can try this too: Take a sheet of paper, curve it into a cylinder and close it with sticky tape. Then load the cylinder axially by books until it buckles. If the cylinder and the load are nearly perfect, then the cylinder deforms into a Yoshimura pattern. Clearly, reality is not perfect. Nevertheless, several Yoshimura buckles can be recognised in the overloaded cylinder.



Sheet of paper *Yoshimura pattern* *Buckled paper cylinder*

Figure 184. Origami exercise

Buckling of a beam supported by springs

Shells can be understood by studying a beam supported by uniformly distributed springs (fig. 185). The bending stiffness of the beam is EI [Nm²]. The stiffness of the distributed springs is k [N/m²]. The beam is loaded by an axial force P [kN]. The differential equation that describes this beam is

$$EI\frac{d^4w}{dx^4}+P\frac{d^2w}{dx^2}+k\,w=0\,.$$

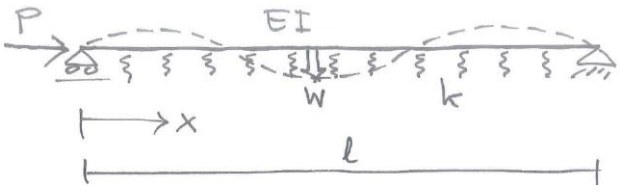

Figure 185. Elastic beam supported by distributed springs

The following buckling shape is proposed

$$w=b\sin\frac{n\pi x}{l}\,,$$

where *n* is the number of half waves of the buckled shape. Substitution of the buckling shape into the differential equation gives the following solution.

```
> w:=b*sin(n*Pi*x/l):
> eq:=EI*diff(w,x,x,x,x)+P*diff(w,x,x)+k*w=0:
> Pcr:=expand(solve(eq,P));
```

$$P_{cr} = \frac{n^2\pi^2 EI}{l^2} + \frac{k\,l^2}{n^2\pi^2}$$

This solution is plotted in figure 186 in dimension less quantities. It shows that for long beams the red line is a good approximation.

$$P_{cr} \approx 2\sqrt{k\,EI}\ .$$

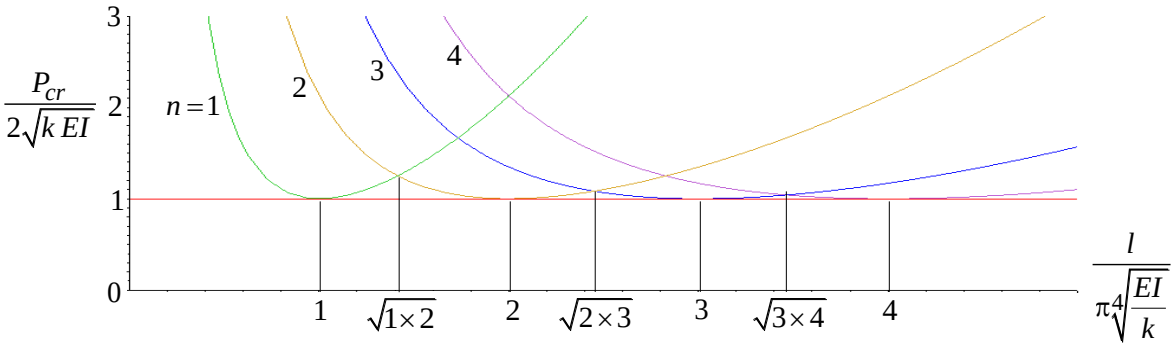

Figure 186. Buckling load as a function of the beam length

Ring buckling of an axially compressed cylinder
Consider a circular cylinder (fig. 187).

$$k_{xx} = 0, \quad k_{yy} = \frac{1}{a}, \quad k_{xy} = 0, \quad \alpha_x = \alpha_y = 1, \quad 0 \le u \le l, \quad 0 \le v \le 2\pi a$$

Somebody proposes the following deformation.

$$u_x = \frac{\nu}{a}\int w(u)\,du, \quad u_y = 0, \quad u_z = w(u)\,.$$

This deformation is axial symmetric and depends on an unknown function *w*. Please note the difference between ν (Poisson's ratio) and *v* (curvilinear coordinate).

Substitution in the 21 Sanders-Koiter equations (p. 54) gives

$$\frac{E\,t^3}{12(1-\nu^2)}\frac{d^4w}{dx^4} + \frac{E\,t}{a^2}w = n_{xx}\frac{d^2w}{dx^2}\,.$$

This is the same differential equation as that of buckling of a beam supported by springs (p. 137). Apparently we can make the following interpretations.

$$\frac{Et^3}{12(1-\nu^2)} = EI, \quad \frac{Et}{a^2} = k, \quad n_{xx} = -P$$

Using this analogy, the buckling load of a not short cylinder is calculated as

$$n_{cr} = -2\sqrt{k\,EI} = \frac{-1}{\sqrt{3(1-\nu^2)}}\frac{Et^2}{a} \qquad \boxed{n_{cr} \approx -0.6\frac{Et^2}{a}}$$

and the buckling length is

$$l_{cr} = \pi\sqrt[4]{\frac{EI}{k}} = \frac{\pi\sqrt{at}}{\sqrt[4]{12(1-\nu^2)}} \approx 1.7\sqrt{at}\,.$$

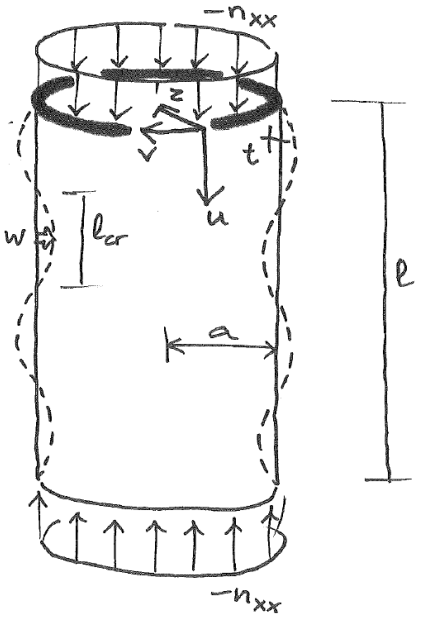

Figure 187. Cylinder coordinate system

Exercise: What cylinder part can be represented by a beam and what part by uniformly distributed springs?

Exercise: Calculate the buckling length of a cylinder made out of a sheet of paper.

Exercise: In what shape does a very long cylinder buckle?

Exercise: What is the difference between the buckling length and the influence length (p. 73)?

Differential equation for shell buckling

The differential equation for shell buckling is an extension of the shallow shell differential equation (p. 59)

$$\frac{E\,t^3}{12(1-\nu^2)}\nabla^2\nabla^2\nabla^2\nabla^2 u_z + E\,t\,\Gamma\Gamma u_z = \nabla^2\nabla^2\left(p_z + n_{xx}\frac{\partial^2 u_z}{\partial x^2} + (n_{xy}+n_{yx})\frac{\partial^2 u_z}{\partial x \partial y} + n_{yy}\frac{\partial^2 u_z}{\partial y^2}\right)$$

It can be easily derived starting with Sanders-Koiter equation 21 (p. 54) by replacing k_{xx} by $k_{xx} + \frac{\partial^2 u_z}{\partial x^2}$ et cetera. This differential equation can be solved analytically for elementary shell shapes and elementary loading. The buckling loads thus obtained are called *critical loads*. There is a large body of literature on this. Scientists who made significant contributions are Rudolf Lorenz, Stephen Timoshenko, Richard Southwell, Richard von Mises, Wilhelm Flügge, Lloyd Donnell. An overview is given by Nicholas Hoff [84] [2].

Buckling load factor
A load factor λ is introduced in the differential equation for shell buckling (p. 139).

$$\frac{E\,t^3}{12(1-\nu^2)}\nabla^2\nabla^2\nabla^2\nabla^2 u_z + E\,t\,\Gamma\Gamma u_z = \nabla^2\nabla^2(\lambda\, p_z + \lambda\, n_{xx}\frac{\partial^2 u_z}{\partial x^2} + \lambda\,(n_{xy}+n_{yx})\frac{\partial^2 u_z}{\partial x \partial y} + \lambda\, n_{yy}\frac{\partial^2 u_z}{\partial y^2})$$

A chessboard buckling pattern is assumed.

$$u_z = c\cos\frac{\pi x}{l_x}\cos\frac{\pi y}{l_y}$$

The following assumptions simplify the mathematics.
$n_{xy} + n_{yx} = 0$ ... the buckles occur in the principal membrane force directions,
$k_{xy} = 0$ ..... the buckles occur in the principal curvature directions.

The buckling pattern and the assumptions are substituted in the differential equation and the critical load factor is solved (appendix p. 211).

[2] Stephen Timoshenko (1878-1972) was born in Ukraine and became a professor at Kyiv Polytechnic Institute. In 1919, he fled for the Bolshevik revolution and ended up in the USA where he became a professor at the University of Michigan and later at Stanford University [Wikipedia].

Richard von Mises (1883-1953) was born in Ukraine. He studied at Vienna University of Technology. He was a pilot during the First World War and afterwards a professor of applied mathematics in Dresden and Berlin. He was Jewish and in 1933 he left nazi Germany to teach in Istanbul. Later he moved to Harvard University, USA [Wikipedia].

Rudolf Lorenz (approximately 1880-1945) was a civil engineer in Dortmund, Germany [84].

Richard Southwell (1888-1970) was a mathematician and engineer. He taught at the University of Cambridge, Oxford and Imperial College London [Wikipedia].

Lloyd Donnell (1895-1997) was an American engineer, professor at Illinois Institute of Technology and Stanford University [Wikipedia].

Wilhelm Flügge (1904-1990) was a German engineer. After the second world war he moved to the USA and became professor at Stanford University [German Wikipedia].

Nicholas Hoff (1906-1997) was born in Hungary. He studied aeronautical engineering at Stanford University before the war and eventually became a professor there. He was a student of Timoshenko [Wikipedia].

$$\lambda_{cr} = \frac{-Et}{\frac{n_{xx}}{l_x^2}+\frac{n_{yy}}{l_y^2}}\left(\frac{\pi^2 t^2}{12(1-\nu^2)}(\frac{1}{l_x^2}+\frac{1}{l_y^2})^2 + \frac{(\frac{k_{xx}}{l_y^2}+\frac{k_{yy}}{l_x^2})^2}{\pi^2(\frac{1}{l_x^2}+\frac{1}{l_y^2})^2} \right)$$

Suppose that buckling is not restrained by edges, then the buckling lengths l_x and l_y are such that the load factor is smallest. This was studied by plotting λ_{cr} as function of l_x and l_y for various values of $n_{xx}, n_{yy}, k_{xx}, k_{yy}$ (appendix p. 211). The result is surprisingly simple. Three buckling modes can occur.

$$\lambda_{cr1} = \frac{-E t^2}{\sqrt{3(1-\nu^2)}} \frac{|k_{yy}|}{n_{xx}} \qquad \lambda_{cr2} = \frac{-E t^2}{\sqrt{3(1-\nu^2)}} \frac{|k_{xx}|}{n_{yy}} \qquad \lambda_{cr3} \approx 0$$

The third buckling mode is due to inextensional deformation. Sometimes these buckling load factors are negative, which shows that we need to reverse the load to cause buckling.

Exercise: Are the formulas for cylinder ring buckling and cylinder chessboard buckling the same?

Exercise: What is the buckling formula for a spherical shell loaded by a vacuum?

Challenge: The numerical study seems to show that

$\lambda_{cr3} < 0$ for $n_{xx}|k_{xx}| + n_{yy}|k_{yy}| > 0$ (not dangerous)

$\lambda_{cr3} = \infty$ for $n_{xx}|k_{xx}| + n_{yy}|k_{yy}| = 0$ (not dangerous)

$\lambda_{cr3} > 0$ for $n_{xx}|k_{xx}| + n_{yy}|k_{yy}| < 0$ (dangerous).

Prove or disprove this.

Challenge: Derive the buckling formula for $n_{xy} + n_{yx} = 0$ and $k_{xx} = k_{yy} = 0$ and $k_{xy} \neq 0$.

Design check of buckling

For design, the buckling load factors should not be in the interval $0 < \lambda_{cr} < 1$.

This can be explained as follows. Consider a free form shell structure. We specify loads, safety factors and load combinations (p. 171). We do a linear analysis to obtain the membrane forces. We do a linear buckling analysis to obtain the buckling load factors for each load combination. Suppose that a buckling load factor is 0.9. This means that when we apply this load combination slowly, the shell will buckle at 90% of the full load. Clearly, this will not do. We need to change the design.

Catelan's surface [3]
The Catelan minimal surface is described by the following orthogonal parameterisation (p. 25).

$$\bar{x} = a\,u\cos v \qquad -1 < u < 1 \qquad -\tfrac{1}{2}\pi < v < \tfrac{1}{2}\pi$$

$$\bar{y} = \tfrac{1}{4}a\left((2u^2+1)\sin 2v + 2v\right)$$

$$\bar{z} = \tfrac{1}{4}a\left((2u^2+1)\cos 2v - 1\right)$$

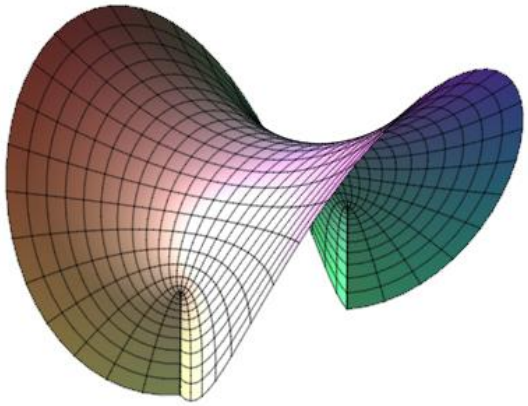

$$k_{xx} = \frac{\cos v}{a\sqrt{u^2+1}(u^2+\cos^2 v)}$$

$$k_{yy} = -k_{xx}$$

$$k_{xy} = \frac{-u\sin v}{a(u^2+1)(u^2+\cos^2 v)}$$

$$\alpha_x = a\sqrt{u^2+\cos^2 v}$$

$$\alpha_y = a\sqrt{(u^2+1)(u^2+\cos^2 v)}$$

Imperfection sensitivity
Before 1930, airplanes consisted of frames covered with a fabric which was painted. However, engineers wanted to build airplanes from aluminium plates that were joined to form a cylindrical shape. Therefore, scientists started to do experiments on cylinders, for example Andrew Robertson [4]. Figure 188 shows the ultimate loads of axially compressed aluminium cylinders. They are much smaller than the critical load. Robertson ends his paper on the subject with "*Further comment as to the insufficiency of these formulae is unnecessary*" [85].

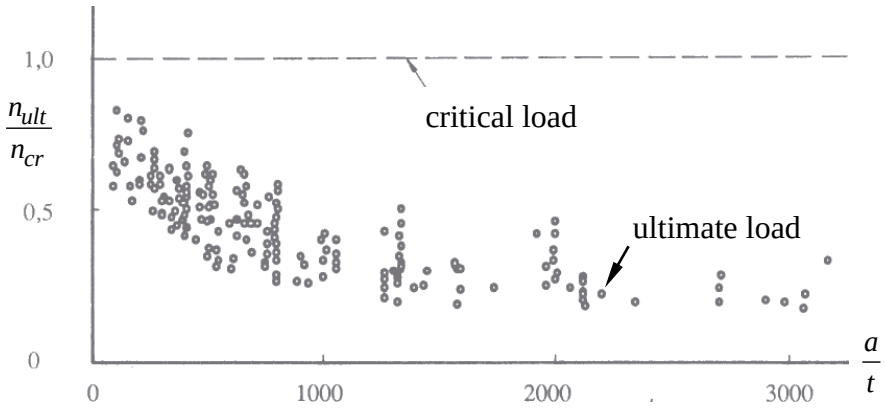

Figure 188. Experimental ultimate loads of 172 axially loaded aluminium cylinders [86]

This difference between theory and experiments is caused by invisible shape imperfections. At first sight, imperfection sensitivity is hard to believe because the experiments were performed very carefully. The aluminium cylinders had perfectly cut edges and were

[3] Eugène Catalan (1814 – 1894) was a Belgian mathematician and professor at the University of Liège [Wikipedia].

[4] Andrew Robertson (1883 – 1977) was a professor of Mechanical Engineering at Bristol University [Wikipedia].

beautifully polished. The cylinders were perfectly centred in the testing machines. The testing machines were modern and very accurate measuring instruments were used. Nonetheless, the ultimate loads were much smaller than the critical loads. Not only compressed cylinders but also bend cylinders and radially compressed domes are very sensitive to shape imperfections.

Experiment

What is the ultimate load of an axially loaded empty beer can? We model the can as an open cylinder. The wall thickness is 0.08 mm the radius is 32.8 mm, Young's modulus is 2.1 10^5 N/mm² and Poisson's ratio is 0.35 (stainless steel). The buckling load (p. 138) is



$$n_{cr} = -0.6\frac{Et^2}{a} = -0.6\frac{2.1\times10^5\times0.08^2}{32.8} = -25.3\ \text{N/mm}$$

$$F_{cr} = 2\pi a\, n_{cr} = 2\times3.14\times32.8\times(-25.3) = -5200\ \text{N}$$

Therefore, it should be able to carry a mass of 520 kg pulled by earth's gravity. Carefully stand on the can and it will – probably – carry your weight. Subsequently, use your thumbs to push a dimple in the can and push it out again. Doing so makes typical clicking sounds. Notice that the imperfections you made are hardly visible. Now, try standing on the can again. It will collapse abruptly. The explanation is imperfection sensitivity.

Puzzle

The large difference between the theoretical buckling load (critical load) and the experimental buckling load (ultimate load) puzzled scientists for approximately 10 years. Is the differential equation wrong? Are the solutions to the differential equation wrong? Are there more solutions that we have not found? Is there some mistake in the experimental set up? Has thin aluminium less stiffness than solid aluminium?

The solution was discovered in 1940 by Theodore von Kármán and Qian Xuesen (钱 学 森 pronounce tsien? sue? sen) [87].[5] They calculated the load-displacement curve after buckling. Figure 189 shows the result of their calculation; n_{xx} is the membrane force in a cylinder and w is the shortening of the cylinder. Note that load on a perfect cylinder can be increased until the critical load after which the strength will drop strongly. This behaviour is typical for shell structures and very different from other structures. Figure 189b shows that very small shape imperfections cause the ultimate load to be much smaller than the critical load.

[5] Von Kármán (1881-1963) and Qian (1911-2009) worked at Caltech (California Institute of Technology) as rocket scientists. They developed the knowledge that later showed necessary for the Apollo program (1961-1972), in which USA astronauts walked on the moon. Von Kármán was Hungarian and he immigrated to the USA in 1930. Qian was Chinese. He immigrated to the USA in 1935 and back to China in 1955 in not friendly circumstances. The discovery of shell imperfection sensitivity was just a footnote in their lives. More on Von Kármán and on Qian can be found in Wikipedia (Qian's name is often spelled as H.S. Tsien).

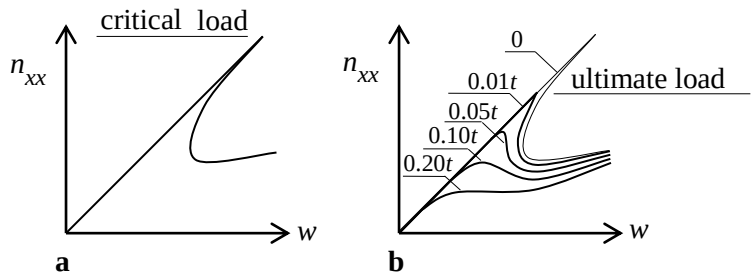

Figure 189. Buckling of cylinders for different shape imperfection amplitudes [87]

Exceptions to imperfection sensitivity
Some shells are not sensitive to imperfections. Radially loaded open cylinders are not because they buckle inextensionally (p. 109). Cylinders with torsion loading ($n_{xy} \neq 0$ or $n_{yx} \neq 0$) are not sensitive to imperfections. A hypar roof (p. 102) is sensitive to imperfections if it buckles in mode 1 or 2 but not if it buckles in mode 3 (p. 140).

Koiter's law [6]
Equilibrium of a perfect system can be described by

$$\lambda = \lambda_{cr}\left(1 - c_1 w - c_2 w^2\right),$$

Where λ is the load factor, λ_{cr} is the critical load factor, w is the amplitude of the deflection, c_1 and c_2 are constants characterising the given structure. There are three types of post critical behaviour (fig. 190). Type I behaviour occurs when $c_1 = 0$ and $c_2 < 0$. The structure is not sensitive to imperfections. Type II behaviour occurs when $c_1 = 0$ and $c_2 > 0$. The structure is sensitive to imperfections. Koiter showed that the ultimate load factor is equal to

$$\lambda_{ult} = \lambda_{cr}\left(1 - 3\left(w_0 \tfrac{1}{2}\rho\sqrt{c_2}\right)^{\frac{2}{3}}\right),$$

Where ρ is a coefficient depending on the imperfection shape and w_0 is the imperfection amplitude. Type III behaviour occurs when $c_1 > 0$. The structure is very sensitive to imperfections. The ultimate load factor is equal to

$$\lambda_{ult} = \lambda_{cr}\left(1 - 2\left(w_0 \rho c_1\right)^{\frac{1}{2}}\right).$$

This is called *Koiter's half power law*.

Properly supported flat plates display type 1 behaviour; They buckle at small normal forces. After buckling the load can be increased substantially. Most thin shells display type III behaviour.

[6] Warner Koiter (1914-1997) was professor at Delft University of Technology at the faculties of Mechanical Engineering and Aerospace Engineering (1949-1979). He wrote his dissertation during the Second World War, while hiding from Arbeitseinsatz, and published it in 1945 just after the war [88]. The English translation appeared in 1967 [89]. It became famous because it quantifies the imperfection sensitivity of thin shells.

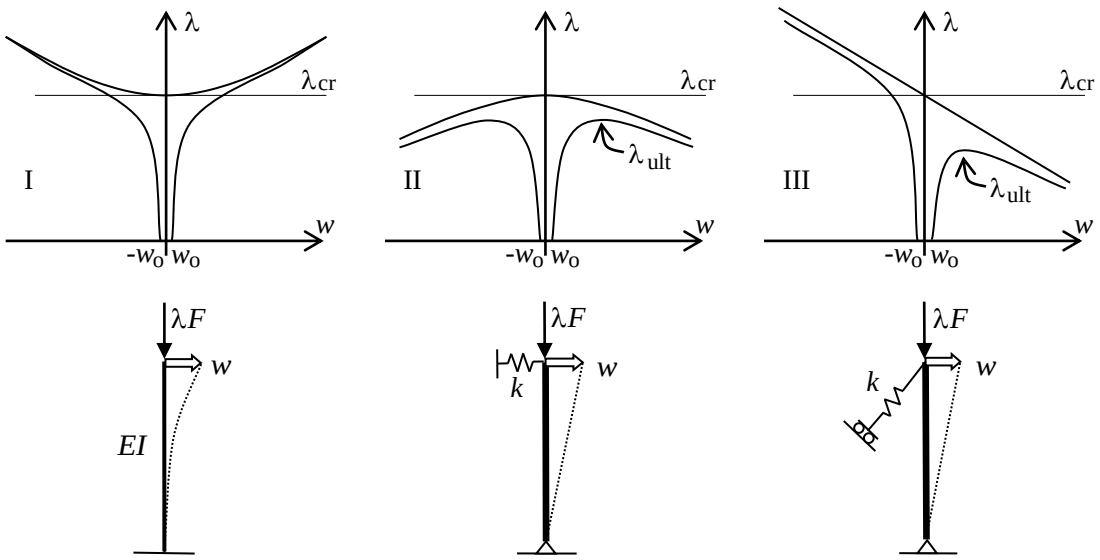

Figure 190. Three types of post buckling behaviour according to Koiter

Knock down factor

In shell design often the following procedure is used. First the critical load is computed by using the formula or a finite element program. Then this loading is reduced by a factor *C* that accounts for imperfection sensitivity. This factor is called "knock down factor". The result needs to be larger than the design loading. Often it is determined experimentally. For example, for reinforced concrete sewer pipes loaded in bending the following knock down factor is used.

$$C = 1 - 0.73(1 - e^{-\frac{1}{16}\sqrt{\frac{a}{t}}}).$$

The range in which it is valid is $0.5 < \frac{l}{a} < 5$ and $100 < \frac{a}{t} < 3000$ where *l* is the pipe length [90].

If little information is available the following knock down factor can be used.

$$\boxed{C = \frac{1}{6}}$$

This is based on figure 188 in which all of the tests show an ultimate load more than 0.166 times the critical load.

Linear buckling analysis

Finite element programs can compute critical load factors λ_{cr} and the associated normal modes. This is called a linear buckling analysis. A finite element model has as many critical load factors as the number of degrees of freedom. We can specify how many of the smallest critical load factors the software will compute. If the second smallest buckling load is very close (say within 2%) to the smallest buckling load we can expect the structure to be highly sensitive to imperfections.

Often, the critical load factors need to be multiplied by the knockdown factor. The results need to be larger than 1. Consequently, if all critical load factors are larger than 6, the structure is safe for buckling.

Linear buckling analyses are performed on shell models without imperfections. We could add shape imperfections, however, this would not solve anything. The shape imperfections grow slowly during loading and this is not included in a linear buckling analyses. For imperfections to grow we need to perform a nonlinear finite element analysis (p. 146).

Ship design
A steel ship consists of plates strengthened by stiffeners. A linear buckling analysis of the ship model produces critical load factors for each plate that buckles. However, flat plates buckle in Koiter's mode I (p. 144) which does not cause failure. We are interested in buckling of big curved parts of the ship because these go in Koiter's mode III which does cause failure. A computer cannot tell the difference between plate buckling and shell buckling. The only thing we can do is go through the load factors from small to large, look at each buckling mode and continue until we see buckling that involves more than one plate. This can take much time because a large ship consists of hundreds of plates and has many load combinations.

Oil tanker
In 2000 the oil company Shell had 150 oil tankers in its fleet. In 2019 just 15. The modern oil tankers are more than 300 m long which is much larger than the old ones. (Advantages of large tankers are less fuel cost and fewer collisions because there are fewer ships at sea.) A new oil tanker costs approximately 120 000 000 euro.

Old single hull oil tankers had a single steel shell between the sea and the oil. The tankers were divided in oil tanks. These tanks were sometimes filled with sea water as ballast for levelling the ship. When the ballast water was pumped out the sea was polluted. Also in collisions the sea was polluted. Nowadays, double hull tankers are common. Double hull tankers have two steel shells between the oil and the sea (figure 139). They also have separate tanks for oil and for ballast water. A problem of the double hull tankers is that the ballast tanks corrode. Despite efforts to paint the ballast tanks, the double hull tankers do not last long. The average life time of oil tankers is 10 years.

Figure 139. … [… p.]

An oil tanker is designed for 20 year. It has three structural limit states: yielding, fatigue and buckling. It has many load cases and about 20 load combinations (table 10).

Current computer capacity is not sufficient to perform a finite element analyses of a tanker in all its details. Therefore, first a rough model is made of the tanker without details. Subsequently, submodels are made of tanker parts. The edges of a submodel are loaded by forces and moments that are automatically transferred from the rough model. This method is called submodelling. For buckling analysis the submodels are much larger than the area of interest because otherwise the free submodel edge would influence the buckling load.

Table 14. Load cases of an oil tanker

Nonlinear finite element analysis
When a shell design is ready it is sensible to check its performance by nonlinear finite element analyses. In these analyses the loading is applied in small increments for which the displacements are computed. Figure 191 shows the results of finite element analyses of a simply supported shallow dome.

The ultimate load is mainly affected by shape imperfections, support stiffness imperfections and yielding or cracking. When these are measured and included in the finite element model, then the predicted ultimate load has a deviation less than 10% of the experimental ultimate load [91].

Clearly, before a shell has been build we cannot measure the imperfections. Instead these are estimated. For example, the amplitude of the geometric imperfections is estimated by the designer and the builder. Often, the analyst will assume that the shape of the geometric imperfections is the first buckling mode. He or she will add this imperfection to the finite element model.

It seems logical that an imperfection shape equal to the buckling shape gives the smallest ultimate load. For columns this is true. However, for shells there exists no mathematical proof of this. Therefore, another imperfection shape might give an even smaller ultimate load [93]. Of course, the analyst can consider only a few imperfection shapes.

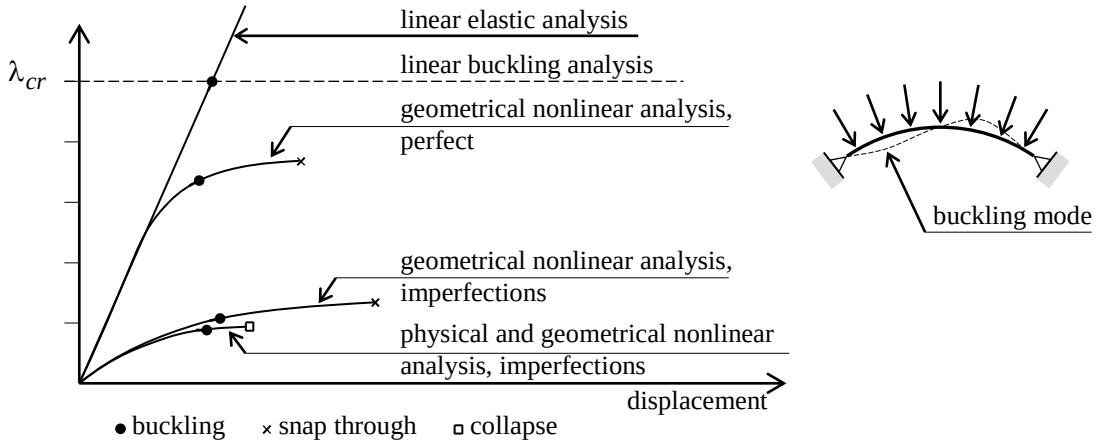

Figure 191. Shell finite element analyses of a steel spherical dome [93]

Mystery solved
The critical and ultimate load of shell structures can be determined by both analytical and numerical analysis. However, these analyses are complicated and many engineers and scientists feel that we still do not understand imperfection sensitivity [94]. Here it is argued that shell buckling is not a mystery at all.

In nonlinear finite element analyses we see that when a small load is applied the shell deforms in a buckling mode. The buckling mode increases the shape imperfections of the shell. The deformation is very small and invisible to the naked eye. Nonetheless, the deformation changes the curvature, in some locations the curvature has become larger and in other locations the curvature has become smaller. It also changes the membrane forces. Inwards buckles have extra compression and outward buckles have extra tension. When the load is increased the curvatures and membrane forces change further. At some location the Gaussian curvature becomes negative and the compression membrane force becomes large. At this location a local buckle starts. It has a larger length than the earlier buckling mode. This local buckle grows quickly, other buckles occur next to it and this spreads through the shell in a second. The shell collapses.

In other words, the shell buckling formulas do not work because the real local curvature and the real local membrane force are very different than computed by a linear elastic analysis of a perfect structure.

Measuring shape imperfections
The accurate shape of a shell structure can be measured by a laser scanner. The result is a point cloud that can be visualised by a CAD program (fig. 192). There is a simple way to extract shape imperfections from a point cloud. Load the point cloud in software Rhinoceros and fit a NURBS (p. 9) through the cloud. Choose the distance of the control points equal to

the imperfection length. This fit will not follow the shape imperfections because the control points are too far apart. The software can compute the distance between a point and the NURBS. The software does this for all points in the cloud and gives a histogram of these distances (fig. 193). The largest distance is the imperfection amplitude *d*.

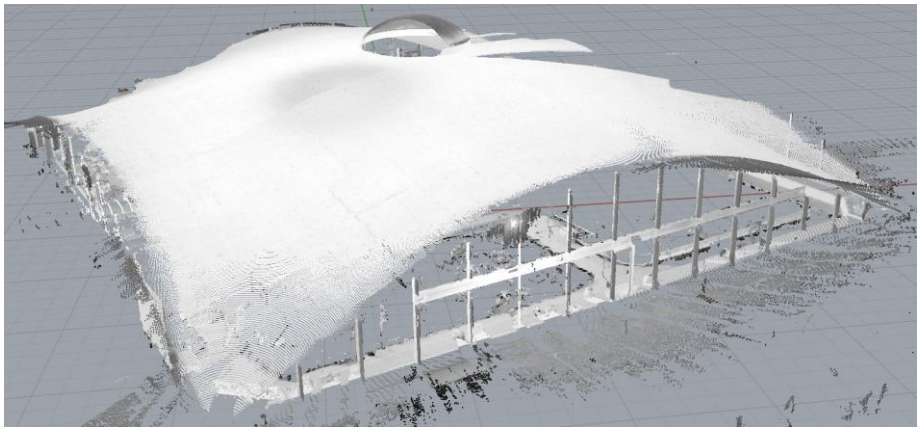

Figure 192. Point cloud of a swimming pool in Heimberg, Switzerland. The laser scanner was positioned inside. All points that are not on the shell were removed later by hand, for example walls, light fittings, swimming children [95].

Bart Elferink and Peter Eigenraam (student and teacher at Delft University) scanned four reinforced concrete shell roofs that were built by the team of Heinz Isler around 1970. The result is

$$d = \frac{1}{108} A^{0.3} l^{0.4}$$

where *d* is the imperfection amplitude (5% characteristic value), *A* is the surface area of the shell and *l* is the imperfection length. The partial safety factor is 1.4 [95].

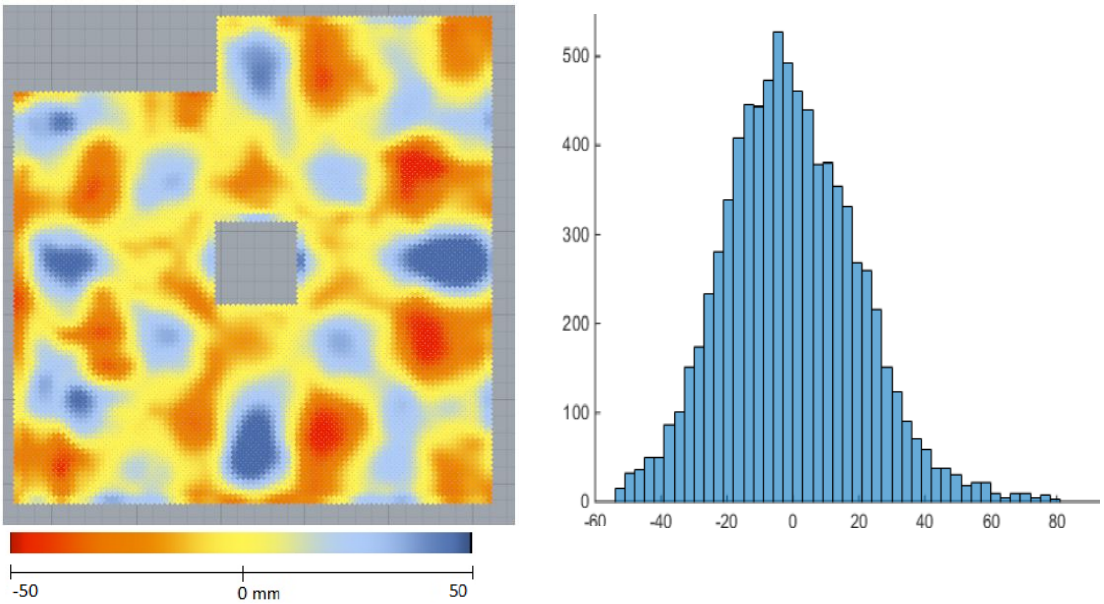

Figure 193. Shape imperfections in the shell roof of Heimberg swimming pool [95]

Exercise: Why do we choose the imperfection length equal to the buckling length?

Stiffeners
If a shell would buckle, it is technically better to use some of the shell material to design stiffeners (fig. 194).

The argument that proves this statement is simple. By putting material in another position the cross-section area stays the same. Therefore, membrane stiffness does not change and the membrane forces do not change. The bending moments in thin shells are small anyway. Consequently, the stresses do not change and it does not affect the strength of the cross-section (yielding or crushing). The material change does increase the moment of inertia, the bending stiffness and the buckling load. Q.E.D.

Of course, "technically better" can be overruled by "expensive to build", "difficult to clean", "just ugly" et cetera.

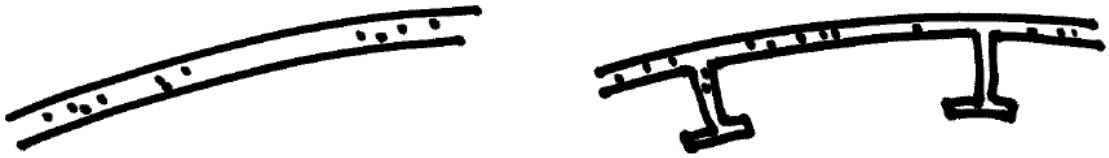

Figure 194. Cross-sections of two shell parts; left without stiffeners and right with stiffeners. Note that the cross-section areas are the same while the moments of inertia are different.



Exercise: Have you noticed that small animals like spiders have an exoskeleton and large animals like elephants have a skeleton? At what size does the transition occur? You can study this by considering a drop of water enclosed by a spherical shell. The water is loaded by gravity and the shell is supported in a point. What is the largest membrane force in the shell? What thickness is required for strength? Subsequently, enlarge the diameter until the shell buckles. At this diameter the designer needs to consider stiffeners or replace the shell by a space truss. I look forward to hearing what diameter you found.[7]

CNIT
The world largest shell structure is in Paris (fig. 196). I was built in 1956 to 1958 as an exhibition centre for machines. It is called "centre des nouvelles industries et technologies" (CNIT). Nowadays, the shell covers shops, restaurants, offices, a convention centre, a hotel and a subway station (fig. 197). Despite its size the shell is easily overlooked due to the eye catching Grande Arche, which was built next to it in 1985 to 1989. To go there, take any public transportation to La Défense Grande Arche.

Architects:	Robert Camelot, Jean de Mailly and Bernard Zehrfuss
Engineers:	Nicolas Esquillan (shell) and Jean Prouvé (façade)
Consultant:	Pier Luigi Nervi
Contractors:	Balancy et Schuhl, Boussiron, Coignet
Construction time:	2.5 years
Structure:	Two layers of reinforced concrete, spaced 2 m, connected by reinforced concrete walls
Shell material:	6070 m^3 of reinforced concrete

[7] An incomplete solution to this problem is $2a \sim \frac{f^3\sqrt{1-\nu^2}}{\rho g E^2}$, where $2a$ is the transition diameter, symbol ~ is read as "is proportional to", f is the material strength, ν is Poisson's ratio, ρ is the specific mass of water, g is the gravitational acceleration and E is Young's modulus.

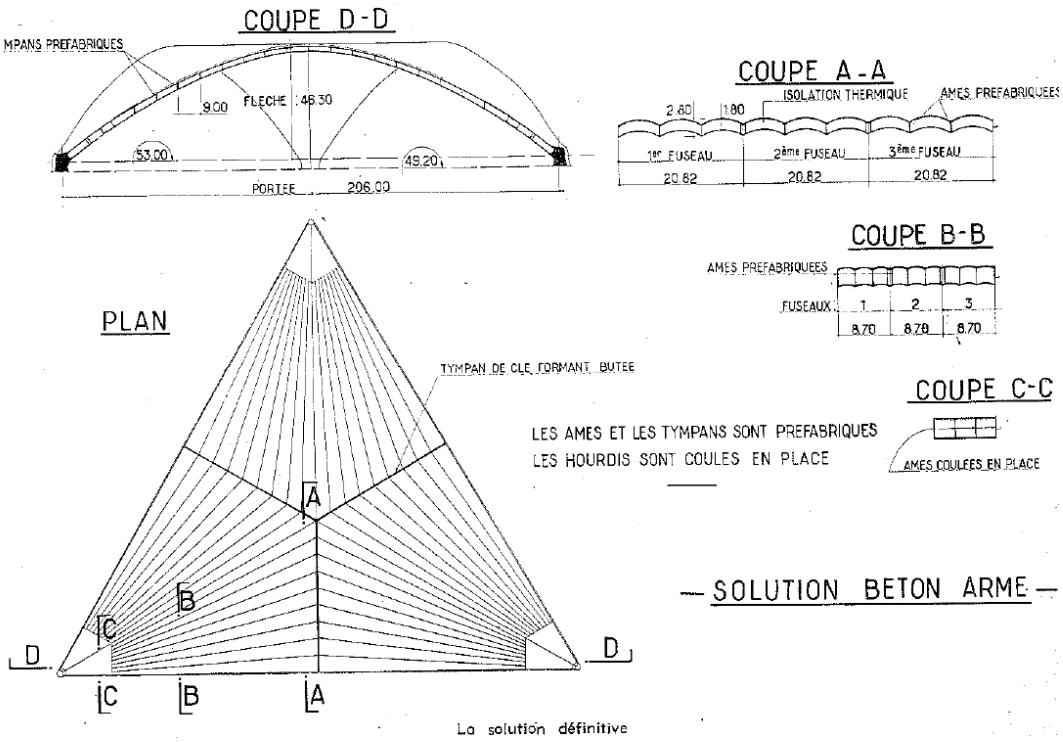

Figure 195. CNIT design by Esquillan [96]



Figure 196. CNIT in 1960 [97]



Figure 197. CNIT interior in 2010 [98]

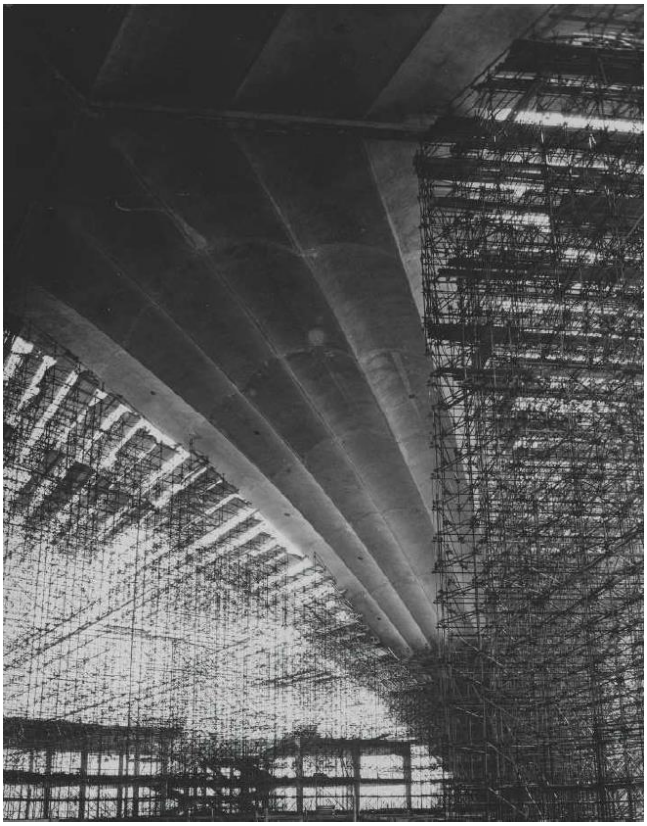

Figure 198. CNIT scaffolding [99]

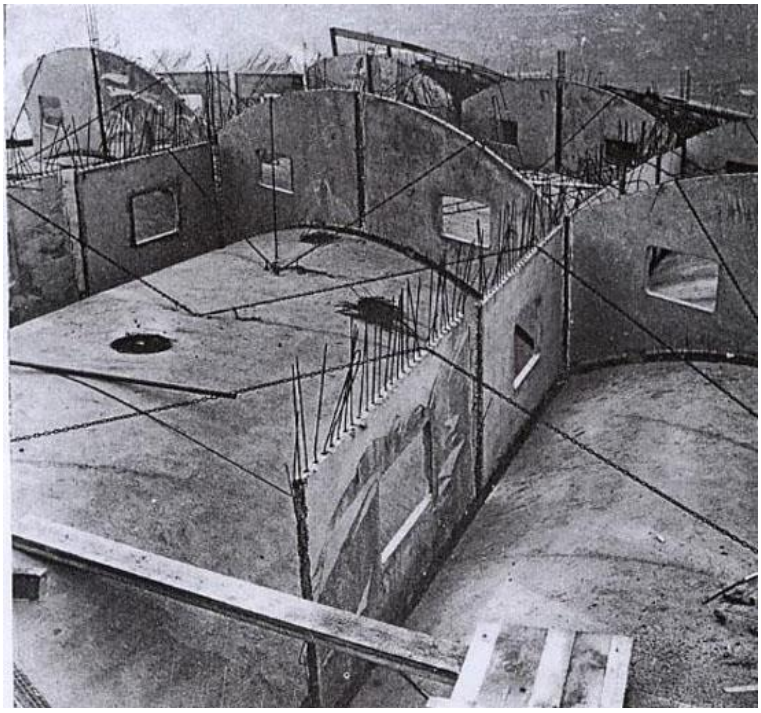

Figure 199. CNIT during construction, visible are the bottom shell and the prefab walls [100]

Each corner of the shell is supported by a large reinforced concrete block that distributes the load over the lime stone underground. The three blocks are connected to each other by three prestressed tension rods [101].

Buckling, yielding or crushing?
In steel columns there is interaction between buckling and yielding. This is mostly caused by rolling stresses and welding stresses. In this note, the theory is summarised and extended to shells.

Relative slenderness is defined as

$$\beta = \sqrt{\frac{n_p}{n_{ult}}} .$$

where, n_p is the yielding or crushing membrane force and n_{ult} is the buckling membrane force without yielding or crushing.

If $\beta >> 1$ then buckling occurs before yielding or crushing.
If $\beta << 1$ then plastic failure or crushing occurs before buckling.
If $\beta \approx 1$ then interaction occurs between buckling and yielding or crushing.

The equation can be rewritten as

$$\beta = \sqrt{\frac{-f\,t}{C\frac{-0.6Et^2}{a}}} = \sqrt{\frac{1.67}{C}\frac{f}{E}\frac{a}{t}}$$

Table 18 shows that a shell made of plastic is more likely to buckle than the same shell made of glass.

Table 18. Properties of materials … and β for C = 1/6 and a / t = 30

Material	Young's modulus E	Compressive strength f	E/f	β
Glass	70000 N/mm²	50 N/mm²	1400	0.5
Concrete	35000	40	875	0.6
Aluminium	70000	110	636	0.7
Steel	210000	350	600	0.7
Wood (Pine)	13000	40	325	1.0
Plastic (Acrilic)	2300	70	33	3.0

Exercise: What percentage of shells fails due to buckling and not due to yielding or crushing? Assume uniform distributions of the material properties $33 \le \frac{E}{f} \le 1400$, geometry $30 \le \frac{a}{t} \le 1000$ and knock down factor $\frac{1}{6} \le C \le 1$. (The exact answer is $\frac{102499-90(\ln 2+\ln 3)}{132599} 100\,\%$.)

Buckling curves for computational analysis

Figure 200 shows buckling curves for steel columns based on hundreds of experiments [102]. The curves can be adopted for shell structures too. Unfortunately, there is no experimental conformation.

```
> Phi:=0.5*(1+alpha*(beta-0.2)+beta^2):
> G:=1/(Phi+sqrt(Phi^2-beta^2)):
> alpha:=0.13: f1:=simplify(G): # ao
> alpha:=0.21: f2:=simplify(G): # a
> alpha:=0.34: f3:=simplify(G): # b
> alpha:=0.49: f4:=simplify(G): # c
> alpha:=0.76: f5:=simplify(G): # d
> plot({f1,f2,f3,f4,f5, 1/beta^2}, beta=0..3,0..1);
```

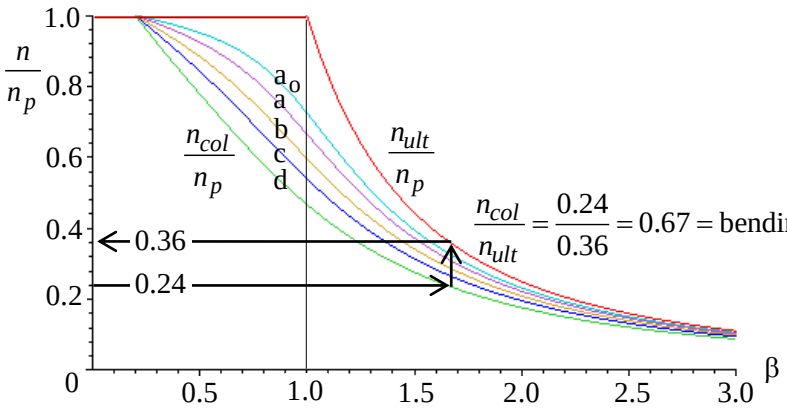

$\frac{n_{col}}{n_{ult}} = \frac{0.24}{0.36} = 0.67 =$ bending stiffness reduction factor at force $n = 0.24 n_p$

Figure 200. Eurocode buckling curves for steel columns

When a steel cross-section has residual stresses from rolling or welding and it is loaded in compression, then local yielding can occur. This reduces the bending stiffness, which reduces the buckling load. Residual stresses can be included in finite element models, however, this takes much modelling time and computation time. There is a much easier way to include residual stresses in a finite element analysis. Rewrite the eurocode buckling curves (fig. 200) and implement a reduction factor $\frac{n_{col}}{n_{ult}}$ on the bending stiffness as a function of the normal force $\frac{n}{n_p}$ (fig. 201) [103]. The derivation below has been performed by Maple.

```
> Phi:=0.5*(1+alpha*(beta-0.2)+beta^2):
> G1:=1/beta^2:
> G2:=1/(Phi+sqrt(Phi^2-beta^2)): # ECCS buckling curve
> opl:=solve(G=G2,beta): beta:=opl[2]:
> alpha:=0.13: f1:=simplify(G2/G1): # ao
> alpha:=0.21: f2:=simplify(G2/G1): # a
> alpha:=0.34: f3:=simplify(G2/G1): # b
> alpha:=0.49: f4:=simplify(G2/G1): # c
> alpha:=0.76: f5:=simplify(G2/G1): # d
> plot({f1,f2,f3,f4,f5},G=0..1);
```

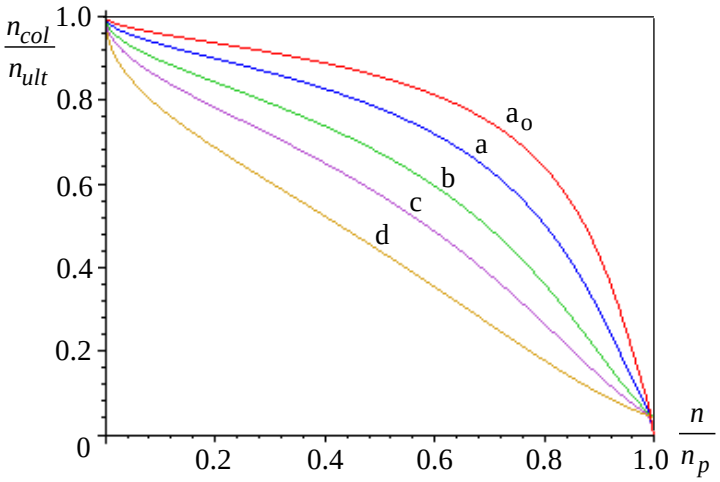

Figure 201. Reduction factor of the initial bending stiffness as a function of the normal force

Hyperboloid

A circular hyperboloid of one sheet is defined by $\frac{\bar{x}^2}{a^2}+\frac{\bar{y}^2}{a^2}-\frac{\bar{z}^2}{ab}=1$.

An orthogonal parameterisation (p. 25) is

$$\bar{x}=a\sqrt{1+u^2}\cos v$$
$$\bar{y}=a\sqrt{1+u^2}\sin v$$
$$\bar{z}=\sqrt{ab}\,u$$

$$-2<u<2$$
$$-\pi<v<\pi$$

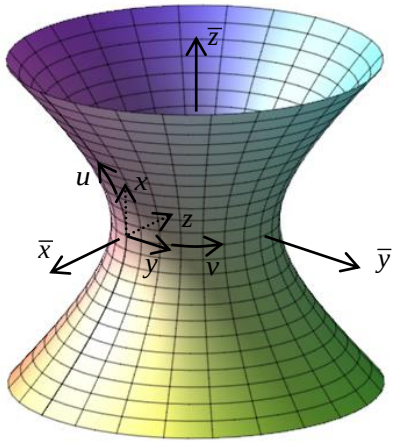

$$k_{xx}=\frac{-1}{b\sqrt{1+(1+\frac{a}{b})u^2}^3}$$
$$k_{yy}=\frac{1}{a\sqrt{1+(1+\frac{a}{b})u^2}}$$
$$k_{xy}=0$$
$$\alpha_x=a\sqrt{\frac{b}{a}+\frac{u^2}{1+u^2}}$$
$$\alpha_y=a\sqrt{1+u^2}$$

Gravity

Suppose that gravity acts in the negative $\bar{z}$ direction. The self-weight $\rho g t$ of the shell needs to be decomposed in the local coordinate system (p. 19).

$$p_x=-\rho g t\frac{\partial\bar{z}}{\partial x}\qquad p_y=-\rho g t\frac{\partial\bar{z}}{\partial y}\qquad p_z=\pm\sqrt{(\rho g t)^2-p_x^2-p_y^2}$$

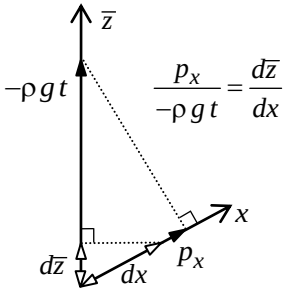

Applied to a hyperboloid (p. 155) the result is

$$p_x=\frac{-\rho g t}{\sqrt{1+\frac{a}{b}\frac{u^2}{1+u^2}}}\qquad p_y=0\qquad p_z=\frac{-\rho g t u}{\sqrt{u^2+\frac{b}{a}(1+u^2)}}$$

Exercise: Solve n_{xx} and n_{yy} for a hyperboloid loaded by gravity.

Ferrybridge

Three reinforced concrete cooling towers collapsed in Ferrybridge, UK in 1965. Fortunately, nobody was injured. The cooling towers were part of a group of eight at a coal-fired power station (fig. 200). The base diameter of the towers was 88 m and the shell thickness was 127 mm. The ratio a/t is 44000/127 = 350. They were 115 m high [105].

The towers had been completed in 1964. At November 1st 1965 it was storming. (The wind speed was 44 m/s at the top edge, which occurs once every 5 years in Ferrybridge.) Vortices occurred between the towers of the first row (fig. 201). These vortices loaded the towers of the second row. The vortex frequency was approximately the same as the natural frequency of the towers (0.6 Hz). An eyewitness said that some towers where moving like belly dancers. Within an hour three collapsed [106].[1]

[1] Despite the strong vibrations, the committee that investigated the collapse concluded that vortex induced vibration was not the real problem. The reason for this conclusion was that not only the second row of towers but all towers were seriously damaged at November 1st. The real problem was that an incorrect wind load had been used in design. The committee did not blame somebody for the collapse.

The construction costs of the original towers was £290 000 each. The collapsed towers were replaced and all towers were strengthened with extra thickness of reinforced concrete. Engineers found ways to operate the remaining towers during reconstruction. If the power station had been temporarily closed, it would have been very expensive for England. In 2016, the power station was permanently closed to reduce CO_2 emission [Wikipedia].



Figure 200. Three collapsed cooling towers at Ferrybridge, UK

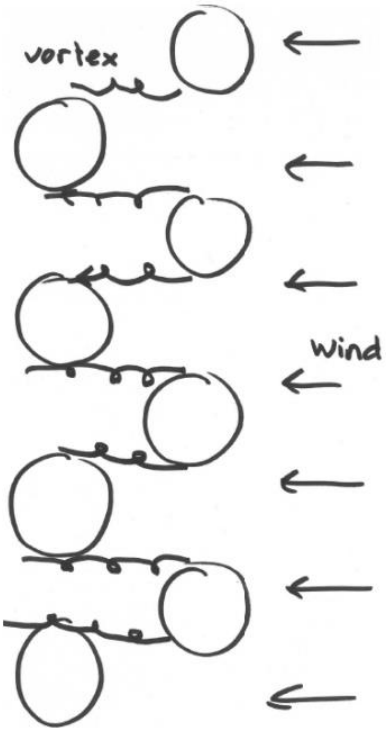

Figure 201. Vortex loading on the towers

Modal analysis

A *normal mode* is a deformation in which a shell can vibrate. The *natural frequency* f_n is the number of times this deformation occurs in a second. The unit of frequency is Hertz (Hz). [2] Often the radian frequency ω is used, which is measured in radians per second. The definition is $\omega = 2\pi f$. A finite element program can compute the normal modes and natural frequencies of a shell structure. A finite element model has as many normal modes and natural frequencies as the number of degrees of freedom. For example, if a shell model has 5000 nodes then it has 5000 x 6 = 30000 degrees of freedom. It also has 30000 normal modes and natural frequencies. A real shell has an infinite number of normal modes and natural frequencies. Natural frequencies are sorted from small to large. The smallest is called *fundamental frequency*. A finite element program does not need to compute all natural frequencies. The user can specify the number of the smallest natural frequencies that will be computed.

The code was unclear, the code was interpreted wrongly and communications between the designers and the wind tunnel experts went wrong [105].

[2] Heinrich Hertz (1857-1894) was a physicist. He worked at the University of Karlsruhe, where he built a machine that detected radio waves for the first time [Wikipedia].

Figure 202 shows six normal modes and natural radian frequencies of a simply supported shallow spherical shell [108]. Young's modulus E is 2000 N/mm², Poisson's ratio ν is 0.3, the length and width are 10 m, the thickness t is 100 mm, the radius a is 20 m and the specific mass ρ is 7850 kg/m³.

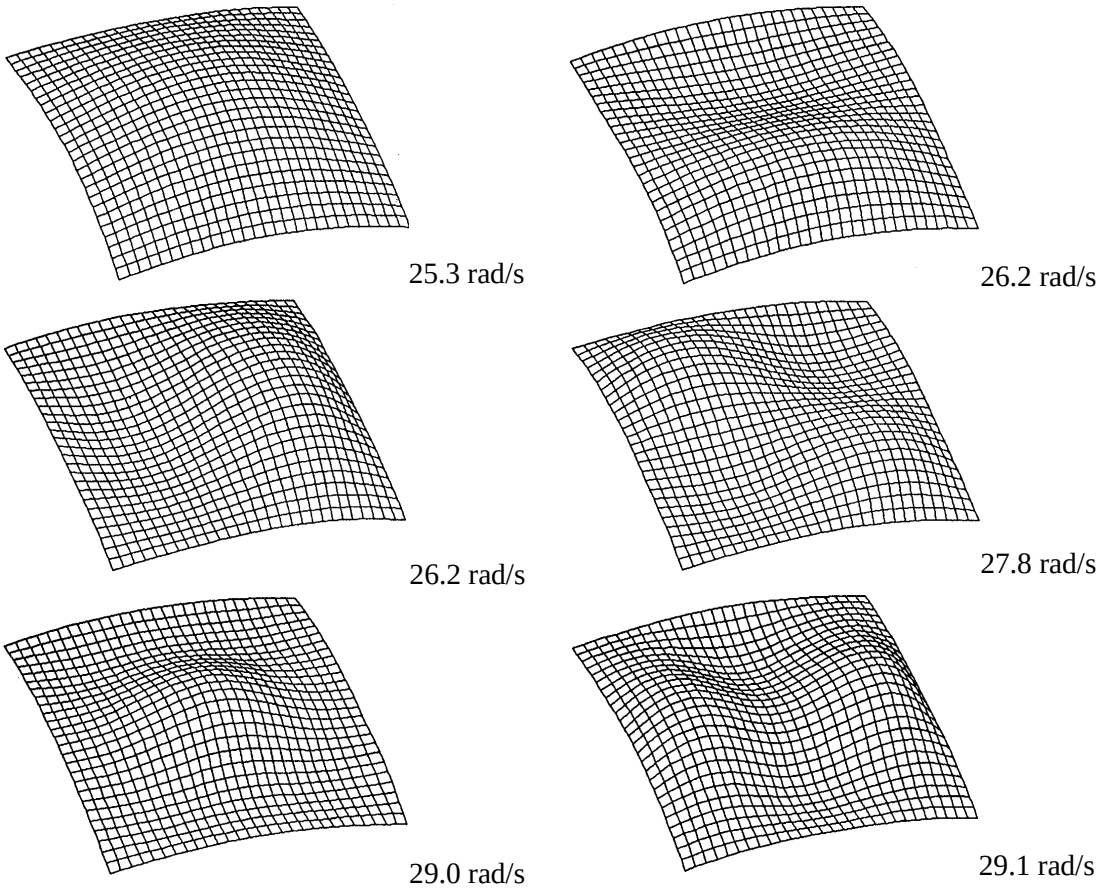

Figure 202. Normal modes and natural frequencies of a shallow spherical shell

Rigid body modes

If a structural model is not properly supported then a linear finite element analysis (p. 82) gives an error message: singular stiffness matrix. This means that the computer is determining the displacements and it cannot decide how large they are.

If a structural model is not properly supported then a modal analysis (p. 156) does not give an error message. Instead it also computes rigid body modes with natural frequencies $f_n = 0$ Hz.

A totally free structure has 6 independent rigid body modes; 3 translations in perpendicular directions and 3 rotations around perpendicular directions. Note that a modal analysis does not determine the magnitude of any normal mode. This is why it does not give an error message for unsupported structures.

Equation of motion

The shell differential equation for dynamic behaviour can be simply derived from the shell buckling differential equation (p. 139) by adding inertia forces to the load (d'Alembert's principle [3]).

[3] Jean d'Alembert (1717-1783) was a French gentlemen scientist. He was an orphan but inherited a fortune and did not work for a living [Wikipedia].

$$\frac{E t^3}{12(1-\nu^2)}\nabla^2\nabla^2\nabla^2\nabla^2 u_z + E t \Gamma\Gamma u_z = \nabla^2\nabla^2\left(p_z + n_{xx}\frac{\partial^2 u_z}{\partial x^2} + (n_{xy}+n_{yx})\frac{\partial^2 u_z}{\partial y \partial x} + n_{yy}\frac{\partial^2 u_z}{\partial y^2} - \rho t \ddot{u}_z\right)$$

In this t is the shell thickness and $\ddot{u}_z$ is the second derivative of the perpendicular displacement to time.

Wave numbers

The wave pattern of a normal mode has peaks and valleys. The number of peak-and-valleys in a cross-section is the wave number. For example in Figure 202 the top right normal mode has wave number 1 in one direction and wave number 1/2 in the other direction.

In beams and plates a small wave number corresponds to a small natural frequency. However, in shells this is not always the case. For example Figure 203 shows the natural frequencies of a cylinder that is simply supported at both edges. This graph has been analytically derived by K. Forsberg and published in the book of Arthur Leissa in 1973 [109]. Every crossing point of a curved line with a vertical line represents a natural frequency. The slenderness ratio is a/t = 500. m is the wave number in the axial direction and n is the wave number in the circumferential direction. In the graph l is the length and R is the radius of the cylinder. Suppose that the ratio l/R = 2. A simple normal mode occurs for m = ½ and n = 2 (fig. 204). In the graph we read a corresponding normalised natural frequency of approximately 0.3 (fig. 203, green circle). However, the smallest natural frequency is 0.05 which occurs for m = ½ and n = 8 (fig. 203, blue circle). This natural mode is shown in Figure 204 right hand side. In fact, in the graph we can count 19 more modes that have smaller frequencies than the simple mode (fig. 203, red circles). Many more exist between the graph lines and outside the area of the graph.

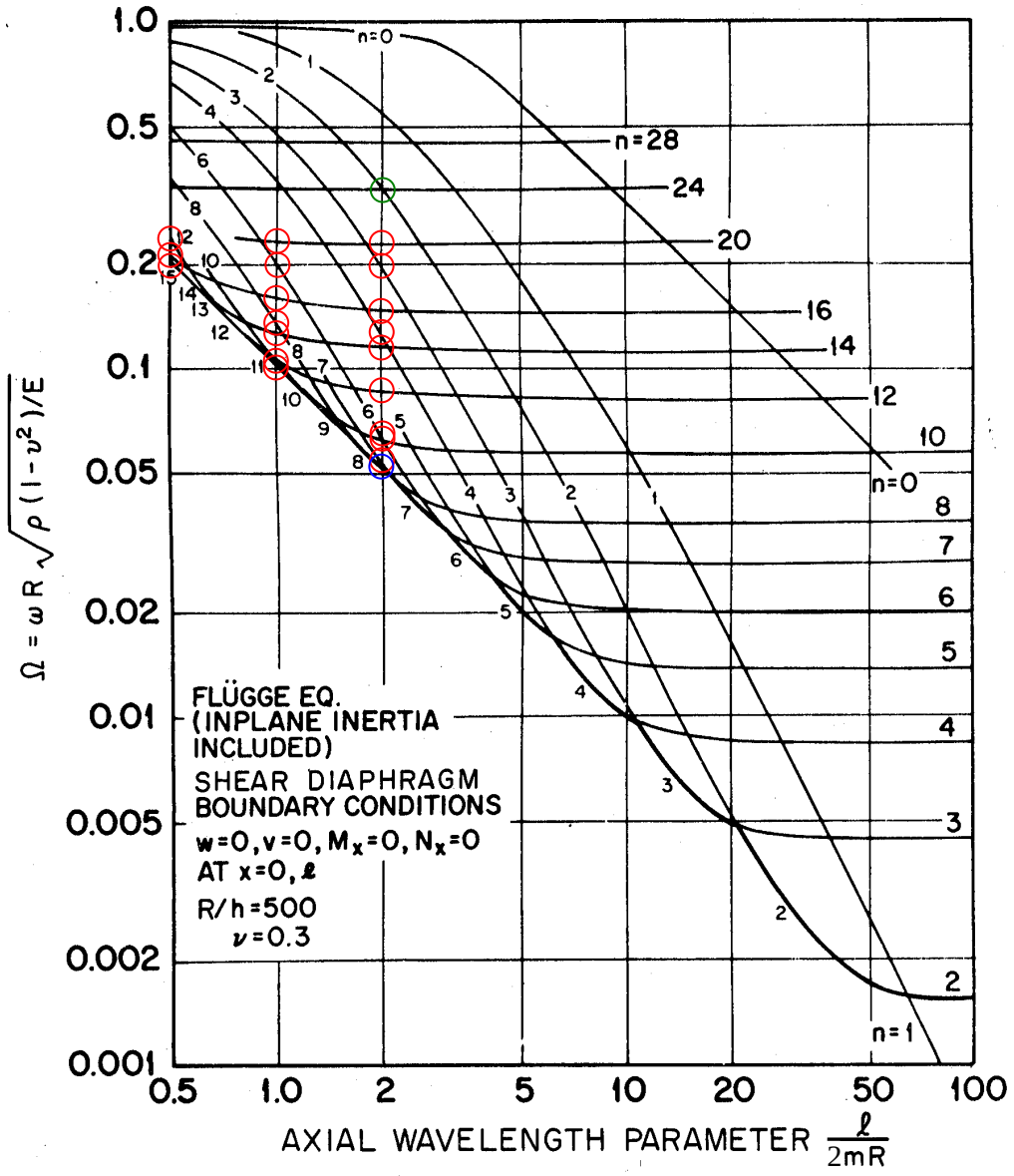

Figure 203. Dispersion curves of a cylinder with diaphragms at each end [109 p.62]

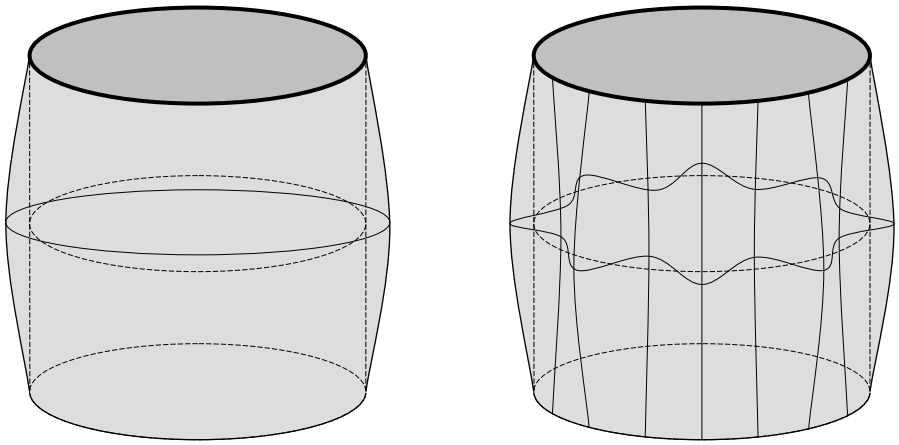

m = ½, *n* = 2, Ω = 0.3

m = ½, *n* = 8, Ω = 0.05

Figure 204. Normal modes of the cylinder

Festoon

Typical in vibration analysis and also in buckling analysis are graphs like figure 203. The envelope of these curves is shown as a thick line. It is called festoon. We have borrowed the word from decorators.



Vibration experiments

Suppose we shake a shell at some frequency and we observe the wave numbers. Such an experiment has been done with an aluminium cylinder that is clamped at one edge and free at the other. The wall thickness is 0.0255 in., the radius is 9.538 in. and the length is 24.63 in. Figure 205 shows the experimental and the analytical results. In this graph *m* is not the wave number but just a number assigned to the normal modes. An excellent agreement is found between experiment and theory. Other experiments also show an excellent agreement [109]. This confirms the correctness of the Sanders-Koiter equations (p. 54).

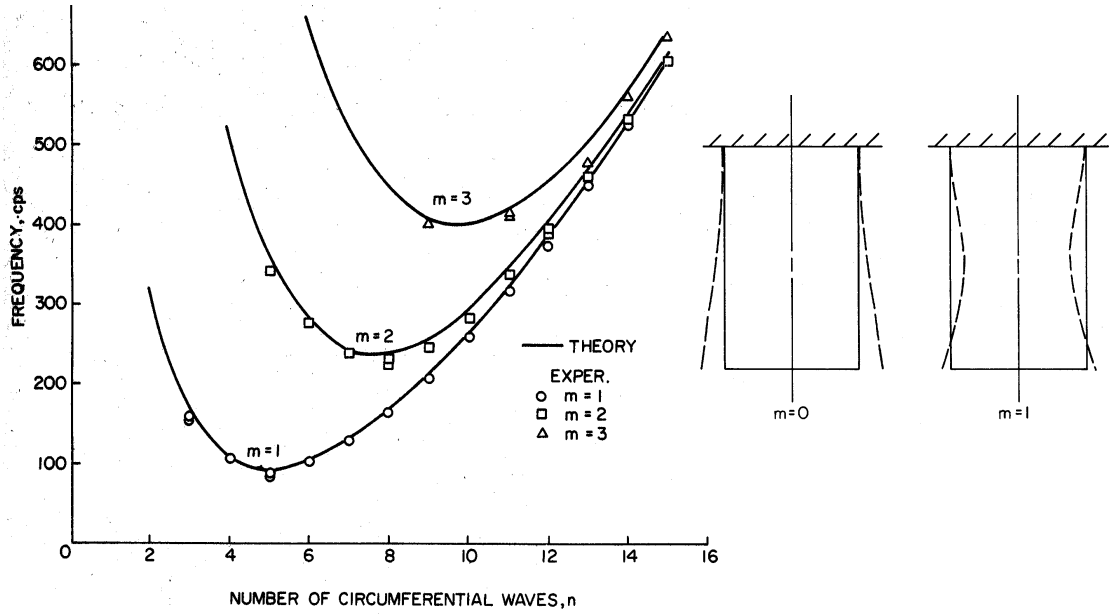

Figure 205. Natural frequencies for a clamped-free aluminium cylinder [109 p.118]

Resonance

A shell can be loaded by a harmonic force, for example a rotating machine or jumping people. If this loading has the same frequency as any of the shell natural frequencies, it will vibrate strongly in associated normal mode. Also other dynamic loading can excite a shell in a normal mode, for example storms and earthquakes. The dominant frequencies of storms vary up to 1 Hz. The dominant frequencies of earthquakes vary up to 10 Hz (fig. 206).

In other words, when you press the modal analysis (p. 156) button, the computer shows the natural frequencies of your structure. If these are larger than 10 Hz you do not have a resonance problem.

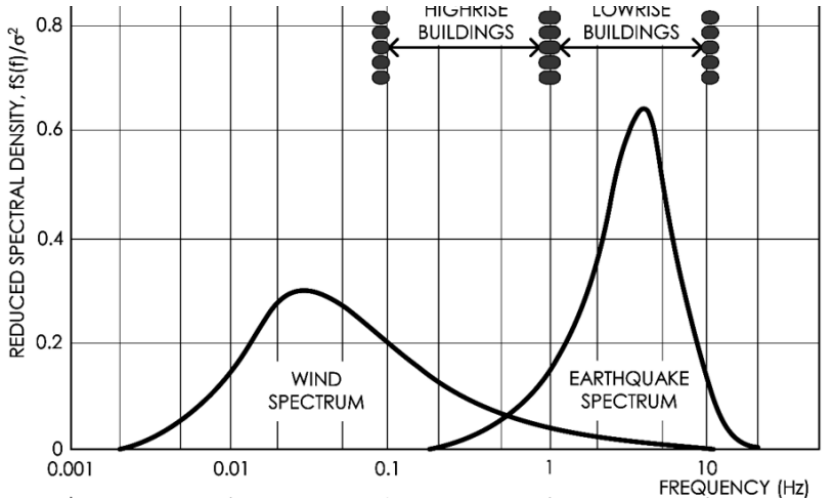

Figure 206. Natural frequencies need to be larger than the dominant frequencies of the load [110]

Inextensional deformation
If the smallest natural frequency of a shell is very small than the deformation is probably inextensional. The corresponding wave number will be small too. This behaviour is opposite to described in the previous sections. It can be explained as that a shell that can move inextensionally is not really a shell but rather a thin curved plate (see shell behaving like a plate p. 114)

Hemispheres
Free vibration of a thin hemispherical shell was first studied by Lord Rayleigh [4] in 1881 [111, p 11]. He assumed inextensional deformation (p. 109) and derived the natural frequencies. The smallest natural frequency is [5]

$$f_n = 0.2407 \frac{t}{a^2} \sqrt{\frac{E}{\rho(1+\nu)}},$$

where ρ is the mass density for example in kg/m³.

Resonance of a wine glass
The frequencies that people can hear vary from 20 Hz to 20 000 Hz. The human voice can produce frequencies up to approximately 1000 Hz. This can be used to break a wine glass. For proof see

http://www.youtube.com/watch?v=sH7XSX10QkM
http://www.youtube.com/watch?v=dU0OqVDl7kc&feature=g-vrec

Spheres
Free vibration of a thin spherical shell was first studied by Horace Lamb in 1882 [112]. [6] A detailed study was also made by Wilfred Baker in 1961 [113]. [7] The smallest natural frequency is

[4] The real name of Lord Rayleigh was John Strutt (1842-1919). When his father died, he inherited a title and a 7000 acres family estate. He left the management of the land to his younger brother and devoted his time to physics at Cambridge University. In 1904, he received a Nobel prize for discovering the gas argon [Wikipedia].

[5] The coefficient 0.2407 in the formula has been obtained by finite element analysis. Rayleigh assumed an unknown factor in his derivation and did not obtain this coefficient. Remarkably, also other early scientists who studied hemispherical shells (Zwingli 1930, Naghdi 1962, Kalnins 1963) failed to obtain the right coefficient.

$$f_n = \frac{1}{2\pi a}\sqrt{\frac{E}{\rho}}\sqrt{\frac{7+3\nu-\sqrt{(7+3\nu)^2-16(1-\nu^2)}}{2(1-\nu^2)}} \approx 0.12\frac{1}{a}\sqrt{\frac{E}{\rho}}.$$

It has been derived from the shell membrane equations (p. 38). Note that this natural frequency does not depend on the shell thickness. The equation is very accurate. For $a/t = 20$ its error is 0.3% [114]. For a smaller thickness it is even more accurate. The equation is suitable for checking finite element software.

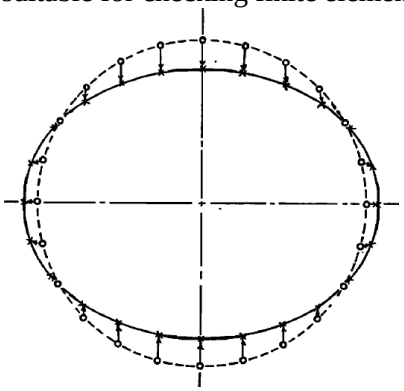

Figure 207. Mode shape of a spherical shell [113] (symmetrical around the vertical axis)

Exercise: Lamb ends his paper with a prediction. "*I find that a thin glass globe 20 centimètres in diameter should, in its gravest mode, make about 5350 vibrations per second.*"[112] Does this indeed follow from the formula?

Exercise: Consider a hemisphere and a sphere of similar material, size and thickness. The sound of the sphere is much higher than the sound of the hemisphere. What causes this?

Cylinders

Circular cylinder shells can vibrate in beam modes and in shell modes. In a beam mode it bends up and down while the cross-section does not deform ($n = 1$). In a shell mode the centre line remains straight and the cross-section deforms ($n = 2, 3, 4\ldots$). For long cylinders a beam mode gives the smallest natural frequency. For short cylinders a shell mode gives the smallest natural frequency.

Table 14 shows the smallest natural frequencies of beam modes and of shell modes for several types of support. Figure 208 shows these natural frequencies as a function of the cylinder length. The table and the figure do not exactly match. In the table the shell frequencies are straight line approximations, while in the figure the festoons (p. 159) of the exact solutions are shown. Wilhelm Flügge was the first scientist to solve cylinder shell natural frequencies in 1943 [114 p. 627]. The compact presentation of Figure 208 has been made by Chris Calladine in 1983 [114 p. 651].

Table 14. Smallest natural frequencies of cylinder shells for various boundary conditions [9, p.651]

a		$f_n = \frac{7.0}{2\pi}\frac{a}{l^2}\sqrt{\frac{E}{\rho}}$	f	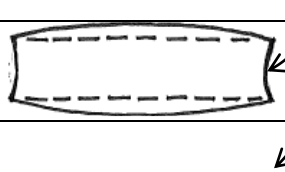 $f_n = \frac{2.4}{2\pi l}\sqrt{\frac{t}{a\sqrt{1-\nu^2}}}\frac{E}{\rho}$

[6] Horace Lamb (1849–1934) was professor of mathematics in Cambridge, England [Wikipedia].

[7] Wilfred Baker (1924–1991) was an explosions expert and accident investigator at Southwest Research Institute, San Antonio, Texas. He started the company BakerRisk [www.bakerrisk.com].

b	$f_n = \frac{11}{2\pi}\frac{a}{l^2}\sqrt{\frac{E}{\rho}}$	g	$f_n = \frac{3.0}{2\pi l}\sqrt{\frac{t}{a\sqrt{1-\nu^2}}\frac{E}{\rho}}$
c	$f_n = \frac{2.5}{2\pi}\frac{a}{l^2}\sqrt{\frac{E}{\rho}}$	h	$f_n = \frac{1.4}{2\pi l}\sqrt{\frac{t}{a\sqrt{1-\nu^2}}\frac{E}{\rho}}$
d	$f_n = \frac{16}{2\pi}\frac{a}{l^2}\sqrt{\frac{E}{\rho}}$	i	$f_n = \frac{3.6}{2\pi l}\sqrt{\frac{t}{a\sqrt{1-\nu^2}}\frac{E}{\rho}}$
e	$f_n = \frac{16}{2\pi}\frac{a}{l^2}\sqrt{\frac{E}{\rho}}$	j	$f_n = \frac{1}{2\pi}\sqrt{\frac{3}{5}}\frac{t}{a^2\sqrt{1-\nu^2}}\sqrt{\frac{E}{\rho}}$

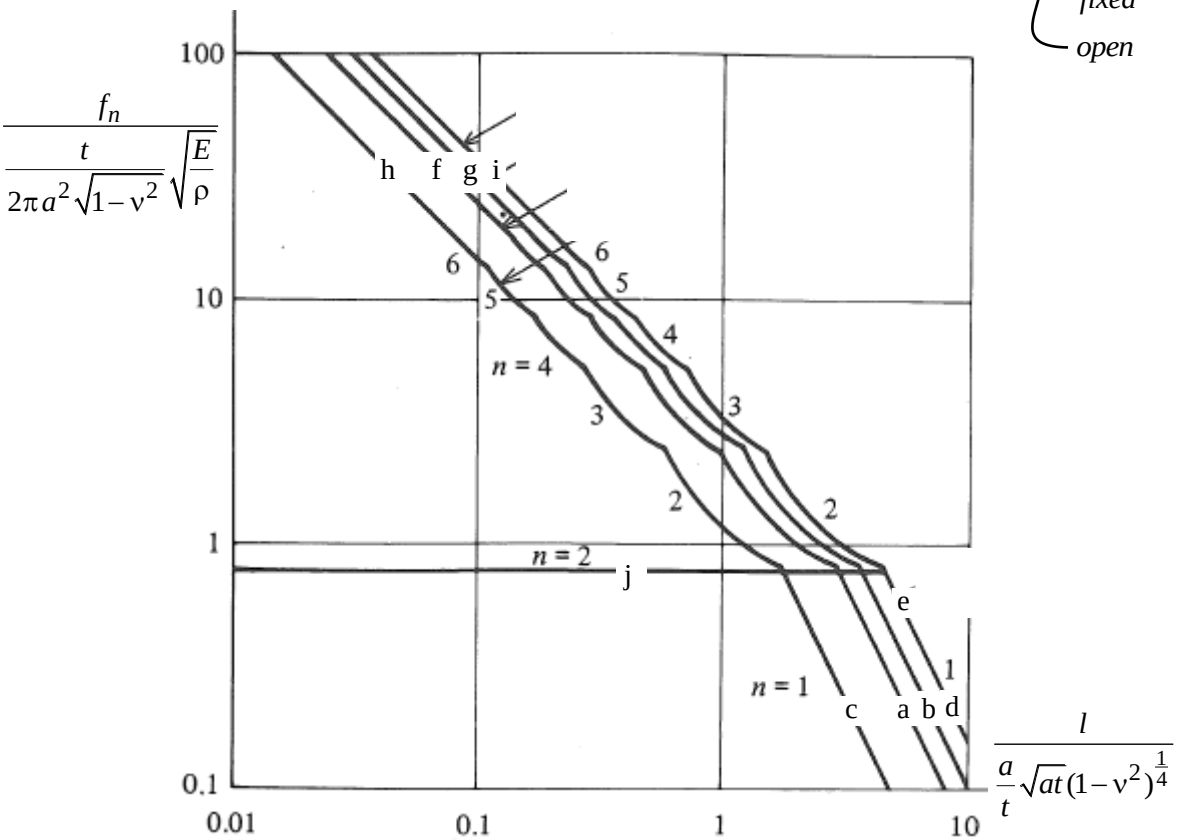

Figure 208. Smallest natural frequencies of cylinder shells for various boundary conditions [114] [8]

Exercise: Which curve in figure 208 is the festoon of figure 203?

Membrane force

A membrane force changes natural frequencies. Tension increases and compression decreases the natural frequencies. For example, consider a simply supported cylindrical shell (Table 14, f). It is loaded by an axial force *F*. The natural frequency is

$$f_n = f_{no}\sqrt{1-\frac{F}{F_{ult}}},$$

[8] Note that the author of figure 208 must have been very smart. He writes 7 quantities *f*n, *E*, ν, ρ, *a*, *t*, *l* into just 2 dimensionless quantities and represents 10 equations in one graph. Others need over 100 graphs to display the same information.

where f_{no} is the natural frequency without loading and F_{ult} is the axial **buckling** load [115]. Note that when the cylinder almost buckles the natural frequency is almost zero. The normal mode does not change due to the axial load. The formula is not only valid for the fundamental frequency but also for higher natural frequencies provided that the **buckling mode** has the same shape as the normal mode (higher buckling modes). This property can be used for monitoring structural damage (see measuring vibrations p. 164)

Shell vibration literature
Between 1880 and 1980, scientists solved many shell problems. Robert Blevins collected the natural frequency formulas and published these in his book [115]. However, analytical solutions can only be derived for simple shapes, like spheres, cylinders, cones and curved panels. Fortunately, around 1980, computers became powerful tools. Between 1960 and 2000, scientists developed the finite element method (p. 82). Nowadays, it is a simple task to compute natural frequencies of shells of any shape, with any loading and any supports.

Natural frequency of a square shell
Consider a square shell with diaphragm boundary conditions (p. 70) at each edge (fig. 209). The shell has a small curvature (shallow), a uniform in plane edge load and a uniform surface load. Its smallest natural frequency is

$$f_n = \sqrt{\underbrace{\frac{\pi^2}{12(1-\nu^2)}\frac{Et^2}{\rho l^4}}_{\text{bending stiffness}} + \underbrace{(k_m^2 + k_{xy}^2)\frac{E}{4\pi^2\rho}}_{\text{curvature}} + \underbrace{\frac{n_{xx}+n_{yy}}{4\rho t l^2} - \frac{(1-\nu^2)n_{xy}^2}{71.7\rho E t^4}}_{\text{membrane forces}}}$$

In this equation the contributions can be observed of bending stiffness, curvature and membrane forces. The equation was derived by substituting $u_z = \cos\frac{\pi x}{l}\cos\frac{\pi y}{l}\cos 2\pi f t$ in the equation of motion (p. 157) and it has been validated and extended by finite element analysis.[9]

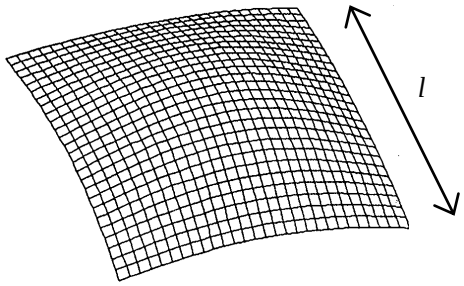

Figure 209. Square shell with diaphragm boundary conditions

Exercise: Check the natural frequency formula by applying it to figure 202. Can we also use the formula to calculate the natural frequency of mode 4?

Exercise: What is the contribution of curvature to the natural frequency of Enneper's surface (p. 164) with diaphragm boundary conditions?

[9] The contribution of *km* has been found by John Sewall in 1967 [116]. The term with *nxx* + *nyy* has been found by Edmond Szechenyi in 1971 [117]. The term with *nxy* has been found by Roland van Dijk in 2014 [118]. The contribution of *kxy* has been found analytically and confirmed numerically by Yordi Paasman in 2016 [119]. The Gaussian curvature *kG* has no significant influence, which was shown by Joep Sluijs in 2017 [120].

Challenge: For which size *l* is the formula for the smallest natural frequency of a square shell (p. 163) no longer accurate?

Enneper's surface

Enneper's [10] surface (fig. 210) is a minimal surface (p. 24) described by

$$\bar{x} = 2au(1+v^2-\tfrac{1}{3}u^2)$$

$$\bar{y} = -2av(1+u^2-\tfrac{1}{3}v^2)$$

$$\bar{z} = 2a(u^2-v^2)$$

$$k_{xx} = \frac{-1}{a(1+u^2+v^2)^2}$$

$$k_{yy} = \frac{1}{a(1+u^2+v^2)^2}$$

$$k_{xy} = 0$$

$$\alpha_x = 2a(1+u^2+v^2)$$

$$\alpha_y = 2a(1+u^2+v^2)$$

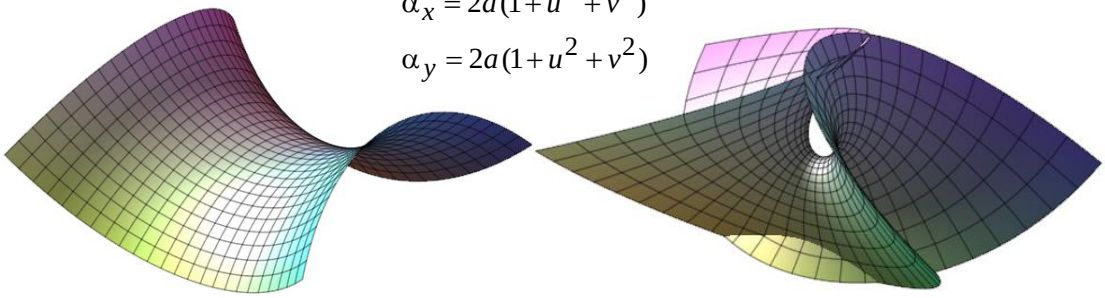

$-\frac{1}{2} < u < \frac{1}{2}$ $-\frac{1}{2} < v < \frac{1}{2}$ $-2 < u < 2$ $-2 < v < 2$

Figure 210. Enneper's surface; a shallow part and a deep part

Measuring vibrations

Vibrations can be observed by changes in the strain at some point of a structure. A strain gauge is a small sensor for measuring strains. It is carefully glued onto the surface of a structure. There is a long thin wire in a strain gauge (fig. 211). When this wire is extended its electrical resistance changes. In a simple test setup the strain gauge is connected to a box which is connected to a laptop computer (fig. 212).

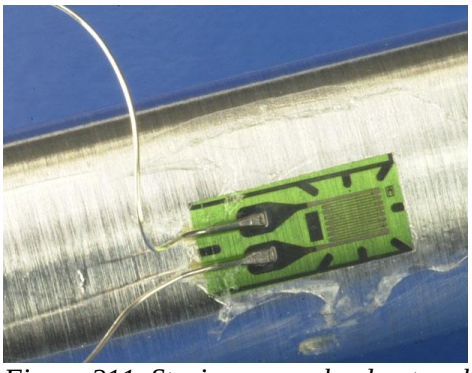

Figure 211. Strain gauge glued onto a bar

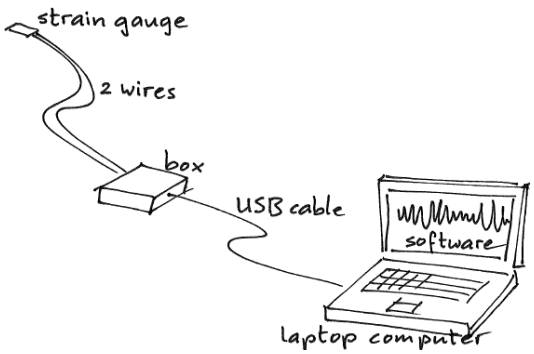

Figure 212. Simple test set-up for measuring vibrations

The box contains electronics which does two things. 1) It measures the electrical resistance of a strain gauge with a circuit called Wheatstone bridge. This produces a voltage that changes between approximately -2.5 and 2.5 Volts. 2) It translates the analog voltage into digital numbers (sequences of 0 and 5 Volts) and puts these on the USB cable. The digital numbers are read and stored by the software on the laptop computer.

[10] Alfred Enneper (1830–1885) was professor of mathematics in Göttingen [Wikipedia].

A strain gauge costs approximately €10. Unfortunately, they cannot be removed without breaking. The box and software cost approximately €200 (for example Mantracourt DSCUSB).

Spectrum

A measured signal can be approximated by adding a number of sine functions and cosine functions. An example is the block signal of figure 213. A very good approximation can been obtained when a large number of sine functions is used. This approximation is called a Fourier series.[11]

Apparently the following frequencies are in the block signal: $1/(2\pi)$ with an amplitude of 1.23, $3/(2\pi)$ with an amplitude of 0.30 and $5/(2\pi)$ with an amplitude of 0.10. A plot of this result is called the spectrum of the block signal (fig. 214).

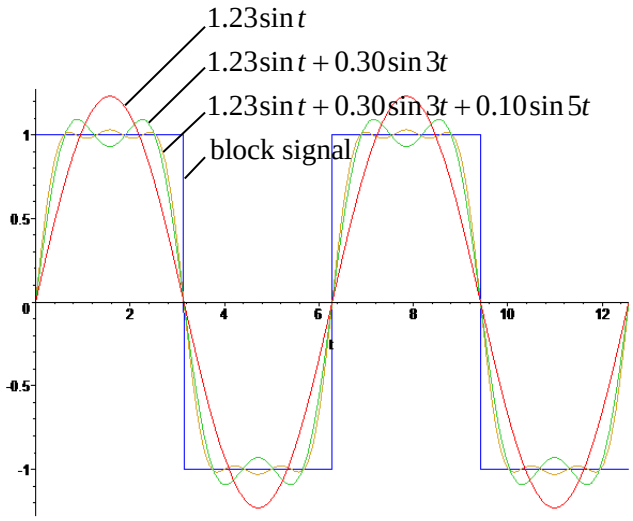

Figure 213. Fourier series approximations of a block signal

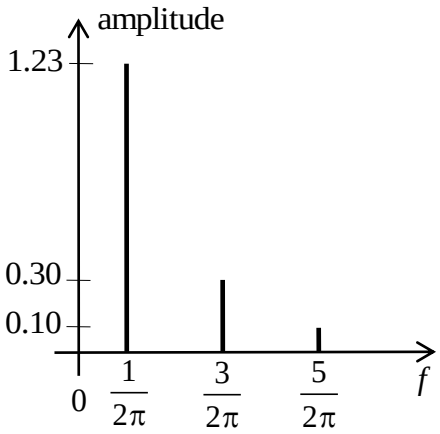

Figure 214. Spectrum of a block signal

Fast Fourier transform

A fast Fourier transform (FFT) is an algorithm for computing the spectrum (p. 165) of a signal. Figure 215 shows an example signal. (Micro strain as a function of the time step number, the time step is 0.01 s.)

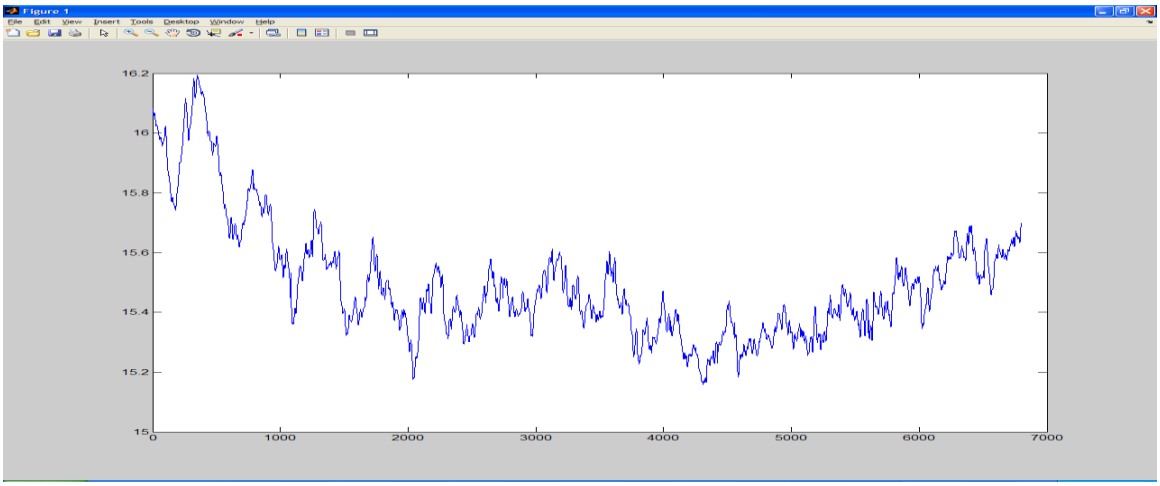

[11] Joseph Fourier (1768–1830) was a French physicist. He is also known for conjecturing the greenhouse effect of the Earth's atmosphere [Wikipedia].

Figure 215. Measured signal

The following Matlab code is used for plotting the spectrum shown in figure 216. In this example the peaks of the spectrum are natural frequencies.

```
>> a = [16.0832 16.0825 16.0823 .. 15.6987];
>> Dt = 0.01
>> y = a - mean(a)
>> N = length(y)
>> plot([0:N-1]/Dt/N, abs(fft(y)))
>> axis([0 1 0 600])
```

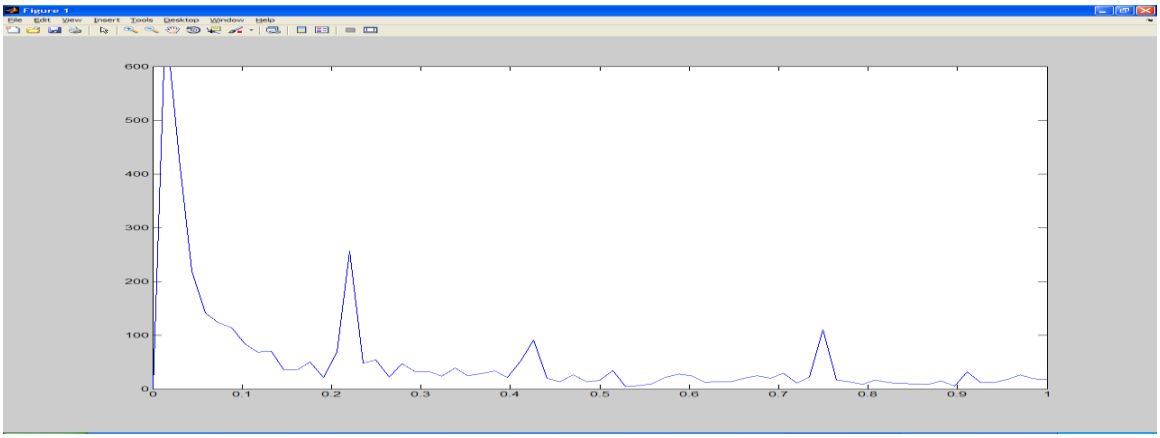

Figure 216. Spectrum of the signal

Sampling theorem
When measuring vibrations (p. 164), in every time step the strain is recorded. A high frequency *f* may not be noticed. To be noticed and determined accurately the time step needs to be substantially smaller than 1/(2*f*). This is called the *sampling theorem* [121].

Transient analysis
A transient analysis is a dynamic finite element computation. The loading is specified starting at $t = 0$ and varies in time. The response is computed in many very small time steps. For large structures it takes several hours to compute the response to just one minute of loading. A storm lasts for approximately 6 hours, therefore, transient analysis is not suitable for simulating the behaviour to this loading. An earthquake lasts for less than a minute, therefore, this loading can – and needs – to be analysed with a transient analysis. Note that the word "transient" means "lasting only a short time".

In a transient analysis it is important that the specified time step is sufficiently small. Halve the time step to see if it is (see mesh refinement p. 84 and apply this to time). It is also important to specify realistic damping ratio's (p. 167) for the right modes.

Damping ratio
The amount of damping is expressed in a damping ratio ζ. (Refer to your dynamics text book for the definition of the damping ratio.) The damping ratio can be determined experimentally by exiting a structure in a normal mode, removing the load and observing how the vibrations decay (fig. 217). The *logarithmic decrement* δ is calculated with

$$\delta = \frac{1}{n} \ln \frac{x_0}{x_n},$$

where x_0 is an amplitude and x_n is the amplitude n peaks later.

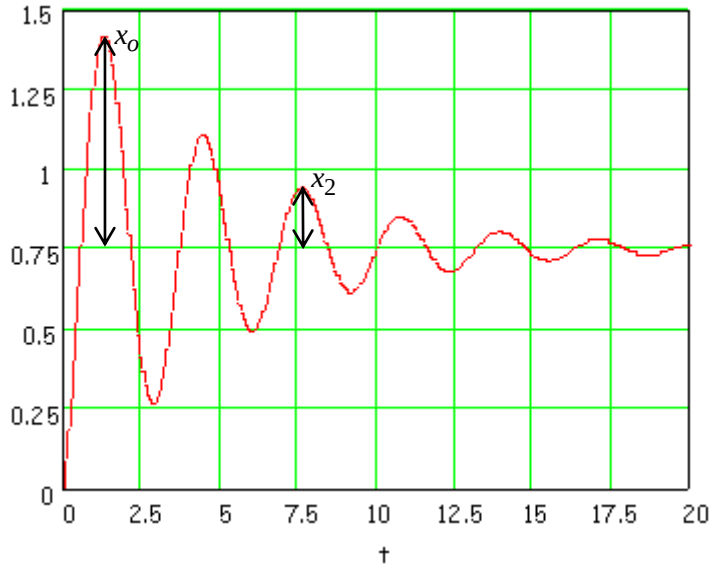

Figure 217. Damping of a mass spring system

The damping ratio is calculated with

$$\zeta = \frac{\delta^2}{\sqrt{4\pi^2 + \delta^2}} .$$

Some results are:
Reinforced concrete structures under service loading ζ = 4%,
Reinforced concrete structures under ultimate loading ζ = 5%,
Welded steel structures ζ = 2%,
Bolted steel structures ζ = 6%.

Damping ratio distribution
Different normal modes of a structure can have different damping ratios. In a transient analysis (p. 166) they need to be specified. In many programs *Rayleigh damping* can be selected. In this method the damping matrix is a combination of the mass matrix and the stiffness matrix. Sometimes Rayleigh damping is referred to as proportional damping. An advantage of Rayleigh damping is that the transient analysis is faster than with other damping methods. The damping ratios need to be specified for two modes. The software interpolates the other ratios almost linearly (fig. 218). It is recommended to specify damping of the first normal mode and the highest occurring normal mode [122]. To find out which is the highest mode, increase the number of the second dampened mode until there is no change in important results.

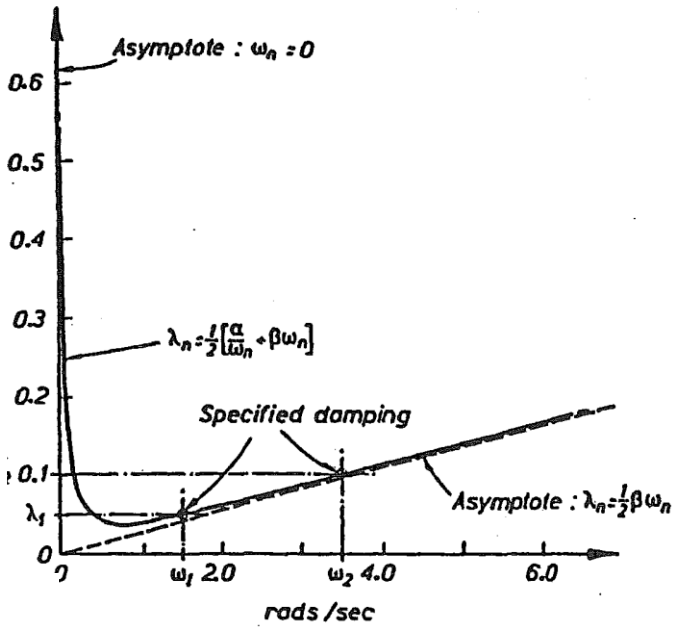

Figure 218. Damping ratio as a function of the frequency in case of Rayleigh damping [122]

Acceptable vibrations

People are disturbed by feeling and seeing vibrations. Figure 219 shows what most people experience. An acceleration of 0.2 m/s^2 is often acceptable.

	perception	acceptability in buildings	structural effects	examples
A	very unpleasant	not acceptable	danger of collapse	- earthquake
B	unpleasant	not acceptable	local damage	- emergency braking of a car
C	strongly noticeable	hardly acceptable	cracks in masonry	- in a tram or elevator
D	well noticeable	only rough work	small cracks	- start of seasickness
E	noticeable	shortly in rooms	no influence on building	
F	hardly noticeable	acceptable	no influence	
G	not noticeable			

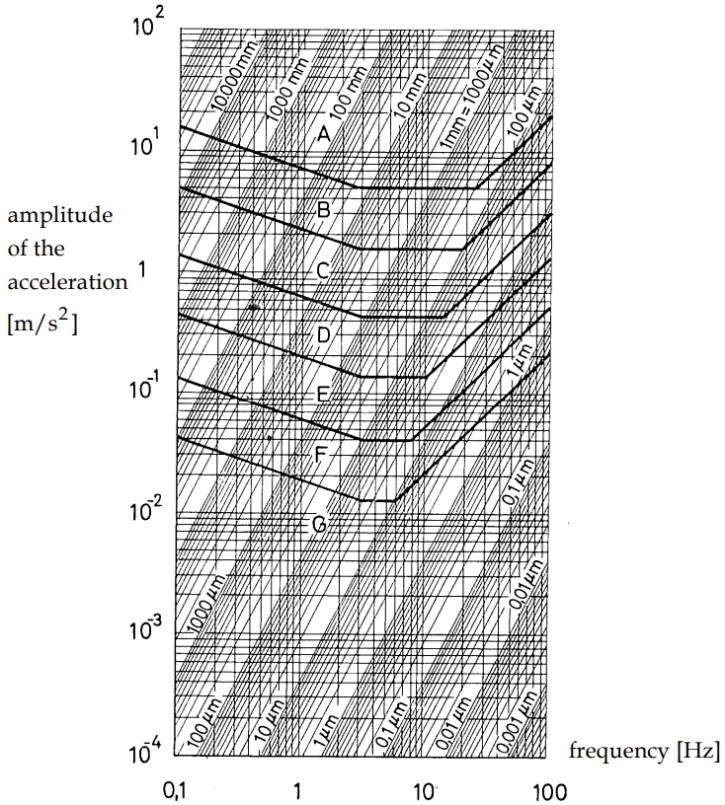

Figure 219. Perception of vibrations [H. van Koten, "Grenzen voor dynamische beweging", TNO-IBBC, rapport BI-67-107, 1967 (in Dutch)]

Exercise: The shell roof of a museum vibrates with a frequency of 1 Hz and an amplitude of 1 mm. Do visitors feel dizzy?

Shell acoustics
The interior of a reinforced concrete shell roof is often smooth without the usual beams, bars, cables and columns that clutter the view. However, as a consequence, the reflection of sound can be unexpectedly strong. The architect needs to consider this and perhaps consult an acoustic expert.

Many shells have a funny acoustic property called whispering gallery. When you stand inside close to the shell and whisper something then on the other side of the shell somebody can hear it clearly. This is because sound waves are guided by the hard curved surface. The name has been derived from the famous whispering gallery in St. Paul's Cathedral (p. 43).

Sounds outside should not enter a building. For this mass is needed. A 70 mm thick reinforced concrete shell might not be sufficient.

Design improvements
If a design has vibration problems it needs to be improved. For frame structures it is often possible to change a design such that the loading frequency is in between two natural frequencies. However, for a shell structure this probably is not possible because the natural frequencies are very close to another (see fig. 202). Therefore, the smallest natural frequency of a shell needs to be larger than the loading frequency (fig. 206).

Also it is possible to add dampers to solve vibration problems. (An example is the dampers used in cars.) Dampers are effective but also expensive. A transient analysis (p. 166) can be performed to determine the effect of dampers. However, the damping ratio (p. 167) of the structure itself also has a large influence and it is difficult to estimate accurately. Therefore, it

is difficult to determine whether dampers are really needed. A practical approach is to design damper positions but not include dampers in the structure. If later the structure starts to vibrate, dampers can still be placed. The designer needs to tell everybody that he or she is following this approach, otherwise later he or she might be blamed for making a bad design.

Limit state function
Consider a frame that carries a roof terrace. It is loaded by wind load W and live load L (fig. 223). Plastic analysis shows that mechanisms occur at

$$W = 4\frac{M_p}{l^2}, \qquad W + 2(2-\sqrt{2})L = 4\sqrt{2}\frac{M_p}{l^2}, \qquad W + 2L = 8\frac{M_p}{l^2}$$

A *limit state function* describes collapse of this frame (fig. 224). We engineers have many synonyms for limit state function, such as *yield contour*, *interaction diagram*, *utilisation*, *yield locus*, *response surface*, *strength hypothesis, unity check*. Surely, this shows that the concept is important to us.

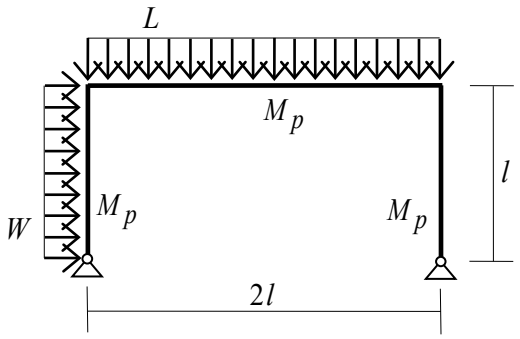

Figure 223. Frame structure with load

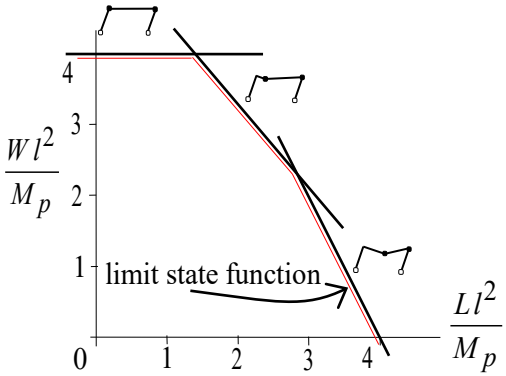

Figure 224. Limit state function

Limit state
A *limit state* is described by the following information.
- An event, for example *deflection* > 52 mm or *collapse*
- A small probability
- Load combinations for which the event shall not occur
- A limit state function (p. 171). Equation or software that checks if the event occurs

Approximation of the limit state function
Suppose we design a frame that is loaded by wind W and live load L (Fig. 223). The load combinations are

$0.2\,W_c$ and $1.4\,L_c$ ……	Hardly any wind and a large roof party
$1.6\,W_c$ and $0.3\,L_c$ ……	Storming and some furniture left on the roof

In this, W_c and L_c are the 5% characteristic values of the loads (or something similar).

We estimate the column and beam dimensions (first design) and enter these into a frame analysis program. We use the moments to design better dimensions for the columns and beam (second design). We repeat the frame analysis. Now, the beam stresses are somewhat too large and the column stresses are much below yield. So, we choose a somewhat larger beam cross section and smaller column cross sections (final design). We repeat the frame analysis and all stresses are fine.

Each of the three designs can be visualised by a limit state function (p. 171) Figure 225 shows how this may look like. The final design can carry each load combination and is not much stronger than it needs to be. We can safely approximate the final limit state function with the envelop of the load combinations (fig. 226).

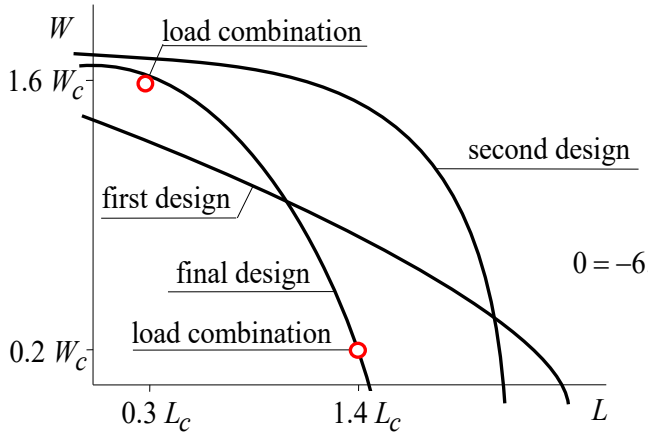

Figure 225. Three limit state functions

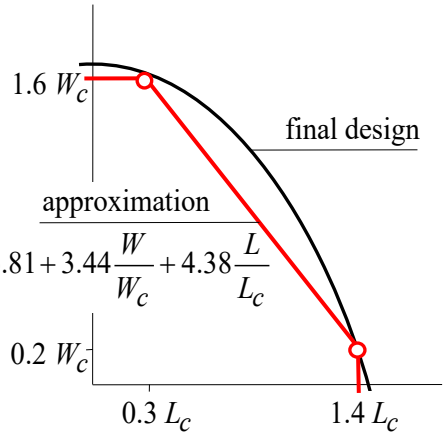

Figure 226. Approximation of the limit state function of the final design

```
> #     Z = a + b*W + c*L
> eq1:= 1 = a + b*1.0*Wc + c*1.0*Lc:
> eq2:= 0 = a + b*1.6*Wc + c*0.3*Lc:
> eq3:= 0 = a + b*0.2*Wc + c*1.4*Lc:
> solve({eq1,eq2,eq3},{a,b,c});
```

a = -6.81 b = 3.44/Wc c = 4.38/Lc

Monte Carlo analysis

The atomic bomb was developed from 1941 to 1945, in Los Alamos, USA. The development continued with the hydrogen bomb. It involved more than 130.000 people and was top secret [Wikipedia]. One of the researchers was Stanisław Ulam.[2] He worked on neutron diffusion and had an idea that he explained as follows.

"*... in 1946 ... I was convalescing from an illness and playing solitaires. The question was, what are the chances that ... solitaire laid out with 52 cards will come out successfully? After spending a lot of time trying to estimate them by pure combinatorial calculations, I wondered whether a more practical method than "abstract thinking" might not be to lay it out say one hundred times and simply observe and count the number of successful plays. This was already possible to envisage with the beginning of the new era of fast computers, and I immediately thought of problems of neutron diffusion ... I described the idea to John von Neumann,* [3] *and we began to plan actual calculations.*" [Wikipedia]

They needed a code name for their work and chose *Monte Carlo*, which refers to the Monte Carlo Casino in Monaco, where Ulam's uncle used to gamble with money borrowed from relatives [Wikipedia].

So, in a Monte Carlo structural analysis, a computer repeats the following experiment many times. Draw values of steel strength, concrete strength, self-weight, snow load, wind load, et cetera from their distributions and perform a finite element analysis. Do the unity checks. The failure probability is the number of failures over the number of experiments (fig. 228).

[2] Stanisław Marcin Ulam (1909–1984) was a Polish-American scientist in the fields of mathematics and nuclear physics [Wikipedia].

[3] John von Neumann (1903–1957) was a Hungarian-American mathematician and computer scientist [Wikipedia].

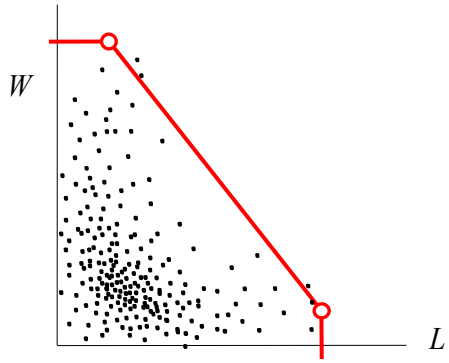

Figure 228. Monte Carlo analysis. Three of 200 analyses are outside the limit state function; the failure probability is 3/200.

Turkstra's rule

Meteorologists measure wind. In their records they find the largest wind speed in 50 years at some location. This is represented by a probability distribution (fig. 231). They can also draw the distribution of the largest wind speed in any 10 year period and the distribution of the largest snow depth in any 50 year period. These distributions are called *extreme value distributions* for example the Gumbel distribution describes storms well. [4]

The meteorologist can also plot the *joint* probability distribution of wind speed and snow depth (fig. 229). This distribution is of the largest in a day. A Monte Carlo analysis of 1000 000 design lives needs 1000 000 × 50 years × 365 days = 18 250 000 000 simulations. This takes too much time, even on a modern computer.

We could assume that all loads reach their 50 year maximum at the same time. So, the largest storm in the design life occurs at the same time as the largest snow depth and at the same time as the largest floor load. Clearly, this is very unlikely and it leads to very expensive structures.

In 1970, Carl Turkstra proposed a solution.[5] Let's consider all loads at their daily value except for one that has its extreme value [123]. In this way we use the extreme value distributions and not the joint distributions. The number of simulations is now 1000 000 × 3, if there are 3 load cases. The method does not take much time and is reasonably accurate.

	wind load distribution	snow load distribution	floor load distribution
combination 1	*extreme*	daily	daily
combination 2	daily	*extreme*	daily
combination 3	daily	daily	*extreme*

[4] Emil Gumbel (1891–1966) was a German mathematician. He taught statistics in Heidelberg and Paris. He was active in politics and often spoke against the Nazi party. He and his family had to leave Europe in 1940. He became a professor at Columbia University, USA [Wikipedia].

[5] Carl Turkstra (1936–2022) was a professor at the Polytechnic Institute of New York, Brooklyn. In 1989, aged 52, he left academia to lead the family lumber business in Canada. His parents were Dutch immigrants who settled in Hamilton, Canada in 1927.
[online obituary: https://www.legacy.com/ca/obituaries/thespec/name/carl-turkstra-obituary?id=40027708]

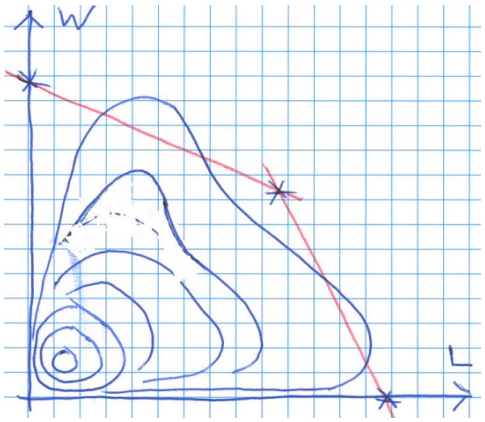

Figure 229. Joint distribution of W and L (Only daily distributions are possible)

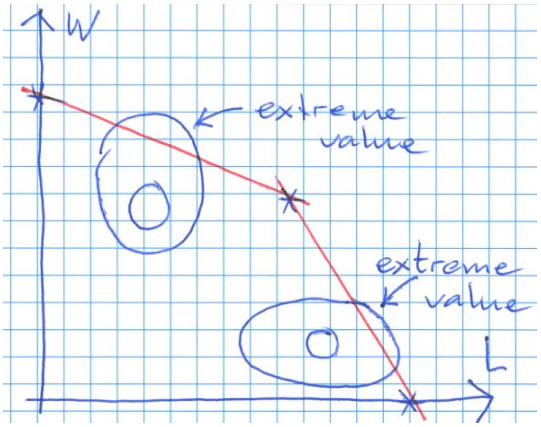

Figure 230. Turkstra's approximation (50 year extreme value distributions)

Drawing a number

In a Monte Carlo analysis, the software draws numbers out of probability distributions. How do we program this? It is best explained with an example. The Gumbel cumulative distribution function is (fig. 231)

$$F = \exp(-\exp(\frac{u-x}{\alpha})) \quad \text{where} \quad u = \mu - 0.5772\,\alpha \quad \text{and} \quad \alpha = \sigma\sqrt{6}/\pi\,.$$

The inverse is

$$x = \mu - \sigma\frac{\sqrt{6}}{\pi}\left(0.5772 + \ln(-\ln(F))\right).$$

We draw a random number between 0 and 1, assign this to F and calculate x. The Python code is

```
x=mean-stdev*0.7797*(0.5772+math.log(-math.log(random.random())))
```

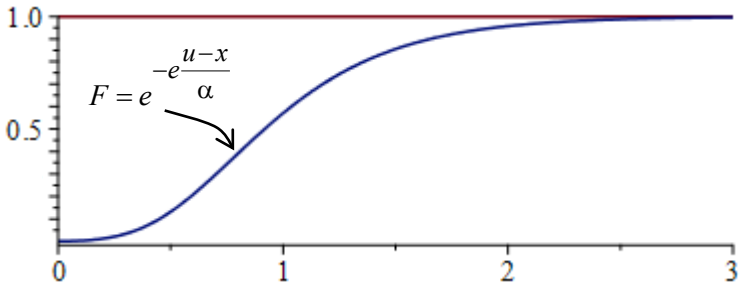

Figure 231. Cumulative distribution function (CDF) of the Gumbel distribution ($\mu = 1$, $\sigma = 0.5$)

Exercise: Plot the probability density function (PDF) of the Gumbel distribution.

Software

It is not difficult to write a program that computes failure probabilities. A simple Python program can be downloaded from

phoogenboom.nl\b17_Python_Monte_Carlo.txt

The program uses the Monte Carlo method, Turkstra's rule and the envelope of the load combinations. The program does 1000 000 simulations, which takes a few seconds.

The program has a remarkable property. Each material and each load can be represented by two ratios.

bias = characteristic value / mean
coefficient of variation = standard deviation / mean

If we change the input numbers, but these ratios stay the same, the failure probability stays the same. Note that these ratios have no unit.

Exercise: Does failure probability depend on the units of the input values?

Challenge: We need 2000 failures for computing the failure probability with less than 5% error. Sometimes this rule is not true and the error is larger than 5%. How often does this happen? (Poisson distribution. [6])

Human error

Engineers make mistakes. Of course we have procedures to catch our mistakes on time. Nonetheless, most structural failures are due to human error [125]. Often we find out during construction. We cannot statistically predict the magnitude of these errors. Therefore, they are not included in the calculation of failure probabilities. If you now think that calculating structural failure probabilities is just an academic exercise, you are right. However, is there a better way to make our structures safe?

Annual failure probability

The software produces the failure probability in the design life, for example 50 years. For a design life of 49 years, we need to adjust the extreme value distributions (p 176). The *annual* failure probability in year 50 can be obtained by subtracting the 49 year failure probability from the 50 year failure probability. The annual failure probability varies from year to year. The annual failure probability is highest in the first year of a structure's life, unless fatigue is important [126]. An approximation of the annual failure probability is

$$P_{fa} \approx \frac{P_{fd}}{n}$$

where

P_{fa} …. annual failure probability

P_{fd} ..... probability of failure in the design life

n ..... design life in years

This formula is accurate for structures with much variable load compared to self-weight.

Failure probability per year is checked with a personal safety (p. 176) requirement. Failure probability per design life is compared to an economic safety (p. 177) target.

Changing the period of a Gumbel distribution

The period of the Gumbel distribution can be changed. For example, we have the distribution for the largest in 50 year and we need the distribution for the largest in 100 year. The standard deviation σ stays the same. The mean μ becomes $\mu + \sigma\frac{\sqrt{6}}{\pi}\ln\frac{100}{50}$.

[6] Siméon Poisson (1781-1840) was a French mathematician. On Wikipedia is a list of things named after him. It is more than 50 long ... and missing is Poisson's ratio of elasticity theory.

Suppose that the largest in 1 year has a normal distribution. It can be shown that the largest in 50 years approximately has a Gumbel distribution. The same occurs for the log normal distribution and many other distributions.

Personal safety
Consider a citizen of a civilised country. This person can die due to an accident, a health problem, murder et cetera. Figure 232 shows the probability of dying in one year as a function of age. A few of these deaths are due to structural collapse.

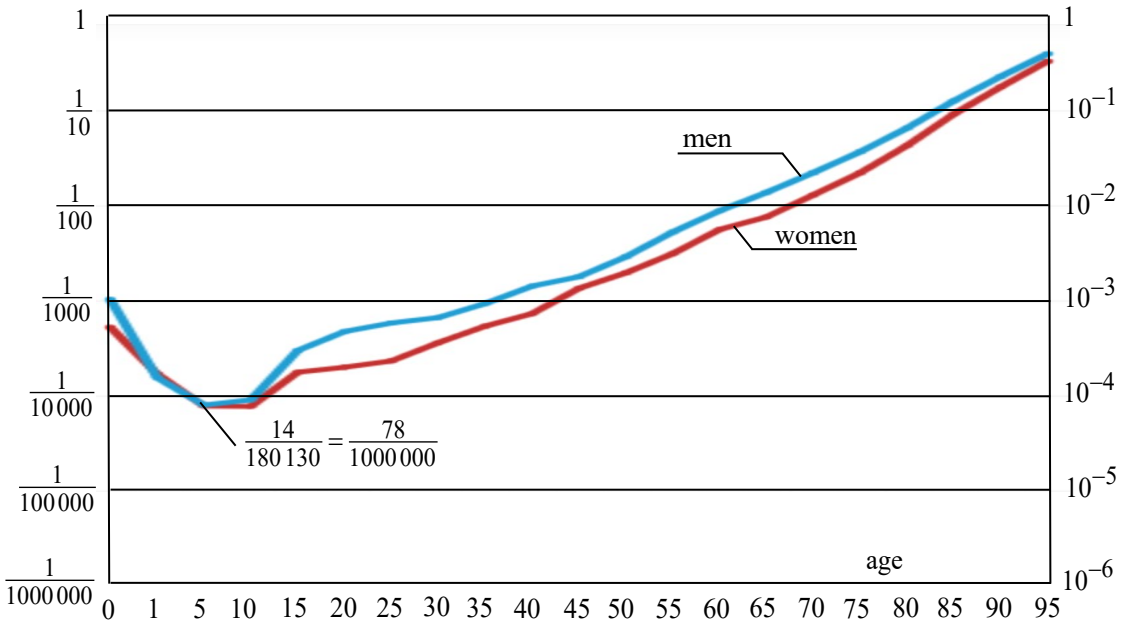

Figure 232. Probability of dying of a Flemish (Belgian) citizen in 2017 [127]. The data behind the curves shows that in 2017 the number of 70 year old men in Flanders was 142 852 of which 3187 died. Another example is that in 2017 the number of 5 year old girls in Flanders was 180 130 of which 14 died; 11 due to sickness.

A father and his 5 year old daughter go to an amusement park in Paris. This father would not enter the park, if it would increase her probability of dying. Fortunately, the park structures are designed for a collapse probability of 1/1000 000 a year. This is negligible because 1/1000 000 + 77/1000 000 = 78/1000 000 (see fig. 232). We engineers say: “Keep her safe and do not worry about structural collapse.”

Calculating with probabilities
Consider two events A and B. Event A occurs with a probability 0.1. Event B occurs with a probability 0.2. A and B are independent. This means that occurring of A has no influence on the probability that B occurs and the other way around.
The probability that A or B occurs is 0.1 + 0.2 = 0.3.
The probability that A and B occur is 0.1 × 0.2 = 0.02.

Henk
On a typical day, Henk is at home (13 hours), at school (6 hours), in the shopping mall (2 hours) or outdoors (3 hours). His home has a modern load bearing structure with a failure probability of 10/1000 000 per year. The dominant load in Henk’s city is storm. Henk and his housemates would recognise serious storm damage and go to the neighbours’ house right away. Henk’s school has a beautiful large shell roof with a failure probability of 200/1000 000 in its design life of 50 years or 4/1000 000 per year. If this roof would buckle, very few of the present students or teachers would survive. Henk’s mall has a steel frame structure with

an annual failure probability 10/1000 000. If a column would fail, the other columns still carry the floors and roof. Perhaps 3 of the about 200 shoppers would die by falling parts.

The probability of Henk dying in a structural collapse this year is

Henk is in the mall *and* the mall collapses *and* Henk dies.

$$P_f = 13/24 \times 10/1000\,000 \times 0 + 6/24 \times 4/1000\,000 \times 1 + 2/24 \times 10/1000\,000 \times 3/200$$
$$= 0 + 1/1000\,000 + 0.013/1000\,000$$
$$= 1.013/1000\,000$$

which is acceptable (see personal safety p. 176). This example shows that large shell roofs really need to have small failure probabilities for the ultimate limit state.

Exercise: Change Henk's calculation into your situation. Include a beautiful shell structure that you want to build. Is the conclusion the same?

Exercise: In the Netherland are about 10 000 000 buildings, 10 000 bridges and 17 000 000 people. Clearly, any significant collapse is reported in the news and you have read about it. How many of these buildings and bridges collapsed last year? How many people died in those accidents? Is the probability of dying in a structural collapse less than 1/1000 000?

Economic safety

Let us look at a structure as a business investment only. We can do so shamelessly because personal safety is covered above (see personal safety p. 176). The expected cost C_e of a building is

$$C_e = C_l + C_s + C_n + P_f C_f$$

where

C_l ..... Cost of the land

C_s ..... Cost of the load bearing structure, often just 10% of the building costs

C_n ..... Cost of all non-structural parts of the building, like windows, interior walls, bathrooms

P_f ..... Probability of structural failure in the design life

C_f ..... Failure cost, for example, value of the building (depreciated), destroyed machines, lost production, loss of experienced employees, liability payments

To bring P_f down, we need to increase C_s (fig. 234). Consequently, there is an optimal P_f for which C_e is smallest.

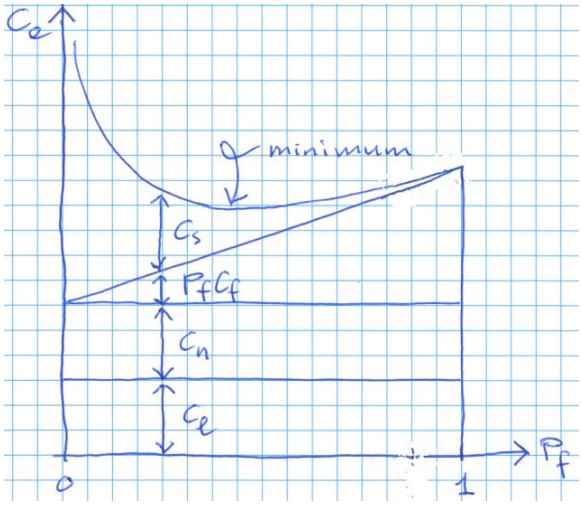

Figure 234. Expected cost of a building

This calculation has been performed for many buildings in developed countries. Table 13 shows the results for 12 situations.

1) A new building. It is being designed and will be build.
2) An existing building. The structure is deteriorated and the load is increased. The structure needs to be checked. Actual dimensions and material properties can be measured which reduces uncertainty. Repair and strengthening is expensive.

1) Wind is the dominant load. Stability walls that resist storms are large and expensive.
2) Wind load is not dominant.

1) Consequence class 1 (CC1) House, agricultural building, green house, storage building.
2) Consequence class 2 (CC2) Office, 5 storey house, hotel, apartment, shop, school, hospital, industry building.
3) Consequence class 3 (CC3) High rise, building with 16 or more storeys, hospital with 4 or more storeys, grandstand, exhibition hall, concert hall, large public buildings [129].

Table 13. Optimal failure probabilities (ULS) in the design life of structures based on costs only [130]

consequence class	new building		existing building	
eurocode EN 1990	no wind	wind	no wind	wind
CC1	$\frac{480}{1\,000\,000}$	$\frac{11000}{1\,000\,000}$	$\frac{2600}{1\,000\,000}$	$\frac{36000}{1\,000\,000}$
CC2	$\frac{72}{1\,000\,000}$	$\frac{2600}{1\,000\,000}$	$\frac{480}{1\,000\,000}$	$\frac{11000}{1\,000\,000}$
CC3	$\frac{8}{1\,000\,000}$	$\frac{480}{1\,000\,000}$	$\frac{72}{1\,000\,000}$	$\frac{480}{1\,000\,000}$

Note that economic safety is a target, while personal safety (p. 176) is a requirement that must be fulfilled regardless of the target.

Exercise: If you were to die now, society would loose the tax that you will pay in your life. Calculate how much this is. This really large number is used to represent you or any other person in the optimisation of structural failure probability.

Exercise: Economic safety (design life) can be governing over personal safety (annual). For which situations in table 13 is this so for a frame structure? And which for a shell roof?

Challenge: 1) Design a thin steel dome roof for a building in Amsterdam. 2) Calculate its construction costs. 3) Calculate its failure probability. 4) Change the thickness and continue at step 2. 5) Plot expected cost as a function of failure probability. 6) Read the optimal failure probability.

Table 14: Statistics for the city of Amsterdam [133]

		distribution	μ	σ/μ
Concrete compressive strength, C35		normal	… N/mm^2	…
Steel tensile strength, …		normal	… N/mm^2	…
Office floor load,	1 day largest	gamma	0.50 kN/m^2	0.4 + A/(10 m^2)
	1 year largest	Gumbel		
	50 year largest	Gumbel	1.50 kN/m^2	0.4
Wind load	1 hour largest	Weibull	0.10 kN/m^2	1.0
	1 year largest	Gumbel	…	
	50 year largest	Gumbel	1.00 kN/m^2	0.25

Safety index β

Often, we use the safety index β to express failure probability. This is a number between 2 and 5. It can be computed by

$$\beta = \sqrt{W(\frac{1}{2\pi P_f^2})}$$

Where $W()$ is the Lambert function and P_f is the failure probability. Examples are

P_f	$\frac{10\,000}{1000\,000}$	$\frac{1000}{1000\,000}$	$\frac{100}{1000\,000}$	$\frac{10}{1000\,000}$	$\frac{1}{1000\,000}$	$\frac{0.1}{1000\,000}$	$\frac{0.01}{1000\,000}$
β	2.34	3.09	3.73	4.26	4.76	5.20	5.62

Strength of chains

A long chain is less strong than a short chain. This has been thoroughly analysed by Waloddi Weibull (pronounce Vy-bull) in 1939 [7] [131]. A chain link has a strength with a mean μ_1 and a standard deviation σ_1. A chain breaks when one of the links breaks. Thus, it does not break when link one does not break and link two does not break and link three does not break and so on. The breaking probability can be calculated from

$$1 - P_{fc} = (1 - P_{fl})(1 - P_{fl})(1 - P_{fl})... = (1 - P_{fl})^n \ .$$

where P_{fc} is the chain breaking probability, P_{fl} is the link breaking probability and n is the number of links. Weibull understood that the left tail is important. He made a simple distribution that can have any left tail (Fig. 235). The probability that the strength is smaller than x is

[7] Waloddi Weibull (1887-1979) was a professor in Royal Institute of Technology, Stockholm, Sweden. He did research on shock waves, fatigue and reliability [Wikipedia][132].

$$P_{fl} = 1 - e^{-(\frac{x}{\lambda})^k}$$

where λ and k are constants. It can be shown that the chain design strength x_c can be calculated from the link design strength x_l with the following formula. The formula is correct for any breaking probability.

$$\boxed{x_c = x_l \, n^{-\frac{1}{k}}}$$

The constant k can be solved from the equation

$$\Gamma^2(1+\frac{1}{k})(1+\frac{\sigma^2}{\mu^2}) - \Gamma(1+\frac{2}{k}) = 0 \qquad \frac{1}{k} \approx 0.83\frac{\sigma}{\mu}$$

The coefficient of variation σ/μ of the chain is the same as that of the link. Some values are; steel 0.08; timber 0.18; concrete 0.15 [133].

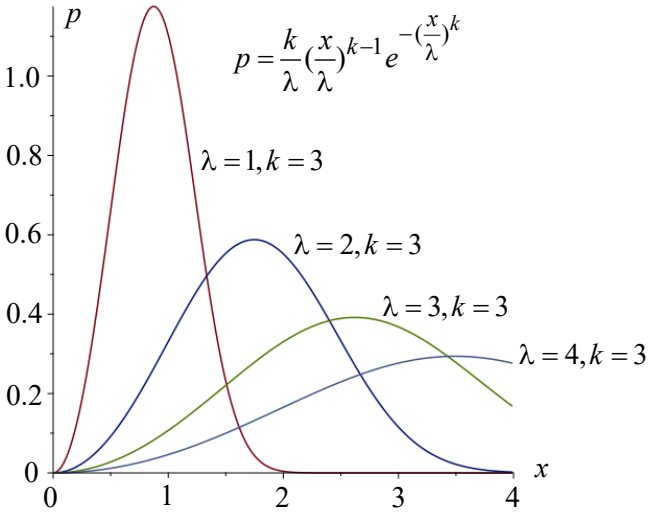

Figure 235. Weibull probability density function

For example, a chain is made of 700 steel links. The design strength of a 10 link chain is 130 kN. The constant k is 15.3. The design strength of the 700 link chain is

$$130 \times 70^{-\frac{1}{15.3}} = 98 \text{ kN}$$

Exercise: Derive the chain strength formula.

Statistical size effect

We can think of a large shell as an assembly of parts. In most shells breaking of one part does not lead to collapse of the shell. So it does not behave like a chain (strength of chains p. 179). However, sometimes it does, for example mutually supporting barrel vaults (Fig. 235). Many engineers include this in the calculations by reducing the design strength of the materials by the factor

$$n^{-\frac{1}{k}}.$$

This is called *statistical size effect* of material strength [134]. In other words, a large structure fails at a smaller stress than a small structure.



Figure 235. Bridge over the river Maas at the city of Nijmegen in the Netherlands built in 2013

Professional size effect
Consider an engineer at the beginning of her career. She starts designing reinforced concrete components. If one of her components break, somebody is likely to get hurt and she will feel terrible. Moreover, she is self-employed and could be liable for the medical costs. It would be like she got hurt herself too. In her career she will design approximately 10 000 components. When she retires, it will be like she is living under 10 000 components at the same time. She makes the decision that she wants to be as safe as other people. She reduces the design strength of reinforcing steel by a factor (strength of chains p. 179)

$$10\,000^{-\frac{1}{15.3}} = 0.55 \ ,$$

and the design strength of concrete by a factor

$$10\,000^{-\frac{1}{7.91}} = 0.31 \ .$$

Exercise: Study the following changes in the above calculation;
- often nobody gets hurt,
- she will design less than 10 000 components,
- some of the structures that she worked on will have been demolished when she retires,
- she is not liable because she performs all calculations according to the correct code of practice.

Literature

1 E.P. Popov, S.J. Medwadowski, *Concrete Shell Buckling*, American Concrete Institute, SP-67, Detroit, 1981
2 R. Hooke, *Lectiones Cutlerianæ*, or A collection of lectures: physical, mechanical, geographical, & astronomical, London, Printed for John Martyn, 1679
3 R. Elwes, *Maths 1001*, Quercus 2010, p.124
4 W. Kragting, Optimal Prestressing of Membrane Structures, M.Sc. report, Delft University of Technology, 2004
5 S.P. Timoshenko, S. Woinowsky-Krieger, *Theory of Plates and Shells*, second edition, McGraw-Hill, 1959. p. 443
6 K. Riemens, De optimale koepel, Bachelor project, Delft University of Technology, 2011 online: http://homepage.tudelft.nl/p3r3s/BSc_projects/eindrapport_riemens.pdf (In Dutch)
7 D.J. Struik, *Lectures on classical differential geometry*, second edition, Dover publications, New York, 1988
8 C.R. Calladine, *Theory of Shell Structures*, Cambridge University Press,1983
9 N.N. Alimina, S. Triatmodjo, The amalgamation style of Rumah Gadang in architecture and interior of Istano Basa Pagaruyung in Batusangkar, Indonesia: iconography-iconology analysis, *Cogent Arts & Humanitie*s, Vol. 12, No. 1, 2025
10 Anonymous, St. Paul's cathedral, Gift shop booklet, Scala Publishers Ltd, London, 2011
11 Anonymous, St. Paul's cathedral, Gift shop poster, London, 1999
12 P.C.J. Hoogenboom, R. Spaan, Shear Stiffness and Maximum Shear Stress of Round Tubular Members, 15th *International Offshore and Polar Engineering Conference* (ISOPE-2005), Seoul, June 19-24, 2005, Vol. 4, pp. 316-319
13 A.E.H. Love, The Small Free Vibrations and Deformation of a Thin Elastic Shell, *Philosophical Transactions of the Royal Society of London*, Vol. 179, 1888, pp. 491-546
14 A.E.H. Love, *A treatise on the mathematical theory of elasticity*, Cambridge University press, Volume 2, 1893
15 W. Flügge, *Statik und Dynamik der Schalen*, Springer-Verlag, Berlin, 1934 (in German).
16 R. Byrne, Theory of small deformations of a thin elastic shell, University of California, *Publications in Mathematics* (new series), 1944, Vol. 2, pp. 103-152.
17 V.V. Novozhilov, *The theory of thin shells*, translated by P.G. Lowe, edited by J.R.M. Radok, Noordhoff, Groningen, 1959.
18 E. Reissner, Stress strain relations in the theory of thin elastic shells, *Journal of Mathematical Physics*, 1952, Vol. 31, pp. 109-119.
19 P.M. Naghdi, On the theory of thin elastic shells, *Quarterly Applied Mathematics*, 1957, Vol. 14, pp. 369-380.
20 A.E.H. Love, *A treatise on the mathematical theory of elasticity*, second edition, Cambridge University press, New York, 1906
21 J.L. Sanders, An improved first approximation theory for thin shells, National Aeronautics and Space Administration (NASA) Report No. 24, Washington, DC, 1959.
22 W.T. Koiter, A consistent first approximation in the general theory of thin elastic shells, Report, Delft University of Technology, 1959.
23 W.T. Koiter, A consistent first approximation in the general theory of thin elastic shells, *Proceedings of IUTAM Symposium* On the Theory of Thin Elastic Shells, Delft 24-28 August 1959, North-Holland publishing company, Amsterdam 1960, pp 12-33.
24 D.H. van Campen, Levensbericht W.T. Koiter, Huygens Institute - Royal Netherlands Academy of Arts and Sciences (KNAW), *Levensberichten en herdenkingen*, 1999, Amsterdam, pp. 7-12
25 L.H. Donnell, A new theory for the buckling of thin cylinders under axial compression and bending, *Transactions of the American Society of Mechanical Engineers*, 1934, Vol. 56, pp. 759-806.
26 L.S.D. Morley, An improvement on Donnell's approximation for thin-walled circular cylinders, *Quarterly Journal of Mech. Applied Mathematics*, 1959, Vol. 12 (Part 1), pp. 89-99.

27 Anonymous, *Caltech Alumni News*, December 1948, online (20-08-2022) https://calteches.library.caltech.edu/642/2/Alumni.pdf, excerpt: “J.H. Wayland, M.S. '35, PhD. '36, has been appointed Associate Professor of Applied Mechanics at the Institute, to succeed Ralph E. Byrne, Jr., who died on September 17.“
28 Anonymous, *1940 U.S. Census*, online (20-08-2022) https://www.ancestry.com/1940-census/usa/California/Ralph-E-Byrne-Junior_2j5w9x, excerpt: “… Age 28, born abt 1912, Birthplace Missouri, Gender Male, Race White, Home in 1940 803 South Oakland Avenue Pasadena …,”
29 J. Blaauwendraad, *Plates and FEM, Surprises and Pitfalls*, Springer, 2010, p 77.
30 R. Zwennis, Spanningen in de rand van koud vervormde glasplaten, Bachelor project, Delft University of Technology, June 2013, (In Dutch), online: http://homepage.tudelft.nl/p3r3s/BSc_projects/eindrapport_zwennis.pdf
31 … Palazzetto dello sport, …
32 J. Blaauwendraad, J.H. Hoefakker, *Structural Shell Analysis, Understanding and Application*, Springer, 2014, 305 pp.
32b Y. Gorash, D. MacKenzie, On cyclic yield strength in definition of limits for characterisation of fatigue and creep behaviour, *Open Engineering*, Vol. 7 (2017) p. 126–140
33 H.W. Babel, R.H. Christensen, H.H. Dixon, Design, fracture control, fabrication, and testing of pressurized space-vehicle structures, Chapt 23 in *Thin-shell structures; Theory, experiment and design*, Y.C. Fung, E.E. Sechler (editors) Prentice-Hall, New Jersey, 1974.
34 Anonymous, *Isogrid design handbook*, McDonnel Douglas Astronautics Company, California, 1973
43 O.C. Zienkiewicz, R.L. Taylor, *The finite element method*, 4th edition, 1991, Vol. 2, Chapter 3.
44 B.M. Irons, The SemiLoof Shell Element, *Conference on Finite elements for thin shells and curved members* in Cardiff, 20–21 May 1974, Editors D.G. Ashwell, R.H. Gallagher, John Wiley & Sons, New York, N.Y. 1976, pp. 197–222
45 O.C. Zienkiewicz, R.L. Taylor, *The finite element method*, 4th edition, 1991, Vol. 2, Chapter 5.
46 H.W. Loof, The economical computation of stiffness of large structural elements, *International Symposium on Electronic Digital Computers in Structural Engineering*, University of Newcastle upon Tyne, 4-8 July 1966.
48 I. Cormeau, Bruce Irons: A non-conforming engineering scientist to be remembered and rediscovered, *International journal for numerical methods in engineering*, Vol. 22 (1986) pp. 1-10
49 E.M.J. Vicca, Werken met schaalelementen, Bachelor project in Structural Engineering, Delft University of Technology, 2016
50 J.U. de Jong, Eindige-elementenmethode voor schaalconstructies, De werkelijke nauwkeurigheid van schaalelementen in Ansys, Bachelor project in Structural Engineering, Delft University of Technology, 2015.
51 M. Farchich, Eindige-elementenmethode voor schaalconstructies, De nauwkeurigheid in SCIA-Engineer, Bachelor project, Delft University of Technology, June 2021, online http://homepage.tudelft.nl/p3r3s/BSc_projects/eindrapport_farchich.pdf
52 G.E. Moore, Cramming more components onto integrated circuits. *Electronics*, Vol. 38, Number 8, April 19, 1965
53 T. Belytschko, H. Stolarski, W.K. Liu, N. Carpenter, J.S.-J. Ong, Stress projection for membrane and shear locking in shell finite elements, *Computational Methods in Applied Mechanical Engineering*, Vol. 51 pp. 221-258, 1985
54 W.H. Press, B.P. Flannery, S.A. Teukolsky, W.T. Vetterling, *Numerical Recipes in Pascal, The Art of Scientific Computing*, Cambridge University Press, 1989.
55 …, Zeckendorf Plaza dimensions, …
58 M. Kuijvenhoven, P.C.J. Hoogenboom, Particle-spring method for form finding grid shell structures consisting of flexible members, *IASS Journal*, Vol. 53 (2012), No. 1, pp. 31–38
59 J.O. Løset, Viking ships and Norse wooden boats, website, vikingskip.com/index.htm, retrieved April 2025

60 J. Blaauwendraad , J.H. Hoefakker, *Structural shell analysis, Understanding and application*, Springer, Dordrecht, 2014
61 C.F. Gauß, *Disquisitiones generales circa superficies curvas*, Oct. 8, 1827, Commentationes societatis regiae scientarium Gottingensis recentiores, Göttingen 1873, Vol. 4, pp. 217 - 492 (in Latin)
62 T.E. Boothby, *Historic Preservation of Thin-Shell Concrete Structures*, online, 26 May 2012, http://www.engr.psu.edu/ae/thinshells/module%20III/case_study_3.htm
63 H. Bösiger, The building of Isler shells, *IASS Journal*, Vol. 53 (2011) No. 3, pp. 161-169
64 E. Ramm, Heinz Isler shells – the priority of form, *IASS Journal*, Vol. 53 (2011) No. 3, pp. 143-154
65 T. Kotnik, J. Schwartz, The architecture of Heinz Isler, *IASS Journal*, Vol. 53 (2011) No. 3, pp. 185-190
67 E. Reissner, Stresses and small displacements of shallow spherical shells II, *Journal of Mathematics and Physics*, Vol. 25 (1946), pp. 279-300
68 Ho Kwang-chien and Chen Fu, A simplified method for calculating double curvature shallow shells under the action of concentrated loads, *Acta Mechanica Sinica*, Vol. 6 (1963) No. 1, pp. 19-37 (in Chinese)
69 C.R. Caladine, Theory of shell structures, Cambridge University press, 1983
70 A. Semiari, *Doorbuiging van schalen door puntlasten*, Bachelor report, Delft University of Technology, 2012
73 N. Ramos, *Concentrated loads on anticlastic shells*, Bachelor report, Delft University of Technology, June 2012, online http://homepage.tudelft.nl/p3r3s/BSc_projects/eindrapport_ramos.pdf
74 Hoogenboom PCJ, Yu Chenjie, Taneja K, Moments due to concentrated loads on thin shell structures, *HERON*, Vol. 61 (2016), No. 3, pp. 153-165
75 D. Staaks, *Koud torderen van glaspanelen in blobs*, MSc report, Eindhoven University of Technology, the Netherlands, 2003
75b M. Bonthuis, Twisted plate behaviour, Assignment for course CIEM5301 Shell Structures, Delft University of Technology, Faculty of Civil Engineering, 2024, online: https://phoogenboom.nl/BSc_projects/eindrapport_bonthuis.pdf
76 P.C.J. Hoogenboom, P.A. de Vries, R. Houtman, Requirements for cutting patterns of smooth membrane structures, *IASS Journal*, Vol 50 (2009), No. 1. pp. 23-32
77 G. Darboux, *Leçons sur la théorie génerale des surfaces*, Vol. 4, Gauthier-Villars, 1896, p. 455.
78 H.W. Loof, Eenvoudige formules voor de buigingsstoringen in hypparschalen, die volgens beschrijvenden zijn begrensd, Technische Hogeschool Delft, Faculteit Civiele Techniek, 1961
79 T.M. Tran, Nauwkeurigheid ontwerpformules voor buigende momenten in hypar-daken, Beoordeling nauwkeurigheid formules van Loof, Bachelor project, Delft University of Technology, 2015, online: http://phoogenboom.nl/BSc_projects/eindrapport_tran.pdf
80 H.W. Loof, Schalen I, collegedictaat b17a, 4de druk, TH Delft, 1984
81a M. Westerhof, Extensieloze vervorming van schaalconstructies, Bachelor project, Delft University of Technology, 2024, in Dutch, online: https://phoogenboom.nl/BSc_projects/eindrapport_westerhof.pdf
81b M. Ketchum, Memoirs of Milo Ketchum, online, http://www.ketchum.org/-milo/index.html
82 P.K. Malhotra, T. Wenk, M. Wieland, Simple Procedure for Seismic Analysis of Liquid-Storage Tanks, *Structural Engineering International*, 2000, No. 3, pp. 197-210.
83 Y. Yoshimura, On the Mechanism of Buckling of a Circular Shell under Axial Compression, NACA Technical memorandum, No. 1390, Sec 7.7, 1955.
84 N.J. Hoff, The perplexing behaviour of thin circular cylindrical shells in axial compression, report SUUDAR No. 256, Stanford University 1966.
85 A. Robertson, The strength of tubular struts, *Proceedings of the Royal Society A, Mathematical, physical and engineering sciences*, Vol. 121, Issue 788, Dec. 1928
86 V.I. Weingarten, E.J. Morgan, P. Seide, Elastic Stability of Thin-Walled Cylindrical and Conical Shells under combined Internal Pressure and Axial Compression, *AIAA Journal*, Vol. 3, 1965, pp. 500-505.

87 Th. von Kármán, L.G. Dunn, H.S. Tsien, The influence of Curvature on the Buckling Characteristics of Structures, *J. Aero. Sci.*, 7(7) , 1940, pp. 276-89 (Sec. 7.7).
88 W.T. Koiter, *Over de Stabiliteit van het Elastisch Evenwicht*, Publisher H.J. Paris, Amsterdam, 1945 (In Dutch).
89 W.T. Koiter, NASA Technical Translation F10,833, 1967.
90 M. Farshad, *Design and Analysis of Shell Structures*, Kluwer Academic Publischers, Dordrecht, 1992.
91 J. Arbocz, Shell Buckling Research at Delft 1976-1996, Report TU Delft, 1996.
93 L.A. Samuelson, S. Eggwertz, *Shell Stability Handbook*, Elsevier Science Publishers LTD, Essex, 1992.
94 I. Elishakov. *Resolution of the twentieth century conundrum in elastic stability*. Florida Atlantic University, USA, 2014.
95 B. Elferink, P. Eigenraam, P.C.J. Hoogenboom, J.G. Rots, Shape imperfections of reinforced concrete shell roofs, *HERON*, Vol. 61 (2016) No. 3, pp. 177-192.
96 CNIT, …
97 CNIT, …
98 CNIT, …
99 CNIT, …
100 CNIT, …
101 Michel Pré, The CNIT–La Défense Railway Station in Paris: Answers to Complex Constraints, *Structural Engineering International*, Vol. 28, 2018, Issue 2, Pages 157-160 , Published online: https://www.tandfonline.com/doi/full/10.1080/10168664.2018.1450698
102 H. Beer, G. Schulz, Bases théoriques des courbes européenes de flambement, *Construction Métallique*, No. 3 (Sept 1970), pp. 37-57
103 Xia Wenjing, P.C.J. Hoogenboom, Buckling analysis of offshore jackets in removal operations, *Proceedings of OMAE conference*, June 19-24 2011, Rotterdam
105 D.N. Ford, Ferrybridge cooling towers collapse, in *When technology fails, Significant technological disasters, accidents, and failures of the twentieth century*, edited by N. Schlager, 1994, pp. 267-270.
106 H.C. Shellard, Collapse of cooling towers in a gale, Ferrybridge, 1 November 1965, *Weather*, Vol. 22, No. 6, June 1967, pp 232-240
108 S. Naomis, P.C.M. Lau, *Computational Tensor Analysis of Shell Structures*, Eds. Brebbia and Orszag, Vol 58, Springer-Verlag, Berlin, 1990.
109 A.W. Leissa, *Vibration of Shells*, NASA, Washington D.C. 1973
110 D. Boggs, J. Dragovich, The nature of wind loads and dynamic response, *Proceedings of ACI Symposium Performance-based design of concrete building for wind loads*, SP-240, 2006, pp. 15-44
111 Lord Rayleigh, On the Infinitesimal Bending of Surfaces of Revolution, *Proceedings of the London Mathematical Society*, Vol. 13 (1881), pp. 4-16
112 H. Lamb, On the vibrations of a spherical shell, *Proceedings of the London Mathematical Society*, Vol. s1-14, Issue 1, November 1882, pp. 50-56
113 W.E. Bakker, Axisymmetric modes of vibration of thin spherical shell, *The journal of the Acoustical society of America*, Vol. 33 (1961), No. 12, pp. 1749-1758.
114 C.R. Calladine, *Theory of shell structures*, Cambridge University Press, 1983
115 R.D. Blevins, *Formulas for natural frequency and mode shape*, Van Nostrand Reinhold company, 1979, ISBN 0-442-20710-7.
116 J.L. Sewall, Vibration Analysis of Cylindrically Curved Panels with Simply Supported or Clamped Edges and Comparison with Some Experiments, NASA Report NASA-TN-D-3791, Langley Research Center, 1967.
117 E. Szechenyi, Approximate Formulas for the Determination of the Natural Frequencies of Stiffened and Curved Panels, *Journal of Sound and Vibration*, Vol. 14 (1971), No. 3, pp 401-418.
118 R. van Dijk, Eigenfrequentie van belaste panelen, Delft University of Technology, Bachelor project, 2014 (In Dutch).

119 Y. Paasman, Eigenfrequentie van gekromde panelen, Delft University of Technology, Bachelor project, 2016 (In Dutch).
120 J. Sluijs, Eigenfrequentie van gekromde panelen; Uitbreiding van de ontwerpformule voor zadelvormige panelen, Delft University of Technology, Bachelor project, 2017 (In Dutch).
121 Anonymous, Nyquist–Shannon sampling theorem, *Wikipedia*, www.wikipedia.org, 2012
122 A.J. Carr, Ruaumoko Computer Program Library, University of Canterbury, Department of Civil Engineering, New Zealand, 2000
123 C.J. Turkstra, Theory of structural design decisions, *SM Studies Series* No. 2. Ontario, Canada: Solid Mechanics Division, University of Waterloo, 1970
125 K.C. Terwel, S.J.T. Jansen, Critical factors for structural safety in the design and construction phase, *Journal of Performance of Constructed Facilities*, ASCE, Vol. 29 (2015) No. 3
126 R. de Vries, R.D.J.M. Steenbergen, J. Maljaars, Annual reliability requirements for bridges and viaducts, *HERON* Vol. 68 (2023) No. 2, p. 91-122
127 Agentschap Zorg en Gezondheid, Sterfterisico's volgens leeftijd [online publicatie], Brussel [geraadpleegd op 7 februari 2023], beschikbaar op: www.zorg-en-gezondheid.be/cijfers/
129 Anonymous, *Probabilistic Model Code*, online http://www.jcss.ethz.ch/JCSSPublications/PMC/PMC.html August 2007.
130 R.D.J.M. Steenbergen, A.C.W.M. Vrouwenvelder, Safety philosophy for existing structures and partial factors for traffic loads on bridges, *HERON* Vol. 55 (2010) No. 2.
131 W. Weibull, ”A Statistical Theory Of The Strength Of Materials”, Ingeniörsvetenskapsakademiens Handlingar Nr 151, 1939, Generalstabens Litografiska Anstalts Förlag, Stockholm
132 R.B. Abernethy, "Dr. E. H. Waloddi Weibull 1887-1979", internet, http://www.barringer1.com/weibull_bio.htm, retrieved 20 Feb. 2014
133 A.C.W.M. Vrouwenvelder, J.K. Vrijling, "Probabilistisch ontwerpen", reader, Delft University of Technology, 1987, (In Dutch)
134 Z.P. Bažant, "Size effect on structural strength", Wikipedia, http://en.wikipedia.org/wiki/Size_effect, retrieved 20 Feb. 2014
135 A.S. Thorndike, C.R. Cooley, J.F. Hye, The structure and evolution of flow fields and other vector fields, Journal of Physics A: Mathematical and General, Vol. 11, No. 8, pp. 1455-1490, 1978
136 W.J. van Straalen, Invarianten van tensoren, De onafhankelijkheid van assenstelsels rondom umbilics, Bacheloreindwerk, Delft University of Technology, 2013 (in Dutch) online: http://homepage.tudelft.nl/p3r3s/BSc_projects/eindrapport_van_stralen.pdf
137 P.C.J. Hoogenboom, Reinforced Solid, Wikipedia, 2008
138 J. van Hulst, Invarianten van gecombineerde tensoren, Uitknikken van schaalconstructies, bacheloreindproject, Technische Universiteit Delft, Faculteit Civiele Techniek en Geowetenschappen, juni 2018 (In Dutch with English summary), online: https://phoogenboom.nl/BSc_projects/eindrapport_van_hulst.pdf

Appendix. Optimal arch

An arch with a sagitta of about 40% of the span needs the least material. This appendix presents the proof.

For an evenly distributed load q [N/m] the arch has a parabolic shape (fig. 1).

$$y = s\left(1+2\frac{x}{l}\right)\left(1-2\frac{x}{l}\right), \tag{1}$$

where l is the span and s is the sagitta.

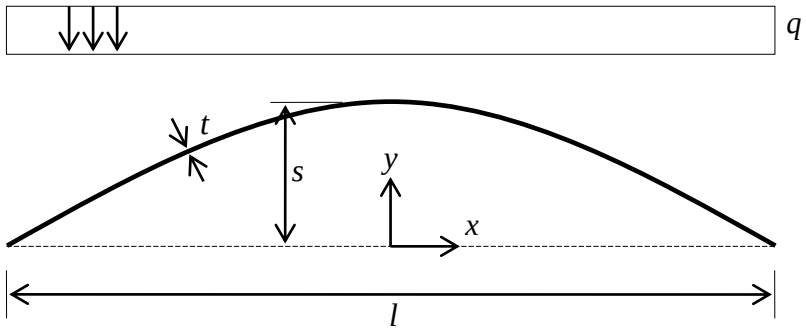

Figure 1. Parabolic arch

The volume of the arch is

$$Vol = \int_{x=-\frac{1}{2}l}^{\frac{1}{2}l} t\,w\,dz\,, \tag{2}$$

where $t = t(x)$ is the thickness, w is the width and dz is a small distance along the arch. The thickness t is related to the axial force $N = N(x)$.

$$t\,w\,f = N\,, \tag{3}$$

where f is the compressive strength of the material. The axial force N in the arch has a vertical component V and a horizontal component H (fig 2.).

$$\frac{N}{V} = \frac{dz}{dy} \tag{4}$$

This is valid for $x < 0$. The vertical components V need to be in equilibrium with the loading q (fig. 2).

$$V = -x\,q \tag{5}$$

This is valid for $x < 0$.

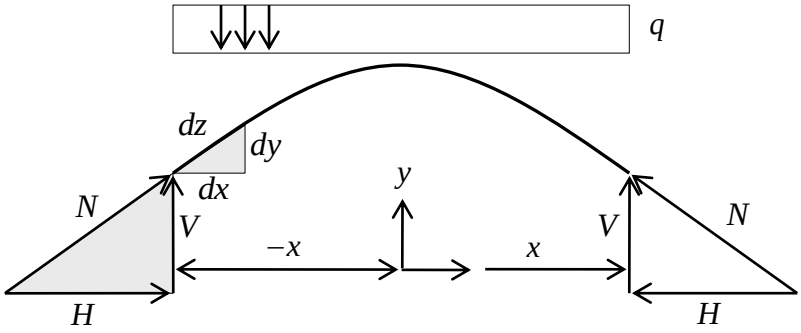

Figure 2. Section forces

Substitution of equations 3 to 5 in equation 2 gives

$$Vol = 2 \int_{x=-\frac{1}{2}l}^{0} \frac{-xq}{f} \frac{dz^2}{dxdy} dx \tag{6}$$

Using the Pythagorean theorem $dz^2 = dx^2 + dy^2$ we obtain

$$\frac{dz^2}{dxdy} = \frac{1}{\frac{dy}{dx}} + \frac{dy}{dx}. \tag{7}$$

Substitution of equations 1 and 7 in equation 6 and evaluation of the integral gives

$$Vol = ql \frac{16s^2 + 3l^2}{24 f s}. \tag{8}$$

For the minimum volume it holds

$$\frac{dVol}{ds} = 0, \tag{9}$$

from which s can be solved.

$$s = \frac{\sqrt{3}}{4} l \approx 0.4l \tag{10}$$

Q.E.D.

Appendix. Optimal dome

A dome with a sagitta of about 30% of the span needs the least material. This appendix presents the proof.

The shape is assumed to be a spherical cap (fig. 3).

$$y = -\sqrt{a^2 - x^2}\ .$$

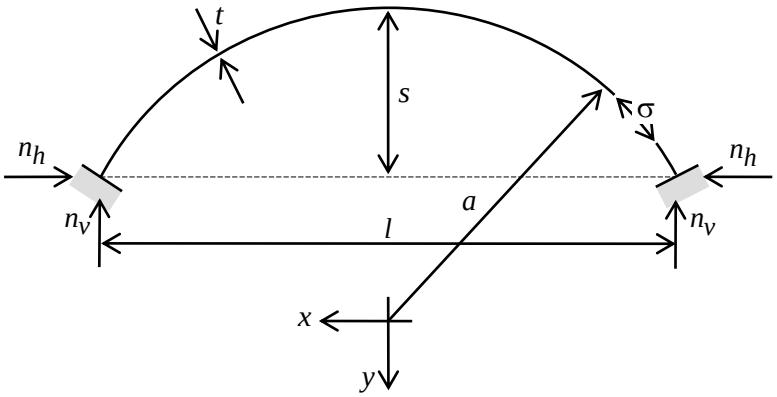

Figure 3. Dome dimensions and coordinate system

The radius of curvature is

$$a = \frac{s}{2} + \frac{l^2}{8s}\ .$$

The dome surface area is

$$A = \int_{\varphi=0}^{2\pi} \int_{x=0}^{\frac{1}{2}l} \sqrt{dx^2 + dy^2}\, x\, d\varphi = 2\pi \int_{x=0}^{\frac{1}{2}l} \sqrt{1 + (\frac{dy}{dx})^2}\, x\, dx = \pi a \left(2a - \sqrt{4a^2 - l^2} \right). \qquad (1)$$

We assume the thickness t to be constant. The vertical support reaction is

$$n_v = \frac{A \rho g t}{\pi l},$$

Where ρ is the specific mass, g is the gravitational acceleration. The horizontal support reaction is

$$n_h = n_v \left. \frac{dx}{dy} \right|_{x=\frac{1}{2}l} = a \rho g t \left(\frac{2a}{\sqrt{4a^2 - l^2}} - 1 \right).$$

The meridional stress in the dome foot is

$$\sigma = \frac{1}{t} \sqrt{n_v^2 + n_h^2} = 2 \frac{a^2 \rho g}{l^2} (2a - \sqrt{4a^2 - l^2})\ . \qquad (2)$$

The hoop stress in the dome foot is smaller than the meridional stress. The stress in the dome top is

$$\lim_{l \downarrow 0} \sigma = \tfrac{1}{2} a \rho g$$

We assume that the dome is fixed at the support. The thickness for which the dome almost buckles is [1] (see buckling p. 140)

$$\sigma_{cr} = \frac{1}{C\sqrt{3(1-\nu^2)}} \frac{E t}{a} \quad \Rightarrow \quad t = C\sqrt{3(1-\nu^2)}\, \frac{\sigma a}{E}, \tag{3}$$

where $1/C$ is the knockdown factor for including imperfections. The material volume V of the dome is found by substituting (1), (2) and (3) in

$$V = A\, t,$$

which can be evaluated to

$$V = \left(2a - \sqrt{4a^2 - l^2} \right)^2 \frac{a^4}{l^2} \frac{2\pi\rho g}{E} C\sqrt{3(1-\nu^2)}.$$

This can be rewritten in dimensionless quantities

$$\frac{VE}{2\pi\rho g l^4 C\sqrt{3(1-\nu^2)}} = \left(2\frac{a}{l} - \sqrt{4\frac{a^2}{l^2} - 1} \right)^2 \frac{a^4}{l^4}, \text{ where } \frac{a}{l} = \tfrac{1}{2}\frac{s}{l} + \tfrac{1}{8}\frac{l}{s}.$$

Figure 4 shows the dimensionless material volume as a function of $\frac{s}{l}$.

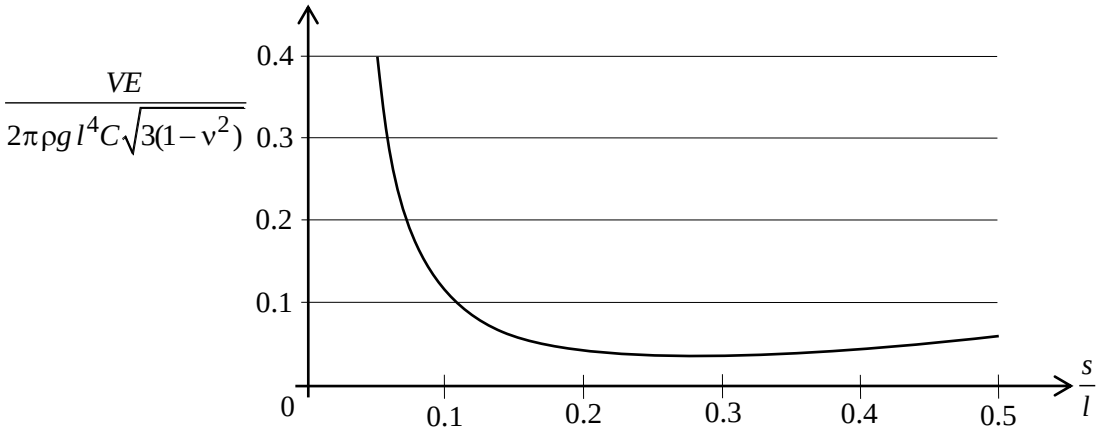

Figure 4. Material volume V as a function of sagitta s

The roots of $\frac{dV}{ds}$ are $s = -\frac{\sqrt{3}}{2}l,\ -\frac{\sqrt{3}}{6}l,\ \frac{\sqrt{3}}{6}l,\ \frac{\sqrt{3}}{2}l.$

[1] Thin domes almost always buckle before yielding or crushing. It can be shown that for yielding or crushing to occur due to self-weight the span l needs to exceed 1 km.

Therefore, the minimum material volume occurs at $\frac{s}{l}=\frac{\sqrt{3}}{6}\approx 0.3$. Q.E.D.

The optimal $\frac{s}{l}$ value does not depend on the material *E*, ν, ρ, it does not depend on the span *l*, it does not depend on the imperfections *C* and it does not depend on the gravity *g* (earth or moon).

The thickness at minimum volume is $t=\frac{2}{9}C\sqrt{3(1-\nu^2)}\,\frac{\rho g l^2}{E}$.

Since $C\sqrt{3(1-\nu^2)}\approx 6\sqrt{3(1-0.27^2)}=10$,

the thickness is approximately $t=\frac{20}{9}\frac{\rho g l^2}{E}$.

The thickness can be written as $\frac{Et}{2\rho g l^2}C\sqrt{3(1-\nu^2)}=\frac{a^3}{l^3}\left(2\frac{a}{l}-\sqrt{4\frac{a^2}{l^2}-1}\right)$.

Figure 5 shows the dimensionless thickness as function of $\frac{s}{l}$. For $\frac{s}{l}$ values larger than 0.3 the thickness does not change much.

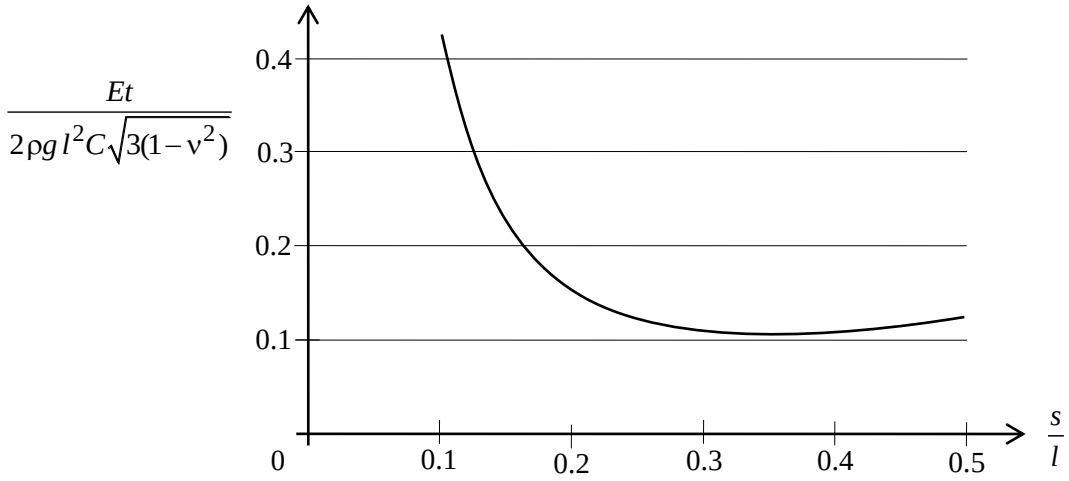

Figure 5. Thickness t as a function of the sagitta s

In this derivation it is assumed that the thickness is everywhere the same. However, the stress in the top is 25% smaller than in the foot of the dome. Therefore, the top can be 25% thinner. A varying thickness would give a somewhat different optimum sagitta.

The horizontal support reaction of the optimal dome is evaluated to $n_h=\frac{1}{3}l\rho g t$.

Appendix. Curvature tensor

This appendix proves that curvature is a tensor. Consider a point on a shell middle surface. In this point are a local coordinate system *x*, *y*, *z* and a rotated local coordinate system *r*, *s*, *z*. A point (*x*, *y*) can be expressed in (*r*, *s*) by

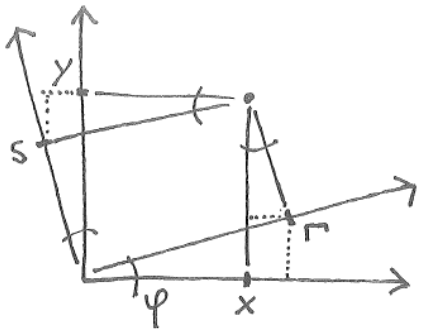

$$x = r\cos\varphi - s\sin\varphi$$
$$y = r\sin\varphi + s\cos\varphi$$

The shell middle surface can be described by (see page 21)

$$z = \tfrac{1}{2}k_{xx}x^2 + k_{xy}xy + \tfrac{1}{2}k_{yy}y^2$$

Only second order terms are included because higher order terms are much smaller close to the origin of the local coordinate system. Substitution of the former into the latter gives

$$z = \tfrac{1}{2}k_{xx}(r\cos\varphi - s\sin\varphi)^2 + k_{xy}(r\cos\varphi - s\sin\varphi)(r\sin\varphi + s\cos\varphi) + \tfrac{1}{2}k_{yy}(r\sin\varphi + s\cos\varphi)^2$$

The definition of curvature is (see page 20)

$$k_{rr} = \frac{\partial^2 z}{\partial r^2}, \quad k_{ss} = \frac{\partial^2 z}{\partial s^2}, \quad k_{rs} = \frac{\partial^2 z}{\partial r \partial s}$$

Substitution of the former into the latter gives

$$k_{rr} = k_{xx}\cos^2\varphi + k_{yy}\sin^2\varphi + k_{xy}2\sin\varphi\cos\varphi$$
$$k_{ss} = k_{xx}\sin^2\varphi + k_{yy}\cos^2\varphi - k_{xy}2\sin\varphi\cos\varphi$$
$$k_{rs} = (k_{yy} - k_{xx})\sin\varphi\cos\varphi + k_{xy}(\cos^2\varphi - \sin^2\varphi)$$

A quantity that can be transformed to another coordinate system by these equations is by definition a tensor (dimensions 2, rank 2). Q.E.D.

The transformation equations can be rewritten as

$$k_{rr} = \tfrac{1}{2}(k_{xx} + k_{yy}) + \tfrac{1}{2}(k_{xx} - k_{yy})\cos 2\varphi + k_{xy}\sin 2\varphi$$
$$k_{ss} = \tfrac{1}{2}(k_{xx} + k_{yy}) - \tfrac{1}{2}(k_{xx} - k_{yy})\cos 2\varphi - k_{xy}\sin 2\varphi$$
$$k_{rs} = \qquad\qquad -\tfrac{1}{2}(k_{xx} - k_{yy})\sin 2\varphi + k_{xy}\cos 2\varphi$$

and as

$$\begin{bmatrix} k_{rr} & k_{rs} \\ k_{rs} & k_{ss} \end{bmatrix} = \begin{bmatrix} \cos\varphi & \sin\varphi \\ -\sin\varphi & \cos\varphi \end{bmatrix} \begin{bmatrix} k_{xx} & k_{xy} \\ k_{xy} & k_{yy} \end{bmatrix} \begin{bmatrix} \cos\varphi & -\sin\varphi \\ \sin\varphi & \cos\varphi \end{bmatrix}$$

and as

$$k_{ij} = \sum_{m=x,y} \sum_{n=x,y} k_{mn}\, t_{mi}\, t_{nj} \qquad i = r,s \quad j = r,s$$

The equations can be plotted by Mohr's circle.

Appendix. Membrane force tensor

This appendix shows that shell membrane forces can be transformed to another coordinate system in almost the same way as regular tensors. Consider a local coordinate system *x*, *y*, *z* and a rotated local coordinate system *r*, *s*, *z*. Consider two small triangular shell parts.

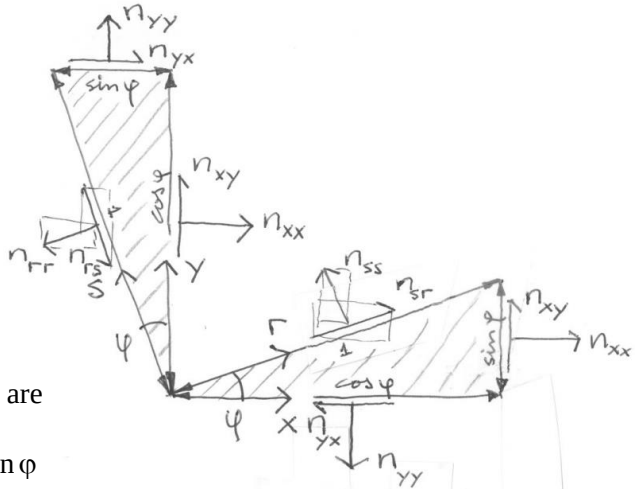

The equilibrium equations of these parts are

$$n_{rr}1\cos\varphi - n_{rs}1\sin\varphi = n_{xx}\cos\varphi + n_{yx}\sin\varphi$$
$$n_{rs}1\cos\varphi + n_{rr}1\sin\varphi = n_{yy}\sin\varphi + n_{xy}\cos\varphi$$
$$n_{sr}1\sin\varphi + n_{ss}1\cos\varphi = n_{yy}\cos\varphi - n_{xy}\sin\varphi$$
$$n_{ss}1\sin\varphi - n_{sr}1\cos\varphi = n_{xx}\sin\varphi - n_{yx}\cos\varphi$$

This can be written as

$$n_{rr} = n_{xx}\cos^2\varphi + n_{yy}\sin^2\varphi + (n_{xy}+n_{yx})\sin\varphi\cos\varphi$$
$$n_{ss} = n_{xx}\sin^2\varphi + n_{yy}\cos^2\varphi - (n_{xy}+n_{yx})\sin\varphi\cos\varphi$$
$$n_{rs} = (n_{yy}-n_{xx})\sin\varphi\cos\varphi + n_{xy}\cos^2\varphi - n_{yx}\sin^2\varphi$$
$$n_{sr} = (n_{yy}-n_{xx})\sin\varphi\cos\varphi + n_{yx}\cos^2\varphi - n_{xy}\sin^2\varphi$$

and as

$$n_{rr} = \tfrac{1}{2}(n_{xx}+n_{yy}) + \tfrac{1}{2}(n_{xx}-n_{yy})\cos 2\varphi + \tfrac{1}{2}(n_{xy}+n_{yx})\sin 2\varphi$$
$$n_{ss} = \tfrac{1}{2}(n_{xx}+n_{yy}) - \tfrac{1}{2}(n_{xx}-n_{yy})\cos 2\varphi - \tfrac{1}{2}(n_{xy}+n_{yx})\sin 2\varphi$$
$$n_{rs} = \tfrac{1}{2}(n_{xy}-n_{yx}) - \tfrac{1}{2}(n_{xx}-n_{yy})\sin 2\varphi + \tfrac{1}{2}(n_{xy}+n_{yx})\cos 2\varphi$$
$$n_{sr} = -\tfrac{1}{2}(n_{xy}-n_{yx}) - \tfrac{1}{2}(n_{xx}-n_{yy})\sin 2\varphi + \tfrac{1}{2}(n_{xy}+n_{yx})\cos 2\varphi$$

and as

$$\begin{bmatrix} n_{rr} & n_{rs} \\ n_{sr} & n_{ss} \end{bmatrix} = \begin{bmatrix} \cos\varphi & \sin\varphi \\ -\sin\varphi & \cos\varphi \end{bmatrix} \begin{bmatrix} n_{xx} & n_{xy} \\ n_{yx} & n_{yy} \end{bmatrix} \begin{bmatrix} \cos\varphi & -\sin\varphi \\ \sin\varphi & \cos\varphi \end{bmatrix}$$

and as

$$n_{ij} = \sum_{m=x,y} \sum_{n=x,y} n_{mn}\, t_{mi}\, t_{nj} \qquad i = r,s \quad j = r,s$$

Appendix. Asymmetric tensors

This appendix gives the properties of the membrane force tensor.

Invariants

$n_{xx} + n_{yy}$ (trace)
$n_{xx}n_{yy} - n_{xy}n_{yx}$ (determinant)
$n_{xy} - n_{yx}$

Principal values (no shear stress, eigenvalues)

$$n_1 = \frac{n_{xx} + n_{yy}}{2} + \sqrt{(\frac{n_{xx} - n_{yy}}{2})^2 + n_{xy}n_{yx}} \qquad \varphi = \arctan\frac{n_1 - n_{xx}}{n_{yx}} \qquad \varphi = \arctan\frac{n_2 - n_{xx}}{n_{yx}}$$

$$n_2 = \frac{n_{xx} + n_{yy}}{2} - \sqrt{(\frac{n_{xx} - n_{yy}}{2})^2 + n_{xy}n_{yx}} \qquad \varphi = \arctan\frac{n_{yy} - n_1}{n_{xy}} \qquad \varphi = \arctan\frac{n_{yy} - n_2}{n_{xy}}$$

Largest and smallest normal force

$$\frac{n_{xx} + n_{yy}}{2} + \sqrt{(\frac{n_{xx} - n_{yy}}{2})^2 + (\frac{n_{xy} + n_{yx}}{2})^2} \qquad \varphi = \tfrac{1}{2}\arctan\frac{n_{xy} + n_{yx}}{n_{xx} - n_{yy}} + \tfrac{1}{2}\pi$$

$$\frac{n_{xx} + n_{yy}}{2} - \sqrt{(\frac{n_{xx} - n_{yy}}{2})^2 + (\frac{n_{xy} + n_{yx}}{2})^2} \qquad \varphi = \tfrac{1}{2}\arctan\frac{n_{xy} + n_{yx}}{n_{xx} - n_{yy}}$$

Largest and smallest shear force

$$-\frac{n_{xy} - n_{yx}}{2} + \sqrt{(\frac{n_{xx} - n_{yy}}{2})^2 + (\frac{n_{xy} + n_{yx}}{2})^2} \qquad \varphi = -\tfrac{1}{2}\arctan\frac{n_{xx} - n_{yy}}{n_{xy} + n_{yx}}$$

$$\frac{n_{xy} - n_{yx}}{2} + \sqrt{(\frac{n_{xx} - n_{yy}}{2})^2 + (\frac{n_{xy} + n_{yx}}{2})^2}$$

Mohr's circle

…..

Appendix. Compatibility equation

In this appendix the shell compatibility equation (p. 57) is checked.

```
> ux:=  c1 +   c2*u +   c3*v +   c4*u^2 +   c5*u*v +   c6*v^2 +   c7*u^3 +   c8*u^2*v +   c9*u*v^2 +
c10*v^3:
> uy:=c11 + c12*u + c13*v + c14*u^2 + c15*u*v + c16*v^2 + c17*u^3 + c18*u^2*v + c19*u*v^2 +
c20*v^3:
> uz:=c21 + c22*u + c23*v + c24*u^2 + c25*u*v + c26*v^2 + c27*u^3 + c28*u^2*v + c29*u*v^2 +
c30*v^3:
> epsilonxx:=diff(ux,u)/alphax-kxx*uz+kx*uy:
> epsilonyy:=diff(uy,v)/alphay-kyy*uz+ky*ux:
> gammaxy:=diff(ux,v)/alphay+diff(uy,u)/alphax-2*kxy*uz-kx*ux-ky*uy:
> phix:=-diff(uz,u)/alphax-kxx*ux-kxy*uy:
> phiy:=-diff(uz,v)/alphay-kyy*uy-kxy*ux:
> phiz:=1/2*(-diff(ux,v)/alphay+diff(uy,u)/alphax-kx*ux+ky*uy):
> kappaxx:=diff(phix,u)/alphax-kxy*phiz+kx*phiy:
> kappayy:=diff(phiy,v)/alphay+kxy*phiz+ky*phix:
> rhoxy:=diff(phix,v)/alphay+diff(phiy,u)/alphax+(kxx-kyy)*phiz-kx*phix-ky*phiy:
> l:=-diff(epsilonxx,v,v)/alphay^2 + diff(gammaxy,u,v)/alphax/alphay - diff(epsilonyy,u,u)/alphax^2:
> r:=-kyy*kappaxx + kxy*rhoxy - kxx*kappayy:
> u:=0: v:=0: kx:=0: ky:=0: kxx:=kxy^2/kyy:
> simplify(l-r);
                        0
```

Q.E.D.

Appendix. Cylinder equation

In this appendix the shell cylinder equation (p. 74) is derived.

```
> ux:=-nu/a*int(w(u),u): uy:=0: uz:=w(u):
> pz:=0:
> kxx:=0: kyy:=-1/a: kxy:=0: alphax:=1: alphay:=1:
> ky:=diff(alphay,u)/alphay/alphax: kx:=diff(alphax,v)/alphax/alphay:
> epsilonxx:=diff(ux,u)/alphax-kxx*uz+kx*uy:
> epsilonyy:=diff(uy,v)/alphay-kyy*uz+ky*ux:
> gammaxy:=diff(ux,v)/alphay+diff(uy,xs)/alphax-2*kxy*uz-kx*ux-ky*uy:
> phix:=-diff(uz,u)/alphax-kxx*ux-kxy*uy:
> phiy:=-diff(uz,v)/alphay-kyy*uy-kxy*ux:
> phiz:=1/2*(-diff(ux,v)/alphay+diff(uy,u)/alphax-kx*ux+ky*uy):
> kappaxx:=diff(phix,u)/alphax-kxy*phiz+kx*phiy:
> kappayy:=diff(phiy,v)/alphay+kxy*phiz+ky*phix:
> rhoxy:=diff(phix,v)/alphay+diff(phiy,u)/alphax+(kxx-kyy)*phiz-kx*phix-ky*phiy:
> nxx:=E*t/(1-nu^2)*(epsilonxx+nu*epsilonyy):
> nyy:=E*t/(1-nu^2)*(epsilonyy+nu*epsilonxx):
> nxym:=E*t/(2*(1+nu))*gammaxy:
> mxx:=E*t^3/(12*(1-nu^2))*(kappaxx+nu*kappayy):
> myy:=E*t^3/(12*(1-nu^2))*(kappayy+nu*kappaxx):
> mxy:=E*t^3/(24*(1+nu))*rhoxy:
> vx:=diff(mxx,u)/alphax+diff(mxy,v)/alphay+ky*(mxx-myy)+2*kx*mxy:
> vy:=diff(myy,v)/alphay+diff(mxy,u)/alphax+kx*(myy-mxx)+2*ky*mxy:
> nz:=(kxy*(mxx-myy)-(kxx-kyy)*mxy)/2:
> nxy:=nxym-nz:
> nyx:=nxym+nz:
> px:=-(diff(nxx,u)/alphax+diff(nyx,v)/alphay+ky*(nxx-nyy)+kx*(nxy+nyx)-kxx*vx-kxy*vy):
> py:=-(diff(nyy,v)/alphay+diff(nxy,u)/alphax+kx*(nyy-nxx)+ky*(nxy+nyx)-kyy*vy-kxy*vx):
> pz:=-(kxx*nxx+kxy*(nxy+nyx)+kyy*nyy+diff(vx,u)/alphax+diff(vy,v)/alphay+ky*vx+kx*vy):
> simplify(px);
                              0
> simplify(py);
                              0
> collect(simplify(pz),w(u));
```

$$\frac{Et}{a^2}w(u)+\frac{Et^3}{12(1-\nu^2)}\left(\frac{d^4}{du^4}w(u)\right)$$

Appendix. Section forces and moments in thick shells

In thin shells the membrane forces, the moments and the shear forces are defined in the same way as in plates (see definition of membrane forces p. 13). For thick shells (p. 13) the definitions are somewhat different because of the curvature (p. 20).

$$n_{xx} = \int_{-\frac{1}{2}t}^{\frac{1}{2}t} (\sigma_{xx}(1-k_{yy}z)+\sigma_{xy}k_{xy}z)dz \qquad n_{yy} = \int_{-\frac{1}{2}t}^{\frac{1}{2}t} (\sigma_{yy}(1-k_{xx}z)+\sigma_{xy}k_{xy}z)dz$$

$$n_{xy} = \int_{-\frac{1}{2}t}^{\frac{1}{2}t} (\sigma_{xy}(1-k_{yy}z)+\sigma_{yy}k_{xy}z)dz \qquad n_{yx} = \int_{-\frac{1}{2}t}^{\frac{1}{2}t} (\sigma_{xy}(1-k_{xx}z)+\sigma_{xx}k_{xy}z)dz$$

$$m_{xx} = \int_{-\frac{1}{2}t}^{\frac{1}{2}t} (\sigma_{xx}(1-k_{yy}z)+\sigma_{xy}k_{xy}z)zdz \qquad m_{yy} = \int_{-\frac{1}{2}t}^{\frac{1}{2}t} (\sigma_{yy}(1-k_{xx}z)+\sigma_{xy}k_{xy}z)zdz$$

$$m_{xy} = \frac{1}{2}[\int_{-\frac{1}{2}t}^{\frac{1}{2}t} (\sigma_{xy}(1-k_{yy}z)+\sigma_{yy}k_{xy}z)zdz + \int_{-\frac{1}{2}t}^{\frac{1}{2}t} (\sigma_{xy}(1-k_{xx}z)+\sigma_{xx}k_{xy}z)zdz]$$

$$v_x = \int_{-\frac{1}{2}t}^{\frac{1}{2}t} (\sigma_{xz}(1-k_{yy}z)+\sigma_{yz}k_{xy}z)dz \qquad v_y = \int_{-\frac{1}{2}t}^{\frac{1}{2}t} (\sigma_{yz}(1-k_{xx}z)+\sigma_{xz}k_{xy}z)dz$$

Exercise: Show that the above definitions comply with Sanders-Koiter equation 18. (Terms with for example $k_{yy}k_{xy}$ can be neglected because they are small.)

Derivation

The equations in the principal directions are simple (see figure); for example

$$n_{rr} = \int_{-\frac{1}{2}t}^{\frac{1}{2}t} \sigma_{rr}(1-k_{ss}z)dz$$

Here it is shown that the kernel

$$\sigma_{rr}(1-k_{ss}z)$$

in the principal directions *r*, *s* becomes

$$\sigma_{xx}(1-k_{yy}z)+\sigma_{xy}k_{xy}z$$

in the general directions *x*, *y*.

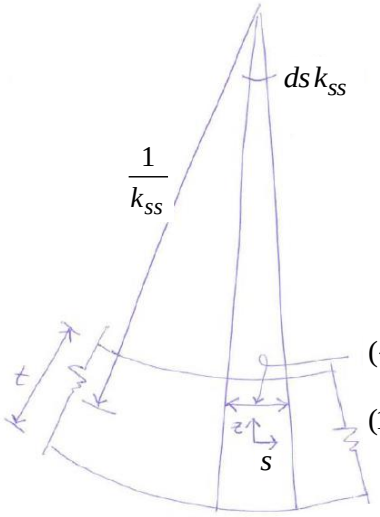

$$n_{rr}ds = \int_{-\frac{1}{2}t}^{\frac{1}{2}t} \sigma_{rr}(1-k_{ss}z)dsdz$$

```
dnrr:=(dnxx+dnyy)/2+(dnxx-dnyy)/2*cos(2*f)+dnxym*sin(2*f):
dnss:=(dnxx+dnyy)/2-(dnxx-dnyy)/2*cos(2*f)-dnxym*sin(2*f):
dnrsm:=              -(dnxx-dnyy)/2*sin(2*f)+dnxym*cos(2*f):
srr:=(sxx+syy)/2+(sxx-syy)/2*cos(2*f)+sxy*sin(2*f):
sss:=(sxx+syy)/2-(sxx-syy)/2*cos(2*f)-sxy*sin(2*f):
srs:=            -(sxx-syy)/2*sin(2*f)+sxy*cos(2*f):
```

```
krr:=(kxx+kyy)/2+(kxx-kyy)/2*cos(2*f)+kxy*sin(2*f):
kss:=(kxx+kyy)/2-(kxx-kyy)/2*cos(2*f)-kxy*sin(2*f):
krs:=           -(kxx-kyy)/2*sin(2*f)+kxy*cos(2*f):
dqr:= dqx*cos(f)+dqy*sin(f):
dqs:=-dqx*sin(f)+dqy*cos(f):
srz:= sxz*cos(f)+syz*sin(f):
ssz:=-sxz*sin(f)+syz*cos(f):

eq0:=krs=0:
f:=solve(eq0,f);
```

$$f := \frac{1}{2}\arctan\left(\frac{2\,kxy}{kxx - kyy}\right)$$

```
eq1:=dnrr=srr*(1-kss*z):
eq2:=dnss=sss*(1-krr*z):
dnrs:=srs*(1-kss*z):
dnsr:=srs*(1-krr*z):
eq3:=dnrsm=(dnrs+dnsr)/2:
opl:=solve({eq1,eq2,eq3},{dnxx,dnxym,dnyy}): assign(opl):
dnxx:=collect(dnxx,sxx);
```

$dnxx := (-kyy\,z + 1)\,sxx + kxy\,sxy\,z$

```
dnyy:=collect(dnyy,syy);
```

$dnyy := (-kxx\,z + 1)\,syy + kxy\,sxy\,z$

```
dnxym:=collect(dnxym,sxy);
```

$$dnxym := \left(-\frac{1}{2}\,z\,kxx - \frac{1}{2}\,z\,kyy + 1\right)sxy + \frac{1}{2}\,kxy\,sxx\,z + \frac{1}{2}\,kxy\,syy\,z$$

```
dnxy:=sxy*(1-kyy*z)+kxy*syy*z;
```

$dnxy := sxy\,(-kyy\,z + 1) + kxy\,syy\,z$

```
dnyx:=sxy*(1-kxx*z)+kxy*sxx*z;
```

$dnyx := sxy\,(-kxx\,z + 1) + kxy\,sxx\,z$

```
simplify(dnxym-(dnxy+dnyx)/2):
```

0

```
eq4:=dqr=srz*(1-kss*z):
eq5:=dqs=ssz*(1-krr*z):
opl:=solve({eq4,eq5},{dqx,dqy}); assign(opl):
dqx:=collect(dqx,sxz);
```

$dqx := (-kyy\,z + 1)\,sxz + kxy\,syz\,z$

```
dqy:=collect(dqy,syz);
```

$dqy := (-kxx\,z + 1)\,syz + sxz\,z\,kxy$

Appendix. Stresses in thick shells

surface $z=\frac{1}{2}t$	$\sigma_{xx}=(\frac{1}{t}+\frac{k_{yy}}{2})n_{xx}+(\frac{6}{t^2}+\frac{k_{yy}}{t})m_{xx}-k_{xy}(\frac{n_{xy}+n_{yx}}{4}+\frac{m_{xy}}{t})$ $\sigma_{yy}=(\frac{1}{t}+\frac{k_{xx}}{2})n_{yy}+(\frac{6}{t^2}+\frac{k_{xx}}{t})m_{yy}-k_{xy}(\frac{n_{xy}+n_{yx}}{4}+\frac{m_{xy}}{t})$ $\sigma_{zz}\approx 0$ $\sigma_{yz}=0$ $\sigma_{xz}=0$ $\sigma_{xy}=(\frac{1}{t}+\frac{k_m}{2})\frac{n_{xy}+n_{yx}}{2}+(\frac{6}{t^2}+\frac{k_m}{t})m_{xy}-k_{xy}(\frac{n_{xx}+n_{yy}}{4}+\frac{m_{xx}+m_{yy}}{2t})$
middle surface $z=0$	$\sigma_{xx}=\frac{1}{t}n_{xx}+\frac{k_{yy}}{t}m_{xx}-\frac{k_{xy}}{t}m_{xy}$ $\sigma_{yy}=\frac{1}{t}n_{yy}+\frac{k_{xx}}{t}m_{yy}-\frac{k_{xy}}{t}m_{xy}$ $\sigma_{zz}\approx 0$ $\sigma_{yz}=\frac{3}{2t}v_y$ $\sigma_{xz}=\frac{3}{2t}v_x$ $\sigma_{xy}=\frac{1}{t}\frac{n_{xy}+n_{yx}}{2}+\frac{k_m}{t}m_{xy}-k_{xy}\frac{m_{xx}+m_{yy}}{2t}$
surface $z=-\frac{1}{2}t$	$\sigma_{xx}=(\frac{1}{t}-\frac{k_{yy}}{2})n_{xx}+(-\frac{6}{t^2}+\frac{k_{yy}}{t})m_{xx}+k_{xy}(\frac{n_{xy}+n_{yx}}{4}-\frac{m_{xy}}{t})$ $\sigma_{yy}=(\frac{1}{t}-\frac{k_{xx}}{2})n_{yy}+(-\frac{6}{t^2}+\frac{k_{xx}}{t})m_{yy}+k_{xy}(\frac{n_{xy}+n_{yx}}{4}-\frac{m_{xy}}{t})$ $\sigma_{zz}\approx 0$ $\sigma_{yz}=0$ $\sigma_{xz}=0$ $\sigma_{xy}=(\frac{1}{t}-\frac{k_m}{2})\frac{n_{xy}+n_{yx}}{t}+(-\frac{6}{t^2}+\frac{k_m}{t})m_{xy}+k_{xy}(\frac{n_{xx}+n_{yy}}{4}-\frac{m_{xx}+m_{yy}}{2t})$

Derivation

```
sxx:=(sxxt+sxxb)/2+(sxxt-sxxb)*z/t: # Bernoulli's hypothesis
syy:=(syyt+syyb)/2+(syyt-syyb)*z/t:
szz:= 0:
syz:=-4*syzm/t^2*(z-t/2)*(z+t/2):
sxz:=-4*sxzm/t^2*(z-t/2)*(z+t/2):
sxy:=(sxyt+sxyb)/2+(sxyt-sxyb)*z/t:
# Definitions of membrane forces, moments and shear forces
eq1:=nxx=int(sxx*(1-kyy*z)+sxy*kxy*z,z=-t/2..t/2):
eq2:=nyy=int(syy*(1-kxx*z)+sxy*kxy*z,z=-t/2..t/2):
nxy:=int(sxy*(1-kyy*z)+syy*kxy*z,z=-t/2..t/2):
```

```
nyx:=int(sxy*(1-kxx*z)+sxx*kxy*z,z=-t/2..t/2):
eq3:=nxym=(nxy+nyx)/2:
eq4:=mxx=int((sxx*(1-kyy*z)+sxy*kxy*z)*z,z=-t/2..t/2):
eq5:=myy=int((syy*(1-kxx*z)+sxy*kxy*z)*z,z=-t/2..t/2):
mxy:=int((sxy*(1-kyy*z)+syy*kxy*z)*z,z=-t/2..t/2):
myx:=int((sxy*(1-kxx*z)+sxx*kxy*z)*z,z=-t/2..t/2):
eq6:=mxym =(mxy+myx)/2:
qx:=int(sxz*(1-kyy*z)+syz*kxy*z,z=-t/2..t/2);
```

$$qx := \frac{2}{3}\, sxzm\, t$$

```
qy:=int(syz*(1-kxx*z)+sxz*kxy*z,z=-t/2..t/2);
```

$$qy := \frac{2}{3}\, syzm\, t$$

```
opl:=solve({eq1,eq2,eq3,eq4,eq5,eq6},{sxxb,sxxt,sxyb,sxyt,syyb,syyt})
: assign(opl):
sxxt:=mtaylor(sxxt,{kxx,kxy,kyy},2);
```

$$sxxt := \left(\frac{6}{t^2} + \frac{kyy}{t}\right) mxx - \frac{kxy\, mxym}{t} + \left(\frac{1}{t} + \frac{1}{2}\, kyy\right) nxx - \frac{1}{2}\, nxym\, kxy$$

```
syyt:=mtaylor(syyt,{kxx,kxy,kyy},2);
```

$$syyt := -\frac{kxy\, mxym}{t} + \left(\frac{6}{t^2} + \frac{kxx}{t}\right) myy - \frac{1}{2}\, nxym\, kxy + \left(\frac{1}{t} + \frac{1}{2}\, kxx\right) nyy$$

```
sxyt:=mtaylor(sxyt,{kxx,kxy,kyy},2);
```

$$sxyt := -\frac{1}{2}\,\frac{kxy\, mxx}{t} + \left(\frac{6}{t^2} + \frac{1}{2}\,\frac{kxx}{t} + \frac{1}{2}\,\frac{kyy}{t}\right) mxym - \frac{1}{2}\,\frac{kxy\, myy}{t} - \frac{1}{4}\, kxy\, nxx + \left(\frac{1}{t} + \frac{1}{4}\, kxx + \frac{1}{4}\, kyy\right) nxym - \frac{1}{4}\, nyy\, kxy$$

```
sxxm:=mtaylor((sxxt+sxxb)/2,{kxx,kxy,kyy},2);
```

$$sxxm := \frac{kyy\, mxx}{t} - \frac{kxy\, mxym}{t} + \frac{nxx}{t}$$

```
syym:=mtaylor((syyt+syyb)/2,{kxx,kxy,kyy},2);
```

$$syym := -\frac{kxy\, mxym}{t} + \frac{kxx\, myy}{t} + \frac{nyy}{t}$$

```
sxym:=mtaylor((sxyt+sxyb)/2,{kxx,kxy,kyy},2);
```

$$sxym := -\frac{1}{2}\,\frac{kxy\, mxx}{t} + \left(\frac{1}{2}\,\frac{kxx}{t} + \frac{1}{2}\,\frac{kyy}{t}\right) mxym - \frac{1}{2}\,\frac{kxy\, myy}{t} + \frac{nxym}{t}$$

```
sxxb:=mtaylor(sxxb,{kxx,kxy,kyy},2);
```

$$sxxb := \left(-\frac{6}{t^2} + \frac{kyy}{t}\right) mxx - \frac{kxy\, mxym}{t} + \left(\frac{1}{t} - \frac{1}{2}\, kyy\right) nxx + \frac{1}{2}\, nxym\, kxy$$

```
syyb:=mtaylor(syyb,{kxx,kxy,kyy},2);
```

$$syyb := -\frac{kxy\, mxym}{t} + \left(-\frac{6}{t^2} + \frac{kxx}{t}\right) myy + \frac{1}{2}\, nxym\, kxy + \left(\frac{1}{t} - \frac{1}{2}\, kxx\right) nyy$$

```
sxyb:=mtaylor(sxyb,{kxx,kxy,kyy},2);
```

$$sxyb := -\frac{1}{2}\,\frac{kxy\, mxx}{t} + \left(-\frac{6}{t^2} + \frac{1}{2}\,\frac{kxx}{t} + \frac{1}{2}\,\frac{kyy}{t}\right) mxym - \frac{1}{2}\,\frac{kxy\, myy}{t} + \frac{1}{4}\, kxy\, nxx + \left(\frac{1}{t} - \frac{1}{4}\, kxx - \frac{1}{4}\, kyy\right) nxym + \frac{1}{4}\, nyy\, kxy$$

Appendix. Increase of the Gaussian curvature

The quantity $-k_{yy}\kappa_{xx} + k_{xy}\rho_{xy} - k_{xx}\kappa_{yy}$ is approximately equal to the increase of the shell Gaussian curvature k_G during loading.

Proof

In the local coordinate system the shell surface can be approximated by (p. 21)

$$z = \tfrac{1}{2}k_{xx}x^2 + k_{xy}xy + \tfrac{1}{2}k_{yy}y^2 .$$

A displacement can be approximated as

$$u_z = u_{zo} + \varphi_x x + \varphi_y y - \tfrac{1}{2}\kappa_{xx}x^2 - \tfrac{1}{2}\rho_{xy}xy - \tfrac{1}{2}\kappa_{yy}y^2 .$$

The deformed shape is

$$z + u_z = u_{zo} + \varphi_x x + \varphi_y y + \tfrac{1}{2}(k_{xx} - \kappa_{xx})x^2 + (k_{xy} - \tfrac{1}{2}\rho_{xy})xy + \tfrac{1}{2}(k_{yy} - \kappa_{yy})y^2 .$$

The curvatures after deformation are

$$\frac{\partial^2 (z + u_z)}{\partial x^2} = k_{xx} - \kappa_{xx} ,$$
$$\frac{\partial^2 (z + u_z)}{\partial x \partial y} = k_{xy} - \tfrac{1}{2}\rho_{xy} ,$$
$$\frac{\partial^2 (z + u_z)}{\partial y^2} = k_{yy} - \kappa_{yy} .$$

Before deformation the Gaussian curvature of the middle surface is

$$k_G = k_{xx}k_{yy} - k_{xy}^2 .$$

After deformation the Gaussian curvature is

$$k_{Gd} = (k_{xx} - \kappa_{xx})(k_{yy} - \kappa_{yy}) - (k_{xy} - \tfrac{1}{2}\rho_{xy})^2 .$$

The increase in Gaussian curvature is

$$k_{Gd} - k_G = -k_{yy}\kappa_{xx} + k_{xy}\rho_{xy} - k_{xx}\kappa_{yy} + \kappa_{xx}\kappa_{yy} - \tfrac{1}{4}\rho_{xy}^2 .$$

The last two terms are very small compared to the other terms and can be neglected for shells with significant curvatures. They cannot be neglected for flat plates.

Q.E.D.

The increase of the Gaussian curvature can also be written as

$$k_{Gd} - k_G = -(k_{yy} - \tfrac{1}{2}\kappa_{yy})\kappa_{xx} + (k_{xy} - \tfrac{1}{4}\rho_{xy})\rho_{xy} - (k_{xx} - \tfrac{1}{2}\kappa_{xx})\kappa_{yy} .$$

Appendix. Umbilical patterns

Identifying umbilical patterns

It is often difficult to recognise the umbilical pattern from the finite element principal directions, especially when several umbilics occur close to each other. Fortunately, they can be recognised computationally too.

Six gradients a_i can be computed from the tensor finite element results around an umbilic.

$$a_1 = \frac{\partial m_{xx}}{\partial x} \quad a_2 = \frac{\partial m_{xx}}{\partial y}$$
$$a_3 = \frac{\partial m_{yy}}{\partial x} \quad a_4 = \frac{\partial m_{yy}}{\partial y}$$
$$a_5 = \frac{\partial m_{xy}}{\partial x} \quad a_6 = \frac{\partial m_{xy}}{\partial y}$$

The directions of the ridges are the roots of

$$f = \frac{a_6 \tan^3\varphi + (a_2 - a_4 + a_5)\tan^2\varphi + (a_1 - a_3 - a_6)\tan\varphi - a_5}{(a_2 - a_4)\tan^3\varphi + (a_1 - a_3 - 4a_6)\tan^2\varphi - (a_2 - a_4 + 4a_5)\tan\varphi - (a_1 - a_3)}.$$

For example, Figure 6 shows f for $a_1 = 1$, $a_2 = 2$, $a_3 = 3$, $a_4 = 4$, $a_5 = 5$, $a_6 = 6$ N/mm². The roots can be computed using the Newton-Raphson algorithm. When the directions of the ridges are known the umbilical pattern can be identified using Figure 172.

Exercise: What umbilical pattern follows from the following?

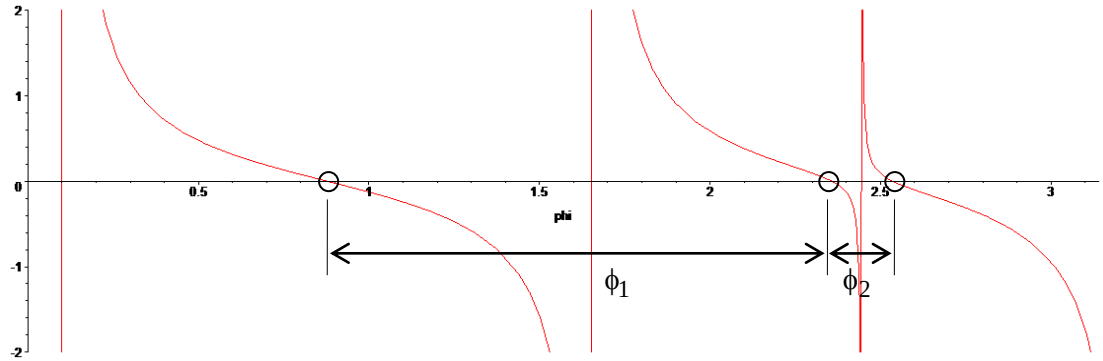

Figure 6. Function f of φ, the three roots are angles of ridges with the x axis

Table 14. Values of a_1 to a_6 for the patterns of figure 171

	a_1	a_2	a_3	a_4	a_5	a_6
Monstar	2	0	0	0	0	3
Star	0	2	0	0	1	0
Lemon	2	0	0	0	0	1
Flame	1	-1	0	0	0	1
Orthogonal	0	1	0	0	0	0

Simplified umbilical patterns
For the curvature tensor there is a substantial simplification; $a_5 \equiv a_2$ and $a_6 \equiv a_3$. This follows from applying the curvature definitions (p. 20) to

$$\overline{z} = c_1\overline{x}^2 + c_2\overline{x}\,\overline{y} + c_3\overline{y}^2 + c_4\overline{x}^3 + c_5\overline{x}^2 y + c_6\overline{x}\,\overline{y}^2 + c_7\overline{y}^3 .$$

For the membrane force tensor of plates loaded in plane there is a simplification too; $a_5 \equiv -a_4$ and $a_6 \equiv -a_1$ provided that there is edge load only therefore p_x and p_y are zero. This follows from Sanders-Koiter equation 19 and 20 (p. 54).

Invariants of tensor gradients
The gradients a_i defined in the previous section depend on the direction of the local *x* axis and *y* axis. It is useful to have quantities that do not depend on the coordinate system. The following quantities have this property. They are called invariants. They are valid for all points of a shell, not only for umbilics (p. 124).

$$\delta_1 = (a_1 - a_3)a_6 - (a_2 - a_4)a_5$$
$$\delta_2 = a_1 a_3 - a_5^2 + a_2 a_4 - a_6^2$$
$$\delta_3 = (a_1 + a_3)^2 + (a_2 + a_4)^2$$
$$\delta_4 = (a_3 - a_6)^2 + (a_2 - a_5)^2$$
$$\delta_5 = 4(a_1 a_3 - a_5^2)(a_2 a_4 - a_6^2) - (a_1 a_4 + a_2 a_3 - 2a_5 a_6)^2$$
$$\delta_6 = 4(t_2^2 - 3a_6 t_1)(t_1^2 + 3a_5 t_2) - (t_2 t_1 + 9a_5 a_6)^2 \qquad t_1 = a_1 - a_3 - a_6 \qquad t_2 = a_2 - a_4 + a_5$$

An infinite number of invariants exists. After all, the above six invariants can be added, multiplied et cetera in an infinite number of ways. This does not mean that all invariants can be constructed from the above invariants. Probably, invariants exist that cannot but a mathematical proof of this does not exist as yet.[2]

Interpretation of the invariants of tensor gradients
Invariants (p. 214) do not depend on the direction of the *x* and *y* axis. Physical reality does neither. So, invariants are good candidates to describe physical reality. The following interpretations of invariants have been found.
Invariant δ_1 gives information on the umbilical pattern. Where $\delta_1 > 0$ monstars occur, where $\delta_1 < 0$ stars occur, where $\delta_1 = 0$ orthogonal patterns or nonlinear patterns occur. Where invariant $\delta_6 = 0$ lemons or flames occur. More applications of invariants are likely to be found.

Invariant proof

```
> restart:
> x:=r*cos(f)-s*sin(f):
> y:=r*sin(f)+s*cos(f):
> nxx:=p1+a1*x+a2*y:
> nyy:=p2+a3*x+a4*y:
```

[2] Invariants are not easy to find. Invariant δ_1, δ_5 and δ_6 have been derived by A. Thorndike *et al*. in 1978 [135]. Invariant δ_2, δ_3 and δ_4 have been discovered by Wouter van Stralen in 2013 [136].

```
> nxy:=p3+a5*x+a6*y:
> nrr:=1/2*(nxx+nyy)+1/2*(nxx-nyy)*cos(2*f)+nxy*sin(2*f):
> nss:=1/2*(nxx+nyy)-1/2*(nxx-nyy)*cos(2*f)-nxy*sin(2*f):
> nrs:=              -1/2*(nxx-nyy)*sin(2*f)+nxy*cos(2*f):
> b1:=diff(nrr,r):
> b2:=diff(nrr,s):
> b3:=diff(nss,r):
> b4:=diff(nss,s):
> b5:=diff(nrs,r):
> b6:=diff(nrs,s):
> simplify((b1-b3)*b6-(b2-b4)*b5);
```

$a1\ a6 - a2\ a5 - a3\ a6 + a4\ a5$

Ridge angles as function of constants a_1 to a_6

$$\begin{aligned} n_{xx} &= p + a_1 x + a_2 y \\ n_{yy} &= p + a_3 x + a_4 y \\ n_{xy} &= \quad a_5 x + a_6 y \end{aligned} \tag{1}$$

$$\begin{aligned} x &= r\cos\varphi \\ y &= r\sin\varphi \end{aligned} \tag{2}$$

$$\begin{aligned} n_{rr} &= \tfrac{1}{2}(n_{xx}+n_{yy}) + \tfrac{1}{2}(n_{xx}-n_{yy})\cos 2\varphi + n_{xy}\sin 2\varphi \\ n_{ss} &= \tfrac{1}{2}(n_{xx}+n_{yy}) - \tfrac{1}{2}(n_{xx}-n_{yy})\cos 2\varphi - n_{xy}\sin 2\varphi \\ n_{rs} &= \qquad\qquad -\tfrac{1}{2}(n_{xx}-n_{yy})\sin 2\varphi + n_{xy}\cos 2\varphi \end{aligned} \tag{3}$$

The principal directions γ in the *r*-*s* coordinate system is

$$\tan 2\gamma = \frac{2n_{rs}}{n_{rr} - n_{ss}} \tag{4}$$

For a ridge

$$\gamma = 0 \text{ or } \gamma = \tfrac{1}{2}\pi\,. \tag{5}$$

Substitution of Eqs (1), (2), (3) and (5) in (4) gives

$$0 = \frac{a_6\tan^3\varphi + (a_2 - a_4 + a_5)\tan^2\varphi + (a_1 - a_3 - a_6)\tan\varphi - a_5}{(a_2 - a_4)\tan^3\varphi + (a_1 - a_3 - 4a_6)\tan^2\varphi - (a_2 - a_4 + 4a_5)\tan\varphi - (a1 - a3)} \tag{6}$$

The denominator is important because when any two ridges have an angle of $\pi/2$ the third ridge is cancelled out of this fraction. Therefore, there can be one, two or three roots.

The roots can be computed using, for example, the Newton-Raphson algorithm.
The derivative of Eq. (4) is

$$\frac{d}{d\varphi}\tan 2\gamma = \frac{(t_1\tan^2\varphi + t_2\tan\varphi + t_3)(1+\tan^2\varphi)^2}{((a_2 - a_4)\tan^3\varphi + (a_1 - a_3 - 4a_6)\tan^2\varphi - (a_2 - a_4 + 4a_5)\tan\varphi - (a1 - a3))^2} \tag{7}$$

$$t_1 = a_6(a_1 - a_3 - 4a_6) - (a_2 - a_4 + a_5)(a_2 - a_4)$$
$$t_2 = -2(a_2 - a_4)(a_1 - a_3) - 8a_5a_6$$
$$t_3 = -a_5(a_2 - a_4 + 4a_5) - (a_1 - a_3 - a_6)(a_1 - a_3)$$

Constants a_1 to a_6 as function of the ridge angles

To obtain the patters of fig. 171 we choose a Cartesian coordinate system in an umbilic and assume a linear variation in the second order tensor, for example the normal forces.

$$\begin{aligned} n_{xx} &= p + a_1 x + a_2 y \\ n_{yy} &= p + a_3 x + a_4 y \\ n_{xy} &= \quad a_5 x + a_6 y \end{aligned} \tag{1}$$

Cylinder coordinates are introduced.

$$\begin{aligned} x &= r\cos\varphi \\ y &= r\sin\varphi \end{aligned} \tag{2}$$

The principal direction γ is defined by

$$\tan 2\gamma = \frac{2n_{xy}}{n_{xx} - n_{yy}}. \tag{3}$$

For the ridges holds

$$\gamma = \varphi \tag{4}$$

Substitution of equations (1), (2) and (4) in (3) gives a third degree polynomial in $\tan\varphi$.

$$a_6 \tan^3\varphi + (a_2 - a_4 + a_5)\tan^2\varphi + (a_1 - a_3 - a_6)\tan\varphi - a_5 = 0 \tag{5}$$

Suppose the roots of this polynomial are b_1, b_2 and b_3. Then it can be written as

$$(b_1 - \tan\varphi)(b_2 - \tan\varphi)(b_3 - \tan\varphi) = 0. \tag{6}$$

This can be evaluated as

$$\tan^3\varphi - (b_1 + b_2 + b_3)\tan^2\varphi + (b_1b_2 + b_2b_3 + b_3b_1)\tan\varphi - b_1b_2b_3 = 0. \tag{7}$$

Comparing Eq. (5) to (7) we observe,

$$\begin{aligned} \frac{a_2 - a_4 + a_5}{a_6} &= -(b_1 + b_2 + b_3) \\ \frac{a_1 - a_3 - a_6}{a_6} &= b_1b_2 + b_2b_3 + b_3b_1 \\ \frac{a_5}{a_6} &= b_1b_2b_3 \end{aligned} \tag{8}$$

The roots are the angles of the ridges (fig. 172)

$$\begin{aligned} b_1 &= \tan\varphi_1 \\ b_2 &= \tan\varphi_2 \\ b_3 &= \tan\varphi_3 \end{aligned} \tag{9}$$

Substitution of equations (9) in (8) and evaluation gives

$$\begin{aligned} a_1 - a_3 &= (ccc + ssc + css + scs)\, C \\ a_2 - a_4 &= -(sss + ccs + csc + scc)\, C \\ a_5 &= sss\, C \\ a_6 &= ccc\, C \end{aligned} \tag{10}$$

where C is an unknown factor and

$$\begin{aligned} sss &= \sin\varphi_1 \sin\varphi_2 \sin\varphi_3 \\ css &= \cos\varphi_1 \sin\varphi_2 \sin\varphi_3 \\ scs &= \sin\varphi_1 \cos\varphi_2 \sin\varphi_3 \\ ssc &= \sin\varphi_1 \sin\varphi_2 \cos\varphi_3 \\ ccs &= \cos\varphi_1 \cos\varphi_2 \sin\varphi_3 \\ csc &= \cos\varphi_1 \sin\varphi_2 \cos\varphi_3 \\ scc &= \sin\varphi_1 \cos\varphi_2 \cos\varphi_3 \\ ccc &= \cos\varphi_1 \cos\varphi_2 \cos\varphi_3 \end{aligned} \tag{11}$$

Invariants as a function of the ridge angles

$$\begin{aligned} \delta_1 &= C^2 \cos(\varphi_2 - \varphi_1)\cos(\varphi_3 - \varphi_1)\cos(\varphi_3 - \varphi_2) \\ \delta_3 - 4(\delta_1 + \delta_2) &= (a_1 - a_3 - 2a_6)^2 + (a_2 - a_4 + 2a_5)^2 = C^2 \\ \delta_6 &= \pm 3C^4 \sin^2(\varphi_2 - \varphi_1)\sin^2(\varphi_3 - \varphi_1)\sin^2(\varphi_3 - \varphi_2) \end{aligned} \tag{12}$$

Appendix. Buckling equations

> $nxy := 0 : nyx := 0 : kxy := 0 :$

> $uz := C \cdot \cos\left(\frac{\mathrm{Pi} \cdot x}{lx}\right) \cdot \cos\left(\frac{\mathrm{Pi} \cdot y}{ly}\right) :$

> $G1 := kxx \cdot diff(uz, y, y) - 2 \cdot kxy \cdot diff(uz, x, y) + kyy \cdot diff(uz, x, x) :$

> $G2 := kxx \cdot diff(G1, y, y) - 2 \cdot kxy \cdot diff(G1, x, y) + kyy \cdot diff(G1, x, x) :$

> $D1 := diff(uz, x, x) + diff(uz, y, y) :$

> $D2 := diff(D1, x, x) + diff(D1, y, y) :$

> $D3 := diff(D2, x, x) + diff(D2, y, y) :$

> $D4 := diff(D3, x, x) + diff(D3, y, y) :$

> $P1 := \mathrm{lambda} \cdot (pz + nxx \cdot diff(uz, x, x) + (nxy + nyx) \cdot diff(uz, x, y) + nyy \cdot diff(uz, y, y)) :$

> $P2 := diff(P1, x, x) + diff(P1, y, y) :$

> $P3 := diff(P2, x, x) + diff(P2, y, y) :$

> $eq := \frac{E \cdot t^3}{12 \cdot (1 - \nu^2)} \cdot D4 + E \cdot t \cdot G2 = P3 :$

> $\lambda 1 := solve(eq, \mathrm{lambda}) :$

> $\lambda 2 := \frac{-E\,t}{\frac{nxx}{lx^2} + \frac{nyy}{ly^2}} \cdot \left(\frac{\pi^2 \cdot t^2}{12 \cdot (1 - \nu^2)} \cdot \left(\frac{1}{lx^2} + \frac{1}{ly^2} \right)^2 + \frac{\left(\frac{kxx}{ly^2} + \frac{kyy}{lx^2} \right)^2 + \left(\frac{2 \cdot kxy}{lx \cdot ly} \right)^2}{\pi^2 \cdot \left(\frac{1}{lx^2} + \frac{1}{ly^2} \right)^2} \right) :$

> $simplify(\lambda 1 - \lambda 2);$

$$0$$

> $lx := l \cdot \cos(a) : ly := l \cdot \sin(a) :$

> $\lambda 3 := simplify(\lambda 2) :$

> $\lambda 4 := \frac{-E \cdot t^2}{\sqrt{3 \cdot (1 - \nu^2)}} \cdot \frac{\mathrm{abs}(kxx)}{nyy} :$

> $\lambda 5 := \frac{-E \cdot t^2}{\sqrt{3 \cdot (1 - \nu^2)}} \cdot \frac{\mathrm{abs}(kyy)}{nxx} :$

> $E := 5 : \mathrm{nu} := 0.3 : t := 3 : l := \frac{1}{\mathrm{abs}(kyy)} :$

> $kxx := \frac{1}{150} \cdot \frac{1}{t \cdot \sqrt{(1 - \nu^2)}} : kyy := \frac{-1}{300} \cdot \frac{1}{t \cdot \sqrt{(1 - \nu^2)}} : nxx := \frac{1}{1000} \cdot \frac{E \cdot t}{(1 - \nu^2)} : nyy := \frac{-3}{1000} \cdot \frac{E \cdot t}{(1 - \nu^2)} :$

> $nxx \cdot \mathrm{abs}(kxx) + nyy \cdot \mathrm{abs}(kyy);$

$$-0.00001919935600$$

> $plot\left(\{\lambda 3, \lambda 4, \lambda 5\}, a = 0 .. \frac{\mathrm{Pi}}{2}, -3 .. 2 \right);$

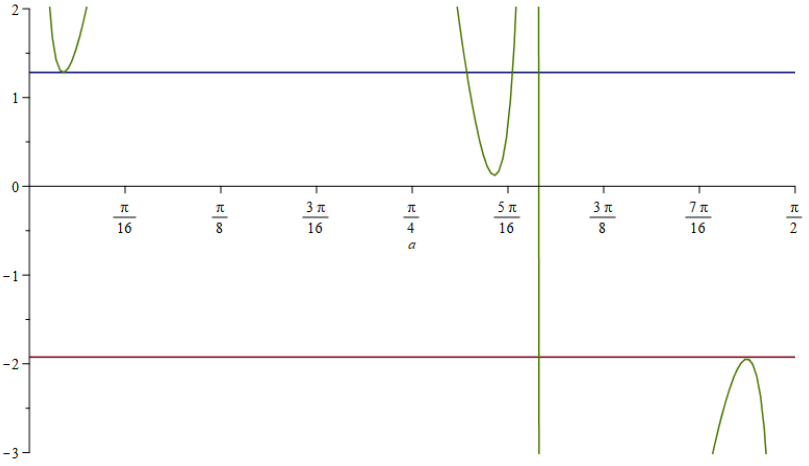

Appendix. 3D reinforcement

Designing
In a small cube of concrete the following reinforcement ratios can be applied [137].

$$\rho_x = \frac{\sigma_{xx} + |\sigma_{xy}| + |\sigma_{xz}|}{f_y}, \qquad \rho_y = \frac{\sigma_{yy} + |\sigma_{xy}| + |\sigma_{yz}|}{f_y}, \qquad \rho_z = \frac{\sigma_{zz} + |\sigma_{xz}| + |\sigma_{yz}|}{f_y}$$

where f_y is the rebar yield strength. If a ratio is negative, no reinforcement is needed.

Sometimes a bit less reinforcement is sufficient too, especially in case of multiple stress states due to multiple load combinations It is convenient to just try less reinforcement and apply the check below.

If the bars are placed in the principal directions than the required reinforcement ratios are

$$\rho_1 = \frac{\sigma_1}{f_y}, \qquad \rho_2 = \frac{\sigma_2}{f_y}, \qquad \rho_3 = \frac{\sigma_3}{f_y}$$

For fibre reinforced concrete the reinforcement ratio is

$$\rho = 4\frac{\sigma_1}{f_y}.$$

Challenge: Derive the factor 4 considering that most fibres are not in the tensile direction and do not have full development length.

Checking reinforcement
Suppose somebody designed reinforcement and we need to check it. For this, the eigenvalues of the following matrix need to be smaller than or equal to zero [143].

$$\begin{bmatrix} \sigma_{xx} - \rho_x f_y & \sigma_{xy} & \sigma_{xz} \\ \sigma_{xy} & \sigma_{yy} - \rho_y f_y & \sigma_{yz} \\ \sigma_{xz} & \sigma_{yz} & \sigma_{zz} - \rho_z f_y \end{bmatrix}$$

Where σ_{xx}, σ_{yy} … et cetera are the computed linear elastic stresses ρ_x, ρ_y, ρ_z are the reinforcement ratios and f_y is the steel yield stress.

This rule can be easily explained. Concrete shrinks while curing, the bars do not, so small cracks are everywhere. The concrete between the bars cannot carry tension. The concrete principal stresses need to be negative. The principals stresses are the eigenvalues of the concrete stress tensor. In the ultimate limit state, the concrete stress tensor consists of the computed linear elastic stresses minus the stresses carried by the reinforcement when yielding.

Crushing of the concrete needs to be checked too. This is explained in the following note.

Checking concrete stresses
Crushing failure of concrete can be checked with the Mohr-Coulomb criterion

$$\frac{\sigma_3}{f_c} + \frac{\sigma_1}{f_t} \leq 1$$

where σ_3 and σ_1 are the smallest (most negative) and largest principal stresses of the concrete stress tensor, f_c is the concrete compressive strength (negative value), f_t is the concrete tensile strength. The latter is not zero because between the shrinkage cracks there are chunks of concrete that are not cracked. These chunks form the compression diagonals.

The Mohr-Coulomb value can be interpreted as following;

- when it is for example 0.87 than 87% of the capacity of the material has been used;
- when it is for example 1.23 than the material is overloaded by 23%. In fact, if this were the real material it would already have been crushed;
- when it is for example -1.30 the material is prestressed which makes it stronger for additional load.

Appendix. Tensors

Tensor properties
The sum of two tensors is a tensor.
$RT_1R^{\mathrm{T}} + RT_2R^{\mathrm{T}} = R(T_1 + T_2)R^{\mathrm{T}}$ Q.E.D.

The product of two tensors is a tensor.
$RT_1R^{\mathrm{T}}RT_2R^{\mathrm{T}} = RT_1R^{-1}RT_2R^{\mathrm{T}} = RT_1IT_2R^{\mathrm{T}} = RT_1T_2R^{\mathrm{T}}$ Q.E.D.

The inverse of a tensor is a tensor.
$RT^{-1}R^{\mathrm{T}} = RT^{-1}R^{-1} = R(RT)^{-1} = (R^T)^{-1}(RT)^{-1} = (RTR^{\mathrm{T}})^{-1}$ Q.E.D.

For example, an eccentricity tensor *e* can be defined.

$$\begin{bmatrix} e_{xx} & e_{xy} \\ e_{yx} & e_{yy} \end{bmatrix}\begin{bmatrix} n_{xx} & n_{xy} \\ n_{yx} & n_{yy} \end{bmatrix} = \begin{bmatrix} m_{xx} & m_{xy} \\ m_{xy} & m_{yy} \end{bmatrix}$$

We know that this eccentricity tensor is a tensor because of the above properties.

Challenge: Suppose that we designed a shell, performed a finite element analysis and want to improve the shape such that the eccentricity is in the middle third. Which rule can be derived for this? Will successive shape improvements converge?

Tensor invariants
A 2×2 tensor has two quantities that do not change when the coordinate system rotates around the *z* axis. Using the moment tensor as an example, these quantities are

$m_{xx} + m_{yy}$	trace
$m_{xx}m_{yy} - m_{xy}^2$	determinant

These quantities are called the invariants. Clearly, the invariants can be added, multiplied et cetera, to produce more quantities that do not change when the coordinate system rotates around the *z* axis. For example,

$m_{xx}^2 + 2m_{xy}^2 + m_{yy}^2$

Exercise: Derive that $m_{xx}^2 + 2m_{xy}^2 + m_{yy}^2$ does not depend on the direction of the coordinate system by combining the invariants.

Exercise: Show that $k_1 = k_m + \sqrt{k_m^2 - k_G}$ and $k_2 = k_m - \sqrt{k_m^2 - k_G}$.

Exercise: Derive the following equations. $k_1^2 + k_2^2 = k_{xx}^2 + 2k_{xy}^2 + k_{yy}^2 = 4k_m^2 - 2k_G$

Exercise: Derive that $\sqrt{\sigma_{xx}^2 - \sigma_{xx}\sigma_{yy} + \sigma_{yy}^2 + 3\sigma_{xy}^2}$ does not change when the coordinate system rotates around the *z* axis.

Reinforcement is a tensor too
The reinforcement that designers choose for concrete shells looks like trajectories. This is because the bars are most efficient when they cross perpendicularly. It would be optimal if the bars follow the stress trajectories in the shell surface. This means four layers of bars; two close to the inner surface and two close to the outer surface. However, usually this is not possible because different load combinations give different stress trajectories. Nevertheless, two layers of practical reinforcement can be described by a second order tensor field. The bar cross-section areas are the principal values a_1 and a_2 in for example mm²/m or kg/m². The reinforcement tensor is

$$\begin{bmatrix} a_{xx} & a_{xy} \\ a_{xy} & a_{yy} \end{bmatrix}.$$

The amount of reinforcement of a small shell part with length l_1 and width l_2 is $a_1 l_2 l_1 + a_2 l_1 l_2$. Per shell area this is $a_1 + a_2$, which is equal to $a_{xx} + a_{yy}$. A computer can determine the reinforcement tensor field as an optimisation problem (three dofs per node.) The objective is to minimise the total amount of reinforcement. The constraints are strength, crack width and development length.

Exercise: Why is $a_1 a_2 \geq 0$?

Invariants of two tensors
When two 2×2 tensors are added or multiplied et cetera, the resulting tensor has the four invariants of the individual tensors and two extra invariants. Using curvature and moment as an example, the extra invariants are

$$k_{xx} m_{xx} + 2k_{xy} m_{xy} + k_{yy} m_{yy}$$
$$k_{xy}(m_{xx} - m_{yy}) - m_{xy}(k_{xx} - k_{yy})$$

More independent invariants of two 2×2 tensors have not been found [138].

Exercise: The invariants of two tensors both occur in the Sanders-Koiter equations. Can you spot them?

Exercise: Derive that $k_{xx} m_{yy} - 2k_{xy} m_{xy} + k_{yy} m_{xx}$ does not change when the coordinate system rotates around the *z* axis.

Exercise: Derive that $\frac{1}{2}\kappa_{xx} m_{xx} + \frac{1}{2}\rho_{xy} m_{xy} + \frac{1}{2}\kappa_{yy} m_{yy}$ does not change when the coordinate system rotates around the *z* axis.